

LLL-Prop-148

## TMX MAJOR PROJECT PROPOSAL

F. H. Coensgen, Project Leader

January 12, 1977

CIRCULATION COPY  
SUBJECT TO RECALL  
IN TWO WEEKS

Prepared for U. S. Energy Research  
& Development Administration under  
Contract No. W-7405-Eng-48.



#### NOTICE

This report was prepared as an account of work sponsored by the United States Government. Neither the United States nor the United States Energy Research & Development Administration, nor any of their employees, nor any of their contractors, subcontractors, or their employees, makes any warranty, express or implied, or assumes any legal liability or responsibility for the accuracy, completeness or usefulness of any information, apparatus, product or process disclosed, or represents that its use would not infringe privately-owned rights.

#### NOTICE

Reference to a company or product name does not imply approval or recommendation of the product by the University of California or the U.S. Energy Research & Development Administration to the exclusion of others that may be suitable.

LLL-Prop-148

TMX MAJOR PROJECT PROPOSAL

F. H. Coensgen, Project Leader

January 12, 1977

#### ACKNOWLEDGEMENTS

The proposal for a new experiment (TMX) is the product of dedicated hard work by many people in the Magnetic Fusion Energy Division at Lawrence Livermore Laboratory. Credit goes to T. K. Fowler and B. G. Logan for the Tandem Mirror Concept that made this proposal possible. The task of determining the physics objectives and parameter regimes of TMX to best evaluate the concept was primarily the effort of D. E. Baldwin, T. K. Fowler, and B. G. Logan. The mechanical and electrical engineering designs were spearheaded by A. K. Chargin and G. E. Vogtlin. F. H. Coensgen and C. C. Damm played an essential role in coordinating the physics and engineering design efforts. Many other participants in this proposal are recognized in various sections that follow. Thanks particularly go to C. McGregor, J. Johnson, J. E. Bailey, and C. D. Seberger for their invaluable aid in the preparation of this manuscript.

## CONTENTS

Acknowledgments . . . . .	ii
(3.110)      Scientific Scope	
Introduction . . . . .	1
Discussion of the Tandem Mirror Concept . . . . .	2
Physics Objectives of the TMX . . . . .	6
Choice of TMX Parameters . . . . .	9
(3.120)      Engineering Description	
Magnet System . . . . .	15
Vacuum System . . . . .	17
Injection System . . . . .	20
Facility . . . . .	24
Control System . . . . .	26
Diagnostics System . . . . .	26
(3.130)      Total Estimated Cost . . . . .	26
(3.140)      Milestones . . . . .	28
(3.150)      Manpower Requirements . . . . .	28
References . . . . .	34
Appendix A.      Physics Considerations for the TMX . . . . .	35
Appendix B.      Tandem Mirror Reactor Scaling . . . . .	93
Appendix C.      TMX Engineering . . . . .	115
Appendix D.      Detailed Cost Breakdown . . . . .	189
Appendix E.      Environmental Impact Assessment . . . . .	199
Exhibit A.      2XIIB Plasma Confinement Experiments . . . . .	203
Exhibit B.      Theoretical Explanation of Present Mirror Experiments and Linear Stability of Larger Scaled Machines . . . . .	215

TMX MAJOR PROJECT PROPOSAL

(3.110) SCIENTIFIC SCOPE<sup>\*</sup>

Introduction

This document describes a new experimental facility that Lawrence Livermore Laboratory (LLL) proposes to construct in order to test the new Tandem Mirror approach to Q enhancement,<sup>1,2</sup> Q being the ratio of fusion power to neutral-beam injection power in a mirror reactor. This facility, to be called the Tandem Mirror Experiment (TMX), could be completed by October 1978 if the project is authorized in February 1977. By utilizing existing equipment and facilities in Bldg. 435 at LLL, the estimated cost is \$11 million, which is about half what the cost would be without these assets.

The Tandem Mirror concept is an outgrowth of the significant advances in mirror physics that have occurred during the past 18 months. Most importantly, dramatic progress has been achieved in predicting, understanding, and controlling high-frequency turbulence in the 2XIIB experiment.<sup>+</sup> We now believe that, as the size of mirror machines is increased, the principal cause of this turbulence — the drift-cyclotron loss-cone mode (DCLC) — will diminish to insignificance, and leakage of plasma out the machines will be governed by "classical" Coulomb scattering. Thus encouraged, we have given renewed attention to means of reducing the classical end losses and thereby enhancing Q.

These developments are thoroughly summarized in the recent report of the Open Systems Technical Review Panel.<sup>3</sup> This report includes an assessment of the Q-enhancement methods discussed with the Panel during its deliberations at LLL, May 10-14, 1976. The report strongly recommends that Q-enhancement be made a goal of the Mirror Program, as did the reports of both the Senior Review Panel<sup>4</sup> and the Fusion Power Coordinating Committee.<sup>5</sup>

---

<sup>\*</sup>Numbers displayed thus (3.110 to 3.150) refer to subsections of Section 3.100 of the *Procedures Governing the Initiation and Fabrication of Major Projects within the Controlled Thermonuclear Research Program* issued by the U.S.A.E.C. Division of Controlled Thermonuclear Research, February 23, 1973 (reissued as ERDA-5, February 1975).

<sup>†</sup>Recent papers titled "The 2XIIB Plasma Confinement Experiments" and "Theoretical Explanation of Present Mirror Experiments and Linear Stability of Larger Scaled Machines," were presented at the IAEA 6th International Conference on Plasma Physics and Controlled Nuclear Fusion Research in Bertchesgaden, Federal Republic of Germany, October 1976. Copies of these papers are included in this proposal as Exhibits A and B.

Although the Tandem Mirror geometry was first published by Kelley in 1967,<sup>6</sup> the full importance of the Tandem Mirror approach to Q enhancement has emerged since the above reviews were completed. Nevertheless, because the idea draws heavily on well-known mirror physics, we have been able to make a rapid theoretical evaluation. Also, the Tandem Mirror idea was concurrently developed by G. Dimov *et al.*<sup>1</sup> at Novosibirsk, and it has been evaluated independently in the Soviet Union with nearly identical conclusions. By now, the concept has had considerable exposure before the plasma physics community, first at a Q-enhancement workshop sponsored by LLL, September 13-17, 1976; then at the IAEA meeting in Berchtesgaden, where Dimov presented it; and most recently at the San Francisco meeting of the APS Division of Plasma Physics. The concept appears to be sound in principle, and it offers interesting possibilities as a pure-fusion reactor at a Q of 5 or more.

#### Discussion of the Tandem Mirror Concept

The Tandem Mirror concept utilizes to advantage one of the features that has contributed to the low Q of mirror systems: the strong, positive, "ambipolar" potential that confines the electrons but ejects low-energy ions. Because the electrons have higher velocities than the ions, they scatter more rapidly; if it weren't for a net positive charge that develops to hold them back, the electrons would be more poorly confined by the magnetic mirrors than the ions. In other words, in a conventional mirror machine the magnetic field confines the ions, but the ions confine the electrons electrostatically. In this way, a positive potential barrier equal to several times the electron temperature develops between where the plasma is most dense and the end walls.

In the Tandem Mirror, the idea is to "plug" the ends of a solenoid electrostatically by means of ambipolar potential barriers created in two mirror machines, one at each end of the solenoid. Most of the fusion power is produced by thermal burning in the solenoid, which may actually ignite. Despite the fact that input power is required to sustain the plasma in the end cells, the overall Q can be high if the plasma volume in the solenoid greatly exceeds that in the end cells. A similar geometry was proposed by Kelley,<sup>6</sup> with the objective of eliminating deleterious effects of the ambipolar potential on mirror confinement of ions in the center cell. We propose to go one step further by creating a potential minimum that confines those ions.

The geometry of the Tandem Mirror is sketched in Fig. 1. High-energy neutral beams maintain dense mirror plasmas in the end cells. The ions lost from the central solenoid are replaced by injection of low-energy neutral beams, gas, or pellets, which are ionized and heated by the hot electrons. The electrons are in turn heated by the energetic ions in the plugs, possibly augmented by external power input such as electron cyclotron resonance heating (ECRH). Thus, the system is characterized by  $E_p \gg T_e > T_c$ , where  $E_p$  is the average ion energy of the plug,  $T_e$  is the electron temperature, which is the same in both plugs and solenoid, and  $T_c$  is the ion temperature in the central cell.

If the density in the plugs  $n_p$  is greater than that in the solenoid  $n_c$ , the requirement of quasi-neutrality establishes a potential difference  $\Phi_c$  between the two regions. For a Boltzmann distribution of electrons,  $\Phi_c$  is given by

$$\Phi_c = T_e \ln \left( \frac{n_p}{n_c} \right). \quad (1)$$

Central-cell ions with energies  $<\Phi_c$  are confined in this axial potential well for a time  $\tau_c$  required for them to diffuse upward in energy above the barrier height. For  $\Phi_c \gtrsim 2T_c$ ,  $\tau_c$  is given by Pastukhov<sup>7</sup> as

$$\tau_c = \tau_{ii} g(R) \left( \frac{\Phi_c}{T_c} \right) \exp \frac{\Phi_c}{T_c}, \quad (2)$$

where  $\tau_{ii}$  is the ion-ion collision time, and  $g(R) = \sqrt{\pi} (2R + 1) \ln(4R + 2)/4R$  is a slow function of the central-cell mirror ratio  $R = B(\text{mirror})/B(\text{solenoid})$ . Substituting Eq. (1) into Eq. (2) gives

$$\tau_c = \tau_{ii} g(R) \left( \frac{T_e}{T_c} \right) \ln \left( \frac{n_p}{n_c} \right) \left( \frac{n_p}{n_c} \right)^{T_e/T_c}. \quad (3)$$

Provided  $T_e \gtrsim T_c$ , a proper choice of injection flux of ions into the solenoid and the plugs (which are subject to conventional mirror confinement) will maintain an arbitrary density ratio  $n_p/n_c > 1$ , so that any enhancement of  $\tau_c$  over  $\tau_{ii}$  is feasible. The temperature inequality  $T_e \gtrsim T_c$  is important to minimize the density ratio required for adequate electrostatic confinement of central-cell ions. Thus, it is advantageous to use heating methods that preferentially heat electrons.

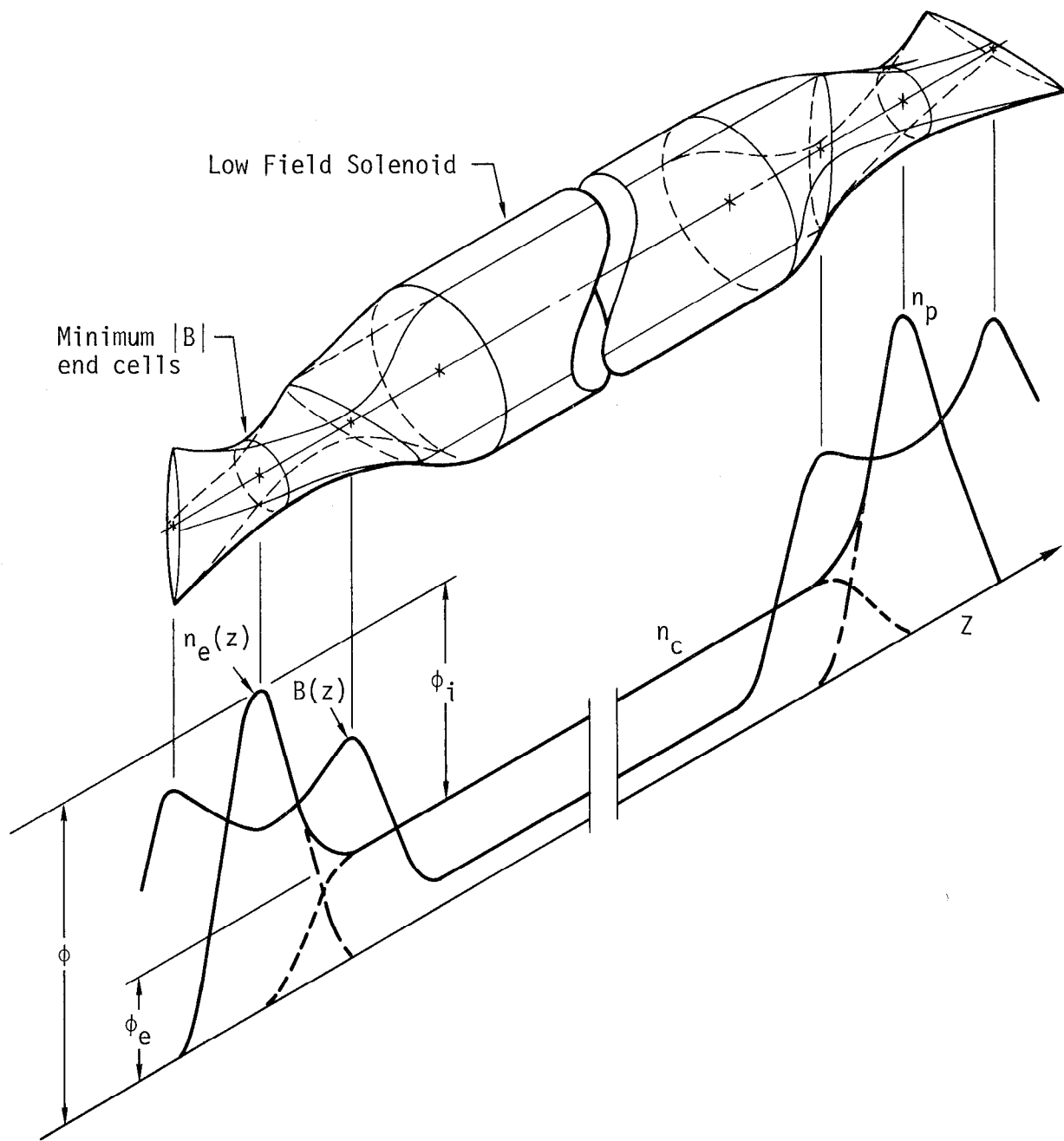


Fig. 1. Tandem mirrors with ambipolar barriers at the ends.

Electrons are confined by a net positive potential  $\Phi_e$  relative to ground; this potential adjusts to a value equalizing the electron losses with the combined ion loss from the plugs and the solenoid. Under most operating conditions,  $\Phi_e$  exceeds  $\Phi_c$  by a factor of 2 to 3.

Because of the enhancement of the confinement time over  $\tau_{ii}$  given by Eqs. (2) or (3), the Q of a Tandem Mirror reactor can considerably exceed unity. If  $P_c$  and  $P_p$  are defined as the externally supplied power per unit volume necessary to sustain the central cell and the plugs, respectively, and  $P_n$  is defined as the nuclear power per unit volume (all in the central cell), the Q of the combined system is

$$Q = \frac{P_p V_p}{P_c V_c + 2P_p V_p} , \quad (4)$$

where  $V_c$  is the volume of the central cell and  $V_p$  is that of a single plug. Under conditions of ignition,  $P_c$  is zero.

In general, Q can assume any value, even if the plug confinement is less than classical. Degraded confinement in the plugs results in increases in  $P_p$ ; to the extent that  $P_p$  is independent of the volumes, Q can be made up by increases in the ratio  $V_c/V_p$  (principally through the ratio of lengths). However, such a circumstance leads to larger net power  $P_n V_c$ , and there is a high priority for near-classical confinement in the plugs. Determining the conditions to obtain classical or nearly classical confinement in a mirror cell is, of course, a primary objective of the mainline Mirror Program as reflected in the current 2XIIB Experiment and the future MX Facility.

An important feature of the Tandem Mirror concept is the possibility of an economical reactor in units of modest power output. Example designs with  $Q = 5$  and electrical power output in the range of 500 to 1000 MW are given in Appendix B.

Perhaps equally important, from the viewpoint of reactor design and development, is the distinct separation of the end cells from the solenoidal region where most of the fusion reactions occur. Thus, the nuclear processes and heat recovery can be isolated from the more sophisticated plasma and magnet technology in the end cells. For example, in the end cells, one might choose to inject ordinary hydrogen beams in order to reduce neutron bombardment of the injector hardware and also to reduce magnet shielding requirements.

Moreover, developments to improve the end cells — to reduce the power input and simplify the design — could proceed quite independently of the main reactor components. As better end plugs are developed, they could be put into service without perturbing the design of the solenoidal magnet, heat exchanger, first wall, and the like. As for the reactor core itself, the straight solenoid is the ultimate in simple and potentially economical magnetic fusion ideas.

#### Physics Objectives of the TMX

The purpose of TMX is to provide a proof-of-principle evaluation of the Tandem Mirror concept as rapidly as possible. To accomplish this, there are three main physics objectives of the experiment:

- To demonstrate the establishment and maintenance of a potential well between two mirror plasmas.

The essence of the Tandem Mirror concept is the extension of the principle of electrostatic confinement to high density by the *in situ* generation of the required potential profile using dense, mirror-confined plasmas as plugs. A first objective of the experiment must be to establish this point by independently controlling the rates of injection of ions into the plugs and into the central cell for a time long compared to the heating time of the electrostatically confined ions.

- To develop a scalable magnetic geometry while keeping macroscopic stability at high beta.

A second essential requirement for a high Q in a tandem mirror system is that the volume of the central cell can be made sufficiently large compared to the volume of the mirror plugs while retaining collisionless guiding-center magnetohydrodynamic (MHD) stability. The best geometry that can be scaled in a literally straightforward manner appears to be two standard minimum- $|B|$  magnetic wells connected to a uniform solenoid. Such a geometry necessarily introduces regions of bad magnetic line curvature at the transitions between solenoid and plugs. The issues of

guiding-center MHD stability are the flute-interchange mode in the system as a whole and, at high  $\beta$  ( $> 0.5$ ), the finite- $\beta$  mirror mode in the plug and ballooning interchange in the solenoid. The TMX system is completely stable to the flute interchange mode, which is anchored by the high-pressure plasma in the minimum- $|B|$  plugs. The mirror and ballooning modes occur only at high  $\beta$ , and the TMX is designed to be stable to both at its nominal operating point and to be able to explore theoretical thresholds for instability. A reactor design would have several features that bear on MHD stability: solenoidal plasma pressure less than 1% of the plug pressure; a solenoid-to-plug volume ratio of several hundred; and mirror ratios modest in the plugs and large in the central cell. The TMX is designed to model a reactor and to explore these issues; therefore, it has pressure and volume ratios that are typical of a reactor and mirror ratios in the plugs and solenoid that are variable over a wide range.

- To investigate the microstability of the plug-solenoid combination in order to maximize the plug-density/injection-power ratio.

The theory of the DCLC mode developed in conjunction with 2XIIB experiments should apply to the mirror plugs of the tandem mirror system; this theory was used to predict the baseline performance of TMX. An important objective of TMX experiments is to verify quantitatively the applicability of this theory to the tandem mirror and to implement further stabilization techniques yet to be proved effective in 2XIIB. For example, with a modest increase in  $r_p/\rho_p$  to about 5 (by increasing the trapped beam current, if necessary by using some 20-keV modules), a small central core with zero or very small radial density gradient can be achieved. Then, large streaming currents are theoretically no longer required for DCLC stability in the central core,<sup>9</sup> and  $T_e$  at the core can increase to near classical values ( $T_e \lesssim E_p/15$ ). An additional feature of DCLC stabilization specifically characteristic of the tandem mirror configuration can be tested in TMX. According to theory, the partial penetration of warm Maxwellian ions from the central cell into

the plugs provides enough low-energy ions for a distribution stable to DCLC in a line-average sense, provided that the length of the plugs can be made sufficiently short (in units of the ion Larmor radius) that the instability will be unable to localize in the unstable region. As for other instability modes, in TMX and also in a tandem mirror reactor the plasma length  $L_p$  in the plug is sufficiently short that the negative-energy modes and the high-frequency convective loss-cone modes are not expected to play a role.

In addition to these primary physics objectives, there are a number of secondary questions that have important reactor implications; these can also be addressed in the TMX facility. Due to its Maxwellian ion distribution, the central cell is stable to velocity-space instabilities, but there might be enhanced radial transport due to pressure-driven drift waves or modes driven by the radial electric field. These processes can be investigated in the system; the central-cell lifetime of 100 ion-ion collision times should be adequate for this purpose. Crucial factors determining the size of a tandem mirror reactor are the fraction of fast alpha particles that can be contained (or eliminated) and the degree to which  $T_e > T_c$  can be maintained. Accumulated thermalized alpha particles will prevent steady-state operation unless they can be selectively transported radially. These issues involving alpha reaction products can be investigated in the TMX experiment by injecting a small percentage of alpha particles into the central cell using a 20-keV helium neutral beam. Loss rates of high-energy alpha particles due to nonadiabaticity and radial transport can then be determined, as well as the rate of accumulation of thermal alpha particles.

### Choice of TMX Parameters

In designing TMX, we adopt the viewpoint that the experiment should be able to meet the above physics objectives as soon as possible to permit a rapid experimental evaluation of the Tandem Mirror concept. To increase confidence in the design and to be able to react quickly to results of future 2XIIB operation, we draw where possible from the 2XIIB experience.<sup>8</sup> Thus, we have chosen neutral injection in the end plugs as the only proven method for obtaining plasmas at high temperatures and density in mirror machines.

The minimum-size neutral injection experiment to meet the goals of TMX is fairly well determined. The scale of the experiment is set by the end plugs; parameters of the central cell follow from those of the plugs. The minimum size of the plug plasma is determined mainly by the minimum focused beam dimension, and the minimum magnet size is set mainly by beam access. Given the plasma length, the minimum magnetic field strength in the plug is set by adiabaticity requirements. Since these same considerations figured prominently as 2XIIB and its neutral-beam system evolved, it is no surprise that we are led to TMX plugs that are very similar to 2XIIB. Calculations of the required beam currents to sustain the plasma, the effects of background gas load, the attainable  $\beta$ , the spatial extent of the plasma, the low energy flux required for stability, and the target plasma and injection currents required for startup all follow from 2XIIB operation under reproducible and, to a considerable extent, theoretically understood conditions.<sup>9</sup> By so doing, we have a performance baseline for the plugs and can focus on the physics of the central cell and the central cell-plug combination that is unique to the tandem mirror configuration.

The neutral-beam system includes the sustaining beams necessary to maintain the plugs in steady state for an interesting period of time and also additional pulsed beams needed during the startup phase. Based on 2XIIB experience as discussed in Appendix A6, the additional startup requirements can be met by beams on hand; we have available up to seventeen 50-A, 20-keV modules from the 2XIIB and Baseball facilities. To meet the sustaining beam requirements, we have focused on either 20-keV or 40-keV beams of the LLL/LBL type that require little or no further development. In the present case, we find little cost difference between 20 and 40 keV, or between hydrogen and deuterium; hence, we opt for 40-keV deuterium beams that turn out to yield a somewhat higher electron temperature and improved confinement. For the pulse length we choose

25 ms, which will turn out to equal the ion lifetime in the center cell for the nominal operating mode, and is therefore the minimum beam duration required to observe ion confinement in the central cell. This choice is made for reasons of cost and schedule. If the initial experiments in TMX go well, the later addition of a long-pulse or quasi-dc sustaining beam system would be highly desirable. This step would entail additional costs and is beyond the scope of the present proposal. Finally, the sustaining beam current must be sufficient to obtain high  $\beta$  in the plugs. One of the important objectives of TMX is to study the  $\beta$  limits due to the mirror mode in the plugs at mirror ratios less than 2.

From the above considerations, we obtain the following plug parameters included in Table 1, which lists nominal operating parameters for TMX:

- Plasma radius  $r_p = 7$  cm and length  $L_p = 40$  cm — same as 2XIIB, determined mainly by the neutral-beam "footprint" (beam size at the position of the plasma).
- Average energy  $E_p = 26$  keV — corresponds to 40-keV injection, taking account of one-half and one-third energy components.
- Midplane magnetic field  $B_p = 10$  kG — determined from adiabaticity scaling from 2XIIB (Appendix A4); corresponds to  $r_p \approx 2\varrho_p$ .
- Beta  $\beta_p = 0.5$  — conservative value from 2XIIB stream-stabilized operation; high beta is needed to get the high density in the plugs that is required in reactor designs.
- Density  $n_p = 5 \times 10^{13} \text{ cm}^{-3}$  — corresponds to  $\beta_p = 0.5$  and  $E_p = 26$  keV.
- Mirror-to-mirror length = 90 cm — determined mainly by required neutral-beam access.
- Sustaining beam pulse length = 25 ms — minimum time to observe ion confinement in the central cell.
- Mirror ratio in the plug  $R_p = 2$  — same as in 2XIIB; however, a much smaller value would be desirable in a reactor, and the TMX field design allows a variation down to  $R_p = 1.3$ .

Having chosen plug parameters, the scale of the central cell follows.

A necessary requirement is MHD stability. As is shown in Appendix A2, because the energy density in the plugs is much larger than in the solenoid, interchange stability follows if the plugs themselves are stable. The TMX design concept of a straight solenoid connecting two minimum- $|B|$  plugs is a natural solution to this requirement. Providing room for the transition from the minimum- $|B|$

geometry to the circular geometry of the solenoid was the main consideration determining the length of the central cell,  $L_c$ , in Table 1. Also, a longer device would not conveniently fit in the existing building. As noted above, determining the upper limits on  $\beta_c$  due to ballooning in the central cell is an important objective of TMX. Beta in the central cell is variable both by varying the density and the field strength. The nominal values of  $B_c$  and density in Table 1 correspond to  $\beta_c = 0.5$ ; the ratio  $B_p/B_c = 20$  in turn fixes the ratio of plasma cross sections in the two regions. A subsidiary requirement to be in the appropriate collisionless MHD regime in order to test ballooning in the central cell is that the ion mean-free-path exceed  $L_c$ . The nominal operating parameters of Table 1 marginally meet this requirement.

It remains to determine the sustaining beam current and hence the number of 40-keV beam modules required per plug as discussed in Appendix A6. This requires knowing  $T_e$  and, because of the electron coupling between the plugs and the central cell, it in fact requires determining the complete operating mode of the system. The necessary formulas, from which the remaining parameters of Table 1 are calculated, are fully developed in Appendix A1 and will not be repeated here. (In deriving the parameters of Table 1, two constants defined in Appendix A1 are taken as  $\lambda = 1.3$  and  $\eta = 8$ .)

As compared to 2XIIB, the main new points in calculating TMX parameters, as developed in Appendix A1, are: (1) the formulas for central-cell confinement, and (2) the relation determining the electron temperature in TMX as given by Eq. (A12). This latter relationship concerns stabilization of the end plugs. The plugs in TMX are designed to function exactly as does the 2XIIB plasma, except that it is the axial loss from the central cell that supplies the flux of low-energy plasma proven successful in reducing fluctuations in 2XIIB. The parameters of the central cell follow from this requirement, once plug parameters are chosen. Ions will be supplied to the central cell by ionization of gas fed into the central cell at a controlled rate, much as in the gas-feed experiments in 2XIIB. The gas will be introduced in the transition region between the plug and the solenoid (see Appendix A5). The ion temperatures of the plugs and central cell are coupled through the electron temperature  $T_e$ , which is determined by the loss current required for stabilization. Stabilization of the plugs by the loss current from the central cell should be much more efficient than methods heretofore employed on 2XIIB. This is because all of the low-energy plasma created by feeding gas into the central cell must pass through the end

Table 1. Nominal deuterium operation parameters for the TMX experiment with gas feed alone.

Parameter	Value
Electron	
Temperature, $T_e$	0.20 keV
Confining potential, $\Phi_e$	1.1 keV
Plug	
Density (assumed uniform over $V_p$ ), $n_p$	$5 \times 10^{13} \text{ cm}^{-3}$
Average energy, $E_p$	26 keV
Plasma length, $L_p$	40 cm
Radius of plasma half-maximum, $r_p$	7 cm
Plasma volume ( $\equiv \pi r_p^2 L_p$ ), $V_p$	$6.3 \text{ l}^3$
Central magnetic field, $B_p$	10 kG
Mirror ratio (axial), $R_p$	2
Mirror-to-mirror length	90 cm
Beta, $\beta_p$	0.5
Ion Larmor radius, $\rho_p$	3.3 cm
Ion current (trapped, per plug), <sup>a</sup> $j_p V_p q$	8 A
Confinement product, $(nT)_p$	$3 \times 10^{11} \text{ cm}^{-3} \cdot \text{s}$
Central cell	
Density (assumed uniform over $V_c$ ), $n_c$	$1.2 \times 10^{13} \text{ cm}^{-3}$
Ion temperature, $T_c$	0.080 keV
Confining ion potential, $\Phi_c$	0.29 keV
Length, $L_c$	5.5 m
Radius, $r_c$	31 cm
Volume ( $\equiv \pi r_c^2 L_c$ ), $V_c$	$1690 \text{ l}^3$
Magnetic field, $B_c$	0.5 kG
Mirror ratio, $R_c$ ; R	40 (to mirrors); 20 (to plug midplane)
Beta (electron + ion), $\beta_c$	0.54
Ion Larmor radius, $\rho_c$	3.7 cm
Ion current, $q j_c V_c$	125 A
Confinement product, $(nT)_c$	$3.1 \times 10^{11} \text{ cm}^{-3} \cdot \text{s}$

<sup>a</sup>Taking account of trapping efficiency and other factors, the necessary 40-keV beam current to provide 8 A of trapped current is 80 A (see Appendix A6).

plugs in order to escape along magnetic lines; in 2XIIB, a large portion of the low-energy plasma does not penetrate the plugs and only leads to unnecessary electron cooling. Thus, even though the TMX plugs are designed after 2XIIB, we calculate and anticipate higher electron temperatures. Again, we refer to Appendix A1 for details.

A different TMX option, listed in Table 1A, is to introduce neutral injection in the central cell in addition to the gas feed. Using only a gas feed to supply cold ions to the central cell results in  $T_c < T_e$ ; this is the case corresponding to the nominal operating parameters of Table 1. A different regime with  $T_c > T_e$  can be explored by supplying a portion of the central-cell current as energetic neutrals that heat the plasma. In a reactor, this mode of operation limits Q to less than 3, but it would be well suited for a "breakeven" experiment to achieve  $Q = 1$  with moderate beam voltages. Again using formulas developed in Appendix A1, Table 1A lists parameters for an experiment in TMX using two 20-keV injectors in the central cell.

Finally, we note that there are two mechanisms discussed in Appendix A3 that might lead to an improved stability of the TMX plugs beyond that of the straightforward 2XIIB scaling. In the tandem mirror configuration, the confined ions from the central cell partly penetrate the plug, and in fact they overlap about one-half of the volume occupied by the plug ions. Preliminary calculations indicate that this may permit a substantial reduction in the required stabilizing flux (at least in a small device like TMX), but the exact magnitude and the parametric dependence of this reduction are not yet available.

A second mechanism for improved stability of the TMX end plugs is the controlled injection of the plugs so as to create an inner core having a "flat-topped" radial density profile. Because the DCLC mode is driven by the density gradient, regions of small or vanishing gradient require little or no stabilizing flux. Experiments of this type are scheduled for 2XIIB and, depending on results, they are also an option in TMX.

Table 1A. Parameters with gas feed plus 20-keV  
neutral beams at 60 A (incident).<sup>a</sup>

Parameter	Value
Electron	
Temperature, $T_e$	0.29 keV
Confining potential, $\Phi_e$	1.5 keV
Plug	
Ion current (trapped, per plug), $j_p V_p q$	5 A
Confinement product, $(nT)_p$	$4.9 \times 10^{11} \text{ cm}^{-3} \cdot \text{s}$
Central cell	
Electron density, $n_c$	$1.9 \times 10^{13} \text{ cm}^{-3}$
Maxwellian density, $n_w$	$1.4 \times 10^{13} \text{ cm}^{-3}$
Energetic tail density (from slowing-down beam), $n_H$	$0.5 \times 10^{13} \text{ cm}^{-3}$
Maxwellian temperature, $T_w$	0.28 keV
Total average energy (including energetic tail), $\bar{E}_c$	2.0 keV
Confining ion potential, $\Phi_c$	0.28 keV
Maxwellian confinement product, $n_w^2 / j_{\text{gas}}$	$6.3 \times 10^{10} \text{ cm}^{-3} \cdot \text{s}$
Overall confinement product, $n_c^2 / j_c$	$1.25 \times 10^{11} \text{ cm}^{-3} \cdot \text{s}$
Radius, $r_c$	16 cm
Magnetic field, $B_c$	1.9 kG
Mirror ratio, $R_c; R$	10.5 (to mirrors); 5.3 (to plug midplane)
Beta, $\beta_c$	0.54
Maxwellian Larmor radius, $\rho_w$	1.7 cm
20-keV Larmor radius, $\rho_{20 \text{ keV}}$	15 cm
Total ion current, $q j_c V_c$	210 A

<sup>a</sup>36 A attenuated in plasma. Plug parameters are the same as in Table 1 except as indicated. The term "Maxwellian" refers to the gas feed ion component; "energetic tail" refers to the beam ion component.

### (3.120) TMX ENGINEERING DESCRIPTION

The principal subsystems of the TMX Major Project are described in the following sections; additional detail is provided in Appendix C.

#### Magnet System

The tandem mirror configuration consists of three connected mirror cells. Identical high-field mirror cells at the two ends are joined by a large, low-field solenoidal cell as shown in Fig. 2. This configuration is provided by a set of coils whose geometry, although fixed, can produce a range of flux shapes by adjustment of the currents in the various coils. Thus, the magnetic field shape becomes an adjustable experimental parameter and, in particular, mirror ratios and conditions for MHD stability can be varied. For the parameter range of primary interest, the pressure-weighted  $\int P_{\parallel} \frac{d\ell}{B}$  stability condition can be realized for the system as a whole.

The winding elements of the end magnets, or plugs, are a Baseball-type coil and a pair of "C" coils nested within the Baseball winding. By changing the ratio of currents in the two types of coils, it is possible to vary the axial mirror ratio between 3.5 and 1.3 and the radial well depth between 0.98 and 1.04. With available power supplies, the central field of the plug may be held constant at 1.0 T over a portion of this range, while the extremes can be realized for a central field above 0.55 T.

The center-cell windings are an existing set of solenoidal coils. A set of segmented Ioffe bars extending the length of the solenoidal section helps in making the transition between the central cell and the plugs.

Force-structure requirements for this magnet set are not severe, and an estimate is included in Appendix C1, as well as details of the magnet design.

In considering the use of superconductor versus copper for these magnets, we have decided in favor of a water-cooled copper conductor. At LLL, we have both the cryogenic capacity to cool a superconducting magnet set of this size and also sufficient power available to energize a copper magnet set for several seconds. The additional cost of superconductor over copper and the added operational complexity of a cryogenic-type experiment determined the choice.

All of the magnet coils are to be wound with hollow, square, copper conductor and are to be operated at near room temperature in a pulsed mode, with an "on" time of about 3 s. Plug magnets will be wound on forms suitable for vacuum impregnation after winding.

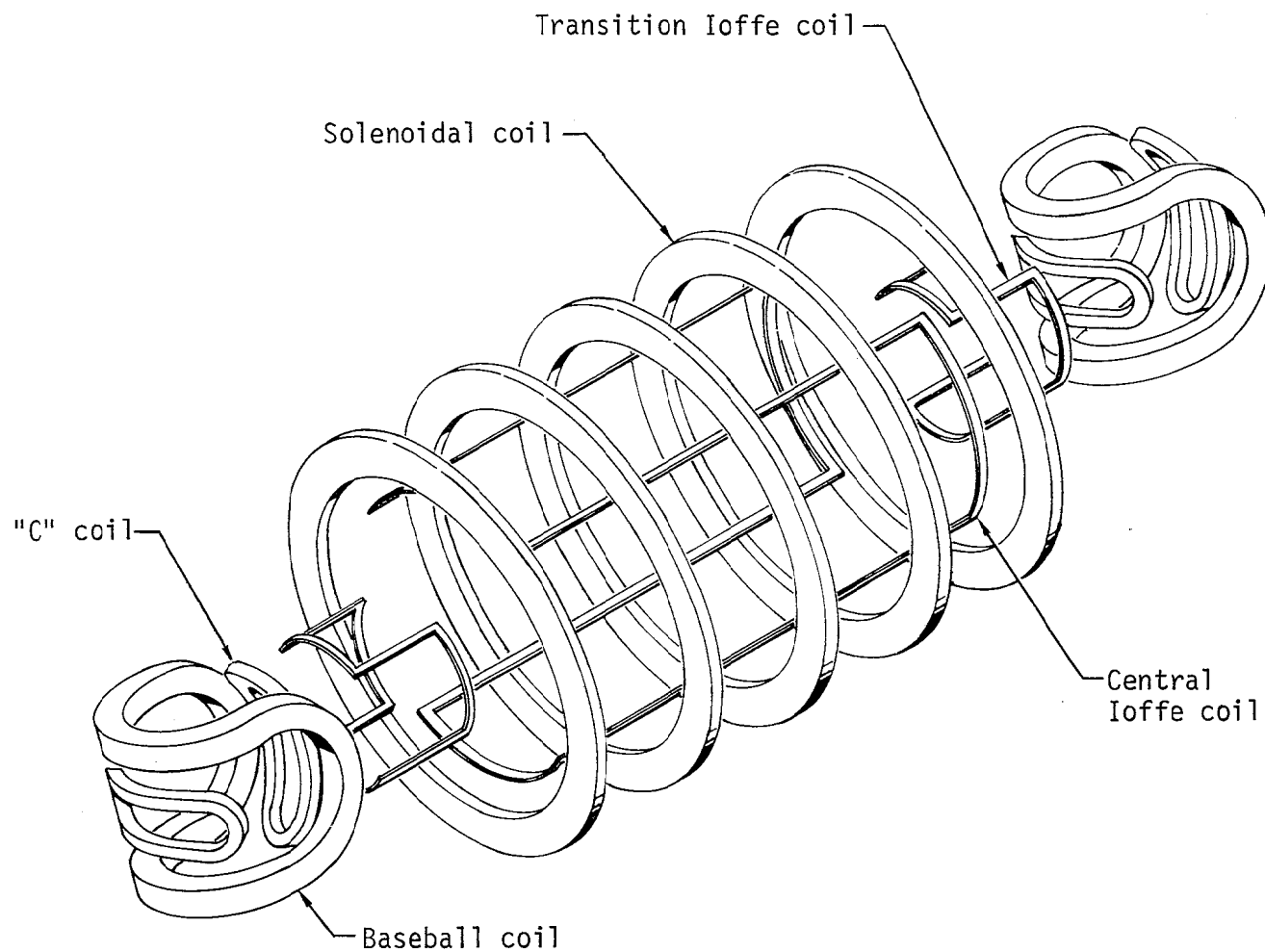


Fig. 2. TMX coil set.

We calculate the peak power for the coils to be about 20 MW and the total stored energy to be 40 MJ. The coils will be cooled by continuously circulating low-conductivity water with a cooling time between each pulse of 2 min. With this duty cycle, the existing 6.5 MW of continuous cooling tower capacity is more than adequate. The plug magnets are designed to match the coils to the available power supplies. The average current density is less than  $2000 \text{ A/cm}^2$ , resulting in a temperature rise of  $60^\circ\text{C}$  in 3 s.

Twenty-five 300-kW dc power supplies are available at LLL and capable of being pulsed at several times rated output. Substation capacity is adequate to power these supplies. Thus, about 20 MW of pulsed dc power is available to drive the magnet set. Further details of the magnet power supply are contained in Appendix C1.

The TMX magnet parameters are summarized in Table 2.

#### Vacuum System

As in all mirror confinement experiments sustained by neutral beam injection, the vacuum requirements are primarily determined by a balance between the rate of charge-exchange loss of trapped ions and the rate of trapping of beam particles.

A schematic of the TMX vacuum system is shown in Fig. 3.

For the plug sections of the system, the vacuum requirement is based on a model in which the plasma core is shielded from impinging gas by a boundary layer of warm plasma. This boundary layer is maintained by 1) particle input from gas and 2) energy input from trapped hot ions through turbulence. This model, discussed in Appendix A9, is derived from an analysis of the vacuum in 2XIIB. From these considerations, we estimate that the plasma can tolerate a gas load on its surface about equal to the hot ion current trapped in the core, without either eroding the plasma surface or seriously degrading the hot-ion temperature. The trapped current per plug for the four 40-keV sustaining beams operating at full rated output is estimated to be 19 A; hence, a gas flow to the surface of this order of magnitude is tolerable.

Both the ambient gas density external to the plasma and molecular streaming from the beam neutralizers contribute to the gas impinging on the plasma. Gas diffusing into the plasma region from the source tanks, the beam dump regions (used to dispose of untrapped beam), and the plasma end dumps all contribute to the ambient gas pressure. These contributions to the gas load are estimated in Appendix C2.

Table 2. TMX magnet parameters.

Parameter	Value
Magnet Type	
Plug (2)	Baseball plus "C" coil pair
Transition	Ioffe bars
Central cell	Solenoids
Distance between inner mirrors	5.5 m
Distance between plug mirrors	0.9 m
Plug central field	1.0 T
Center-cell field <sup>a</sup>	0.05 to 0.3 T
Plug mirror ratio, axial <sup>a</sup>	1.3 to 3.5
Plug mirror ratio, radial <sup>a</sup> (at 10 cm)	0.98 to 1.04
Maximum plasma radius	
In plug	0.2 m
In center-cell	0.7 m
Total stored energy	40 MJ

<sup>a</sup>For some of this range, a field of 1.0 T in the center of the plug can be achieved. The extremes of this range can be attained at somewhat lower plug fields. See Appendix C1.

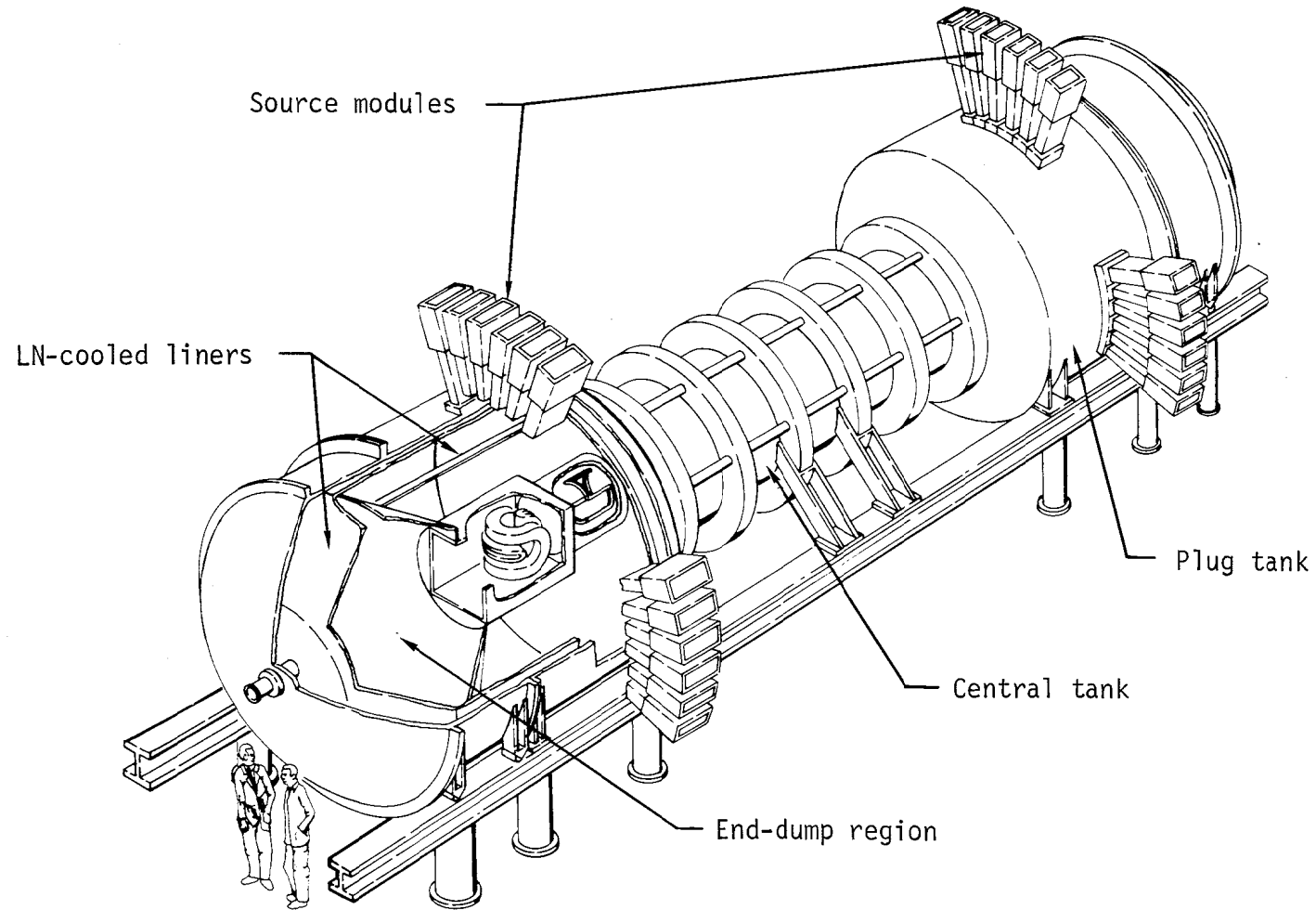


Fig. 3. Schematic of TMX vacuum system.

The other major contribution to the gas load is from the reflux of charge-exchange particles from the walls of the containment region. In Appendix C2, this contribution is conservatively estimated on the basis of unity refluxing, a value consistent with the 2XIIB analysis in Appendix A9. With the smoother metallic walls planned for the TMX system, the reflux coefficient may be less than unity.

The various contributions to the gas load on the plug plasma are summed in Appendix C2 to yield a value comparable to the trapped ion current estimated above. On the basis of these conservative estimates, we expect the plug vacuum to be satisfactory.

The diffuse flow of gas is minimized through the use of large-area active pumping formed by deposition of titanium on liquid-nitrogen-cooled surfaces prior to each containment run. Source gas is differentially pumped in regions separated by minimum-conductance baffles. Reflux of energetic particles is minimized by burial in titanium-coated, water-cooled surfaces located on the magnet walls and in the beam and plasma dump regions.

Table 3 lists the various pumping areas and volumes.

The central cell contains no cooled liners. The gas feed is adjusted to give the required central plasma density, and gas refluxing from the walls is pumped both by the plasma (ultimately exiting through the plugs to the plasma dump region) and by a titanium coating on the walls.

The titanium getter power supplies now in use on 2XIIB will be used for the TMX system.

#### Injection System

The TMX injection system includes two 2XIIB-type plasma generators to form a plasma column for buildup and 24 neutral-beam source modules to generate and sustain the heated plasma. One plasma generator is mounted on each end-dump tank and is located on flux lines that map to the center of each plug magnet.

The neutral-beam modules are mounted 12 to each plug tank, as shown in Fig. 4. This orientation allows for disposal of untrapped beam and optimum differential pumping between source regions and plug magnets. Each group of 6 sources contains 4 modules rated at 20 keV, 50 A and 2 modules rated at 40 keV, 40 A. Both kinds of modules are of the type developed at LBL and in current use on 2XIIB. Specifications for the injector modules are listed in Table 4. Neutral-beam injectors will be individually shielded from the fringe

Table 3. Areas and volume of regions in TMX.

Region	Volume (m <sup>3</sup> )	Pump area (m <sup>2</sup> )
Plug tank		
Plug-coil region	3	10
(each of 2)		
End dump	18	40
(each of 2)		
Injector regions:		
First (each of 4)	5	23
Second (each of 4)	6	20
Dump (each of 4)	9	20
Gas box (each of 2)	<1	0
Plug tank total:	122	352
Central	<u>10</u>	<u>25</u>
Total for machine:	132	377

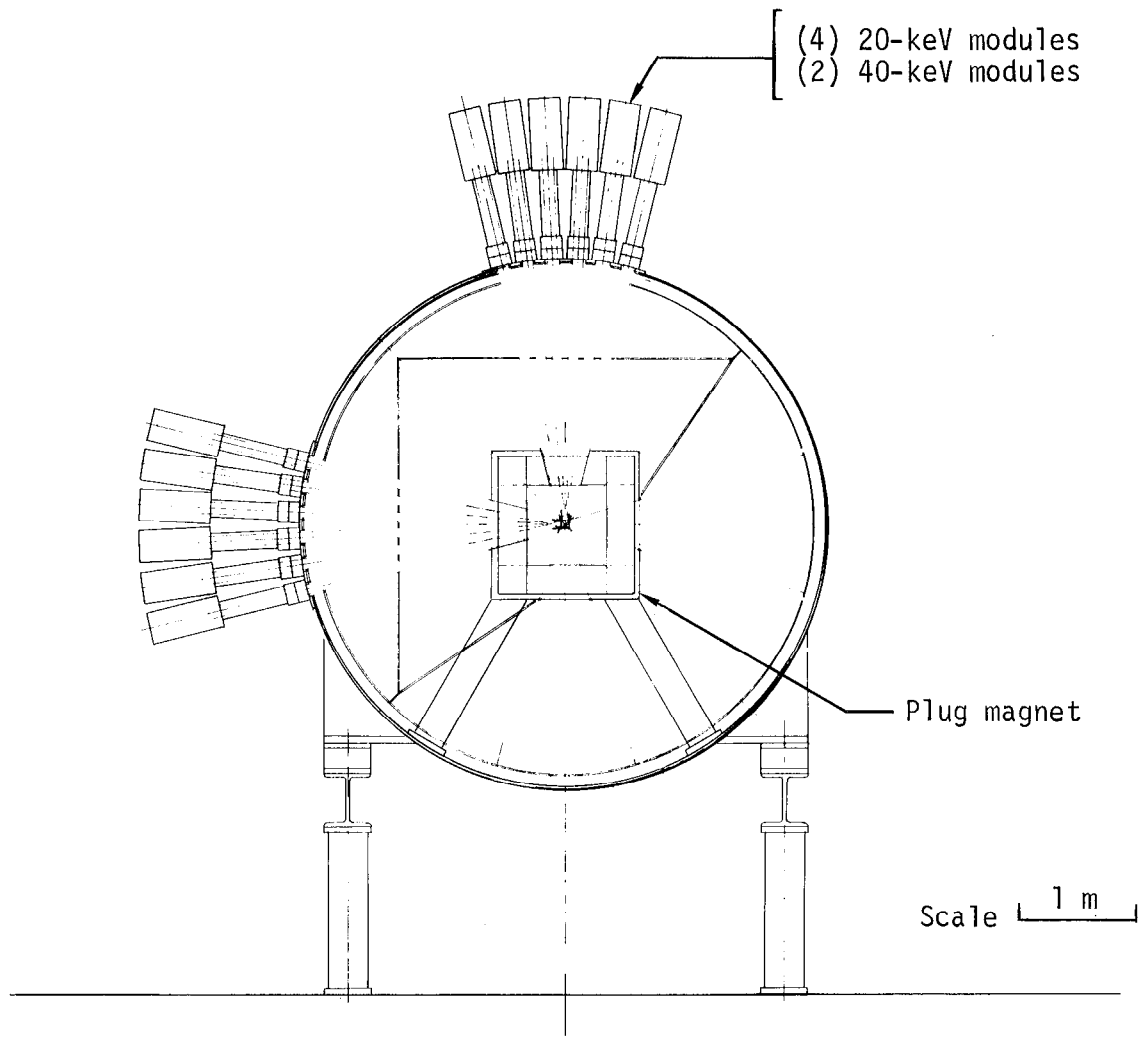


Fig. 4. Schematic of plug injection system.

Table 4. Neutral injector module specifications.

Parameter	20-keV module	40-keV module
Max. neutral-beam energy	20 keV	40 keV
Avg. neutral-beam energy	~15 keV	~29 keV
Power supply drain	80 A	65 A
Extractor current density	0.5 A/cm <sup>2</sup>	0.4 A/cm <sup>2</sup>
Extractor dimensions	7 cm x 35 cm	7 cm x 35 cm
Overall dimensions	20 cm x 58 cm	20 cm x 58 cm
Pulse length	25 ms	25 ms
D <sub>2</sub> gas inlet	30 Torr·l/s	30 Torr·l/s
Beam divergence	±2° W x ±0.5° H	±2° W x ±0.5° H
Beam at plasma (rated value)	50-A neutrals in 10 cm high x 33 cm wide.	40-A neutrals in 10 cm high x 33 cm wide.

magnetic field and individually mounted to the plug vessel through an isolation valve to facilitate maintenance.

The power supplies for the injector system will consist partly of supplies now in use on 2XIIIB, those under construction as part of the Baseball Multi-Beam major project, and some new units to be built. Power supplies will have enough energy storage to power all modules for 25 ms. Details of the power supply complement as well as a more complete description of the injector system are given in Appendix C3.

#### Facility

The TMX experiment will be housed in existing buildings at LLL. The confinement apparatus will occupy the west half of Bldg. 435 in an area previously used by the Baseball II-T experiment. The vacuum vessel will be set in a pit in order to provide full access and overhead clearance and also to minimize radiation shielding. The machine will be flanked by tiers for supporting neutral-beam and streaming-gun power supplies. Magnet power supplies are located in an adjacent building, with cabling to the magnets through existing tunnels. An existing 17-ton bridge crane services the central bay area. All systems will be controlled from racks along the east side of the central bay. An artist's conception of the facility is shown in Fig. 5.

A wall of concrete blocks surrounds the pit area to provide shielding against neutrons. A thickness of 2 ft of concrete is calculated to reduce the neutron flux well below the acceptable level (see Appendix C5).

Plasma diagnostics will utilize much of the existing 2XIIIB equipment located on the second level of the side bay of Bldg. 435. Any necessary expansion will be adjacent to the 2XIIIB diagnostic room. This will allow an efficient use of a central data acquisition facility for either the 2XII area or the TMX area.

Other ancillary equipment will be located adjacent to Bldg. 435, and work areas will be located in outlying rooms at ground level. A total of approximately 21,000 ft<sup>2</sup> of floor space (including tier areas) will be utilized by the experiment.

Appendix C4 describes the facility and the required modifications.

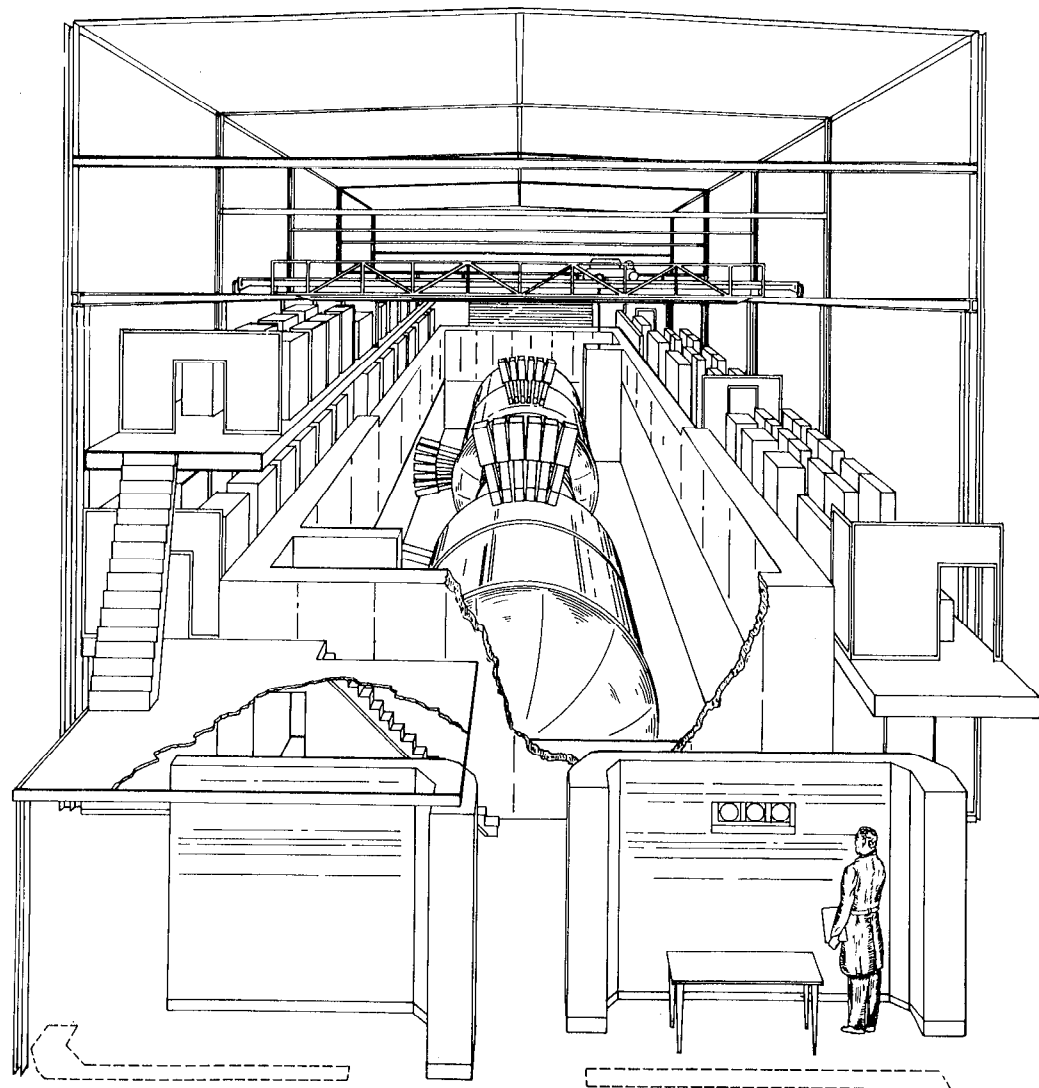


Fig. 5. Conceptual drawing of the TMX facility.

#### Control System

The control system for TMX will be basically a manual system, except that the existing computerized controls for getters and 12 neutral beams on 2XIIB will be utilized.

Vacuum system control will be based on a status map and will provide for easy cycling of the system with interlocks to prevent undesirable operations.

Magnet power supplies will be manually pre-set, and voltages and currents in each coil will be monitored.

Neutral-beam control will be partly computerized, with 12 beams controlled by the existing 2XIIB computer. The other 12 beams will be manually controlled but will include computer-compatible interfacing for possible future upgrading.

Streaming-plasma gun controls will also be manual with computer-compatible interfacing.

The entire system will be safety-interlocked and designed "fail-safe" to provide an environment free of all controllable hazards.

A further description of the control system is included in Appendix C6.

#### Diagnostics System

The diagnostics system will be based on the 2XIIB system, augmented by equipment available from Baseball II-T and by equipment acquired in the interim. Raw data storage and archiving, as well as on-line data processing, will be accomplished by a minicomputer. Data processing and readout between each injection period will enable the experimenter to evaluate the data and direct the course of the experiment.

Additional instrumentation beyond the existing system will be needed because there are three regions of interest on TMX. Also, some new measurements will be required for TMX (see Appendix A8 for a discussion of Diagnostics), including measurements of space potential and low-energy ion spectra; the latter will necessitate incorporation of new instrumentation. Further engineering aspects of the diagnostics requirements are discussed in Appendix C7.

#### (3.130) TOTAL ESTIMATED COST

A summary of TMX costs is given in Table 5. A detailed breakdown of the costs is presented in Appendix D. The total estimated cost by subsystem and

Table 5. TMX cost summary by subsystem (thousands of \$).

	Operating		Equipment		Total
	FY 77	FY 78	FY 77	FY 78	cost
Magnet system	295	950	0	50	1,295
Vacuum system	313	1271	0	0	1,584
Injection system	157	1631	432	149	2,369
Facility	283	773	13	105	1,174
Controls	113	227	75	80	495
Diagnostics	100	500	0	400	1,000
System design and integration	365	617	0	0	982
Administration	127	539	0	0	666
Subtotals:	1753	6508	520	784	9,565
Contingency:		1239		196	1,435
Totals:	1753	7747	520	980	11,000

fiscal year is given in Table 6. The total estimated cost by budget activity and by fiscal year is given in Table 7.

(3.140) MILESTONES

Project milestones are listed in Table 8.

(3.150) MANPOWER REQUIREMENTS

Manpower requirements are listed in Table 9.

Table 6. (3.131) Total cost by subsystem by fiscal year.  
(thousands of \$)

	FY 77	FY 78	Total
<b>Magnet</b>			
Labor <sup>a</sup>	130	366	496
Materials	87	365	452
Overhead	<u>78</u>	<u>219</u>	<u>297</u>
Subtotal:	295	950	1,245
Equipment	-	50	50
Construction	<u>-</u>	<u>-</u>	<u>-</u>
Total:	295	1,000	1,295
<b>Vacuum</b>			
Labor <sup>a</sup>	115	174	289
Materials	130	993	1,123
Overhead	<u>68</u>	<u>104</u>	<u>172</u>
Subtotal:	313	1,271	1,584
Equipment	-	-	-
Construction	<u>-</u>	<u>-</u>	<u>-</u>
Total:	313	1,271	1,584
<b>Injector</b>			
Labor <sup>a</sup>	48	388	436
Materials	81	1,011	1,092
Overhead	<u>28</u>	<u>232</u>	<u>260</u>
Subtotal:	157	1,631	1,788
Equipment	432	149	581
Construction	<u>-</u>	<u>-</u>	<u>-</u>
Total:	589	1,780	2,369
<b>Facility</b>			
Labor <sup>a</sup>	167	246	413
Materials	18	380	398
Overhead	<u>98</u>	<u>147</u>	<u>245</u>
Subtotal:	283	773	1,056
Equipment	13	105	118
Construction	<u>-</u>	<u>-</u>	<u>-</u>
Total:	296	878	1,174

Table 6 continued

	FY 77	FY 78	Total
<b>Controls</b>			
Labor <sup>a</sup>	50	83	133
Materials	33	95	128
Overhead	<u>30</u>	<u>49</u>	<u>79</u>
Subtotal:	113	227	340
Equipment	75	80	155
Construction	<u>-</u>	<u>-</u>	<u>-</u>
Total:	188	307	495
<b>Diagnostics</b>			
Labor <sup>a</sup>	58	250	308
Materials	8	100	108
Overhead	<u>34</u>	<u>150</u>	<u>184</u>
Subtotal:	100	500	600
Equipment	<u>-</u>	400	400
Construction	<u>-</u>	<u>-</u>	<u>-</u>
Total:	100	900	1,000
<b>System design and integration</b>			
Labor <sup>a</sup>	228	386	614
Materials	<u>-</u>	<u>-</u>	<u>-</u>
Overhead	<u>137</u>	<u>231</u>	<u>368</u>
Subtotal:	365	617	982
Equipment	<u>-</u>	<u>-</u>	<u>-</u>
Construction	<u>-</u>	<u>-</u>	<u>-</u>
Total:	365	617	982
<b>Administration</b>			
Labor <sup>a</sup>	62	171	233
Materials	29	265	294
Overhead	<u>36</u>	<u>103</u>	<u>139</u>
Subtotal:	127	539	666
Equipment	<u>-</u>	<u>-</u>	<u>-</u>
Construction	<u>-</u>	<u>-</u>	<u>-</u>
Total:	127	539	666

Table 6 continued

	FY 77	FY 78	Total
Operating contingency	-	1,239	1,239
Equipment contingency	-	196	196
<b>Totals:</b>			
Operating (MDF)	1,753	7,747	9,500
Equipment	520	980	1,500
Construction	—	—	—
<b>Total:</b>	<b>2,273</b>	<b>8,727</b>	<b>11,000</b>

<sup>a</sup> Labor includes those charges defined as "support burden" in normal LLL accounting procedures.

Table 7. (3.132) Total estimated costs  
by budget activity and by fiscal year (thousands of \$).

	FY 77	FY 78	Total
<b>Operating</b>			
Confinement systems	-	-	-
Development and technology	-	-	-
Applied plasma physics	-	-	-
Reactor projects	-	-	-
<b>Major device fabrication</b>			
Labor <sup>a</sup>	858	2,064	2,922
Materials	386	3,209	3,595
Overhead	509	1,235	1,744
Contingency	<u>-</u>	<u>1,239</u>	<u>1,239</u>
Operating subtotal:	1,753	7,747	9,500
<b>Capital equipment</b>			
Equipment	520	784	1,304
Contingency	<u>-</u>	<u>196</u>	<u>196</u>
Equipment subtotal:	520	980	1,500
<b>Construction</b>			
Total:	2,273	8,727	11,000

<sup>a</sup> Labor includes those charges defined as "support burden" in normal LLL accounting procedures.

Table 8. (3.140) TMX construction milestones.

1. Letter of intent	September	1976
2. Complete preliminary design	December	1976
3. Submit proposal	January	1977
4. DMFE decision point	February	1977
5. Initiate site preparation	March	1977
6. Start winding magnets	June	1977
7. Let contract for vacuum tanks	August	1977
8. Complete pit in Bldg. 435	September	1977
9. Install power supply tiers	November	1977
10. Begin installation of neutral beam power supply transmission lines	December	1977
11. Install vacuum tanks	February	1978
12. Begin installation of magnet system	April	1978
13. Begin equipment transfer from 2XIIB	June	1978
14. Begin debug operation of complete TMX system	October	1978

Table 9. (3.150) Total permanent manpower by fiscal year.

	FY 77	FY 78
Equivalent manyears	28.5	67.5
Cost (thousands of \$)	1367.0	3299.0

## REFERENCES

1. G. I. Dimov, V. V. Zakaidakov, and M. E. Kishinevsky, *Fizika Plasmy* 2, 597 (1976); also G. I. Dimov, V. V. Zakaidakov, M. E. Kishinevsky, "Open Trap with Ambipolar Mirrors," in *6th Inter. Conf. Plasma Physics and Controlled Nuclear Fusion Research, Berchtesgaden, Fed. Rep. of Germany, 1976* (IAEA, in preparation), Paper C4.
2. T. K. Fowler and B. G. Logan, "The Tandem Mirror Reactor," Lawrence Livermore Laboratory, Rept. UCRL-78749 (1976); to be published in *Comments Plasma Phys.*
3. *Report of the Open Systems Technical Review Panel*, W. R. Ellis, Chairman, Energy Research and Development Administration, Rept. ERDA-76/140 (1976).
4. *Ibid*, p. 82.
5. *Ibid*, p. 84.
6. G. G. Kelley, *Plasma Phys.* 9, 503 (1967).
7. V. P. Pastukhov, *Nucl. Fusion* 14, 3 (1974).
8. F. H. Coensgen, J. F. Clauser, D. L. Correll, W. F. Cummins, C. Gormezano, B. G. Logan, A. W. Molvik, W. E. Nexsen, T. C. Simonen, B. W. Stallard, and W. C. Turner, "2XIIB Plasma Confinement Experiments," in *Proc. 6th Inter. Conf. Plasma Physics and Controlled Nuclear Fusion Research, Berchtesgaden, Fed. Rep. of Germany, 1976* (IAEA, in preparation), Paper CN-35/C1; also Lawrence Livermore Laboratory Rept. UCRL-78121, Rev. 1 (1976).
9. H. L. Berk, D. E. Baldwin, T. A. Cutler, L. L. Lodestro, N. Maron, L. D. Pearlstein, T. D. Rognlien, J. J. Stewart, and D. C. Watson, in *Proc. 6th Inter. Conf. Plasma Physics and Controlled Nuclear Fusion Research, Berchtesgaden Fed. Rep. of Germany, 1976* (IAEA, in preparation) Paper CN-35/C2; also Lawrence Livermore Laboratory, Rept. UCRL-78125, Rev. 1 (1976).

APPENDIX A. PHYSICS CONSIDERATIONS FOR THE TMX

## CONTENTS

A1.	Confinement and Energetics ( <i>D. E. Baldwin and B. G. Logan</i> ) . . . . .	37
A2.	MHD Stability ( <i>D. E. Baldwin and L. D. Pearlstein</i> ) . . . . .	47
A3.	Microstability ( <i>D. E. Baldwin and L. D. Pearlstein</i> ) . . . . .	51
A4.	Adiabaticity ( <i>D. E. Baldwin and R. H. Cohen</i> ) . . . . .	57
A5.	A Numerical Model for the Cold-Gas Feed ( <i>R. P. Freis and B. G. Logan</i> ) . . . . .	58
A6.	TMX Neutral-Beam Requirements ( <i>F. H. Coensgen, A. W. Molvik, W. E. Nexsen, and T. C. Simonen</i> ) . . . . .	65
A7.	Electron Physics in the Tandem Mirror ( <i>R. F. Post</i> ) . . . . .	68
A8.	Diagnostics for TMX ( <i>B. G. Logan, R. S. Hornady, and W. E. Turner</i> ) .	72
A9.	Plasma/Wall Charge-Exchange Interactions in the 2XIIB Magnetic Mirror Experiment ( <i>B. W. Stallard, F. H. Coensgen, W. F. Cummins, C. Gormezano, B. G. Logan, A. W. Molvik, W. E. Nexsen, T. C. Simonen, and W. C. Turner</i> ) . . . . .	80
A10.	TMX Neutron Yields ( <i>W. E. Nexsen</i> )	
	References . . . . .	89

### A1. CONFINEMENT AND ENERGETICS

In a tandem mirror system, the ions of the plugs and those in the central cell have little direct contact. They interact mainly through the electrons. Mutual collisions in the overlap region can be neglected — for the central-cell ions because of their brief percentage dwell time in the plugs, and for the plug ions because of the relative low density in the central cell.

The key to tandem mirror confinement lies in the electron physics, and particularly in the maintenance of a high electron temperature  $T_e$ . The electrons move freely between the central cell and the plugs, subject only to the relative potential given by

$$\Phi_c = T_e \ln \left( \frac{n_p}{n_c} \right), \quad (A1)$$

where  $T_e$  is the electron temperature, and  $n_p$ ,  $n_c$  are the plug and central-cell densities.

As in any open-ended configuration, the electrons will be electrostatically confined by the drop in ambipolar potential from the plasma bulk to ground; for energies below this confining potential, the electron distribution will be Maxwellian.

We define  $\Phi_e$  as the potential of the central-cell region relative to ground (see Fig. A-1) and  $\Phi_c$  as the potential of the plugs relative to the central cell. The two potentials are determined by different physical processes. The latter potential drop, given by Eq. (A1), is determined by quasi-neutrality. The required equality of electron and ion loss from the tandem-cell system, described below, determines  $\Phi_e/T_e$ .

Throughout this description, we shall neglect all profile effects. All quantities are to be interpreted as representative, or average, quantities.

The electron loss process is properly described by a bounce average of the electron collision operator. The loss process results from collisions suffered in both the plugs and the central cell. We define the volume of a plug  $V_p$  and the central cell  $V_c$  so that the total volume is  $V_c + 2V_p$ . For our purposes here, only the ratio will be significant; for the present design this ratio has the value

$$\frac{V_p}{V_c} = \frac{L_p B_c}{L_c B_p} = 3.6 \times 10^{-3} .$$

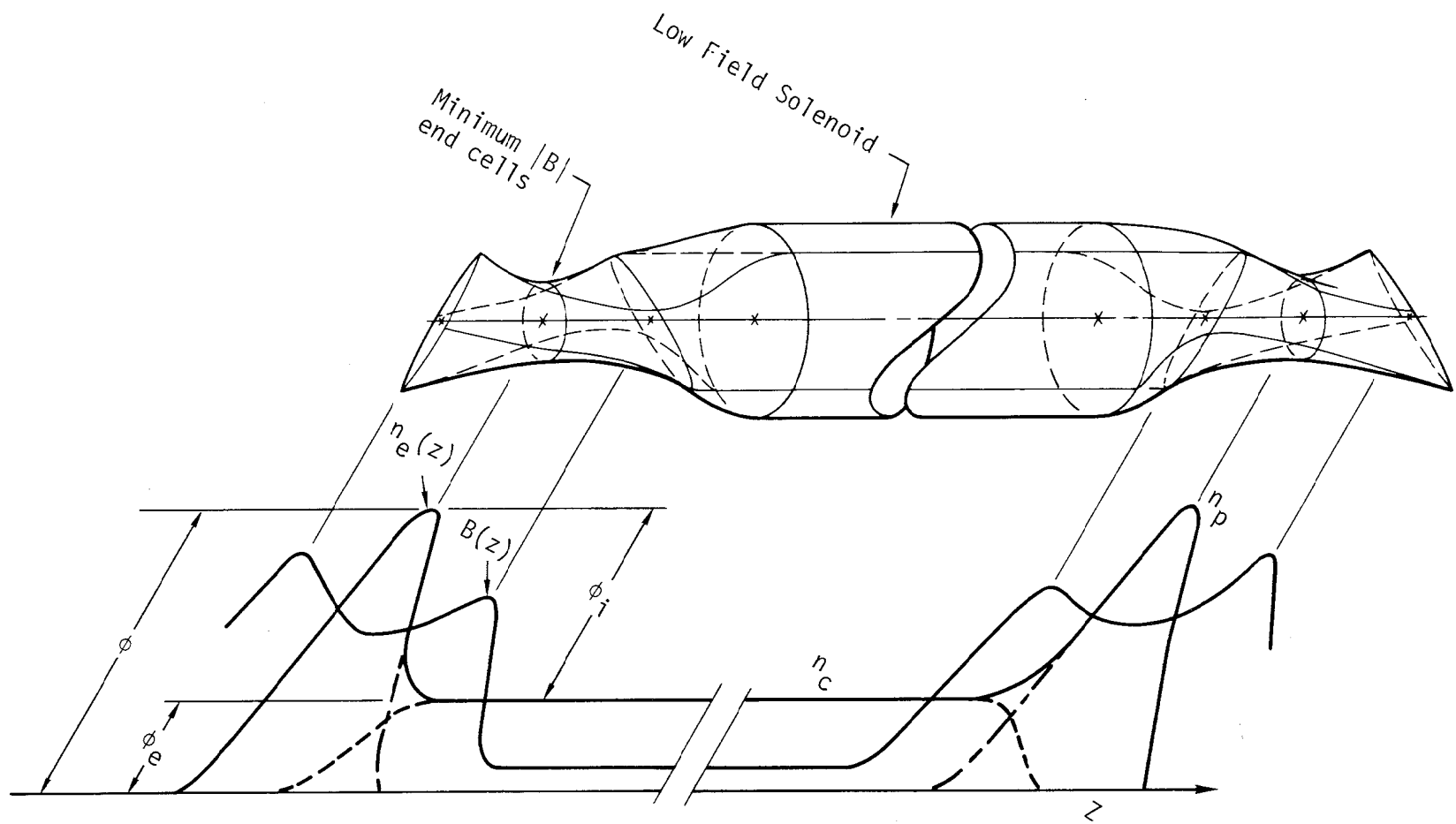


Fig. A-1. Tandem mirrors with ambipolar barriers at the ends.

The electron lifetime is given by the analytical relation of Pastukhov<sup>A1</sup> as modified by a square-well approximation to the bounce average, giving for the electron loss rate

$$\frac{d}{dt} (n_c V_c + 2n_p V_p) = \frac{2(n_c^2 V_c + 2n_p^2 V_p)}{g(R) (n\tau)_{ee}} \left( \frac{T_e}{\Phi_e} \right) \exp \frac{-\Phi_e}{T_e}, \quad (A2)$$

where  $R$  is the mirror ratio from plug to central cell,  $g(R) = \sqrt{\pi} (2R + 1)$ .  $\ln(4R + 2)/4R$  is a slow function of  $R$ , and  $(n\tau)_{ee}$  is the electron-electron 90° scattering-time

$$n\tau_{ee} = 5.63 \times 10^8 T_e^{3/2} \text{ (keV)}$$

when the Coulomb logarithm  $\ln \Lambda = 15$ . The factor 2 appearing in Eq. (A2) is an error corrected from the Pastukhov work<sup>A1</sup>; here it may be interpreted as a doubling of the electron scattering rate beyond that due to self-collision because of their scattering from ions. Introducing the ion net fluxes/volume from the central cell and plugs,  $j_c$  and  $j_p$  respectively,  $\Phi_e/T_e$  is determined by the required equality of the electron loss rate given by Eq. (A2) with the net ion loss

$$\frac{2(n_c^2 V_c + 2n_p^2 V_p)}{g(R) (n\tau)_{ee}} \left( \frac{T_e}{\Phi_e} \right) \exp \frac{-\Phi_e}{T_e} = j_c V_c + 2j_p V_p. \quad (A3)$$

As shown in Appendix A3 on microstability, the experiment will operate in a mode whereby the efflux from the central cell acts as a stream stabilizing the drift-cone mode in the plugs. The net flux  $j_c V_c$  dominates  $j_p V_p$ ; similarly,  $n_c^2 V_c$  dominates  $n_p^2 V_p$ . Equation (A3) may be simplified to read

$$\frac{2n_c^2}{g(R) (n\tau)_{ee}} \left( \frac{T_e}{\Phi_e} \right) \exp \frac{-\Phi_e}{T_e} = j_c. \quad (A4)$$

The ratio  $n_c^2/j_c$  is the confinement product  $(n\tau)_c$  for central-cell ions given by the ion equivalent to Eq. (A2),

$$(n\tau)_c = (n\tau)_{ii} g(R) \left( \frac{\Phi_c}{T_c} \right) \exp \frac{\Phi_c}{T_c}, \quad (A5)$$

where  $\tau_{ii}$  is the  $90^\circ$  self-scattering time for central-cell ions. The ratio  $\Phi_e/T_e$  is given by

$$\left(\frac{\Phi_e}{T_e}\right) \exp \frac{\Phi_e}{T_e} = 2 \sqrt{\frac{m_c}{m_e}} \left(\frac{T_c}{T_e}\right)^{3/2} \left(\frac{\Phi_c}{T_c}\right) \exp \frac{\Phi_c}{T_c}, \quad (A6)$$

where  $m_c$  is the mass of the central-cell ions. Values of  $\Phi_e/T_e \approx 5.5$  will be typical of TMX operation.

Power will be supplied to the TMX experiment via neutral injection into the plugs, although at a later stage alternate schemes such as neutral-beam injection into the central cell are planned. Power is transferred from the energetic plug ions to the electrons and thence to the central-cell ions; for this reason, electron power balance must be considered in conjunction with the ion energetics.

Electrons injected into the central cell at a rate  $j_c V_c$  with zero kinetic energy escape axially with an energy  $\Phi_e$  plus an average kinetic energy  $T_e$  associated with the two degrees of freedom normal to  $B$ . Similarly, those injected into the plugs at a rate  $j_p V_p$  leave with an energy  $\Phi_e + \Phi_c + T_e$ . The electron power balance equation becomes

$$2V_p \kappa \frac{n_p^2 E}{(n\tau)_{drag}} + V_c P_{e-aux} \\ = \frac{3}{2} \frac{n_c^2 (T_e - T_c)}{(n\tau)_{drag}} V_c + (\Phi_e + T_e) j_c V_c + 2(\Phi_e + \Phi_c + T_e) j_p V_p, \quad (A7)$$

where  $(n\tau)_{drag} = 1.4 \times 10^{12} T_e^{3/2}$  (keV) is the energy transfer rate between energetic ions and electrons. The first term on the left side of Eq. (A7) is the electron heating by plug ions of average energy  $E_p$ ;  $\kappa \approx 0.35$  is a factor resulting from averaging the heating power of the plugs over their density profile and taking  $n_p$  as the plug density.  $P_{e-aux}$  represents an auxiliary electron heating power that might be present in a later phase of the experiment. In the description of the reactor models elsewhere in this proposal, the electron heating by alpha particles would enter as this term. The first term on the right side of Eq. (A7) is the power transferred to central-cell ions of temperature  $T_c$ .

The power balance equation for the electrostatically confined ions has a similar form. These ions are injected at low energy, escape from the central cell with average energy  $\Phi_c + T_c$ , and are heated by the electrons. An additional power loss for central-cell ions is that due to charge exchange. For each ionization event giving rise to the particle source for the flux  $j_c$ , there is a charge-exchange event with relative probability  $\sigma_x/\sigma_i$ , where  $\sigma_x$  and  $\sigma_i$  are the respective cross sections for charge exchange and ionization. Such events do not change the density, but replace ions of average energy  $\frac{3}{2}T_c$  with cold ions. The power balance for central-cell ions becomes

$$\frac{3}{2} \frac{n_c^2 (T_e - T_c)}{(n\tau)_{\text{drag}}} + P_{c-\text{aux}} = \left[ \Phi_c + T_c \left( 1 + \frac{3}{2} \frac{\sigma_x}{\sigma_i} \right) \right] j_c, \quad (\text{A8})$$

where  $P_{c-\text{aux}}$  is an auxiliary power analogous to  $P_{e-\text{aux}}$ . Combining Eqs. (A7) and (A8) and neglecting  $j_p V_p$  compared with  $j_c V_c$  as in obtaining Eq. (A6) gives the result

$$\begin{aligned} 2V_p &\leq \frac{n_p^2 E}{(n\tau)_{\text{drag}}} + V_c (P_{c-\text{aux}} + P_{e-\text{aux}}) \\ &= \left[ \Phi_e + T_e + \Phi_c + T_c \left( 1 + \frac{3}{2} \frac{\sigma_x}{\sigma_i} \right) \right] j_c V_c. \end{aligned} \quad (\text{A9})$$

It is convenient to introduce the quantity

$$\eta \equiv \frac{\Phi_e + T_e + \Phi_c + T_c \left( 1 + \frac{3}{2} \frac{\sigma_x}{\sigma_i} \right)}{T_e} - \frac{P_{c-\text{aux}}}{j_c T_e}, \quad (\text{A10})$$

which is dominated by  $\Phi_e/T_e$  and so by Eq. (A6) is slowly varying, with a value of about 8.  $\eta$  represents the energy expended by each electron, both in heating sufficiently to escape and in heating the associated ion to its energy of escape. Because  $\Phi_e + T_e > \Phi_c + T_c$ , more energy is required for the electrons than for the ions to escape. The cooling represented by  $\sigma_x T_c / \sigma_i$ , which might be offset by a non-zero  $P_{c-\text{aux}}$ , has a weak effect as long as  $P_{c-\text{aux}}/j_c \ll \Phi_e + T_e$ .

Because  $j_c$  is chosen to provide the flux required to stabilize the two plugs, it depends only upon plug parameters and the volume ratio, see Appendix A3, Eq. (A29),

$$j_c = 2.3 \cdot 10^7 \lambda \frac{V_p}{V_c} \frac{T_e^{3/2} n_p}{E_L p} , \quad (\text{A11})$$

where  $T_e$  and  $E_p$  are in keV,  $n_p$  is in  $\text{cm}^{-3}$ , and  $L_p$  is in cm.  $\lambda$  depends upon a number of plug parameters, but scaling from 2XIIB operation, it is taken as having a value in the range 1 to 2. From Eqs. (A9) through (A11), when  $P_{c-aux}$  is zero, there results

$$T_e = 0.031 \left( \frac{\kappa E_p \beta_p B_p^2 L_p}{\lambda \eta} \right)^{1/4}, \quad (\text{A12})$$

where  $\beta_p$  is the  $\beta$  of the plug, and  $B_p$  is the minimum field of the plug in kG. For the nominal TMX operating conditions,  $\lambda = 1.3$ ,  $\eta = 8$ ,  $\kappa = 0.3$ , and other parameters as given in Table 1;  $T_e = 0.2$  keV for  $E_p = 26$  keV, and  $T_e = 0.17$  keV for  $E_p = 13$  keV; and  $j_c = 4.7 \times 10^{14} \text{ cm}^{-3} \cdot \text{s}^{-1}$  for  $E_p = 26$  keV. In the form given by Eq. (A12), the expression for  $T_e$  is identical to that for 2XIIB, assuming that the stabilizing current is the minimum required. The fact that in the tandem-cell system the electrons also heat the central cell is represented by the  $\Phi_c + T_c (1 + \frac{3}{2} \sigma_x / \sigma_i)$  contribution to  $\eta$ , but this effect is small compared to the fundamental energy drain by the electrons.

The plug ions will behave just as those in 2XIIB. At  $T_e = 200$  eV and  $n_p = 5 \times 10^{13} \text{ cm}^{-3}$ , the ion replacement time by charge exchange on the neutral beam is short compared to the electron drag time; therefore, the average ion energy in the plug  $E_p$  will be close to the average of that injected in the whole-half-third energy components. For nominal 20-keV injection, this is 13 keV; for nominal 40-keV, it is 26 keV. The density is determined by the ionization current  $j_p$  balanced with the lifetime by electron drag

$$j_p = \frac{n_p^2}{n \tau_{\text{drag}} \ln(E_p \text{ inj} / E_p \text{ esc})}$$

$$= 6.5 \times 10^{15} \text{ cm}^{-3} \text{ s}^{-1} \quad (\text{A13})$$

at  $n_p = 5 \times 10^{13} \text{ cm}^{-3}$ ,  $T_e = 0.2$  keV, and a ratio of the plug energy of injection to that of escape  $E_p \text{ inj} / E_p \text{ esc} = E_p / (\Phi_e + \Phi_c) = 21$ . For  $V_p = 6.3$  litres, this gives an equivalent trapped ion current of 8 A per plug. (Because of incomplete deposition and the high ratio of charge-exchange to ionization cross sections, the required beam current is some 10 times this value.) For these parameters, Eqs. (A11) and (A13) give the result

$$j_c V_c = 18 j_p V_p,$$

justifying the neglect of the plug current contribution to the electron energy loss.

Given  $T_e$  and  $n_p$ , the central-cell parameters  $T_c$  and  $n_c$  are obtained from energy balance, Eq. (A8), and particle balance

$$j_c = \frac{n_c^2}{(n\tau)_c} \quad (A14)$$

with  $(n\tau)_c$  given by Eq. (A5). Eliminating  $j_c$  from Eqs. (A8) and (A14) (with  $P_{c-aux} = 0$ ) and in Eq. (A2) setting  $g(20) = 4.0$  for  $R = 20$  and  $\ln \Lambda = 15$  gives

$$(n\tau)_c = 1.0 \times 10^{11} T_c^{1/2} \Phi_c \exp \frac{\Phi_c}{T_c} . \quad (A15)$$

The resulting relation between  $T_c/T_e$  and  $\Phi_c/T_c$  is

$$\left( \frac{T_c}{T_e} \right)^{1/2} \left( 1 - \frac{T_c}{T_e} \right) = 9.3 \left[ 1 + \frac{T_c}{\Phi_c} \left( 1 + \frac{3}{2} \frac{\sigma_x}{\sigma_i} \right) \right] \exp \frac{-\Phi_c}{T_c} . \quad (A16)$$

Noting that  $\Phi_c/T_c$  will be near 3.3, Eq. (A16) has the approximate solution

$$\frac{\Phi_c}{T_c} = \ln \left\{ \frac{9.3 \left[ 1 + 0.3 \left( 1 + \frac{3}{2} \frac{\sigma_x}{\sigma_i} \right) \right]}{\left( \frac{T_c}{T_e} \right)^{1/2} \left( 1 - \frac{T_c}{T_e} \right)} \right\}, \quad (A17)$$

or

$$n_c = n_p \left\{ \frac{\left( \frac{T_c}{T_e} \right)^{1/2} \left( 1 - \frac{T_c}{T_e} \right)}{9.3 \left[ 1 + 0.3 \left( 1 + \frac{3}{2} \frac{\sigma_x}{\sigma_i} \right) \right]} \right\}^{T_c/T_e} \quad (A18)$$

From Eq. (A14) is obtained the relation

$$\left(\frac{T_e}{T_c}\right)^{3/2} \left\{ \frac{\left(\frac{T_c}{T_e}\right)^{1/2} \left(1 - \frac{T_c}{T_e}\right)}{9.3 \left[1 + 0.3 \left(1 + \frac{3}{2} \frac{\sigma_x}{\sigma_i}\right)\right]} \right\} \left(\frac{2T_c}{T_e} + 1\right) = 3.3 \times 10^{11} \frac{T_e^{3/2} j_c}{n_p^2}. \quad (A19)$$

Equation (A19) holds for general  $j_c$ , but when  $j_c$  is given by Eq. (A11) and  $T_e$  by Eq. (A12) and the central cell and plug energy densities have been expressed in terms of their  $\beta$  values, Eq. (A19) may be written

$$\left(1 + \frac{T_c}{T_e}\right)^{-1/2} \left(\frac{T_e}{T_c}\right)^{3/2} \left\{ \frac{\left(\frac{T_c}{T_e}\right)^{1/2} \left(1 - \frac{T_c}{T_e}\right)}{9.3 \left[1 + 0.3 \left(1 + \frac{3\sigma_x}{2\sigma_i}\right)\right]} \right\} \left(\frac{2T_c}{T_e} + 1\right) = \frac{1}{3} \frac{\kappa}{n} \frac{E_p V_p}{T_e V_c}. \quad (A20)$$

For  $\sigma_x = \sigma_i$  and  $T_c/T_e$  in the range 0.2 to 0.5, the solution to Eq. (A20) is to a good approximation given by

$$\frac{T_c}{T_e} = 0.083 \ln \left( \frac{2\eta T_e V_c}{\kappa E_p V_p} \right). \quad (A21)$$

For  $\kappa = 0.3$ ,  $\eta = 8$ ,  $T_e = 0.2$ ,  $E_p = 26$ , and  $V_c/V_p = 375$ , this gives  $T_c/T_e = 0.40$  and  $n_c = 0.22 n_p$ .

In the mode of operation from which the foregoing operating point was obtained, the current flux  $j_c$  was specified by that necessary to stabilize the plugs according to 2XIIIB scaling. As such, this represents a conservative operating point for TMX. As discussed in Appendix A3, it may be true that, because of the spatial overlap of the central-cell and plug plasmas, less

central-cell flux is required than that given by Eq. (A11). As long as  $j_c V_c \gg j_p V_p$ , the foregoing equations can be used to evaluate the effects on  $T_e$ ,  $T_c$ , and  $n_c$  by such a favorable turn of events. If we view such a change in the required  $j_c$  as a change in the value of  $\lambda$  in Eq. (A11),  $T_e$  from Eq. (A12) scales as  $\lambda^{-1/4}$  and the right side of Eq. (A19) as  $\lambda^{5/8}$ . Specifically, reducing  $\lambda$  by a factor of 10 in the foregoing example raises  $T_e$  to 350 eV (at  $E_p = 26$  keV) and  $T_c/T_e$  to 0.52, and gives  $n_c = 0.16 n_p$ . For constant  $n_p$ ,

$$j_p \propto T_e^{-3/2} \propto \lambda^{3/8}$$

and so

$$\frac{j_p}{j_c} \propto \lambda^{-5/8},$$

and for this example  $j_c V_c = 4.3 j_p V_p$ . Calculations involving further reductions in  $j_c$  necessitate retaining  $j_p V_p$  appearing on the right side of Eq. (A7).

If the plugs are completely stable, e.g., either by virtue of the overlap of Maxwellian and loss-cone distribution or by creation of a radial profile having a flat central portion, there is no requirement on the flux  $j_c$ . As an example of the improvements to be realized for classical operation, we impose the condition that the total current from the central cell equal that from the plugs, which is typical of the reactor regime,

$$j_c V_c = 2 j_p V_p.$$

In this case the electron energy balance equation, Eq. (A9), becomes

$$\frac{n_p^2 E}{(n\tau)_{drag}} = 2\eta T_e \frac{n_p^2}{(n\tau)_p}. \quad (A22)$$

[A factor  $\kappa$  has been discarded in Eq. (A22) because we assume that the same  $n_p^2$  average appears on both sides of the equation.] Assuming the plug lifetime to be governed by classical scattering, we write

$$n\tau_p = 2.8 \times 10^{10} E_p^{3/2} \log R_p = 8.4 \times 10^9 E_p^{3/2}.$$

giving for  $\eta = 8$ ,

$$T_e = E_p / 24 ,$$

or  $T_e = 1.08 \text{ keV}$  for  $E_p = 26 \text{ keV}$ . The depression of  $T_e$  below the nominal  $E_p / 15$  of a single-cell, classical mirror is due to the increase in  $\eta$  from 5.5 to 8 and the doubling of the electron loss current represented by the factor 2 in Eq. (A22). The plug current for this case at  $E_p = 26 \text{ keV}$  is

$$j_p = \frac{n_p^2}{(n\tau)_p} = 2.2 \times 10^{15}$$

and

$$j_c = 1.6 \times 10^{13}$$

Given in Table 1A is the effect of auxiliary neutral-beam heating of the central cell with 36-A attenuated current (60-A incident current). The most dramatic effect is on the increase of  $T_c$ ;  $T_e$  is relatively little affected.

We take

$$P_{c-aux} = f_c \bar{E}_b \frac{I_b (\text{attenuated})}{V_c} ,$$

where  $f_c$  is the fraction of the injected power transferred to the ions, taken as 0.5,  $\bar{E}_b = 13 \text{ keV}$ , and  $V_c$  is reduced by 3.8 due to the necessity for increasing  $B_c$  to 1.9 kG to accommodate both the increased pressure and the large gyroradii of injected ions. Thus,  $P_{c-aux} = 5.3 \times 10^{-4} \text{ kW} \cdot \text{cm}^{-3}$  when  $I_b$  (attenuated) = 36 A the total of which is effective due to charge-exchange heating of the central-cell ions. Particle balance, Eq. (A14), is unaffected when the beam current is included in  $j_c$ , although for  $(n\tau)_c$  we use a formula that more accurately agrees with the results of a Fokker-Planck code at lower values of  $\Phi_c / T_c$  than does Eq. (A5),

$$(n\tau)_c = 8 \times 10^{10} T_c^{3/2} \left( 1 + \frac{\Phi_c}{T_c} \right) \exp \frac{\Phi_c}{T_c} .$$

In summary, the electron temperature is determined by how the heating power of the plugs balances the electron energy drain associated with the central-cell flux required to stabilize the plugs. If the current required for stability can be reduced below the 2XIIIB-based design value, there will be a concomitant increase in  $T_e$ .

## A2. MHD STABILITY

The end plugs of the TMX magnetic field are designed to have absolute minimum-B over the mirror ratio seen by the high-pressure plasmas. However, the central cell has sufficient bad curvature to force the vacuum average over the entire system to be bad also. Magnetohydrodynamic (MHD) interchange stability therefore rests heavily on having the high-pressure plugs stabilize the central cell in a pressure-weighted average. The interchange stability criterion is approximately<sup>A2</sup>

$$\delta \int \frac{d\ell}{B} p_{\parallel}(B) < 0, \quad (A23)$$

where  $p_{\parallel}(r) = w(\alpha, \beta) \hat{p}_{\parallel}(B)$ .

The separation of the pressure into a product of functions of the flux coordinates  $\alpha, \beta$  and  $B$  is a consequence of the omnigenous character of particle drift orbits in the quadrupole symmetry of the TMX magnetic fields (particles with different pitch angles drift on the same drift surface). Because the ratio of plasma pressure to magnetic field in the good-curvature plugs exceeds that in the bad-curvature central cell by a factor of more than 30, the criterion Eq. (A33) is easily satisfied for the TMX magnet design, and stability for sufficiently low  $\beta$  is accordingly assured. In this respect, the MHD stability picture is similar to that in 2XIIB under stream-stabilized operation. In that experiment, the magnetic field is also  $\int d\ell/B$  unstable when integrated from vacuum wall to vacuum wall. However, the presence of the high-pressure plasma, localized in the good well between the mirrors, acts to stabilize the whole flux tube, as would be expected on the basis of the  $\int dp_{\parallel}/B$  stability.

The more substantial questions are those relating to the  $\beta$ -limits in the central cell imposed by ballooning interchange modes for which the drives are local bad curvature and  $E \times B$  rotation. The rotation depends upon the radial distribution of the ambipolar potential, which is quite model-dependent. For purposes of obtaining conservative stability limits, we shall here assume the extreme situation that the potential drops to zero at the plasma boundary. The plasma in the central cell has a roughly 2:1 ratio of electron to ion pressures. A general treatment of ballooning stability requires application of the guiding-center fluid energy principle in nonsymmetric geometry. However, for the TMX configuration the strong stability of the plugs results in a substantial simplification. They effectively anchor perturbations, introducing a line-tying boundary condition on displacements of the central cell.

To determine the rigidity of the plugs to magnetic perturbations and thereby to demonstrate their anchoring capability, recall that bending a field line requires an energy proportional to the square of the Alfvén speed  $V_A$  divided by the connection length. This energy is to be compared with the potential energy of the drive for instability, with the two contributions weighted with the volumes of the respective flux tubes. When the drive is the local bad curvature of the central cell, this yields a condition for rigidity of the plugs given by

$$\frac{2L_p \pi^2 V_{A,p}^2}{B_p^4 L_p^2} > \frac{(T_e + T_c)}{R_c r_c} \left( \frac{2R_c}{m_c B_c} \right),$$

or

$$\frac{\frac{B_p^2}{\beta_p B_{p,\text{vac}}^2}}{\frac{2(T_e + T_c)}{\pi^2 E_p}} \left( \frac{B_p L_p}{B_c r_c} \right) \approx 0.06, \quad (\text{A24})$$

where  $V_{A,p}$  is the Alfvén speed in the plug,  $R_c$  is the central-cell (bad) curvature, and  $r_c$  is the central-cell radius. For the purpose of the flux tube volume weighting of the instability drive, it is assumed that only a fraction  $2r_c/L_c$  of the central cell contributes to the drive; the ratio  $L_p B_p / r_c B_c$  is about 25. The ratio  $(T_e + T_c)/E_p$  is very small, less than 0.01; the condition Eq. (A24) is therefore easily satisfied, with the right side having a value  $\approx 0.06$ . For rotation acting as the drive, rigidity of the plugs follows a form similar to the case of the magnetic drive, except that the full central cell can drive the mode,

$$\frac{2L_p}{B_p} \frac{V_{A,p}^2}{L_p^2} > \left( \frac{c E_c}{r_c B_c} \right)^2 \frac{L_c}{B_c},$$

giving

$$\frac{\frac{B_p^2}{\beta_p B_{p,\text{vac}}^2}}{\frac{2(T_e + T_c)}{\pi^2 E_p}} \left( \frac{r_c E_c}{\phi_e} \right)^2 \left( \frac{e \phi_e}{E_p} \right)^2 \left( \frac{L_p \rho_p}{r_p^2} \right)^2 \frac{L_c B_p}{L_p B_c} \approx 0.5, \quad (\text{A25})$$

or

$$\beta_p < 2 \frac{B_p^2}{B_{p,\text{vac}}^2} .$$

Based upon the conservative assumption that the potential drops to zero at  $r_c$ , i.e., that  $E_c r_c / \phi_e \approx 1$ , the right-hand side of Eq. (A25) is about 0.5. For more shallow potential gradients throughout the plasma, it is correspondingly reduced. Both of these cases illustrate the fact that unstable perturbations must be isolated from the plug and that appropriate stability calculations are those treating the central cell as line tied, i.e., as suffering perturbations that vanish at the plugs.

Ballooning interchange instability driven by the bad curvature of the central cell, assuming that perturbations are line tied at the plugs, characteristically requires  $\beta_c$  close to unity. It can be shown that the long uniform region does not affect the mode, which must be flute in this region. The connection length must, therefore, be equal either to the radius of curvature  $R_c$  or to the radius  $r_c$ , which are nearly equal. More detailed calculations have been carried out using an expansion of the energy principle developed to study ballooning in a long, thin, line-tied, axisymmetric mirror.<sup>A3</sup> The resulting  $\beta_c$  limits vary from 0.31 to 0.75 at vacuum mirror ratio 20, and from 0.20 to 0.54 at vacuum mirror ratio 40, depending upon the model used for the magnetic field. This problem is currently under investigation. By varying the central-cell magnetic field  $B_c$ , the  $\beta_c$  can experimentally be varied from 0.08 to 0.5 to study all ballooning limits.

The situation with regard to rotation is similar. Recent calculations<sup>A4</sup> show that the most severe rotation-driven mode has  $m = 1$  and finite  $k_z$ ; it is antisymmetric in  $z$ , having a node at  $z = 0$ . The stability criterion obtained in that work was

$$(2\pi)^2 \frac{v_{A,c}^2}{L_c^2} > \left( \frac{c E_c}{r_c B_c} \right)^2 ,$$

or

$$\frac{\beta_c}{1-\beta_c} < 2(2\pi)^2 \left(\frac{\Phi_e}{E_c r_c}\right)^2 \left(\frac{T_e}{q\Phi_e}\right)^2 \left(\frac{r_c^2}{L_c \rho_c}\right)^2 \frac{T_c(T_e + T_c)}{T_e^2} \approx 0.39. \quad (A26)$$

Again taking the most extreme case  $E_c r_c / \phi_e \approx 1$ , the right-hand side for the parameters of Table 1 has the value 0.39, or the  $\beta_c$  limit is 0.28. Thus, even if the total potential drop from the plasma center to the wall occurs over the plasma itself, the  $\beta_c$  lies within the range of variation of  $B_c$ . To the extent that some or all of the drop occurs outside the plasma, stability is correspondingly improved - meaning that from Eq. (A26)  $\beta_c$  could be correspondingly increased.

For the parameters of Table 1A describing neutral injection into the central-cell, the right side of Eq. (A24) becomes 0.2, of Eq. (A25) becomes 0.15, and of Eq. (A26) becomes 1.4. The general tendency of curvature-driven ballooning is for the  $\beta$  limit to increase with decreasing mirror ratio. Thus, stability to all MHD ballooning modes is also theoretically assured for the higher central-cell pressure resulting from the beam heating.

### A3. MICROSTABILITY

In the catalogue of possible loss-cone driven instabilities,<sup>A5</sup> behavior of the plugs should be dominated by the required stability of the drift-cyclotron loss-cone (DCLC) mode discussed below. The high-frequency convective mode requires an axial magnetic scale length greater than about 65 ion Larmor radii in order for scattering by this mode to dominate classical electron drag. Similar scale lengths are required for the negative mass instabilities. The designed TMX scale lengths fall well within this limit. The high- $\beta$ , anisotropy-driven Alfvén ion-cyclotron mode has not been observed in 2XIIB at  $\beta$  values well above the TMX design value of  $\beta_p = 0.5$ . Recent theoretical results indicate that the stability of this mode in 2XIIB is due to the combined small axial and radial sizes of the plasma, measured in units of the ion Larmor radius. While theoretical effort in understanding this mode continues, there seems to be no evidence at all from 2XIIB operation that it would be observed in the TMX experiment.

In 2XIIB operation, the observed fluctuations thought to be DCLC are stabilized by the injection of low-energy ions into or beyond the mirror regions. Theory<sup>A5</sup> describes the diminution of the fluctuating electric fields to a penetration of a flux of this injected cold plasma through the hot plasma in sufficient quantity to fill the low-energy portion of the loss cone of the energetic confined ions. The TMX system is designed to operate in the same way, with the loss flux from the central cell acting as the low-energy current necessary to stabilize the plugs.

An important issue is the amount of central-cell flux required for stability of the plugs, because this has a direct effect on the electron temperature. In deriving the minimum operating point of the TMX, we have assumed that the plugs follow exactly the 2XIIB scaling laws. However, as described later, certain aspects of the stability question peculiar to the tandem mirror configuration are still under study. There are reasons to believe that, due to these effects, less central-cell flux might be required, in which case the affected parameters would correspondingly improve.

All loss-cone instabilities are driven by the nonmonotonicity of

$$F(v_{\perp}) = \int dv_{\parallel} f_{ion},$$

where  $f_{ion}$  is the ion distribution function. For mirror-confined plasmas,  $F$  vanished for energies less than  $q\Delta\Phi/(R-1)$ , where  $\Delta\Phi$  is the drop in ambipolar potential to the mirror throat, and  $R$  is the mirror ratio. For isolated mirror plasmas having radii less than roughly  $40\rho_i$  (where  $\rho_i$  is the ion Larmor radius), stability is achieved only by the partial filling of this void. The role of the stream is seen as continually supplying the density required for stability against a loss rate that is the inverse transit time of ions of energy  $q\Delta\Phi$  axially out of the plasma, approximately  $L_p^{-1} \sqrt{\Delta\Phi/m_i}$ . In the 2XIIIB scaling applicable for radii  $\approx 2$  to  $3\rho_i$ , the ratio of the density of such unconfined ions to that of the confined ions of average energy  $E_i$  is

$$n_{unconfined} \propto \frac{\Delta\Phi}{(R-1)E_i} n_{confined},$$

so that the flux necessary to stabilize a mirror deuterium plasma with that radial scale length, density  $n_p$ , average ion energy  $E_p$ , and electron temperature  $T_e$  is given by

$$J_{stab} = 2.3 \times 10^7 \lambda \frac{T_e^{3/2} n_p}{E_p L_p}. \quad (A27)$$

The parameter  $\lambda$  contains a number of model-dependent factors and is best determined by comparison with experiment. It has the theoretical value

$$\lambda = \frac{1}{4(R-1)} \left( \frac{\Delta\Phi}{T_e} \right)^{3/2} \approx 1.3 \text{ in 2XIIIB,} \quad (A28)$$

where  $\Delta\Phi$  is the drop in ambipolar potential from the midplane to the mirror throat, and  $R$  is the total mirror ratio including  $\beta$ -enhancement. The value 1.3 agrees to within 25 to 50% with the measured end-loss currents from 2XIIIB under marginally stable conditions (just before bursting), and we shall assume that Eq. (A28) holds for variation of  $\Delta\Phi/T_e$  and  $R$  as well.

Noting that Eq. (A27) describes the total stabilizing end-loss current required for a single mirror cell (i.e., the sum of that lost out of the two mirrors), we see that if the plugs follow the 2XIIIB scaling then Eq. (A27) would also be the total current necessary to stabilize the two end plugs of a tandem mirror system. This is to be supplied by a central cell having a volume ratio to that of the plugs

$$\frac{V_c}{V_p} = \frac{L_c B_p}{L_p B_c} .$$

The required flux per unit volume injected into the central cell is

$$j_c = 2.3 \times 10^7 \lambda \frac{V_p}{V_c} \frac{T_e^{3/2}}{E_p L_p} \frac{n_p}{n_e} . \quad (A29)$$

The total central-cell flux  $V_c j_c$  dominates by a factor of 5 to 10 the total flux  $2 j_p V_p$  lost from the plugs; the ion flux from the entire system is therefore adequately approximated by  $V_c j_c$  alone. This value of  $j_c$  is the one used in Eq. (A11).

If the behavior of the TMX plugs in the presence of microinstabilities is the same as that of 2XIIB, the flux per unit volume given by Eq. (A27) is sufficient to reduce their fluctuation level to the point that their ion lifetime is dominated by electron drag — see Appendix A1 on scaling laws for the system. (Parenthetically, because this stabilizing flux is weakly scattered by the residual fluctuations to partially fill the low-energy portion of the loss-cone, the stability of other loss-cone driven modes such as the high-frequency convective and negative-energy modes would also be beneficially affected.) Based upon the 2XIIB operations, confidence in the effectiveness of this stream in stabilizing the plugs is very high. An important question, the theoretical answer to which cannot be fully given at this time, is the degree to which the microstability properties of the plugs are altered by virtue of the tandem mirror configuration. To describe the means by which this question is being addressed and how estimates are made for the tandem mirror behavior, it is convenient to first review the means by which warm plasma is seen as stabilizing single-cell mirror machines.

The conventional theoretical method for analyzing the warm plasma stabilization of a hot-mirror-confined plasma has been to add a warm Maxwellian component of density  $n_w$  and temperature  $T_w$  to the hot, loss-cone confined component having density  $n_H$  and average energy  $T_H$ . Analysis of the DCLC dispersion relation yields a stability boundary in the plane of  $n_w/n_H$  versus  $T_w/T_H$ . Generally, this curve shows a minimum in the density ratio at a temperature ratio that depends upon the plasma radial scale length (see Fig. A-2); for 2XIIB parameters,  $r_p/\rho_i \approx 2$  to 3, the minimum  $n_w/n_H \approx 5\%$  occurs at  $T_w/T_H \approx 3 T_e/T_H$ , which is a measure of the hole in the ion distribution

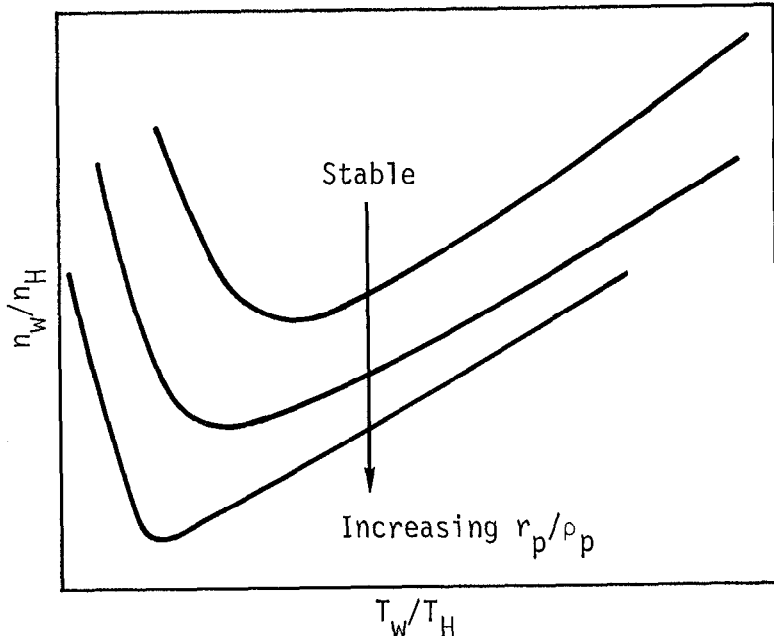


Fig. A-2. Shown are the qualitative dependencies of the warm to hot plasma density ratios on their respective temperature ratios for various radial scale lengths measured in ion gyroradii.

function created by the ambipolar potential drop to the mirror throat  $\sqrt{3}T_e$ . This required density led to the required flux given by Eq. (A27).

The occurrence of the minimum in the required density ratio has a simple physical interpretation. For values of  $T_w/T_H$  too large, the warm ions are too spread in velocity space, so that for a given density they cannot fill the hole. For values of  $T_w/T_H$  too small, the energy distribution of the combined warm and hot species becomes bimodal, and the plasma becomes unstable to "double-humped" modes. The quasi-linear model shows that the nonlinear effect of these double-humped modes is to heat the lower energy component, removing the double-humped character of the total energy distribution function.

The tandem mirror configuration is modeled by forcing the warm component to be nonsymmetric with respect to the midplane of the plug. On the solenoid side, the warm density is taken as equaling at the mirror the density  $n_c$  of the solenoid and as following a Boltzmann law as it penetrates the ambipolar potential associated with the hot plug plasma. On the side of the plug away from the solenoid, only the density resulting from the escaping flux is present.

The stability analysis leading to the warm plasma density requirement upon which Eq. (A27) was based neglected the overlapping Maxwellian plasma confined by the electrostatic barrier associated with the plug. Only the influence of the free-streaming, unconfined warm plasma was included. In gas- and stream-stabilized operation of 2XIIIB, where the external plasma was of very low temperature, only that portion actually passing through the hot plasma was found to affect stability, and this behavior is assumed to persist in the TMX plugs.

The inclusion of the overlapping plasma renders the plasma properties very nonuniform along the magnetic field, and the detailed predictions are still under study. The specific complication is the degree to which the eigenfunction penetrates into the solenoidal side of the plug. However, it is possible to draw certain qualitative conclusions that are based on infinite-medium theory and or results known from conventional mirrors. Specifically, the overlapping plasma will affect stability differently, according to its temperature. If its temperature is low compared to the hole temperature, it may actually be destabilizing, since its inclusion adds a region that is potentially "double-humped" unstable. If the overlapping warm plasma has a temperature comparable to, or slightly greater than, the electron temperature, this plasma has a strong stabilizing effect, since it is very effective in filling the hole in velocity space — at least on the side of the plug facing the solenoid.

Based upon 2XIIB, if the central-cell temperature is too low, the plugs will simply heat the central-cell loss ions to the point where the combination is no longer double-hump unstable. Theoretical results that model 2XIIB operation show that this heating of a low-energy component can proceed without affecting the higher-energy trapped component. Because of the possible wide variety of phenomena depending upon the central-cell ion temperature, the independent control of this temperature provided by the neutral injection into the central cell is of special importance.

The theoretical analysis under development will solve an eigenvalue equation along the magnetic field, through the plug. In so doing, it will correctly account for the nonsymmetric character of the configuration and the degree to which modes can localize in unstable regions. In addition, knowledge of the wave function will supply the necessary information to calculate the heating of the central-cell ions that results. Preliminary results indicate that, within the range of the experiment, there is a sensitivity on the axial length of the plasma due to the importance of eigenfunction localization.

Another parameter of importance in determining the stream requirement, even for a conventional mirror, is the density scale length measured in units of the ion gyroradius, nominally called  $r_p/\rho_p$ . Decreasing this parameter reduces the phase velocity of unstable waves; this in turn has the effect of reducing both the value of the minimum in  $n_w/n_H$  and the  $T_w/T_H$  at which it occurs (see Fig. A2). For the ratio of ion-to-electron energies in the plugs,  $r_p/\rho_p \gtrsim 5$  is the range for this phenomenon to occur. Because it is the local radial density scale length that is of significance, there is the possibility that by shaping, or flat-topping, the plug density profile, the central flux tube will require less stabilizing flux from the solenoid, and the electron temperature on that flux tube will rise accordingly. Experiments of this type are planned for 2XIIB; based upon success there, they may be tried in TMX.

#### A4. ADIABATICITY

A measure of nonadiabatic effects is the local adiabatic energy limit, the energy at which particles somewhere in the plasma volume experience a loss rate due to nonadiabaticity that is equal to the loss rate due to all other processes. For 2XIIB, an estimate of this limit based on the axial field variation as derived from the long, thin, equilibrium approximation (LTA) (using a Gaussian pressure profile with scale distance 20 cm) yields an energy limit of only 14 keV at  $\beta = 0.5$ .<sup>A6</sup> When account is made of the finiteness of the gyroradius at the energy limit compared to the radial scale length of the plasma, this limit is raised. A quadratic model for the radial dependence of  $B$  gives an estimate of over 32 keV; in an appreciable range of energy above this limit, the nonadiabatic diffusion coefficient averaged over all particles is at most of order of the diffusion coefficient due to other processes. One indication that the latter is the more appropriate energy estimate is the observed confinement of 20-keV ions in 2XIIB.

For the TMX plugs, similar estimates based on the LTA give 18 keV if finite orbit effects are neglected and 34 keV if they are included. These estimates are raised when corrections to the LTA are included.

For 2XIIB, the guiding-center equilibrium codes VEPEC and McGUS<sup>A7</sup> predict central field values higher than that predicted by the LTA:

$$B^2 = (1 - \beta) B_{\text{vac}}^2, \quad (\text{A30})$$

where  $\beta \equiv 8\pi p_\perp / B_{\text{vac}}^2$ , and  $B_{\text{vac}}$  is the vacuum field at the plug midplane (but  $B$  is lower than that measured experimentally). It is thus seen that LTA overestimates the finite- $\beta$  field depression, and that finite curvature, neglected in the LTA, partially accounts for the disparity; the remainder is presumably due to finite-orbit effects. The vacuum field of the TMX plugs will be shorter than that in 2XIIB; hence, curvature effects are larger. Guiding-center equilibrium models indicate that the field depression of TMX, including curvature, yields a depression factor at  $\beta = 0.5$  of about 1.25, instead of the value of 1.41 given by LTA. This is the same as the depression in LTA for  $\beta = 0.36$ .

Using  $\beta_{\text{eff}} = 0.36$  as an effective value in Eq. (A30) and applying our conventional calculation, for nominal TMX operation we obtain an estimate of 38 keV for the energy limit if finite orbit effects are neglected and 68 keV if they are included.

## A5. A NUMERICAL MODEL FOR THE COLD-GAS FEED

A computer program has been developed to calculate the buildup and steady state of a plasma fed by cold gas. At issue is the degree to which cold gas, fed to the boundary of the central-cell plasma, can penetrate sufficiently by such means as multiple charge exchanges, generation of Franck-Condon neutrals, and diffusion to act effectively as a volume source of cold ions. The cold gas is molecular D<sub>2</sub> confined in a gas box to a small fraction of the central region of a tandem mirror configuration. The computational model is a one-dimensional slab, representing the region of the gas box, with the plasma in the center, symmetrically bombarded by D<sub>2</sub> from both sides. The effects of the tandem mirror configuration are included by 1) using appropriate end-loss terms, 2) scaling the source terms proportionally to the gas box volume and the loss terms proportionally to the total volume, and 3) maintaining the electron temperature at a fixed value (200 eV). The code solves the one-dimensional, time-dependent, fluid equations for the ion density and temperature and the neutral-gas densities. Three neutral atomic gas D components are created, each at a different energy, due to the interaction of the D<sub>2</sub> with the electrons. The atomic processes included in the calculations are listed in Table A-1.

Table A-1. Atomic processes included in numerical model of the cold-gas feed.

Process	Code label	kT of resultant atoms
(A) D <sub>2</sub> + e → D + D <sup>+</sup> + 2e	n <sub>A</sub>	3 eV
(B) D <sub>2</sub> + e → D + D + e	n <sub>A</sub>	2.5 eV
(C) D <sub>2</sub> + e → D + D <sup>+</sup> + 2e	n <sub>C</sub>	9 eV
(D) D + E → D <sup>+</sup> + e	—	—
(E) D <sup>+</sup> + D → D + D <sup>+</sup>	n <sub>E</sub>	kT

The governing plasma-density and energy-transport equations are:

$$\frac{\partial n}{\partial t} = - \frac{\partial (D_{ie} + D_{ii})}{\partial x} \frac{\partial n}{\partial x} + n [(n_{AT} + n_{CT} + n_{ET}) \sigma v_D + D_{2T}(\sigma v_A + \sigma v_C)] \frac{V_G}{V_T} - \frac{n^2}{(n\tau)} , \quad (A31)$$

and

$$\begin{aligned} \frac{\partial T}{\partial t} &= \frac{T}{n} \frac{\partial (D_{ie} \frac{\partial n}{\partial x})}{\partial x} - \frac{1}{n} \frac{\partial}{\partial x} \left( \frac{5}{3} T D_{ii} \frac{\partial n}{\partial x} - \frac{2nT}{m\Omega^2 \tau_i} \frac{\partial T}{\partial x} \right) \\ &+ v_{31} \frac{\partial n}{\partial x} + v_{33} \frac{\partial T}{\partial x} + \frac{T_e - T}{\tau_{ie}} \\ &+ D_{2T} [\sigma v_A (T_A - T) + \sigma v_C (T_C - T)] \frac{V_G}{V_T} \\ &+ \sigma v_D \frac{V_G}{V_T} [n_{AT} (T_A - T) + n_{CT} (T_C - T)] - \frac{2}{3} \frac{n}{(n\tau)} \phi , \end{aligned} \quad (A32)$$

where the subscripts A through E refer to the atomic processes listed,  $\sigma v$ 's are the appropriate reaction rates,  $V_G$  and  $V_T$  are the gas-box volume and total volume already mentioned,  $m$  is the ion mass, and  $D_{ie}$ ,  $D_{ii}$ ,  $(n\tau)$ ,  $\tau_{ie}$ ,  $\tau_i$ ,  $\tau_e$ ,  $\Omega^2$ ,  $v_{31}$ ,  $v_{33}$  and  $\phi$  are given in the following equations:

$$D_{ie} = - \frac{n(T_e + T)}{m_e \Omega^2 \tau_e} , \quad (A33)$$

$$D_{ii} = D_{ie} \left( \frac{\rho}{n} \frac{\partial n}{\partial x} \right)^2 \left( \frac{m}{m_e} \right)^{1/2} , \quad (A34)$$

$$(n\tau) = \frac{\sqrt{m}}{2} \frac{(T)^{3/2}}{\pi e^4 \ln \lambda} (1 + \frac{\phi}{T} K) e^{\phi/T} + \frac{n L_T}{V_s} , \quad (A35)$$

$$\tau_{ie} = \frac{3m_e}{8 \sqrt{2\pi} \ln \lambda e^4 n} \left( \frac{T}{m} + \frac{T_e}{m_e} \right)^{3/2} , \quad (A36)$$

$$\tau_j = \frac{3}{4} \frac{m_j}{\sqrt{\pi}} \frac{(T_j)^{3/2}}{\ln \lambda e n_j^4}, \quad j = i, e, \quad (A37)$$

$$\Omega_j = \frac{eB}{m_j c}, \quad j = i, e, \quad (A38)$$

$$v_{31} = \frac{2}{3} \frac{1}{n} D_{ie} \left[ \frac{T}{n} \frac{\partial n}{\partial x} + \frac{\partial T}{\partial x} \right], \quad (A39)$$

$$v_{33} = - \frac{2}{3} \frac{1}{m_e \Omega_e \tau_e^2} \left[ \frac{T}{n} \frac{\partial n}{\partial x} + \frac{\partial T}{\partial x} \right], \quad (A40)$$

$$K = \frac{\sqrt{\pi}}{2} \frac{(2R_m + 1) \ln (4R_m + 2)}{2R_M}, \quad (A41)$$

$$\phi = T_e \ln \left( \frac{n}{n_p} \right). \quad (A42)$$

$R_M$  is the mirror ratio,  $n_p$  is the plasma density in the outer mirror plugs, and  $v_s$  is the plasma thermal velocity. In Eq. (A31) and (A32), each of the individual terms can be arbitrarily set to zero. This not only facilitates code checking, but also allows the effect of each physical process to be determined. More will be said of this in the section on results.

The gas density equations are

$$\frac{\partial n_A}{\partial t} + v_A \frac{\partial n_A}{\partial x} = n \left\{ [D_2(x) \alpha + D_2(-x)(1-\alpha)] (2 \sigma v_B + \sigma v_A) - n_A (\sigma v_D + \sigma v_E) \right\} \quad (A43)$$

$$\frac{\partial n_C}{\partial t} + v_c \frac{\partial n_C}{\partial x} = n \left\{ \sigma v_C [D_2(x) \alpha + D_2(-x)(1-\alpha)] - n_C (\sigma v_D + \sigma v_E) \right\}, \quad (A44)$$

$$\frac{\partial n_E}{\partial t} + v_s \frac{\partial n_E}{\partial x} = n \left\{ \sigma_{cx} v_A n_{AT} + \sigma_{cx} v_C n_{CT} - n_E (\sigma v_A + \sigma v_B + \sigma v_C) \right\}, \quad (A45)$$

$$\frac{\partial D_2}{\partial t} + v_2 \frac{\partial D_2}{\partial x} = - n D_2 (\sigma v_A + \sigma v_B + \sigma v_c). \quad (A46)$$

The neutrals from processes A and B have been combined as a single gas component.  $v_A$ ,  $v_C$ , and  $v_2$  are the respective gas velocities, assumed constant. These equations describe the gas streaming in from one side; therefore, if we take into account the symmetry of the problem, the total gas density at any point is  $n_{gT}(x) = n_g(x) + n_g(-x)$ , where the origin of  $x$  is at the center of the slab. The parameter  $\alpha$  is the fraction of gas atoms created in the  $D_2$ -e interaction which emerge with forward velocities.

The steady state has been calculated for a system with the following parameters:

$$T_e = 200 \text{ eV}$$

$$D_2 \text{ equivalent current} = 270 \text{ A}$$

$$\frac{v_g}{v_T} = 10^{-3}$$

$$\text{Slab width, } L_x = 2 \text{ cm}$$

$$n_p = 5 \times 10^{13} \text{ particles/cm}^3$$

$$\text{Mirror ratio} = 40$$

With these parameters fixed, three cases have been run, each with different terms included in the density and temperature equations [Eqs. (A31) and (A32)].

- Case 1 neglects all diffusion, transport, and thermal conduction effects in Eqs. (A31) and (A32), i.e.,  $D_{ie} = D_{ii} = v_{31} = v_{33} = 0$ ,  $\tau_i = \infty$ .
- Case 2 restores  $D_{ie}$  and  $D_{ii}$  (particle diffusion) to Eq. (A31) only;
- Case 3 restores  $D_{ie}$  and  $D_{ii}$  to Eq. (1) only and restores  $\tau_i$  (thermal conductivity) to Eq. (A32).

The resultant density and temperature profiles are shown in Figs. A-3 and A-4, respectively.

The values at the slab center are listed in Table A-2. The first point to note is that in all three cases a substantial plasma density is achieved in the center (even if particle diffusion is neglected). As expected, particle diffusion reduces the outer wings on the density profile, resulting in an increase in the central density. Including thermal conductivity causes a significant reduction in the central temperature as well as a flattening of the temperature profile. These calculations are still in process; as the rest of the transport terms are checked out, they will be included in the temperature equation, although their effects are not expected to be large. Probably of more importance will be a more accurate model of the electron temperature, which will soon be added.

The total end-loss plasma current from the central region ( $I_p$ ), defined as

$$I_p = e \int_0^{L_x} \frac{n^2}{(n\tau)} \frac{V_T}{L_x} dx$$

sensitively depends on the profiles of  $n$  and  $T$ . As shown in three sample cases (Table A-2),  $I_p$  is reduced as radial diffusion is included. Future calculations will focus on the ratios of radial plasma currents to end-loss plasma currents and  $D_2$  gas currents to end-loss plasma currents for cases where the end-loss plasma current is optimized to stabilize the plugs.

Table A-2. Plasma density and temperature at  $x = 0$  for three cases.

Case	$n$ (particles/cm <sup>3</sup> )	T (eV)	$I_p$ (A)	Description
1	$0.8 \times 10^{13}$	119	320	No diffusion; no thermal conductivity.
2	$1.2 \times 10^{13}$	110	58	Diffusion; no thermal conductivity.
3	$1.3 \times 10^{13}$	71	30	Diffusion; thermal conductivity.

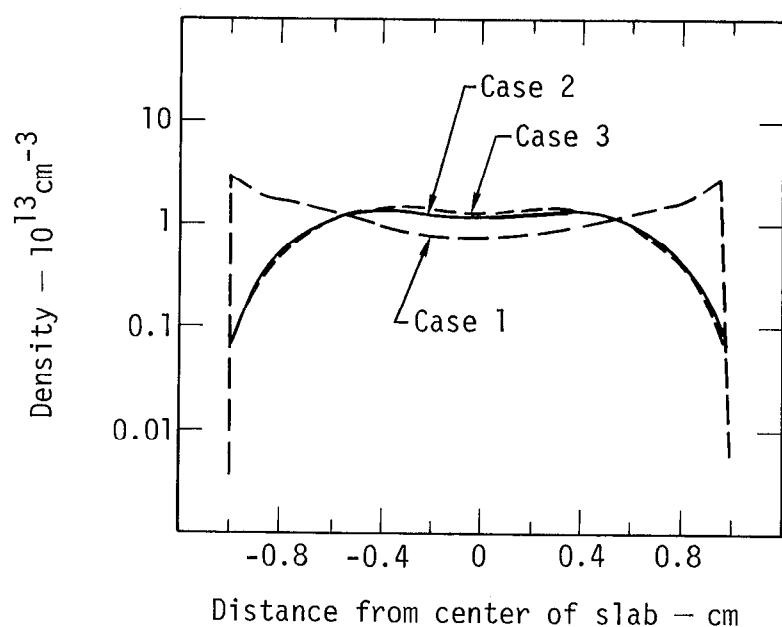


Fig. A-3. Plasma density  $n$  versus distance from center of slab  $x$ .

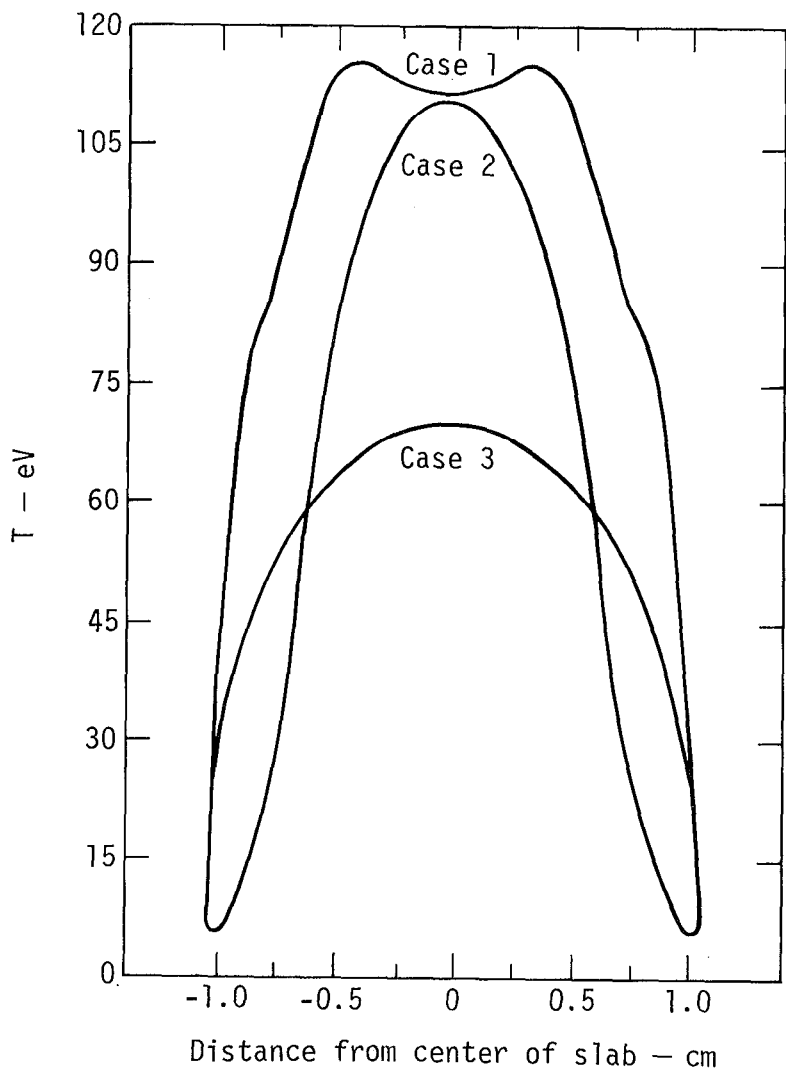


Fig. A-4. Plasma temperature  $T$  versus distance from center of slab  $x$ .

## A6. TMX NEUTRAL-BEAM REQUIREMENTS

The neutral-beam set for each TMX plug includes 8 20-keV modules and 4 40-keV modules that duplicate the beam capability of 2XIIB. Thus, we assure TMX plug parameters equal to achieved 2XIIB plasma parameters and provide the capability of duplicating any further improvement of plasma parameters that may develop in the continuing 2XIIB experiment.

In TMX, we propose to build up the plasma by beam injection in a cold-plasma stream, as has been successfully demonstrated in 2XIIB. Quantitative calculation of buildup from the cold-plasma stream is very model-dependent and therefore not reliable. Consequently, we rely on 2XIIB experience. Whereas buildup is marginally possible at 200 A, to actually achieve the TMX design values of  $\beta \geq 0.5$  and  $r_p \approx 7$  cm injected neutral-beam currents approaching 300 A are required in 2XIIB. Although performance of multiple-beam installations of this size is expected to improve as we gain experience in 2XIIB, the required currents for buildup in the TMX plugs are near the best past performance of the 2XIIB beam system.

The extraction potential of four beams of each TMX plug set is increased to 40 kV. This provides capability to increase the mean ion energy in the plugs from the 13-keV value attained in 2XIIB to the 26-keV value specified in the TMX point design by turning off the 20-keV beams after buildup to the required density or  $\beta$ . Again, the calculation of the transition is very model-dependent, but limited 2XIIB data with only one beam operating at 33 keV indicates that indeed the mean ion energy will rise when the lower-energy beams are turned off. In those runs, the current from the single beam was insufficient to sustain the plasma, so we have no experimental data point for the 40-keV beam current required for the transition.

However, we can estimate the 40-keV beam current required to sustain the plug plasma as follows. We take the electron temperature of  $T_e = 0.2$  keV calculated in Appendix A-1 for a plasma of 7-cm radius and 6.3-litre volume as representative for some plasma profile having an average density and beta equal to the nominal design values  $n_p = 5 \times 10^{13}$ ,  $\beta_p = 0.5$ . The confinement time in the plugs is given by the electron drag time increased by a factor of the logarithm of the ratio of injection energy to energy of escape, roughly the ambipolar potential of the plug. At  $T_e = 0.2$  keV,

$$n\tau = n\tau_{\text{drag}} \ln (E_{\text{inj } p}/E_{\text{esc } p}) = 3 \times 10^{11} \text{ cm}^{-3} \cdot \text{s.}$$

The  $n\tau$  calculated using the quasi-linear code is slightly lower (~17%) than this value due to a residual level of rf turbulence. The trapped current density is then

$$j_p = \frac{n_p^2}{(n\tau)_p} \quad q = 1.3 \text{ mA} \cdot \text{cm}^{-3}.$$

Multiplying this loss current density by the 6.3-litre plasma volume gives a total trapped plug current  $I_{\text{trapped}} \approx 8 \text{ A}$  per plug. For the density and radius of the plug, the trapping efficiency is low; therefore, it is proportional to the density

$$\frac{I_{\text{trapped}}}{I_{\text{beam}}} = 2r_p n_p f_p \sigma_{\text{ionization}}.$$

The coefficient  $f_p \approx 0.5$  is a form factor relating the average line density encountered by the beam to the line density through the plasma center. The cross section for ion and 200-eV electron impact is close to  $3 \times 10^{-16} \text{ cm}^2$ . For a plasma of  $r_p = 7 \text{ cm}$  and  $n_p = 5 \times 10^{13} \text{ cm}^{-3}$ ,

$$I_{\text{trapped}} = 0.1 I_{\text{beam}};$$

so that the required 40-keV beam current for plug sustenance at  $T_e = 200 \text{ eV}$  is 80 A per plug.

Extrapolating the average output of 30 A/module of the 2XIIIB 20-keV beams, we anticipate 24 A/module for the 40-keV beams. In equilibrium, the 96 A provides a modest margin of safety over the calculated required beam current. If this situation occurs, it may be possible to reduce the required stabilizing stream for the plugs by increasing the plasma radius. Such a reduction in stream would have the desirable result of increasing  $T_e$ .

The 20-keV beams represent the majority of the current capacity of the beam set. They have been designed for 25-ms operation in order to assure at least 2XIIIB-quality plug plasmas for the 25-ms duration of the experiment.

Note that on the basis of 2XIIIB data we expect  $n\tau \approx 5 \times 10^{10} \text{ cm}^{-3}$  and  $T_e < 100 \text{ eV}$  at the end of buildup on the plasma stream. The current from the four 40-keV beams is insufficient to sustain the plasma density with this  $n\tau$ . Thus, the transition from stabilization by stream injection to stabilization by plasma loss from the center cell and the increase of the mean ion energy

from 13 to 26 keV may require careful programming of stream and 20-keV beam turnoff to allow  $T_e$  to rise to the point that the 40-keV beams can sustain the density.

## A7. ELECTRON PHYSICS IN THE TANDEM MIRROR

Electrons play a crucial role in the operation of a tandem mirror system. We here review the important element of the electron behavior in such systems, as based on our present understanding.

The magnitude of the confining potential produced by the plugs of a tandem mirror system is proportional to the electron temperature. This temperature in turn is determined by a balance between the rate of heat input to the electrons and the rates of whatever cooling processes are operative.

With respect to electron heating processes as presently envisaged, heat input to the electrons would be derived solely from energy transfer from energetic ions. In TMX, the energetic ions are those in the plugs; in a reactor, alpha particles from the DT reaction would also contribute to the heating.

Electron cooling would arise from two sources. Internally, there is energy transfer between the higher-temperature electrons and the somewhat lower-temperature ions in the central plasma; this cooling rate is moderate and predictable. The second and main source of cooling of the electrons is that which is lost externally, either directly, through escape of the electrons, or through indirect heat-transfer processes. In the direct-loss process, an electron, in order to escape confinement, must possess kinetic energy sufficient to scale the total ambipolar potential barrier, that builds up to bring electron and ion loss rates from the system into equality. In TMX, it typically has a magnitude of order 5 to 6  $T_e$ . Thus, the escape of every electron results in the loss of at least this amount of energy. At a material wall, the electron will have lost most of its kinetic energy to the confining potential. However, the ion with which it is paired will have gained the same kinetic energy in falling down the potential (a hill for the ions) so that much of the energy required for electron loss actually is transferred to escaping ions.

The loss processes just described are understood and predictable in terms of classical collisional processes in the plasma. It is a goal of the TMX experiment, and of the preparatory experiments in 2XIIB that will precede it, to come as close as possible to realizing this theoretical rate.

What additional cooling processes may be present, and what precautions can be taken to limit their impact?

Basically, there are only two processes, both operating external to the plasma confinement region, that we believe can unfavorably influence the

electron cooling rate. Fortunately, it appears that both of these are subject to control. In fact, as will be seen, the tandem mirror concept involves a synergistic factor that will operate to aid the situation.

The first cooling process arises from secondary electrons emitted from the end wall of the confinement chamber under bombardment by the escaping electrons and ions. If no measures are taken to prevent the return of these secondary electrons back along the field lines and into the confinement chamber, each secondary released by an escaping ion will allow the escape of another more energetic electron, resulting in additional cooling. Hobb and Wesson<sup>A8</sup> and Hall<sup>A9</sup> have estimated the magnitude of this additional loss, finding an enhancement factor (for losses across the boundary sheath) of about a factor 3 for a deuterium plasma. This result might be improved in various ways. It is possible to minimize the probability of the release of secondary electrons through optimum choice of materials and wall geometry. It is also possible to prevent their return to the plasma. Suppressor grids, such as employed in vacuum tubes, or permanent magnet multipole fields could be employed to prevent secondaries from escaping from the wall surface. These techniques could be explored in 2XIIB or in auxiliary experiments before implementation in TMX.

The second cooling mechanism operates through the presence of cold plasma in the region between the mirrors and the chamber wall. Here the issues are energy transfer through ionization losses and collisional energy exchange with cold electrons in this exterior plasma. Such plasma can arise naturally if inadequate means are provided to prevent recycling of gas atoms (arising from the neutralization of cold-plasma ions or from wall bombardment) back into the escaping plasma stream. Expansion of the escaping flux line, baffling, and the use of efficient gettered surfaces minimize this problem. Another source of external plasma in 2XIIB is the means used to produce the stabilizing stream. Both the externally supplied stream and the gas box utilized in 2XIIB experiments produce far more cold plasma than is theoretically required for stability — with the result that the excess causes an unnecessary drain on the electron energy. In TMX, where the interior plasma is designed to provide a stabilizing flux matched to the requirement of the plugs, the excess of cooling plasma will not be present.

Experiments without external stream guns and gas sources support our contention that the minimum stabilizing flux does not lead to the accumulation of excessive external plasma. Important in this argument is the theoretical

point that, in the absence of an externally supplied source of low-energy particles, a mirror-confined plasma will achieve marginal stability by sufficiently diffusing confined ions in velocity space to fill its loss cone. Thus, the end-loss current, in the absence of an external source, always has the magnitude of the minimum flux required for stability. Under the above conditions, in particular in the old 2XII in which the appropriate measurements were made, it is known that the density of plasma external to the mirror decayed much faster than that in the mirror trap.

Except in somewhat extreme cases, the cooling effect caused by the recirculation and reionization of wall-neutralized escaping ions can be estimated from the following considerations: Such an ion, if neutralized at the wall and then reionized at any point along a field line connecting a point on the chamber wall to the plasma confinement regions, will result in a net cooling effect of order  $e\phi_e$  per such ion. Part of this cooling will result from the expulsion from the point of ionization of the new ion, accelerated outward by that portion of  $\phi_e$  that lies between the wall and the point at which ionization occurred. The rest of the cooling will result from the inward acceleration and consequent energy exchange of the new electron, the heating of which must ultimately be supplied by the plasma. If  $F$  is the fraction of ions impinging on the surface that are recycled and reionized, then the cooling rate of the plasma electrons will be enhanced by a factor of order  $(1 + F)$ . In extreme cases,  $F$  might actually be larger than unity, corresponding to the release of new gas atoms at the walls by sputtering or other processes. However, with proper design, including the provision of adequate pumping and gettered clean surfaces,  $F$  is reducible to a value much less than 1.0, so that this mode of cooling becomes unimportant. The critical issue here is to ensure that the most probable fate for an escaping ion is that it should be captured on a clean surface, unaccompanied by the reemission of additional atoms, or else that it should be physically removed from the chamber by vacuum pumps.

Care in the design of the end region of TMX should minimize cooling effects such as those described above. However, in the absence of such precautions, it should be noted that there are situations where electron cooling has been observed to be much greater than the amount suggested above. The situations, similar to those which occur in high-density theta pinches, are ones where accumulation of plasma in the exterior region reaches the point where the collision mean free path for the electrons is substantially shorter

than that of the end region. In such situations, the sheath conditions can change and energy can flow out of the mirror region by electron thermal transport at a rate much higher than that which would occur in the presence of only the outward streaming plasma. This circumstance is not typical of mirror confinement, as has been demonstrated in a variety of experiments in the past.

## A8. DIAGNOSTICS FOR TMX

Just as the plugs of the TMX are designed after the 2XIIB plasma, so will be many of the diagnostics, duplicated as required to cover the two plugs. To these are added two new diagnostics designed to measure plasma parameters of special importance to the TMX configuration. The minimum required for the first phase of TMX operation is dictated by the three specific physics objectives of the proposal.

- The primary objective is to measure the potential well created between two mirror plasmas and to relate the central ion confinement product  $n_t c$  to the potential barrier  $\phi_c$ , together with the temperatures  $T_c$  and  $T_e$ . The fundamental scaling law for the barrier height  $\phi_c = T_e \ln(n_p/n_c)$  must be verified; therefore we need to measure  $n_c$  as well as  $n_p$  in both plugs, since they may not be exactly balanced.  
The electron temperature  $T_e$  is a crucial parameter for tandem mirror confinement. To allow confidence in scaling to larger devices, TMX must be sufficiently well diagnosed to assure that the measured  $T_e$  is properly described by a theoretical model. Because conditions external to the plug affect  $T_e$ , as part of this question it should be determined whether the external density  $n_{ext}$  is as low as consistent with measured streaming ion currents  $I_c + I_p$ .
- The second objective is to determine MHD stability in the bad-curvature regions of the transition between plugs and solenoid; this requires looking for low-frequency density fluctuations  $\tilde{n}_c$  in the plasma boundary and correlations in azimuth corresponding to low mode number flutes. The central-cell beta  $\beta_c$  and diamagnetism  $\Delta B_c / B_c$  need to be measured to determine ballooning-mode beta limits. The maximum plug beta  $\beta_p$  needs to be determined as a function of the mirror ratio  $R_{vac}$ ,  $n_p$  and  $E_p$ , and  $\Delta B_p / B_p$ .
- The third important objective is to determine the influence of the central-cell density ratio  $(n_c / n_p)$  and losses (stream current/over plug current,  $I_c / I_p$ ) on the microstability of the plugs (amplitude of ion-cyclotron fluctuations  $\tilde{\phi}_p$ ). To a considerable extent, such measurements will be similar to those carried out in 2XIIB.

Later phases of the experiment, which will deal with issues of radial transport and diffusion and alpha particle adiabaticity and radial losses, will require additional diagnostics not discussed here.

Table A-3 itemizes the plasma parameters to be measured and the appropriate diagnostics. Equipment now in hand from 2XIIB or Baseball is indicated by "yes", including that which is easy to replicate (at minimal cost) for use in two plugs, if desired. Those diagnostics which are yet to be developed are designated "no".

The two diagnostics in Table A-3 having no antecedents in 2XIIB are a neutral analyzer sensitive in the 100-eV range and an ion-beam probe to measure the ambipolar potential. Two designs suggested, respectively, by Turner and Hornady are described below.

#### Low-Energy Ion Analyzer

The electrostatically confined ion distribution in TMX is predicted to be Maxwellian with  $kT \approx 100$  eV and the high-energy tail cutoff at  $\sim 3 kT \approx 300$  eV. Measuring this ion temperature from the distribution of charge-exchange flux leaving the plasma surface with the conventional apparatus of gas-stripping cell and ion energy analyzer would not work because the stripping efficiency is very low at 100 eV — about  $7 \times 10^{-3}\%$  if extrapolated from stripping cells currently used on 2XIIB. We therefore propose to use the time-of-flight neutral-particle analyzer sketched in Fig. A-5. Charge-exchange neutrals from the plasma surface are chopped by a rotating, toothed wheel. As the chopped beam pulse leaves the wheel, it disperses due to the different velocity components. The time distribution of the signal at the detector characterizes the velocity distribution. A Daly detector is used to record the signal. Secondary electrons are accelerated from the negatively biased emitter onto the grounded, aluminized surface of a plastic scintillator viewed by a photomultiplier. Because the mean free path of a 100-eV deuterium atom in a plasma of  $10^{13} \text{ cm}^{-3}$  density is  $\sim 16$  cm, the measurement is located at an ellipsoidal section near one of the end plugs. A 1-keV neutral beam is used to produce a charge-exchange flux originating in the plasma interior.

For a neutral current  $I_0$  incident on the slit of the wheel with Maxwellian temperature  $kT$ , the current arriving at the scintillator  $I_\delta(t)$  is given by

$$I_\delta(t) = \frac{\delta I_0}{\sqrt{\pi}} \frac{1}{(kT)^{3/2}} \int_{E_1}^{E_2} \sqrt{E} \exp(-\frac{E}{kT}) dE,$$

Table A-3. Plasma parameters to be measured with TMX diagnostics.  
(68 data channels)

Plasma Parameters	Diagnostic (no. of systems)	Existing equipment	Remarks
$\phi_p, \phi_c$	Ion-beam probe (2)	No	Needs to be developed. One beam probe for center cell, one for a plug
$T_c$	Low-energy neutral analyzer (1)	No	Needs to be developed. Includes a low-energy neutral beam for calibration.
$T_e$	Thomson scattering system (1)	Yes	Center-cell measurement
$n_p, n_c$	2-mm microwave interferometers (3)	Yes	Measurement in two plugs and in center cell
$E_p$	High-energy neutral analyzers (2)	Yes	15 channel + swinging analyzer
$n_c$ (few kHz)	Langmuir probes (8)	Yes	
$\tilde{\phi}_p$ (few MHz)	rf probe (1)	Yes	
$I_c$	End-loss analyzers (2)	Yes	Including 1 replica
$I_p$	Beam attenuation detectors (2)	Yes	1 10-channel + 1 single-channel
$n_{ext}$	X-band microwave interferometers (2)	Yes	
$\Delta B_p/B_p, \Delta B_c/B_c$	Diamagnetic loops (4)	Yes	

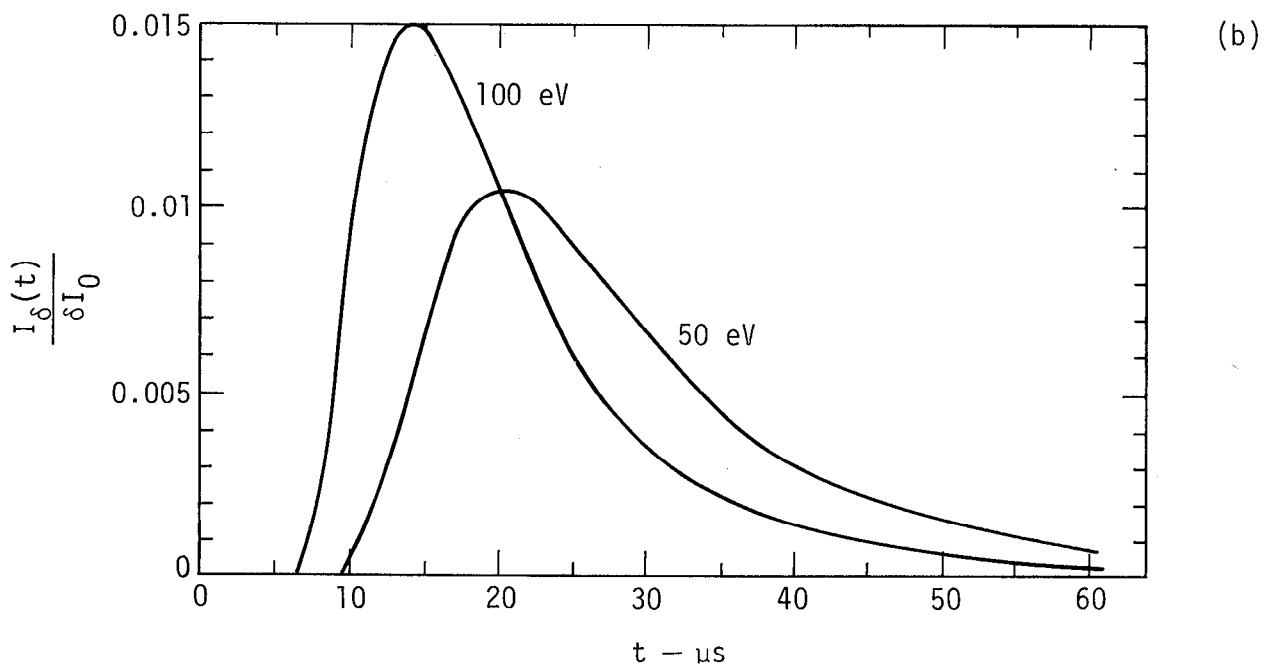
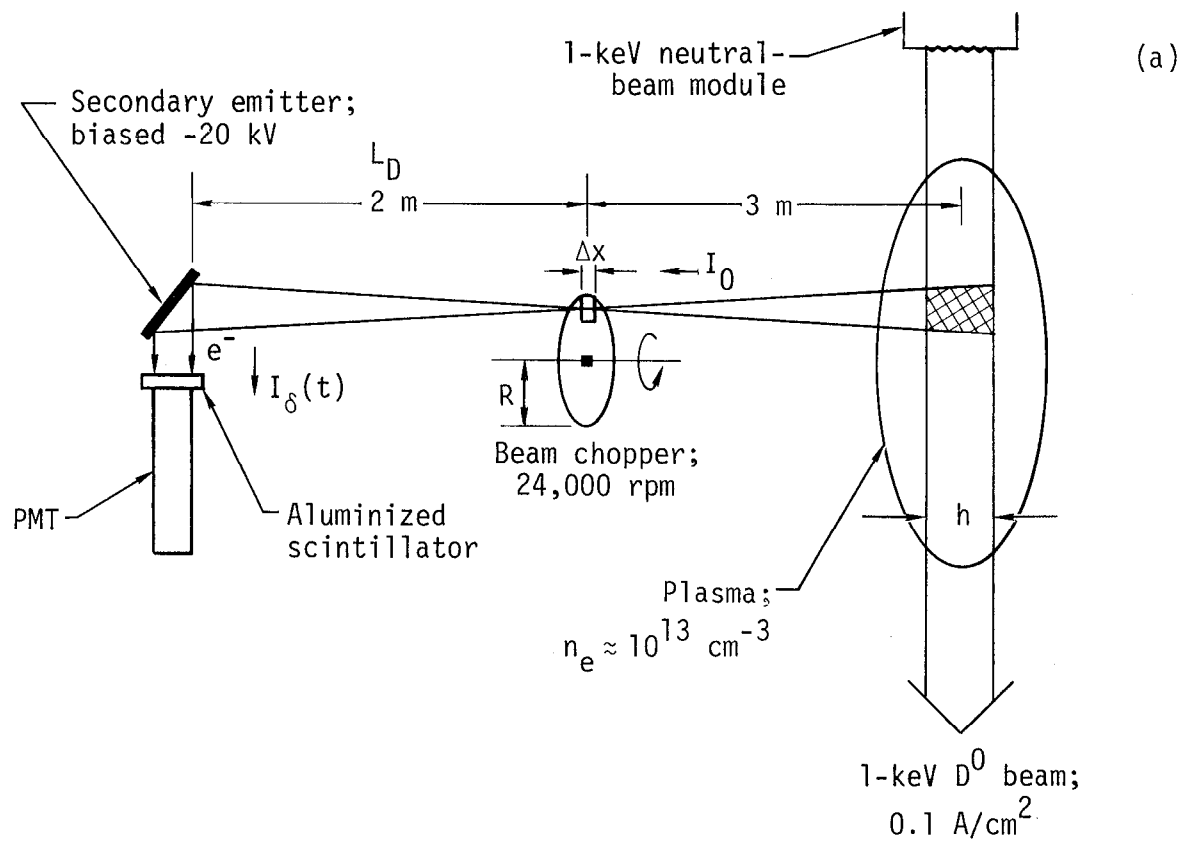


Fig. A-5. Low-energy ion analyzer, showing (a) sketch of analyzer and (b) detector currents versus time for  $kT = 50 \text{ eV}$  and  $kT = 100 \text{ eV}$ .

where  $\delta$  = secondary emission coefficient ( $\approx 0.1$  at 100 eV) and

$$E_1 = \frac{1}{2} M \left( \frac{L_D}{t + \Delta t} \right)^2$$

$$E_2 = \frac{1}{2} M \left( \frac{L_D}{t} \right)^2.$$

The chop time  $\Delta t$  of the neutral current is related to the slit width  $\Delta x$  by  $\Delta x = 2\pi f R \Delta t$  and is determined by the required energy resolution. Taking  $\frac{\Delta E}{E} = 0.05$  at 100 eV and a flight path  $L_D = 200$  cm gives  $\Delta t = 0.5 \times 10^{-6}$  s. For a wheel radius  $R = 10$  cm and rotation frequency  $f = 400$  Hz,  $\Delta x = 1.3 \times 10^{-2}$  cm. The function  $I_\delta / \delta I_0$  that characterizes the pulse at the detector is plotted in the bottom half of Fig. A-5 for  $kT = 50$  eV and  $kT = 100$  eV.

The precision of the measurement of  $kT$  is determined by the total number of counts at the detector. To estimate the number of counts required for a desired precision, we have used the method of maximum likelihood. Assuming the counts recorded by the detector are grouped into bins according to their arrival time, the likelihood function  $\mathcal{L}$  is the multinomial distribution;

$$\mathcal{L}(kT, kT^*) = N! \prod_i \frac{\rho_i^{\eta_i}}{\eta_i!},$$

where

$N$  = total number of counts

$\eta_i$  = number of counts in the  $i^{\text{th}}$  bin

$$\sum_i \eta_i = N.$$

The probability of  $\rho_i$  of a single count falling in the  $i^{\text{th}}$  bin is a function of  $kT$  given by

$$p_i = \int_{t_i}^{t_{i+1}} \frac{2I_\delta(t)}{\delta I_0 \Delta t} dt.$$

In Fig. A-6 we have plotted  $w = \log_e \mathcal{L}$  as a function of  $kT$  assuming a total number of counts  $N = 1000$  and a set of counts  $\{\eta_i\}$  that would be expected for  $kT^* = 100$  eV and a 2-μs integration time. The one-standard-deviation error

limits occur at the points where  $w$  has decreased by 0.5 from the peak value. From Fig. A-6, we see that 1000 counts are sufficient to insure a one-standard-deviation error of 3 eV. This is probably less than the systematic uncertainty that would arise in calibrating the proposed instrument.

The current  $I_0$  falling on the slit of the toothed wheel is

$$I_0 = \frac{e}{4\pi} n_0 n_c \langle \sigma v \rangle_x h \frac{A_{\text{det}} A_{\text{slit}}}{L_D^2},$$

where

$$\begin{aligned} n_0 &= \text{neutral density} \\ n_c &= \text{plasma density} \approx 10^{13} \text{ cm}^{-3} \\ h &= \text{neutral beam height} \approx 7 \text{ cm} \\ A_{\text{det}} &= \text{detector area} \approx 22.8 \text{ cm}^2 \\ A_{\text{slit}} &= \text{slit area} \approx 1.3 \times 10^{-2} \text{ cm}^2 \\ L_D &= \text{length of drift tube} \approx 200 \text{ cm} \\ \langle \sigma v \rangle_x &= \text{charge exchange rate} = 4.5 \times 10^{-8} \text{ cm}^3/\text{s} \end{aligned}$$

for a 1-keV neutral beam with  $j \approx 0.1 \text{ A/cm}^2$ ,  $n_0 \approx 2 \times 10^{10} \text{ cm}^{-3}$ . Inserting this neutral density, we obtain  $I_0 = 4.4 \times 10^9 \text{ A}$ . The number  $N$  of counts arriving at the detector per chop is then

$$N = \frac{1}{2} \frac{\delta I_0 t}{e}$$

$$\approx 400.$$

Thus,  $kT$  is determined with a statistical precision  $\sqrt{\frac{1000}{400}} \times 3 \approx \pm 5 \text{ eV}$  in a single chop. Successive chops, and therefore successive measurements of  $kT$ , could be spaced every 100  $\mu\text{s}$  because 100  $\mu\text{s}$  is adequate time for collection of the low-energy tail of a  $kT = 100 \text{ eV}$  distribution.

We anticipate this diagnostic will require development of a calibration procedure and electronic instrumentation suitable for recording and displaying the time-of-flight spectra.

#### Ion-Beam Probe

A key diagnostic issue in TMX is the measurement of the plasma potential. With the anticipated experimental parameters, it appears that the space

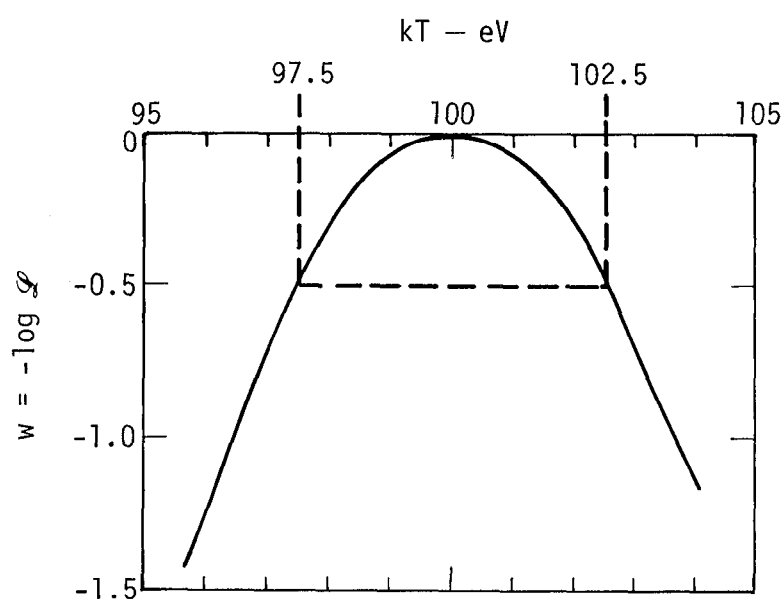


Fig. A-6. Plot of  $w = -\log \mathcal{L}$  versus  $kT$ .

potential, the electron density, and the electron temperature can be measured using various applications of ion-beam probing techniques (A10-12).

In the center solenoidal section, cross-field ion injection of heavy ions (rubidium, cesium) and subsequent detection of the current and energy in the second ionization level produce sufficient information to unfold the space potential, electron density, and electron temperature. This is the usual straightforward application of ion-beam probing, and it can be a valuable diagnostic technique for this experiment.

In the plug section, the usual methods of ion-beam probing are difficult, although still possible. The cross-field ion-probe method would require acceleration potentials near 2 MV in order to inject ions into the mirror; however, the energy change, on the order of 1 kV, is a very small change that would have to be measured.

A better method for measuring the electric potential in the plug is to use a beam of low-energy ( $\sim$ 2-keV) lithium ( $\text{Li}^{++}$ ) ions. A well collimated beam of a few microamperes injected along the magnetic axis into the plasma will ionize to  $\text{Li}^{++}$  ions all along its trajectory, as in the usual cross-field ion-beam diagnostic technique. The  $\text{Li}^{++}$  ions will be electrostatically reflected along a line near the magnetic axis and will return to the detector with an increase in energy, above the injection energy, equal to  $e\phi$ , where  $\phi$  is the plasma potential at the point of creation of the  $\text{Li}^{++}$  ion. Measurement of this energy gain allows the plug potential to be deduced.

Another method from which the plug and central potential may be found by a single measurement is as follows: A  $\text{Li}^{++}$  ion beam is injected along the magnetic axis. In the absence of plasma potential, the time of flight is determined by the initial velocity. By chopping the beam and modulating the energy, the time of flight through the machine may be measured by a detector on the opposite end. The signal on a detector located at the near end disappears when the beam energy exceeds the plug potential. Since the time of flight is determined by the average potential, and the plug potential is known, the central-cell potential  $\phi_c$  may be deduced.

The  $\phi_c$  obtained would rely on the assumption that the potential is constant (zero parallel electric field) within the solenoid region — a good approximation if measurement shows that the density  $n_e$  and field  $B_c$  are uniform.

#### A9. PLASMA/WALL CHARGE-EXCHANGE INTERACTIONS IN THE 2XIIB MAGNETIC MIRROR EXPERIMENT

This appendix discusses wall bombardment by energetic charge-exchange atoms from the 2XIIB mirror-confined plasma.<sup>A13-16</sup> Figure A-7(a) illustrates the basic process. Neutral-beam injection into the plasma results in energetic charge-exchange products bombarding the wall. Backscatter of primary atoms or gas released from the walls can cause charge-exchange loss on the plasma surface if it is not pumped away. To reduce the amount of particle reflux and gas release, the walls in 2XIIB are gettered prior to each shot with several monolayers of titanium. This produces a cleaner surface with the ability to adsorb energetic atoms. Calculations described below show that if hot ions are lost at a rate equal to the charge-exchange loss rate on background gas, then the experimental measurements of buildup of hot-plasma density cannot be explained. This suggests that the hot interior is shielded from the cold gas by a region of lower density and temperature plasma as schematically illustrated in Fig. A-7(b). The required particle confinement in this shield is  $n\tau_s \sim 10^9 \text{ cm}^{-3} \cdot \text{s}$ .

Figure A-8 shows the outline of the plasma and vacuum chamber. The plasma volume is 4.5 to 6.5 litres, whereas the central vacuum chamber volume is 3,400 litres. The plasma radius is 7 to 8 cm, while the average vacuum chamber wall radius is about 50 cm. Along magnetic field lines, the plasma length is 25 to 40 cm, in contrast to the vacuum chamber length of 700 cm. The untrapped neutral beam is dumped into the opposite beam tank 190 cm from the plasma. The large vacuum chamber dimensions, relative to the plasma dimensions, help minimize the effect of plasma/wall interaction.

The principal 2XIIB plasma parameters<sup>A13-15</sup> are  $n_e \leq 1.5 \times 10^{14} \text{ cm}^{-3}$ ,  $\bar{W}_i = 3 - 13 \text{ keV}$ , and  $T_e \leq 85 \text{ eV}$ . The plasma is sustained by a neutral-beam system consisting of 12 neutral-beam injectors operating with extraction energies as high as 20 keV. Up to 4.8 MW of deuterium atoms have been injected. The plasma is maintained in a condition of marginal stability with respect to the drift-cyclotron loss-cone instability by means of a low-energy plasma stream supplied either from a plasma gun or by ionization of gas supplied at the mirror throat.

The charge-exchange flux is peaked near  $90^\circ$  as indicated in Fig. A-8 because ions are initially injected near  $90^\circ$  to the magnetic axis. The ions diffuse principally by electron drag and turbulent diffusion for waves with

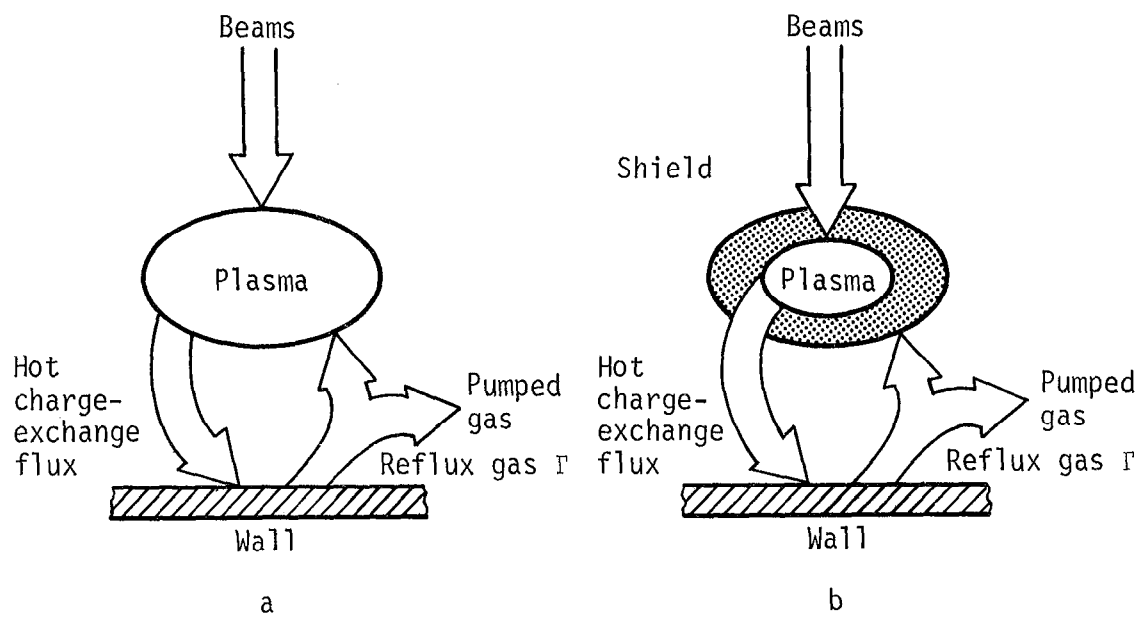


Fig. A-7. Plasma charge-exchange interaction with wall of vacuum chamber:  
 (a) cold gas penetrates directly to the interior, and (b) cold gas  
 is shielded from the interior by a boundary layer.

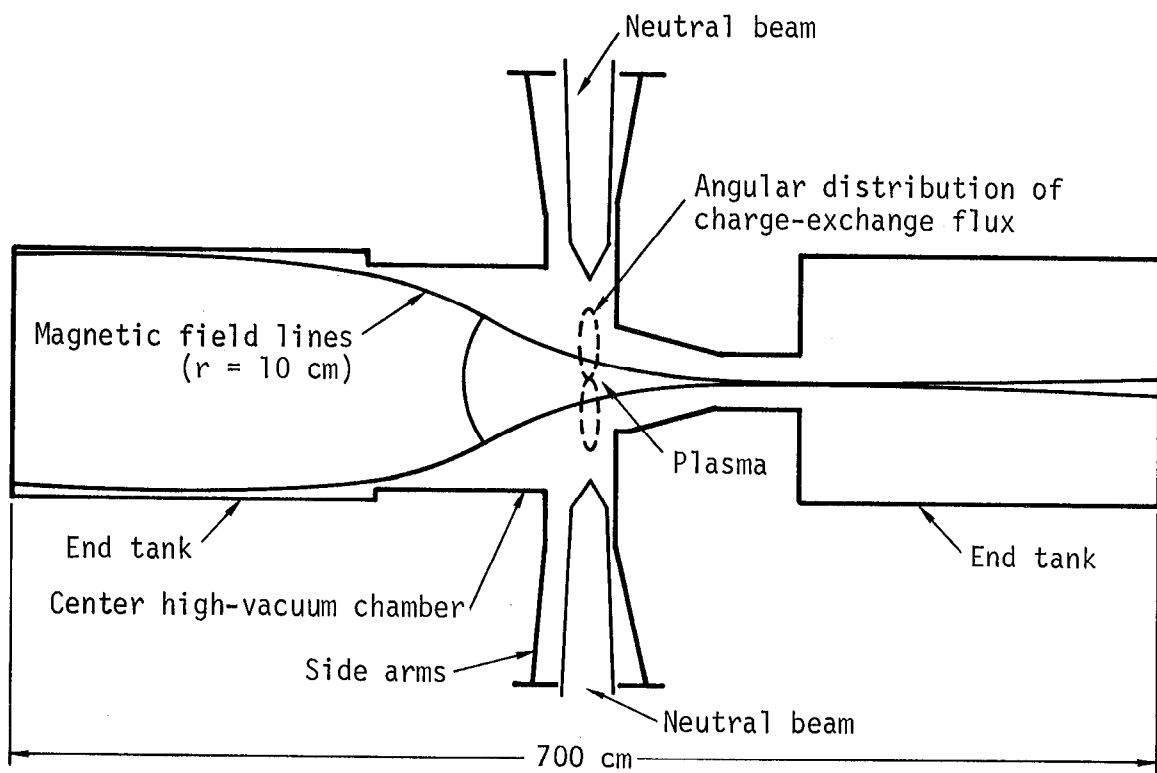


Fig. A-8. To-scale schematic of 2XIIIB plasma and central vacuum chamber.  
Neutral-beam injection is from two 23,000-litre tanks (not shown).

$k_{\parallel} \ll k_{\perp}$ , which do not cause significant angular diffusion. For walls 50 cm from the plasma, the first-wall bombardment flux is  $10^{17}$  atoms  $\text{cm}^{-2} \cdot \text{s}^{-1}$  at a peak power level of  $200 \text{ W} \cdot \text{cm}^{-2}$  for the 5- to 10-ms duration of the experiments.

The neutral charge-exchange flux from the plasma surface is measured by an 11-channel analyzer in the range 0.5 to 39 keV. The measured increase of flux due to background gas is shown in Fig. A-9 for 260 A of injected neutral-beam current. The background gas creating the charge-exchange flux in the figure is produced by wall reflux of plasma ions which charge exchange on the neutral atom beam.

To a good approximation, the background gas density  $n_0$  increases as

$$V \frac{dn_0}{dt} = \Gamma \left( I_{cx} + \frac{1}{4} n_0 v_0 A_p \sigma_x / \sigma_T \right) - \frac{1}{4} n_0 v_0 A_{pump}, \quad (\text{A47})$$

where  $V$  is the volume filled by the gas with speed  $v_0$ . The reflux coefficient  $\Gamma$  is the number of atoms from the wall per incident energetic charge-exchange atom. The first term in the parenthesis,  $I_{cx}$ , is the charge-exchange current from the neutral beam on the hot plasma, while the second term is the charge-exchange current from background gas at the plasma surface. The effective pumping area for cold gas is  $A_{pump} = A_p + s_w A_w + A_x$ . Here  $A_p$ ,  $A_w$ , and  $A_x$  are the areas of the plasma surface, wall, and external pumping opening, respectively, and  $s_w$  is the wall-sticking coefficient. Charge-exchange and total ionization cross sections for cold gas are  $\sigma_x$  and  $\sigma_T$ , respectively. The source of cold gas is wall reflux of energetic charge-exchange neutrals, while pumping is by gettered walls, conducting apertures in the plasma chamber walls, and ionization by the plasma. The ionized gas is assumed to flow along field lines and out the mirrors into the end tanks.

The buildup of charge-exchange flux predicted by Eq. (A47) has been fitted to the data with the curve in Fig. A-9 for two extreme limits. In the first limit, we assume a perfect beam dump, i.e. that untrapped beam current does not cause gas reflux. In the second limit, we assume that all the untrapped beam, as well as charge-exchange current  $I_{cx}$ , causes gas reflux. In the first limit, we fit the measured data with  $\Gamma = 1.5$  and  $v_0$  corresponding to  $E_0 = 14\text{-eV}$  deuterium, whereas in the second limit we find  $\Gamma = 0.5$  and  $E_0 = 3 \text{ eV}$ .

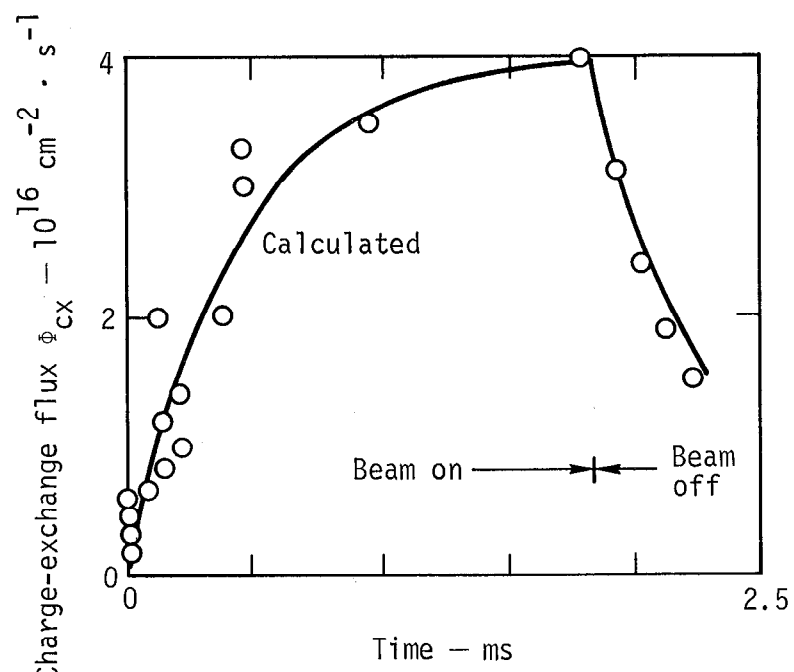


Fig. A-9. Measured and calculated charge-exchange flux versus time.

The expected reflux coefficient has been estimated by averaging the backscattering coefficient, which is a function of energy, over the measured energy distribution of the particles bombarding the surface. For a typical 2XIIIB energy distribution bombarding a clean titanium surface at perpendicular incidence, this coefficient is estimated to be 0.15. The higher values needed to match the experiment are attributed to the angular dependence of backscatter coefficient and to release of gas from the surface.

A radial buildup code<sup>(A17)</sup> (BUILDUP III) computes time-dependent radial density profiles created by injection of neutral beams. This code balances the neutral-beam input with particle losses due to Coulomb losses and erosion of the plasma boundary by background gas. The calculation is one-dimensional, assuming symmetry about the magnetic axis. Particle rate equations for plasma density are solved taking into account neutral beam attenuation and charge-exchange reactions between the injected beam atoms and the plasma ions. Finite Larmor radius effects are treated by simultaneously calculating the guiding center and plasma-particle densities for the ions, assuming circular orbits.

In the calculation, three neutral beams are injected having a current profile similar to the experimental beams. To simulate buildup on a plasma stream, a time-independent, cylindrical plasma target is included in the code. The target density is adjusted to match the initial plasma buildup rates of the calculation and the experiment. To simulate the experimental measurements of plasma density buildup, several input parameters determined from experimental measurements are required. These include the particle confinement parameter  $n\tau$ , the plasma length measured from microwave interferometry, and the wall reflux coefficient obtained by the method already described.

The dashed curve in Fig. A-10 shows a computed radial profile for  $\Gamma = 0$ . The normalized profile is insensitive to charge-exchange losses since the plasma size is determined by beam geometry and plasma ion Larmor radius. Also plotted in Fig. A-10 is a typical profile measured by neutral-beam attenuation through several plasma chords for similar plasma conditions and a normalized Langmuir probe density measurement at 20 cm. The measured and computed profiles are in agreement.

Loss rates by charge exchange are comparable to beam trapping rates for the value of reflux coefficient inferred from the experiment. Consequently, the calculated time dependence of plasma buildup is strongly dependent on  $\Gamma$ ,

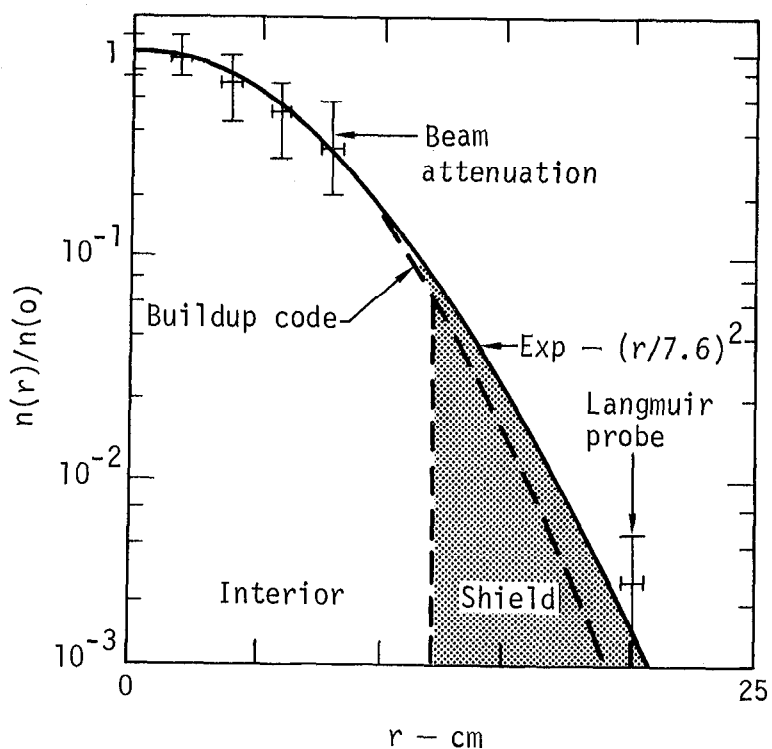


Fig. A-10. Measured and calculated radial density profile normalized to central density.

as shown in Fig. A-11. For these calculations, the computed buildup is insensitive to  $n\tau$  for  $n > 4 \times 10^{10} \text{ cm}^{-3} \cdot \text{s}$ . An important result of the calculation is that good agreement between the experiment and calculation can be obtained only if charge-exchange losses on cold gas are neglected when beams are on during buildup. The calculated dashed curves are shown in Fig. A-11 along with the line density measured by microwave interferometry (solid curve). However, if gas losses are included after beams are turned off, agreement is obtained for the plasma decay rate for values of  $\Gamma$  consistent with Fig. A-9, as shown in Fig. A-11. These calculations suggest that the plasma is shielded from cold-gas losses when beams are on.

Langmuir probe measurements indicate the presence of a plasma density in the  $10^{11} \text{ cm}^{-3}$  range with 16-eV electron temperature at a 20-cm radius. To attenuate several eV energy neutrals, a line density of  $\sim 10^{13} \text{ cm}^{-2}$  is sufficient. For a central density  $n(0) = 5 \times 10^{13} \text{ cm}^{-3}$ , the plasma is one mean free path thick to the gas at  $r = 12 \text{ cm}$ , as indicated schematically in Fig. A-10.

The source of particles and energy for the shield are not clearly evident. However, the following picture is consistent with our present measurements. Particles are supplied to the shield from the cold gas and from the plasma stream. With beams on, the residual ion-cyclotron turbulence level is sufficiently high to heat and mirror trap some of these cold ions. Electrons are heated by these ions as well as by neutral-beam-injected ions trapped in the gas shield. When beams are turned off, the turbulence level decreases and the lifetime of cold ions in the shield is too short to maintain a sufficient density to attenuate the cold gas. Langmuir probe measurements indicate that the shield decays rapidly when the beams are turned off. The hot plasma then decays by charge-exchange erosion at the expected rate, as shown in Fig. A-11.

In summary, the experimental plasma density measurements can be modeled by the buildup code if a plasma shield exists having sufficient density and energy to attenuate cold gas impinging on the plasma surface. Two important consequences of the plasma shield are: first, a reduction in the ion heat loss by cold-gas charge exchange since a relatively cool ion is lost rather than a hot ion; and second, that particle input to the plasma boundary need not be supplied by neutral-beam trapping alone.

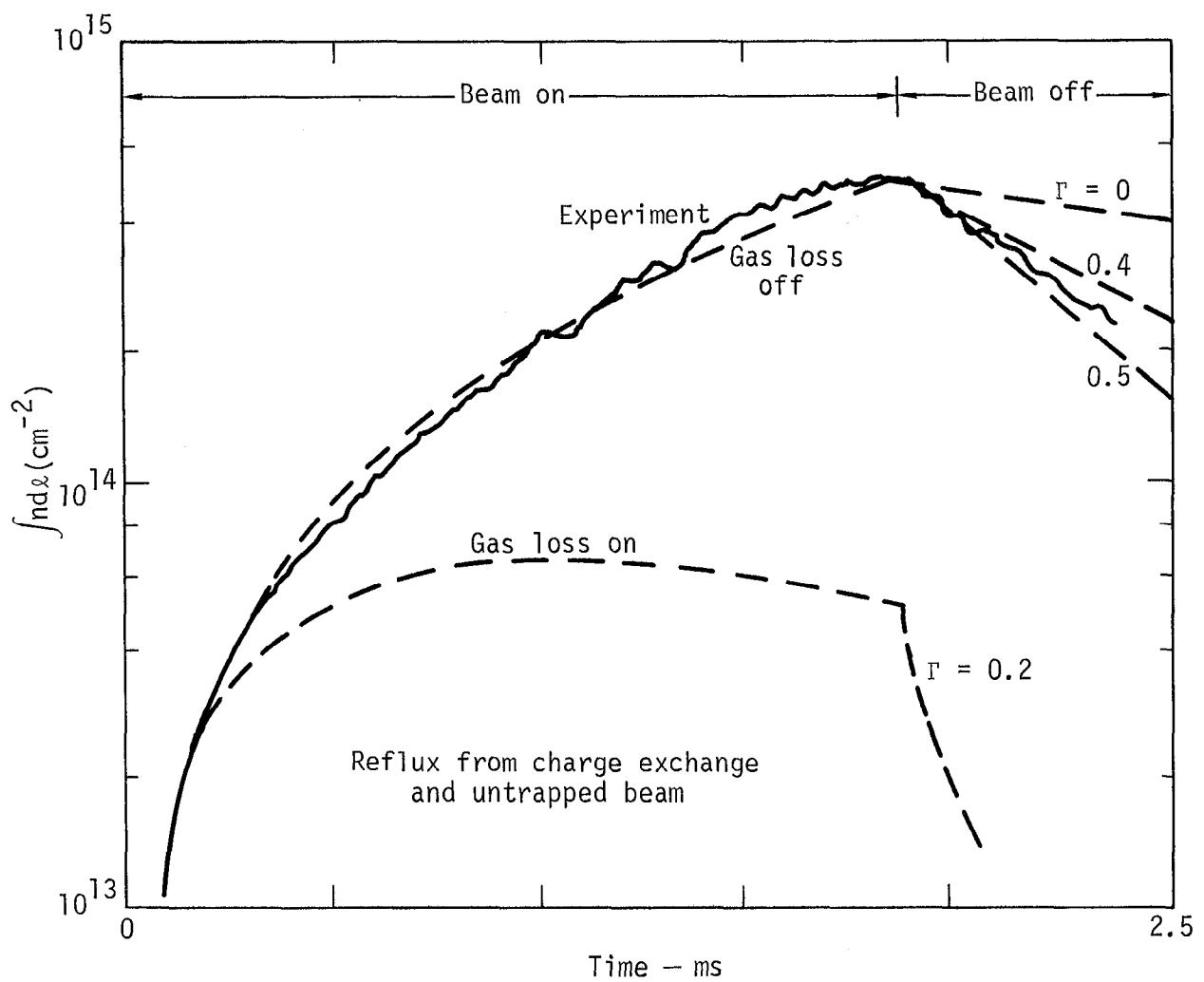


Fig. A-11. Measured and calculated line-density buildup with 260-A, 14-keV neutral-beam injection.

## A10. TMX NEUTRON YIELDS

Operation of TMX with deuterium can result in an appreciable neutron production rate. With a realistic estimate of the duty cycle, it appears that without neutron shielding, the yearly average 40-h/wk occupational exposure limit may be exceeded by personnel stationed closer than 10 m to the plug. Since a successful series of experiments could result in a large increase in the neutron yield over that calculated for the initial set of parameters, we conclude that some neutron shielding should be incorporated in the initial construction.

The neutron yield/plug is

$$Y = 1/3 K \hat{n}^2 \times \pi r_p^2 L_p \langle \sigma v \rangle_{DDn}$$

here  $\hat{n}$  is the peak density,  $r_p$  and  $L_p$  are the plasma radius and length such that

$$N = \hat{n} \times \pi r_p^2 L_p = \text{total number of ions in the plasma,}$$

and

$$K = \frac{\int n^2 dV}{\hat{n}^2 \times \pi r_p^2 L_p} \approx 0.35.$$

The factor of  $\sim 1/3$  applies to plasmas with small  $r_p/a_i$ . It reflects the fact that whereas in an isotropic plasma near-headon collisions produce a large fraction of the neutron reactions, such collisions are rare in plasmas with small  $r_p/a_i$ .

For  $T_p = 26$  keV, we take  $\langle \sigma v \rangle_{DDn}$  equal to  $3 \times 10^{18}$ . From this, it follows that

$$Y = \pi \times 10^{10} \frac{[B(kG)]^4}{[T_i(\text{keV})]^2} \hat{\beta}^2 r_p^2,$$

(taking  $L_p = 40$  cm).

The presently planned TMX parameters are  $\beta = 1/2$ ,  $B = 10$  kG,  $T_i = 26$  keV and taking  $r_p = 7$  cm we find the yield/plug to be

$$y \approx 6 \times 10^{12} \text{ neutrons/s} .$$

The neutron production from the center solenoid can be ignored.

If we assume a pulse repetition rate of 100 25-ms pulses per week (80 h), the average DD source strength is

$$\bar{s}_{DD} = \frac{12 \times 10^{12} \times 0.025 \times 100}{80 \times 3600} \approx 10^8 \text{ neutrons/s} .$$

At a distance of 10 m, the average dose rate is

$$\phi_{DD} = \frac{\bar{s}_{DD}}{4\pi (1000)^2} = \frac{10^8}{4\pi \times 10^6} \approx 8 \text{ neutrons/cm}^2 \cdot \text{s} \approx 1 \text{ mrem/h.}$$

The design yearly average 40 h/wk occupational exposure limit for a facility is 0.5 mrem/h. Since the chosen set of parameters only exceeds this limit by a factor of two, and we have not taken into account the attenuation of the neutrons in the coil structures and tanks, it appears questionable whether shielding would be necessary if this yield was the largest expected from TMX. However, the possible increases in  $\beta$ ,  $r_p$ , and duty cycle could easily lead to between one and two orders of magnitude increase in the average DD source strength.

## REFERENCES

- A1. V. P. Pastukhov, *Nucl. Fusion* 14, 3 (1974).
- A2. L. S. Hall and B. McNamara, *Phys. Fluids* 18, 552 (1975).
- A3. W. A. Newcomb and L. D. Pearlstein, in *Committee Report: LLL Re-evaluation of the Simple Mirror Force Fusion Reactor*, R. W. Moir, Ed., Lawrence Livermore Laboratory Rept. UCID-16736 (1975).
- A4. J. P. Freidberg, private communications.
- A5. D. E. Baldwin, H. L. Berk, J. A. Byers, R. H. Cohen, T. A. Cutler, N. Maron, L. D. Pearlstein, M. E. Rensink, T. D. Rognlien, J. J. Stewart, D. C. Watson, and M. J. Gerver, *Present Status of Mirror Stability Theory*, Lawrence Livermore Laboratory Rept. UCID-17038 (1976).
- A6. R. H. Cohen, G. Rowlands, and J. H. Foote, *Nonadiabaticity in Mirror Machines*, Lawrence Livermore Laboratory Rept. UCRL-78889 (1976); to be submitted to *Phys. Fluids*.
- A7. B. McNamara, D. V. Anderson, J. K. Boyd, J. A. Byers, R. H. Cohen, T. A. Cutler, L. S. Hall, R. F. Post, and M. E. Rensink, "Theory of Mirror Machines at High  $\beta$ ," in *Proc. 6th Inter. Conf. Plasma Physics and Controlled Nuclear Fusion Research, Berchtesgaden, Fed. Rep. of Germany, 1976* (IAEA, in preparation), Paper CN-35/C3; also Lawrence Livermore Laboratory, Rept. UCRL-78123 (1976).
- A8. G. D. Hobbs and J. D. Wess, "Heat Transmission through a Langmuir Sheath in the Presence of Electron Emission, Culham Rept. GLM-R61 (1966).
- A9. L. S. Hall, *Electron Dynamics and the Enhancement of Q in Mirror Magnetic Wells*, Lawrence Livermore Laboratory Rept. UCRL-78296 (1976); submitted to *Nucl. Fusion*.
- A10. J. C. Hosea, F. C. Jobes, R. L. Hickok, A. N. Dellis, *Phys. Rev. Lett.* 30, 839 (1973).
- A11. F. C. Jobes and R. L. Hickok, *Nucl. Fusion* 10, 195 (1970).
- A12. R. E. Reinovsky, W. C. Jennings, and R. L. Hickok, *Phys. Fluids* 16, 1772 (1973).
- A13. F. H. Coensgen, W. F. Cummins, B. G. Logan, A. W. Molvik, W. E. Nexsen, T. C. Simonen, B. W. Stallard, and W. C. Turner, *Phys. Rev. Lett.* 35, 1501, (1975).

- A14. F. H. Coensgen, W. F. Cummins, C. Gormezano, B. G. Logan, A. W. Molvik, W. E. Nexsen, T. C. Simonen, B. W. Stallard, and W. C. Turner, *Phys. Rev. Lett.* 37, 143, (1976).
- A15. F. H. Coensgen, J. F. Clauser, D. L. Correll, W. F. Cummins, C. Gormezano, B. G. Logan, A. W. Molvik, W. E. Nexsen, T. C. Simonen, B. W. Stallard, and W. C. Turner, "2XIIB Plasma Confinement Experiments," in *Proc. 6th Inter. Conf. Plasma Physics and Controlled Nuclear Fusion, Berchtesgaden, Fed. Rep. of Germany 1976* (IAEA, in preparation) Paper CN-35/C1; also Lawrence Livermore Laboratory, Rept. UCRL-78121, Rev. 1 (1976).
- A16. T. C. Simonen, R. H. Bulmer, F. H. Coensgen, W. F. Cummins, C. Gormezano, B. G. Logan, A. W. Molvik, W. E. Nexsen, W. C. Turner, B. W. Stallard, G. E. Vogtlin, and R. R. Vandervoort, *Control of First-Wall Surface Conditions in the 2XIIB Magnetic Mirror Plasma Confinement Experiment*, Lawrence Livermore Laboratory, Rept. UCRL-77600 (1976); to be published in *J. Nucl. Mater.*
- A17. B. W. Stallard, *Radial Plasma Buildup Code for Neutral Beam Injection into a Mirror Machine*, Lawrence Livermore Laboratory, Rept. UCRL-51784 (1975).

APPENDIX B. TANDEM MIRROR REACTOR SCALING

(*B. G. Logan*)

The primary motivation for considering the Tandem Mirror configuration (Fig. B-1) as a mirror fusion reactor is to increase  $Q \equiv$  fusion power/injection power so as to reduce the fractional recirculating power, thereby reducing the cost of power \$/kW(e) net. In addition to an improved  $Q$ , the Tandem Mirror concept incorporates a simple magnetic structure - a low-field solenoid - to confine the main fusion plasma, which should also result in reduced cost of power. Many issues such as microstability, MHD stability, beta limits, impurity and alpha particle trapping, to name a few, must eventually be addressed by theory and experiment before the feasibility of the Tandem Mirror as a reactor can be fully assessed. To be a viable candidate for a reactor, however, the Tandem Mirror concept should offer an economic  $Q$  ( $Q \gtrsim 5$ ) at a reasonable power ( $P_{\text{net}} < 1 \text{ GW}$ ), with stability being assumed. The purpose of this Appendix is therefore limited to showing that the Tandem Mirror does promise a high  $Q$  at moderate power, given classical loss rates, and the availability of high-efficiency, high-energy neutral beams.

In the Tandem Mirror configuration shown in Fig. B-1, the plugs are assumed to be classical mirror machines sustained by high-energy neutral-beam injection. Ion particle losses from the central cell are replenished by injection of low-energy neutral beams or gas at the thin plasma fans in the inner mirror throats. Since electrons exchange rapidly between the plugs and the central cell, the electron temperature  $T_e$  in the plugs will be the same in the central cell. Thus, electrons heated by the energetic ions in the plugs (plug ion energy  $E_p > 10 T_e$ ) can in turn heat the cold ions generated in the central cell, provided the central ion temperature  $T_c < T_e$ . In this way, a fraction of the neutral-beam power required to maintain the plugs can be "reused" to energetically sustain the central cell. In addition to power input from the plugs, the central ions and electrons are both heated by fusion alpha particles born at 3.5 MeV with velocity vectors oriented so that the particles are trapped by the mirrors. Some fraction  $1 > f_\alpha > 0$  of the fusion alphas will be adiabatically confined between the mirrors of the central cell for a sufficient time to thermalize. The partition of alpha energy to ions and electrons depends on  $T_e$ , with more energy going to ions for  $T_e > 33 \text{ keV}$ . When the energy input of the alphas is not sufficient to ignite the central cell, one can consider an external power input to the central cell to augment the power input from the plugs. Since maintaining  $T_e > T_c$  will be desirable to improve central ion confinement, methods such as ECRH that heat electrons are preferred over methods that would heat ions, e.g., energetic neutral injection

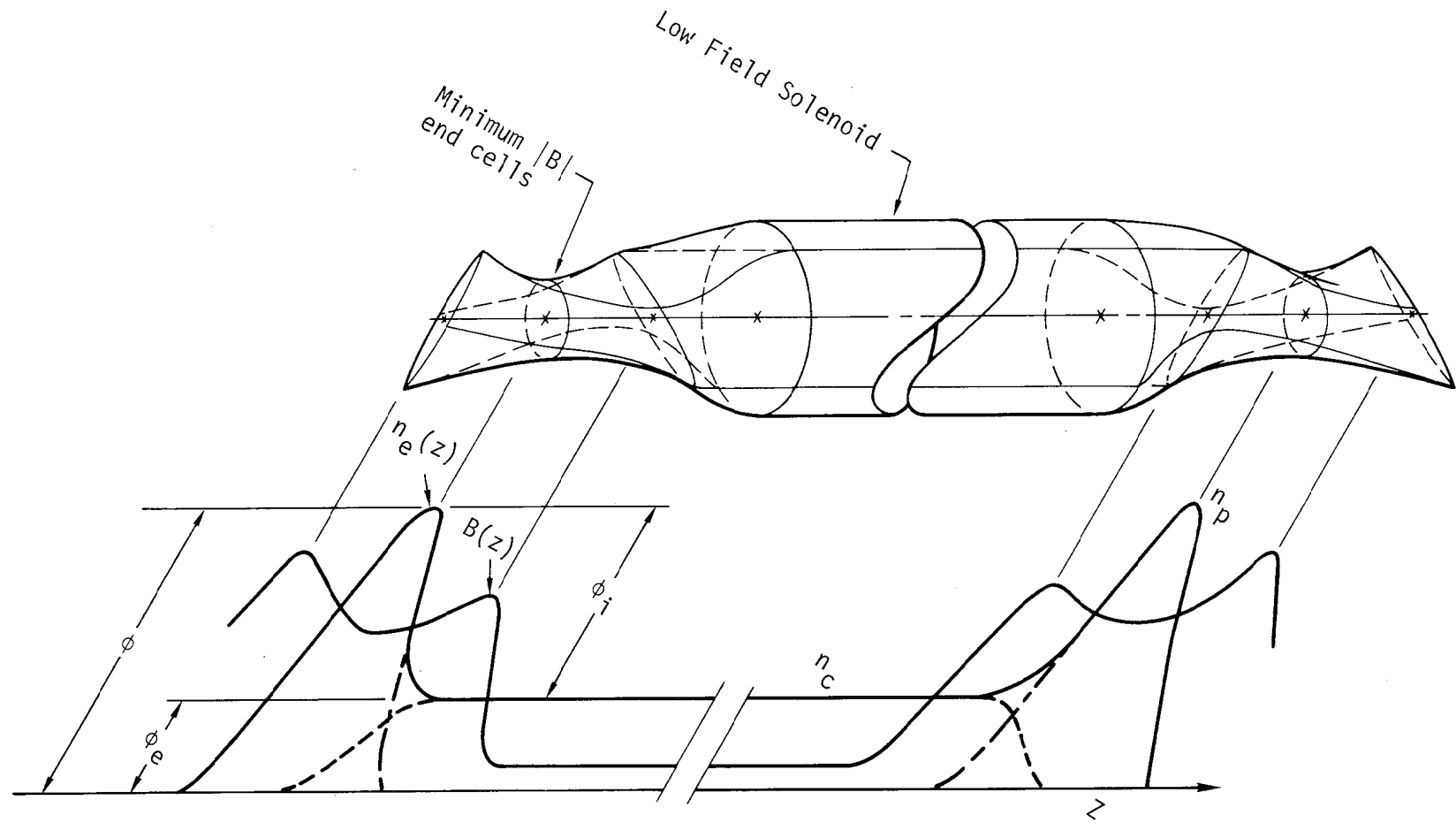


Fig. B-1. Tandem mirror with ambipolar barriers at the ends.

into the central cell. Lacking a clear means of efficiently producing high-power ECRH, we devote primary consideration here to the case where the central cell is sustained solely by electron heating in the plugs and by alpha particles; thus, the entire Tandem Mirror system is powered by high-energy neutral beams injected only into the plugs at the ends.

At  $T_c \approx 20$  to  $40$  keV, the probability for charge exchange of an injected neutral atom in the central cell is several times greater than for ionization. Therefore, associated with the ionization rate needed to replace ion particle losses in the solenoid there is an ion energy loss of  $3$  to  $10 T_c$  per ion created, depending on  $T_c$ . This energy drain by charge exchange from the central ions is sufficient to keep  $T_c < T_e$  even with containment of most of the alphas ( $f_\alpha > 0.5$ ) that would otherwise heat the ions to  $T_c > T_e$ . Because of the peculiar nature of electrostatic confinement of central cell ions in the Tandem Mirror, the improvement in  $nT$  from a lower value of  $T_c/T_e$  more than compensates for the effects of ion energy loss due to charge-exchange cooling. Thus, charge-exchange cooling turns out to be a beneficial effect.

In the following model, we take into account the important effects of ion and electron heating by fast alphas and the pressure of the hot alphas. However, since the equilibrium density of the hot alphas that are doing the heating is typically only 1% of  $n_e$ , the density of hot alphas is neglected, and  $n_e$  is set equal to  $n_c$  in the central cell. The effects of an accumulation of thermalized alphas in the potential well require further investigation beyond the scope of this work. For present purposes, we assume, following Dimov,<sup>B1</sup> that there is some mechanism for removing thermalized alphas, and we neglect their density. In the absence of such a mechanism, the Q's derived will be those of the system before an appreciable alpha ash builds up. Electron energy loss by bremsstrahlung and synchrotron radiation is neglected because it is typically less than 5% of the fusion power. The two ion species used for fuel, deuterium and tritium, are treated as one ion species with an effective mass = 2.5 amu. To ease engineering requirements for the end cells, we assume that the plugs consist of a single injected species - deuterium. Thus, contributions of fusion power from the plugs are neglected whereas the plug injection power is included in determining Q for the system. Because the potential drop  $\phi$  on the outside is greater than the drop  $\phi_c$  on the inside (see Fig. B-1), few of the plug ions will exit into the center cell if all mirror fields are equal. The model simplifies then to one ion species in the center cell and in the plugs, and one electron species throughout.

The magnitude of the potential barrier  $\phi_c$  for the central-cell ions is given by

$$\phi_c = T_e \ln \left( \frac{n_p}{n_c} \right), \quad (B1)$$

where  $n_p$  is the plug density and  $n_c$  is the solenoid density. Pastukhov<sup>B2</sup> shows that for  $\phi_c \gtrsim 2T_c$ , the ion confinement parameter  $(n\tau)_c$  in the center cell is given approximately by

$$(n\tau)_c \approx n\tau_{ii} g(R_c) \left( \frac{\phi_c}{T_c} \right) \exp \left( \frac{\phi_c}{T_c} \right), \quad (B2)$$

where  $\tau_{ii}$  is the Spitzer 90° self-collision time, and  $g(R_c) = \sqrt{\pi} (2R_c + 1) \ln(4R_c + 2)/4R_c$  is a slow function of the central-cell mirror ratio  $R_c = B(\text{mirror})/B(\text{solenoid})$ . For DT ions,  $\ln \Lambda = 20$ , and a typical value of  $R_c = 20$ , Eq. (B-2) [using Eq. (B-1)] becomes

$$(n\tau)_c \approx 8.7 \times 10^{10} T_c^{3/2} \left( \frac{T_e}{T_c} \right) \ln \left( \frac{n_p}{n_c} \right) \left( \frac{n_p}{n_c} \right)^{T_e/T_c} \text{cm}^{-3} \cdot \text{s}, \quad (B3)$$

where  $T_c$  is in keV. The coefficient  $8.7 \times 10^{10}$  obtained from a 2-dimensional Fokker-Planck calculation is 10% lower than that given by Eq. (B2). Eq. (B3) shows the desirability of maintaining  $T_e > T_c$  to enhance the ion confinement for a given density ratio  $n_p/n_c$ .

For the typical case in which the ion loss current from the central cell is at least predominant over the ion loss current from the plugs, one can determine the electron potential  $\phi_e$  (see Fig. B-1) to 5% by assuming equal ion and electron lifetimes in the central cell. This determination is sufficiently accurate even though such equality may be only very roughly satisfied with the finite plug current

$$(n\tau)_e \approx (n\tau)_c. \quad (B4)$$

In Eq. (B4),  $(n\tau)_e$  is given by a formula similar to Eq. (B2), using an electron collision time reduced by a factor of 2 due to collisions of electrons with ions:

$$(n\tau)_e = 9 \times 10^8 T_e^{3/2} \left( \frac{\phi_e}{T_e} \right) \exp \left( \frac{\phi_e}{T_e} \right). \quad (B5)$$

For typical values of  $n\tau = 10^{15} \text{ cm}^{-3}\text{s}$  and  $T_e = 60 \text{ keV}$ , Eq. (B5) gives a value  $\phi_e/T_e = 6$ , which slowly varies with  $n\tau$  and  $T_e$ . For injection energies  $E_{inj} > 20 T_e$  and plug mirror ratios  $R_p = 2.5$ , an approximate formula for  $(n\tau)_p$  derived from Fokker-Planck calculations is given for deuterium by

$$(n\tau)_p \approx 10^{10} E_p^{3/2}, \quad (\text{B6})$$

where  $E_p$  is in keV. With short, fat plasmas at high beta, such as in the 2XIIIB experiment,<sup>B3</sup> an effective mirror ratio  $R_p = 2.5$  might be produced largely be the diamagnetic self-field of the plasma, aided by a slight vacuum mirror ratio of a few percent. The average energy of a plug ion  $E_p$  is less than  $E_{inj}$  due to the drag on colder electrons. An approximate relationship between  $E_p$ ,  $E_{inj}$ , and  $T_e$  based on Fokker-Planck calculations is given by

$$E_p \approx 3.9 \sqrt{T_e E_{inj}}, \quad (\text{B7})$$

which is valid in the range  $20 \lesssim E_{inj}/T_e \lesssim 40$ . All units are in keV. The characteristic equilibration time between ions and electrons given by Spitzer is

$$(n\tau)_{ei} = 10^{12} T_e^{3/2} \quad (\text{B8})$$

for DT ions and  $\ln \Lambda = 20$  in this case. For  $\phi_c > 2T_c$ , we note that both Pastukhov<sup>B2</sup> and recent Fokker-Planck calculations show that the average energy carried out by central ions escaping their potential barrier is  $\phi_c + T_c$ ; correspondingly, the energy carried out by electrons accompanying those ions is  $\phi_e + T_e$ . We can now write down the expressions for power balance for central ions,

$$\frac{n_c^2 \left[ \phi_c + T_c \left( 1 + \frac{3}{2} \frac{\langle \sigma v \rangle_{cx}}{\langle \sigma v \rangle_{ion}} \right) \right]}{(n\tau)_c} = \frac{n_c^2 \left( \frac{3}{2} \right) (T_e - T_c)}{(n\tau)_{ei}} + \frac{1}{4} n_c^2 \langle \sigma v \rangle E_\alpha f_\alpha (1 - f_e), \quad (\text{B9})$$

and for electrons,

$$\begin{aligned}
& \frac{n_c^2(\phi_e + T_e)}{(n\tau)_c} + \frac{n_c^2 \left( \frac{3}{2} (T_e - T_c) \right)}{(n\tau)_{ei}} + \frac{n_p^2(\phi_e + \phi_c + T_e)}{(n\tau)_p(V_c/V_p)} \\
& = \frac{n_p^2 E}{(n\tau)_{ei} (V_c/V_p)} + \frac{1}{4} n_c^2 \langle \sigma v \rangle E \alpha f_\alpha f_e + P_{e-aux}. \tag{B10}
\end{aligned}$$

In Eq. (B9), the factor  $\left( 1 + \frac{3}{2} \frac{\langle \sigma v \rangle_{cx}}{\langle \sigma v \rangle_{ion}} \right)$  appearing

in the first term of the left-hand side represents the energy carried out by charge-exchange cooling per ion created by ionization plus the ion temperature, measured in units of  $T_c$ . For most cases here where  $T_e \gtrsim T_c$ , ionization by electrons is small compared to ionization by ions, so that by calculating electron ionization at  $T_e = T_c$ , this factor can be approximated as a function only of ion temperature, valid in the range of  $10 \lesssim T_c \lesssim 50$  keV:

$$\left( 1 + \frac{3}{2} \frac{\langle \sigma v \rangle_{cx}}{\langle \sigma v \rangle_{ion}} \right) \approx 110 T_c^{-0.8}, \tag{B11}$$

where  $T_c$  is in keV. In the right-hand side of Eq. (B9),  $\langle \sigma v \rangle$  is the DT fusion reaction rate,  $E_\alpha = 3500$  keV is the alpha energy,  $f_\alpha$  is the fraction of fast alphas initially contained, and  $(1 - f_e)$  is the fraction of alpha energy given to ions during their slowing down. An approximate expression for the transfer function  $(1 - f_e)$  from calculations by Rose<sup>B4</sup> is given to within 5% by

$$1 - f_e = 0.29 \ln(T_e) - 0.5. \tag{B12}$$

The transfer function  $f_e$  for electrons appearing in the right-hand side of Eq. (B10) is correspondingly

$$f_e = 1.5 - 0.29 \ln(T_e). \tag{B13}$$

In deriving the electron power balance [(Eq. (B10)], we make use of the fact that an electron source density  $n_c^2/(n\tau)_c$  accompanies the neutral atom sources of the center cell, and an electron source density  $n_p^2/(n\tau)_p$ , diluted by the volume ratio  $V_c/V_p$ , is associated with the energetic neutral injection in the

plugs. Electrons starting from the center cell lose  $\phi_e + T_e$  energy upon escape, whereas electrons starting from the plugs lose a larger amount  $\phi_e + \phi_c + T_e$  corresponding to the higher potential in the plugs. We have explicitly included the electron energy loss term due to the plug current, since it is not negligible compared to the losses from the central cell in cases of small tandem mirror systems at low power levels. In Eq. (B10), the first term in the right-hand side represents the power input to electrons from hot ions in the plugs, the second term is power input to electrons from the alphas, and the third term ( $P_{e-aux}$ ) represents an external power input to electrons per unit volume; e.g., ECRH may be present.

To obtain a self-consistent set of solutions to Eqs. (B1) through (B10), one picks the parameters of plug injection energy  $E_{inj}$ , density ratio  $n_p/n_c$  (or equivalently, the injection source strengths in the plugs and center cell), the fraction of contained alphas  $f_\alpha$ , electron temperature  $T_e$ , and external power/volume ( $P_{e-aux}$ ) in the central cell. Eq. (B9) is then solved numerically for  $T_c$ . Then with  $T_c$  determined, Eq. (B10) is solved for the volume ratio  $V_c/V_p = (\text{solenoid volume})/(\text{volume of both plugs})$ , which can be written in the form

$$\frac{V_c}{V_p} = \left( \frac{n_p}{n_c} \right)^2 \frac{\left[ \frac{E_p}{(n\tau)_{ei}} - \frac{\phi_e + \phi_c + T_e}{(n\tau)_p} + \frac{E_{inj} F_{e-aux}}{(n\tau)_p} \right]}{\left[ \frac{(\phi_e + T_e)}{(n\tau)_c} + \frac{3/2(T_e - T_c)}{(n\tau)_{ei}} - \frac{1}{4} \langle \sigma v \rangle E_\alpha f_\alpha f_e \right]}, \quad (B14)$$

where the parameter  $F_{e-aux}$  is the total auxiliary power input to the central-cell electrons, normalized to the plug injection power:

$$F_{e-aux} = \frac{V_c P_{e-aux}}{n_p^2 V_p E_{inj} / (n\tau)_p}. \quad (B15)$$

The overall system Q  $\equiv$  (solenoid fusion power)/(plug injection power +  $V_c P_{e-aux}$ ) can then be calculated from

$$Q = \frac{\frac{1}{4} (n\tau)_p \langle \sigma v \rangle (17.6 \text{ MeV}) (V_c/V_p)}{(n_p/n_c)^2 (E_{inj}) (1+F_{e-aux})} . \quad (B16)$$

Equation (B16) illustrates the fact that the  $Q$  of a Tandem Mirror system is directly related to the size of the system in terms of the volume ratio  $V_c/V_p$ . To achieve a desired  $Q$ , one therefore generally seeks injection parameters that minimize the volume ratio. Equation (B16) also shows that  $Q$  improves directly with the plug confinement  $(n\tau)_p$ . Since the classical  $(n\tau)_p \propto E_{inj}^{3/2}$ , one desires as high an injection energy in the plugs as is consistent with stopping the beam in the plasma ( $E_{inj} \sim 1 \text{ MeV}$ ). In the conventional mirror reactor, the fusion reaction rate  $\langle \sigma v \rangle$  decreases as  $E_p$  is increased above 100 keV, so that  $Q$  is optimized for injection energies near 100 keV. In a Tandem Mirror, however, one can have ion temperatures in the central cell that maximize  $\langle \sigma v \rangle$ , while at the same time improving  $(n\tau)_p$  by injecting the plugs at a much higher energy. Should the plugs suffer losses greater than classical, the  $Q$  can be recovered by increasing the volume ratio. However, the minimum power for that  $Q$  would be increased. Since  $Q$  is by definition a plasma quantity, the efficiencies of power injection from neutral beams and other external sources such as ECRH are not included. For a  $Q = 5$  to imply an acceptably small recirculating power fraction ( $\lesssim 30\%$ ), it is necessary to have a high efficiency ( $> 80\%$ ) for the power injection.

In his investigations of the Tandem Mirror, Dimov<sup>B1</sup> finds a  $Q = 5$  at a reasonable volume ratio  $V_c/V_p = 410$ , utilizing  $E_{inj} = 1 \text{ MeV}$  in the plugs, alpha heating, and ECRH heating for  $F_{e-aux} = 2.5$  times neutral-beam injection power. He neglects the effects of charge-exchange cooling that are included in our formulation above. If we assume present ECRH efficiencies of less than 20% at 100 GHz ( $n_c = 10^{14} \text{ cm}^{-3}$ ), Dimov's case would not produce net power unless substantial improvements were made in high-frequency microwave tube technology. On the other hand, projecting presently known efficiencies for negative-ion beam generation, stripping losses on background gas, and neutralizer efficiencies for neutral beams indicates that neutral-beam efficiencies should improve with energy, to 80% at 1 MeV or more.

In the following examples, high-energy neutral beams in the plugs are the only external sources of energy present to sustain the system. With or without auxiliary electron heating, development of efficient, high-energy neutral beams will be a key requirement for an economic Tandem Mirror reactor.

Figure B-2 shows the variation of  $Q$  with volume ratio  $V_c/V_p$  for a fixed plug injection power, an injection energy  $E_{inj}$  of 1 MeV, and fixed density ratio  $n_p/n_c = 10$  between the plug and the center cell. The plug power is the only external source of energy ( $F_{e-aux} = 0$ ). Alpha heating at  $f_\alpha = 1$  is included, but for this case it is not enough to sustain the central cell (subignition) because of insufficient  $(n\tau)_c$  at  $n_p/n_c = 10$ . As the volume ratio is increased, the power input per unit volume in the central cell is decreased, so that the equilibrium electron and ion temperatures decrease monotonically with  $V_c/V_p$ . At first,  $Q$  increases with  $V_c/V_p$  because the total central-cell fusion power is increasing faster due to volume increase than the fusion power density is decreasing due to decrease in  $T_c$ . Beyond a certain volume ratio, however, the rate of decline in  $\langle \sigma v \rangle$  with  $T_c$  cannot be compensated for by increases in volume, and  $Q$  decreases rapidly. Increasing the density ratio  $n_p/n_c$  to 16.5 in Fig. B-3, while keeping everything else the same as in Fig. B-2, increases  $(n\tau)_c$  to the point where alpha heating alone can sustain the central cell at  $f_\alpha = 1$  (ignition). Thus  $Q$  increases indefinitely with increasing volume ratio.

Keeping  $E_{inj} = 1$  MeV and  $f_\alpha = 1$ , Fig. B-4 shows the maximum  $Q$  as a function of density ratio  $n_p/n_c$  [increasing  $(n\tau)_c$ ]. The volume ratios that maximize  $Q$  at each value of  $n_p/n_c$  are also plotted as a function of  $n_p/n_c$ . The point is that with sufficient density ratio one can achieve any desired  $Q$ ; but the higher the  $Q$ , the larger the volume ratio and power of the system. The volume ratios for each  $Q$  in Fig. B-4 are close to the minimum ratios if one varies  $n_p/n_c$  to minimize  $V_c/V_p$  for a fixed  $Q$ , rather than maximizing  $Q$  for a fixed  $n_p/n_c$  as in Fig. B-4. Since there is a continuous set of values of density ratio  $n_p/n_c$  and volume ratios  $V_c/V_p$  that can give a certain  $Q$ , one wishes to choose those parameters that will minimize the volume ratio for that  $Q$ , to minimize reactor power.

Associated with a consistent set of parameters  $E_{inj}$ ,  $T_e$ ,  $T_i$ ,  $n_p/n_c$ , and  $V_c/V_p$  for a given  $Q$ , there is a relationship between the plasma pressure in the plugs and the plasma pressure in the solenoid. If one then specifies the maximum betas  $\beta_c$  and  $\beta_p$  in the solenoid and plugs, respectively, the solenoid and plug radii  $r_c$  and  $r_p$ , respectively, are determined by conservation of magnetic flux. These relationships, together with the technological constraint of a maximum plug pressure that can be confined in a maximum field and the economic requirement of a minimum fusion power per unit length in the solenoid, uniquely determine the total fusion power for each set of parameters  $E_{inj}$ ,  $T_e$ ,

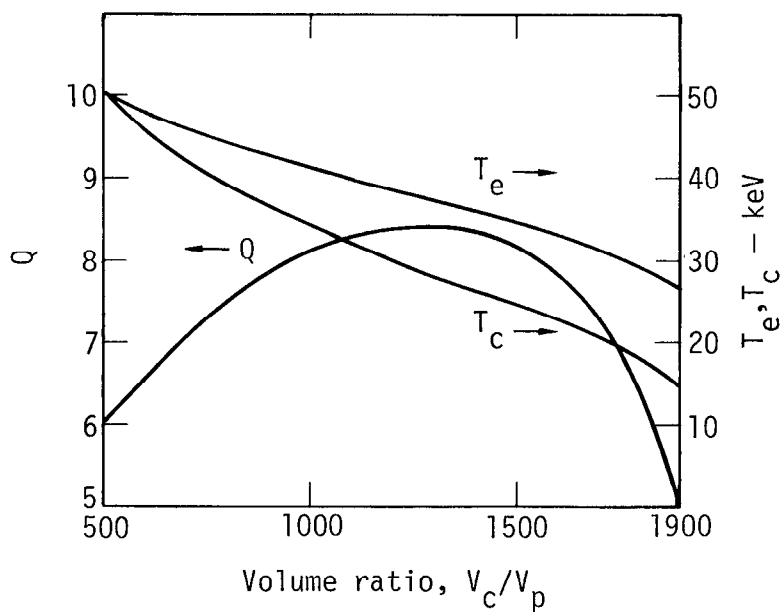


Fig. B-2. Variation of  $Q$ ,  $T_e$ , and  $T_i$  with volume ratio  $V_c/V_p$  (subignition) for  
 $n_p/n_c = 10$   
 $E_{inj} = 1$  MeV  
 $f_\alpha = 1.0$   
 $F_{e-aux} = 0.$

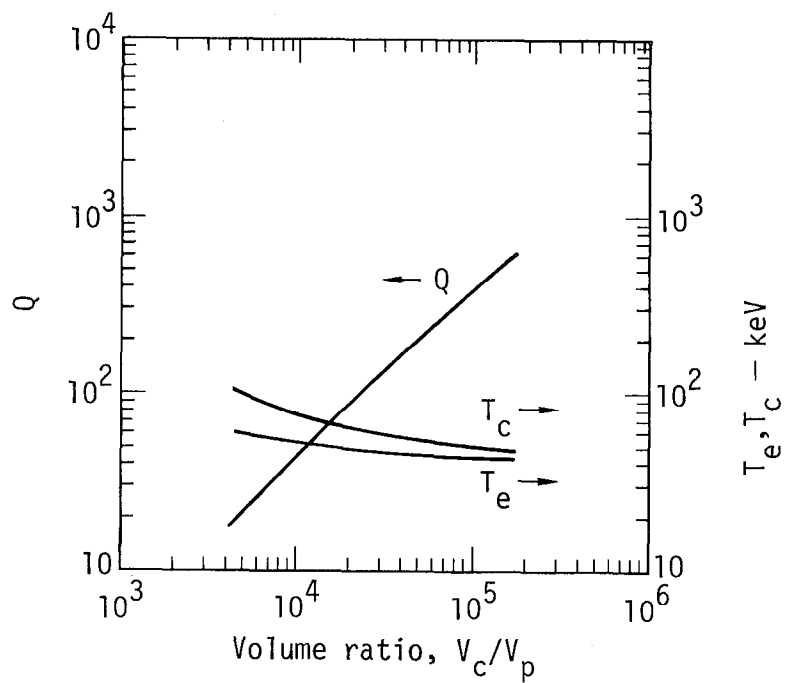


Fig. B-3. Variation of  $Q$ ,  $T_e$ , and  $T_i$  with volume ratio  $V_c/V_p$  (ignition) for  
 $n_p/n_c = 16.5$   
 $E_{inj} = 1$  MeV  
 $f_\alpha = 1.0$   
 $F_{e-aux} = 0$ .

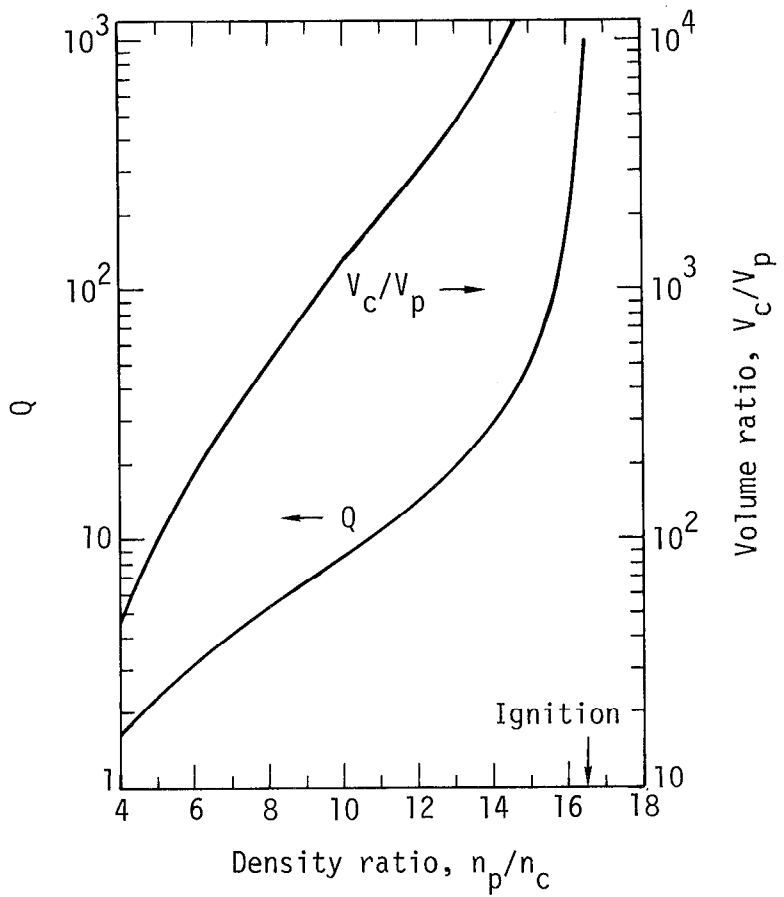


Fig. B-4. Maximum  $Q$  and volume ratio as a function of density ratio for  
 $E_{\text{inj}} = 1 \text{ MeV}$   
 $f_{\alpha} = 1$   
 $F_{\text{e-aux}} = 0.$

$T_i$ ,  $n_p/n_c$ , and  $V_c/V_p$  that give the chosen  $Q$ . The determination of the total fusion power goes as follows: The maximum plug density is determined by the maximum field at the conductor of the plug magnet mirrors  $B_{\max}$ , by the minimum ratio  $R_{\text{vac}} \equiv B_{\max}/B_0$  of the maximum conductor field to the central plug midplane field  $B_0$  outside the plasma that is consistent with the maximum plug beta  $\beta_p$ , and by the average plug perpendicular energy  $0.9 E_p$ :

$$n_p = 2.8 \times 10^{15} \frac{\beta_p B_{\max}^2}{R_{\text{vac}}^2 E_p} \text{ cm}^{-3}, \text{ (maximum)} \quad (\text{B17})$$

where  $B_{\max}$  is in teslas, and  $E_p$  is in keV. The central solenoid density  $n_c$  is determined from the plug density  $n_p$  and the density ratio:

$$n_c = n_p / (n_p/n_c) \text{ cm}^{-3} \text{ (maximum)}. \quad (\text{B18})$$

The minimum solenoid radius  $r_c$  is then found from  $n_c$  and  $\langle \sigma v \rangle$  ( $T_c$ ) and the requirement for a minimum economic fusion power per unit length  $W$  (MW/m at 17.6 MeV/fusion):

$$\frac{1}{4} n_c^2 \langle \sigma v \rangle (\pi r_c^2) (17.6 \text{ MeV}) (1.6 \times 10^{-19}) (10^{-4}) = \left( \frac{\text{MW}}{\text{m}} \right), \quad (\text{B19})$$

or

$$r_c = \frac{6.7 \times 10^7}{n_c} \sqrt{\frac{W}{\langle \sigma v \rangle}} \text{ cm, (minimum)} \quad (\text{B20})$$

where  $W$  is in MW/m, and  $\langle \sigma v \rangle$  is in  $\text{cm}^3 \cdot \text{s}^{-1}$ . Using the relations

$$B_c(\text{inside}) = B_c(\text{outside}) \sqrt{1-\beta_c} \text{ (long, thin approximation)} \quad (\text{B21})$$

$$B_p(\text{inside}) \approx B_p(\text{outside}) (1-\beta_p/2) \text{ (short, fat approximation for 2XIIB-like plasmas)} \quad (\text{B22})$$

and flux conservation

$$A_c B_c(\text{inside}) = A_p B_p(\text{inside}), \quad (\text{B23})$$

one finds an area ratio

$$\frac{A_c}{A_p} = \left( \frac{1 - \beta_p/2}{\sqrt{1 - \beta_c}} \right) \left[ \left( \frac{\beta_c}{\beta_p} \right) \left( \frac{n_p}{n_c} \right) \left( \frac{0.9 E_p}{T_e + T_c + \frac{2}{3} P_\alpha} \right) \right]^{1/2}, \quad (B24)$$

where the hot alpha pressure per unit density  $P_\alpha$  is given by

$$P_\alpha = \frac{1}{4} (n\tau)_{ea} \langle \sigma v \rangle E_\alpha f_\alpha f_e \approx 10^{11} T_e^{3/2} \langle \sigma v \rangle E_\alpha f_\alpha f_e. \quad (B25)$$

The plug radius  $r_p$  is then given by

$$r_p = r_c / \sqrt{A_c/A_p} \text{ cm (minimum).} \quad (B26)$$

The minimum plug length  $L_p$  for one plug is most likely limited by a geometric aspect ratio  $a_s$ :

$$L_p = a_s r_p / 100 \text{ m,} \quad (B27)$$

where  $a_s$  is a constant of order unity set by the relationship of radial and longitudinal field gradients in the plugs. Approximating the plug and solenoid volumes as cylinders of areas  $A_p$  and  $A_c$  and lengths  $L_p$  and  $L_c$ , respectively, we determine the minimum solenoid length  $L_c$  from the volume ratio, area ratio, and the minimum plug length:

$$L_c = \left( \frac{V_c}{V_p} \right) \left( \frac{A_p}{A_c} \right) 2L_p \text{ m, (minimum).} \quad (B28)$$

From the requirement of  $W$  (in MW/m), we have the minimum fusion power  $P_F$

$$P_F = W L_c. \quad (B29)$$

Putting Eqs. (B17) through (B28) together gives the following expression for  $P_F$ :

$$P_F = 2.3 \times 10^{-2} W^{3/2} \left( \frac{V_c}{V_p} \right) \left( \frac{n_p}{n_c} \right)^{1/4} \left[ \frac{\sqrt{1-\beta_c}}{\beta_c^2 \beta_p^{2/3} (1-\beta_p/2)} \right]^{3/2} \frac{(T_e + T_c + P_\alpha)^{3/4}}{\sqrt{\langle \sigma v \rangle}} .$$

$$\left( \frac{R_{vac}}{B_{max}} \right)^2 E_p^{1/4} a_s (\text{MW}), \quad (B30)$$

where  $W$  is in MW/m,  $T_e$ ,  $T_c$ , and  $E_p$  are in keV,  $\langle \sigma v \rangle$  is in  $\text{cm}^3 \cdot \text{s}^{-1}$ , and  $B_{max}$  is in teslas. The required fusion power per unit length  $W$  will in general increase with decreasing  $Q$  because the ratio of net power to fusion power  $P_{net}/P_F$  will decrease with decreasing  $Q$ . At a  $Q = 5$ , assuming an injection efficiency  $n_{beams} = 0.8$ , a thermal cycle efficiency  $n_{thermal} = 0.4$ , a direct converter efficiency  $n_{DC} = 0.6$ , and a blanket multiplication factor  $M = 1.2$ , the ratio  $P_{net}/P_F \approx 0.4$ . For a given  $Q$ , the minimum  $W$  for a given \$/kW will depend primarily on how cheaply the long, low-field central solenoid can be manufactured. Although such costs are not yet precisely determined, for the following examples at  $Q = 5$ , we take  $W = 20 \text{ MW/m}$ , or  $P_{net} = (8 \text{ MW/m}) L_c$ , believing that the solenoid ( $B_c \approx 20 \text{ kG}$ ) will be sufficiently simple to build for a few million dollars a metre.

When Eq. (B30) is evaluated for several parameter sets  $E_{inj}$ ,  $T_e$ ,  $T_i$ ,  $n_p/n_c$ , and  $V_c/V_p$  that give the same  $Q$ , the minimum fusion power is always found to occur near the parameter set having minimum volume ratio  $V_c/V_p$ . Thus, the volume ratio parameter is the best guide for determining minimum fusion power for a given  $Q$ .

For tandem mirror systems of moderately high  $Q$  ( $Q \approx 5$ ), in which the plugs furnish a power to the center-cell electrons comparable to or larger than the alpha power input, the plug injection energy is the most important parameter in determining the minimum volume ratio to achieve the  $Q$ . Figure B-5 shows the minimum net power  $P_{net}$  as a function of  $E_{inj}$ , keeping  $Q = 5$ ,  $B_{max} = 16.5 \text{ T}$ ,  $R_{vac} = 1.1$ ,  $\beta_p = 1$ ,  $\beta_c = 0.7$ ,  $W = 20 \text{ MW/m}$ , and  $a_s = 1.33$  (spherical plugs). At each injection energy, the volume ratio and  $P_{net}$  are minimized against  $T_e$  and the density ratio  $n_p/n_c$ . Figure B-5 shows that the minimum power does not depend sensitively upon the fraction of contained alphas at higher injection energies. However, at injection energies less than 1 MeV, the fraction  $f_\alpha$  makes more of a difference — a factor of 3 at  $E_{inj} = 600 \text{ keV}$ .

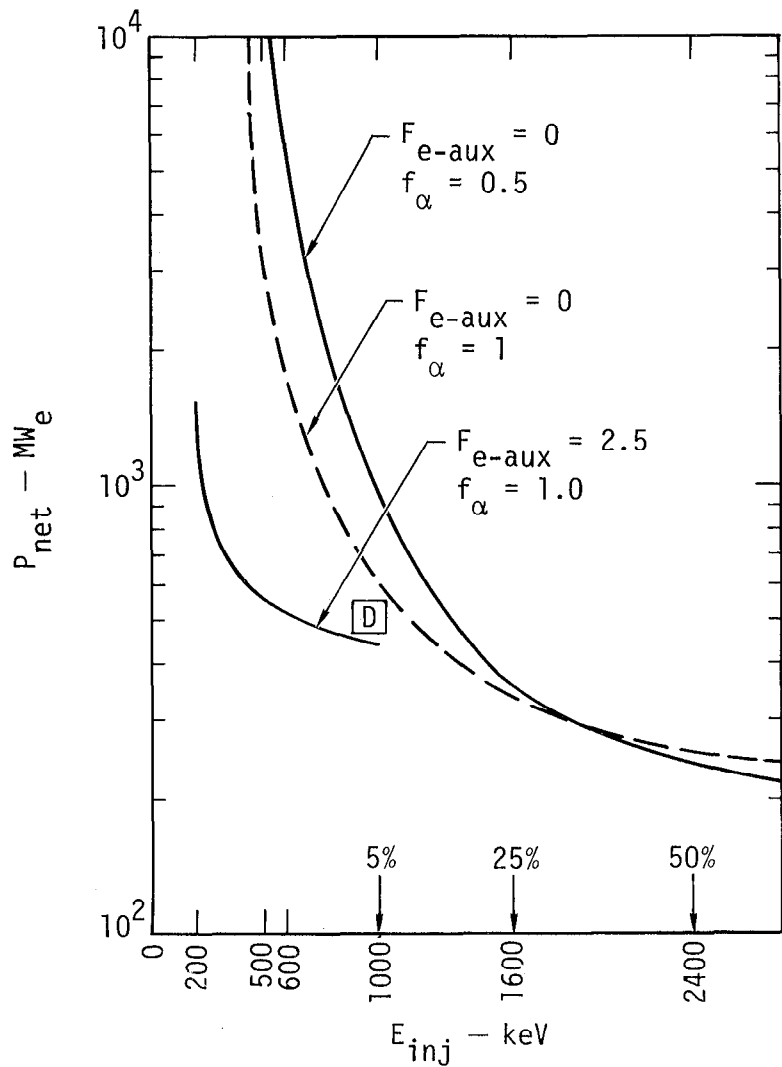


Fig. B-5. TMX net power versus  $E_{inj}$  for  
 $Q = 5$  (17.6 MeV/fusion)

$B_0 = 15$  T (midplane)

$\beta_p = 1$  ( $R_{eff} = 2.4$ )

$\beta_c = 0.7$

$W = 20$  MW<sub>th</sub>/m

$a_s = 1.333$  (spherical plugs)

$f_\alpha$  = fraction of hot alpha particles contained

$n_\alpha \approx 0$  (no thermalized alpha particles)

$\eta_{beams} = \eta_{ECRH} = 0.8$ ;  $\eta_{dc} = 0.6$ ;  $\eta_{thermal} = 0.4$

D = Dimov's case with  $f_\alpha = 1$  and  $F_{e-aux} = 2.5$

Beam transmissions at 5%, 25%, and 50% are indicated.

At  $E_{inj} = 1$  MeV, the minimum powers for Q's other than 5 can be scaled from Fig. B-5 according to the volume ratio associated with each Q in Fig. B-4. To see the beneficial effects of having an auxiliary electron heating input, the curve labeled  $F_{e-aux} = 2.5$  in Fig. B-5 gives the variation of  $P_{net}$  with  $E_{inj}$  using a power  $V_c P_{e-aux}$  equal to 2.5 times the neutral-beam power in the plugs. To compare  $P_{net}$  directly while keeping the recirculating power fraction constant, the same efficiency of 80% is assumed for the auxiliary electron heating as for the neutral beams. Figure B-5 shows that such extra electron heating, if it were that efficient, would allow operation at somewhat lower plug injection energies (since the requirement for high  $E_{inj}/T_e$  ratios to heat electrons is relaxed). Even in this case, however, one would desire  $E_{inj} \gtrsim 400$  keV to minimize power, since at lower injection energies the classical  $(n\tau)_p$  is rapidly decreasing. As a comparison with the model developed here, the point "D" indicated in Fig. B-5 is the value of  $P_{net}$  evaluated by Eq. (B30) for Dimov's parameters at  $F_{e-aux} = 2.5$ ,  $f_\alpha = 1$ , and  $Q = 5$ .

A practical limitation on using higher plug injection energies is the fact that the  $\ln d_1$  through the diameter of the plugs is decreasing with  $E_{inj}$  for the minimum  $P_{net}$  cases in Fig. B-5, while the required  $\ln d_1$  to attenuate the beams increases with  $E_{inj}$ . Values of  $E_{inj}$  at which the transmitted beam fractions are 5%, 25%, and 50% are indicated. The loss of net power and increase in recirculating power fraction implied by the wasted beam power will probably set a limit on  $E_{inj}$  between 1 and 1.6 MeV.

In summary, it appears that given a favorable outcome on the development of efficient high-energy neutral beams and classical loss rates for the plugs, moderately high Q's of 5 or greater are possible in a Tandem Mirror reactor at less than one GW(e) net power. Parameters for one example are given in Table B-1.

Table B-1  
Tandem mirror reactor parameters for  $Q = 5$ ,  $P_{net} = 620 \text{ MW(e)}$

Technology	Central cell	Plugs (each)
$E_{inj} = 1 \text{ MeV}$	$T_e = 50 \text{ keV}$	$E_p = 880 \text{ keV}$
$W = 20 \text{ MW/m}$	$T_c = 47 \text{ keV}$	$\phi = \phi_e + \phi_c = 410 \text{ kV}$
$B_{max} = 16.5 \text{ T}$	$\phi_c = 111 \text{ kV}$	$B_p = 15 \text{ T}$
$R_{vac} = 1.1$	$B_c = 2.2 \text{ T}$	$\beta_p = 1.0$
$n_{beams} = 0.8$	$\beta_c = 0.7$	$B_{pi} = 7.5 \text{ T}$
$\eta_{thermal} = 0.4$	$B_{ci} = 1.2 \text{ T}$	$n_p = 7.1 \times 10^{14} \text{ cm}^{-3}$
$\eta_{direct converter} = 0.6$	$n_c = 7.9 \times 10^{13} \text{ cm}^{-3}$	$r_p = 52 \text{ cm}$
$M = 1.2$	$r_c = 130 \text{ cm}$	$L_p = 100 \text{ cm (sphere)}$
$F_{e-aux} = 0$	$L_c = 77 \text{ m}$	$I_p = 155 \text{ A}$
	$I_c = 570 \text{ A}$	
	$P_F(17.6 \text{ MeV}) = 1550 \text{ MW}$	
	$f_\alpha = 1.0$	

References

- B1. G. I. Dimov, V. V. Zakaydakov, and M. Ye. Kishievsky, "Open Trap with Ambipolar Mirrors," in *Proc. 6th Inter. Conf. Plasma Physics and Controlled Nuclear Fusion Research, Berchtesgaden, Fed. Rep. of Germany, 1976* (AIEA, in preparation) Paper C4.
- B2. V. P. Pastukhov, *Nucl. Fusion* 14, 3 (1974).
- B3. B. G. Logan, J. F. Clauser, F. H. Coensgen, D. L. Correll, W. F. Cummins, C. Gormezano, A. W. Molvik, W. E. Nexsen, T. C. Simonen, B. W. Stallard, and W. C. Turner, *Phys. Rev. Lett.* 37, 1468 (1976).
- B4. D. T. Rose, *Feasibility of Power by Nuclear Fusion*, Oak Ridge National Laboratory, Rept. ORNL-TM-2204 (1968).

APPENDIX C. TMX ENGINEERING

D. P. Atkinson, M. O. Calderon, W. O. Chapin, A. K. Chargin, F. F. Chen  
R. N. Clark, B. S. Denhoy, J. N. Doggett, S. G. Homann,  
G. A. Leavitt, J. D. Lee, K. W. Mortensen, D. L. Pehrson,  
G. A. Pence, G. G. Pollock, T. L. Rossow, P. D. Siemens,  
M. S. Singh, S. R. Thomas, Jr., G. E. Vogtlin, and A. F. Waugh

## Contents

C1.	Magnet System . . . . .	119
	Introduction . . . . .	119
	Winding Geometry and Magnetic Field Shape . . . . .	119
	Magnet Structure . . . . .	123
	Magnet Construction . . . . .	130
	Thermal Design . . . . .	130
	Magnet Power Supply System . . . . .	134
C2.	Vacuum System . . . . .	139
	Introduction . . . . .	139
	Components of the Vacuum System . . . . .	139
	Surface Pumping . . . . .	139
	LN Liners . . . . .	142
	Plasma and Injector Dumps . . . . .	142
	Gas Load Sources . . . . .	142
	Neutral-Beam/Plasma Interaction . . . . .	144
	Molecular-Gas/Plasma Interaction . . . . .	145
	Gas-Balance Analysis . . . . .	145
C3.	Injection System . . . . .	150
	General Description . . . . .	150
	Injector Magnetic Shielding . . . . .	156
	Isolation Valves . . . . .	156
	Target-Plasma Generator . . . . .	157
	Gas Stabilization System . . . . .	157
	Neutral-Beam Power Supplies . . . . .	157
	Target-Plasma Generator Power Supply . . . . .	161
C4.	Facility . . . . .	164
	Description . . . . .	164
	Building and Site Preparation . . . . .	164
	Building Modifications and Additions . . . . .	166
	External Vacuum Pumping System . . . . .	172

C5.	Neutron Shield Design and Analysis . . . . .	174
	Introduction . . . . .	174
	Analytical Model . . . . .	175
	Monte Carlo Calculations . . . . .	178
	Shielding Cost/Benefit . . . . .	178
	Summation . . . . .	182
C6.	Control Systems . . . . .	183
	Vacuum Control System . . . . .	183
	Getter Control System . . . . .	183
	Magnet Control System . . . . .	183
	Personnel Safety Interlocks . . . . .	183
	Neutral Beam and Streaming Gun Control . . . . .	183
C7.	Diagnostic System . . . . .	185
C8.	References . . . . .	186

## C1. MAGNET SYSTEM

### Introduction

The TMX magnet system, as shown in Fig. C-1, consists of two "Baseball" coils, four "C" coils, two "transition" Ioffe coils, one "center" Ioffe coil, and five central solenoidal coils. The Baseball coils enclose the "C" coils, and together they are referred to as the "plug coils".

The design strategy for the TMX magnet system is governed by the requirement that the shape of the magnetic field be adjustable so that it can be an experimental parameter. This implies a number of coils whose geometries, although fixed, can produce a range of flux shapes by varying currents in the different coils. The most important parameters are adjustable mirror ratios and changeable conditions for magnetohydrodynamic (MHD) stability.

The results of a trade-off study of a superconductor versus a copper magnet weighed in favor of copper. Many of the items that make up the cost of a magnet system were about the same in either case. At LLL, we have both the cryogenic capacity to cool a superconducting magnet set of this size and sufficient power available to energize a copper magnet set. It was the additional cost of superconductor over copper and the added operational complexity of a cryogenic experiment that led us to choose a water-cooled copper conductor.

### Winding Geometry and Magnetic Field Shape

The tandem mirror configuration consists of three connected mirror machines: two small high-field mirror machines (the plugs) and a large low-field solenoidal cell located between the high-field regions (see Fig. C-1). To improve the MHD stability conditions, the plug coils are oriented 90° with respect to each other about the longitudinal axis of the machine.

Each plug consists of a pair of "C" coils nested within the lobes of a Baseball coil. Figures C-2 and C-3 show the basic configuration and the proposed dimensions. These coils have the synergistic ability to cover the range of operating conditions necessary to satisfy the physics parameters.

By varying the contributions from the baseball coil (axial mirror ratio,  $R_{\parallel} = 1.25$ , and radial mirror ratio at  $r = 10$  cm,  $R_{\perp 10} = 1.08$ ) and the "C" coils ( $R_{\parallel} = 4.25$ ,  $R_{\perp 10} = 0.98$ ), it is possible to produce a minimum- $|B|$  plug field

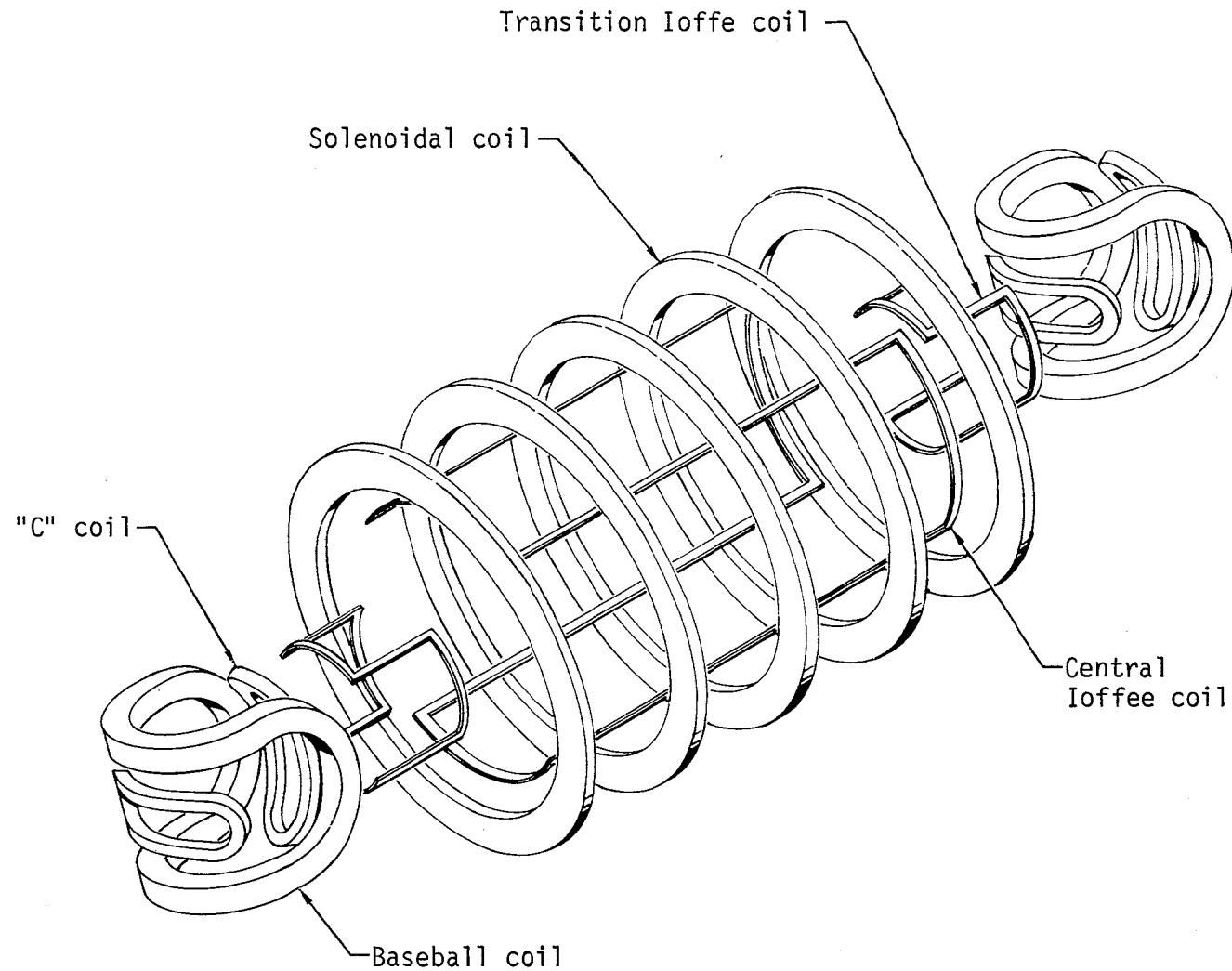


Fig. C-1. TMX coil set.

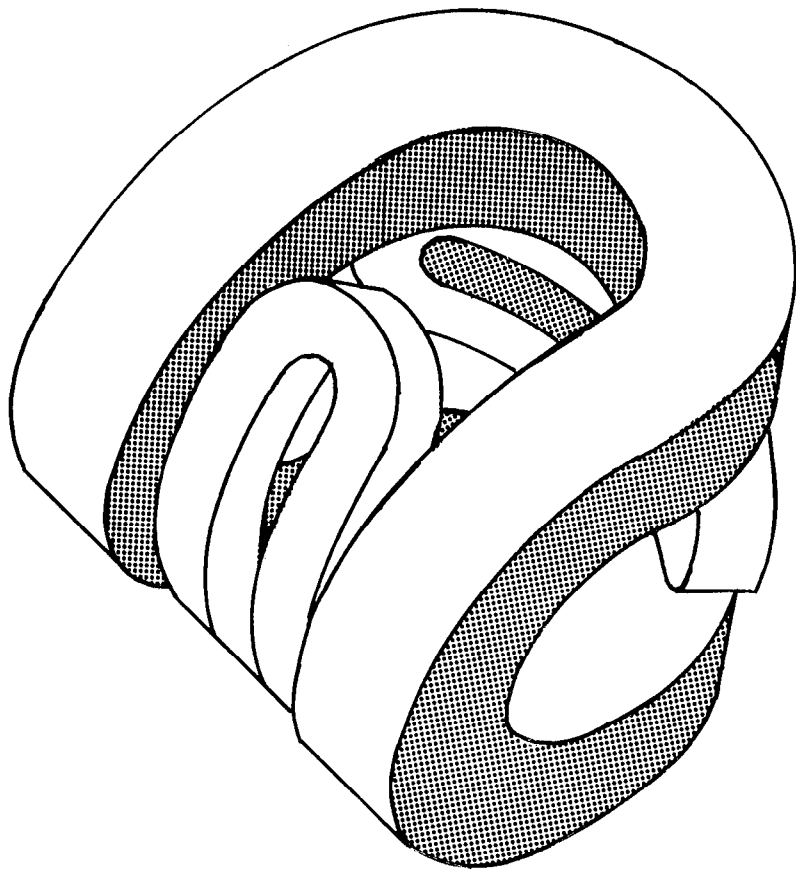


Fig. C-2. Plug coil winding.

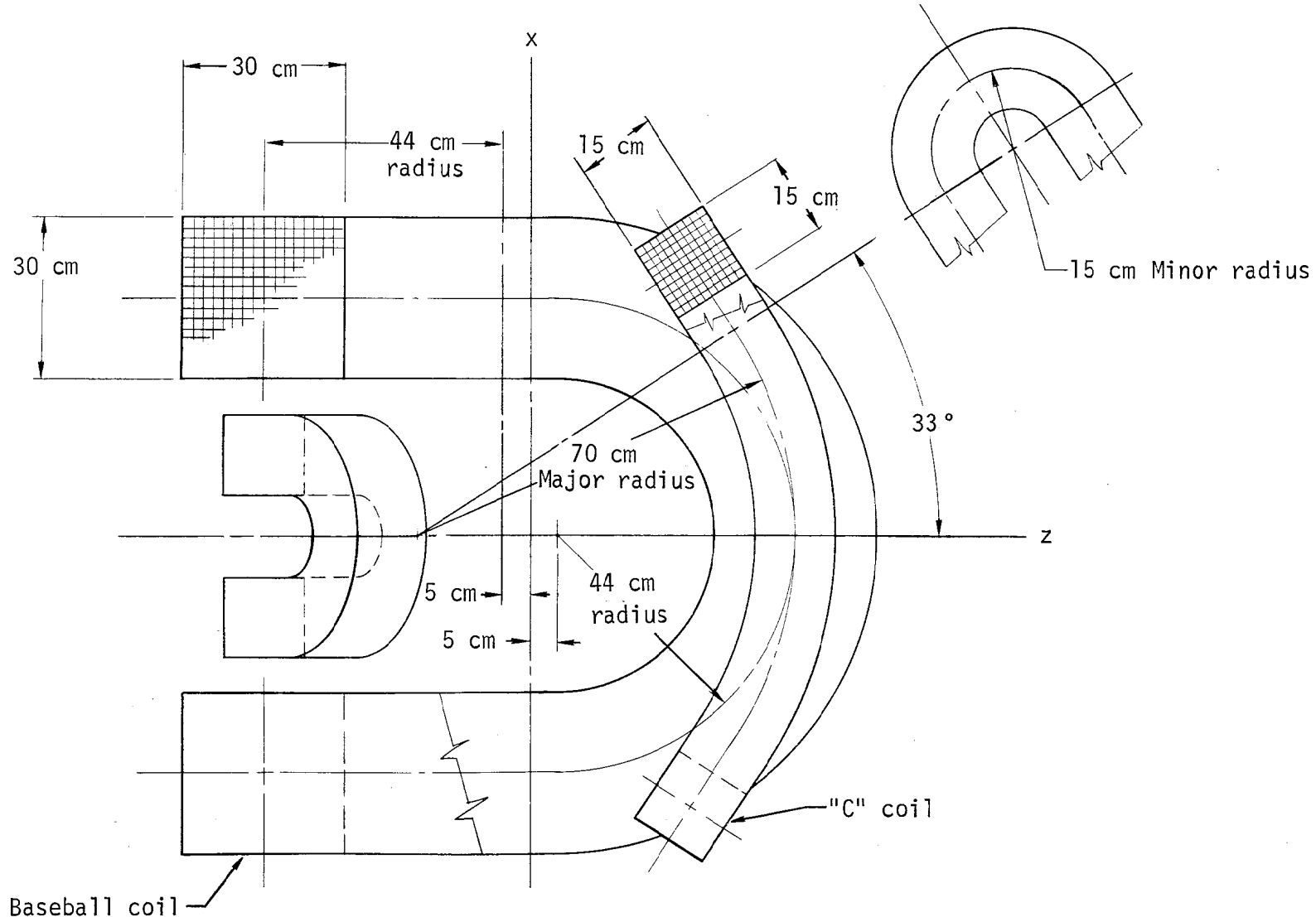


Fig. C-3. Plug coil conductor bundles.

configuration with an axial mirror ratio from 1.3 to 2.8. Corresponding to this range of  $R_{\parallel}$ , the maximum central field strength of the plug, as limited by available power supplies, is 1.0 T. Figure C-4 shows the central field strength of the plug as a function of current ratios when the maximum available power is being used. In addition to the minimum- $|B|$  configuration, the plugs can operate in a nonminimum- $|B|$  mode with large "C" coil current to baseball current ratios ( $I_c/I_{BB} > 2.1$ ). This coil set can also provide an unequal axial mirror ratio, but not with a minimum- $|B|$  configuration.

The center-cell windings are an existing set of solenoidal coils (Fig. C-1) from a previous experiment and cause no particular design problems. Transition coils are required to transform the fan-shaped field lines from one plug  $90^\circ$  to enter the other plug. A Ioffe bar set extending the length of the solenoidal section accomplishes this  $90^\circ$  transform of the plug flux bundles, but it also tends to make the middle of the center cell a minimum- $|B|$  mirror machine. In this design, we incorporate a Ioffe bar set between each plug and the solenoidal region; this bar set can also achieve circularization of the fan-shaped field lines, but with a nonminimum- $|B|$  center cell. Therefore, it will be possible to determine experimentally the optimum field shape for the center cell in a tandem mirror configuration.

Figure C-5 illustrates the magnetic flux shape typical of this coil set. For the purpose of illustration, the field line plots for a case with  $R_{\parallel} = 2.1$ ,  $R_{\perp} = 1.04$ , plug central field of 1.0 T, and center-cell field of 0.1 T are included as Figs. C-6 and C-7. In these plots, the field lines at 0-, 5-, 10-, 15-, and 20-cm radius are plotted on an axial cross section with a back-ground of constant- $|B|$  contours. These plots illustrate the mapping of the flux tubes of the plug centers into the flux tube of the center cell. For the cases shown, the center-cell field shape is solenoidal to within 10% through a length of 3.5 m. The field-shape calculations were done using an updated version of the MAFCO computer code.<sup>C1</sup> In Table C-1, we list the significant magnet parameters.

#### Magnet Structure

With the exception of the central-cell Ioffe bar set and solenoidal coils, all the coils are inside the vacuum system (Fig. C-8).

The internal coils are supported from the walls of the vacuum vessel against gravitational and gross axial magnetic forces. The major magnetic loads will be those trying to change the shape of the Baseball and "C" coils. However, due to symmetry, these may be self-reacted, independently of external structures.

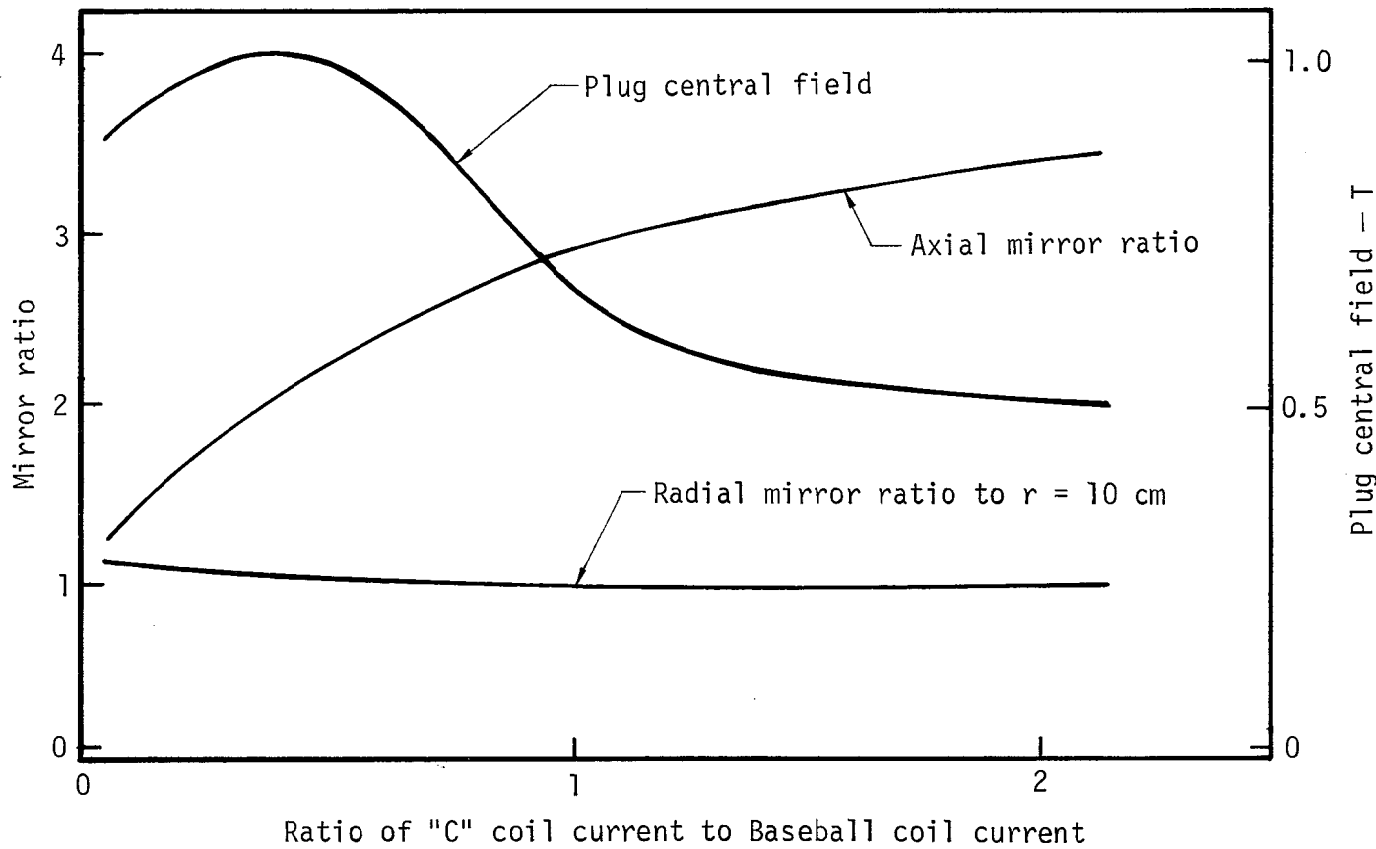


Fig. C-4. Range of magnetic-field parameters for the plug coils.

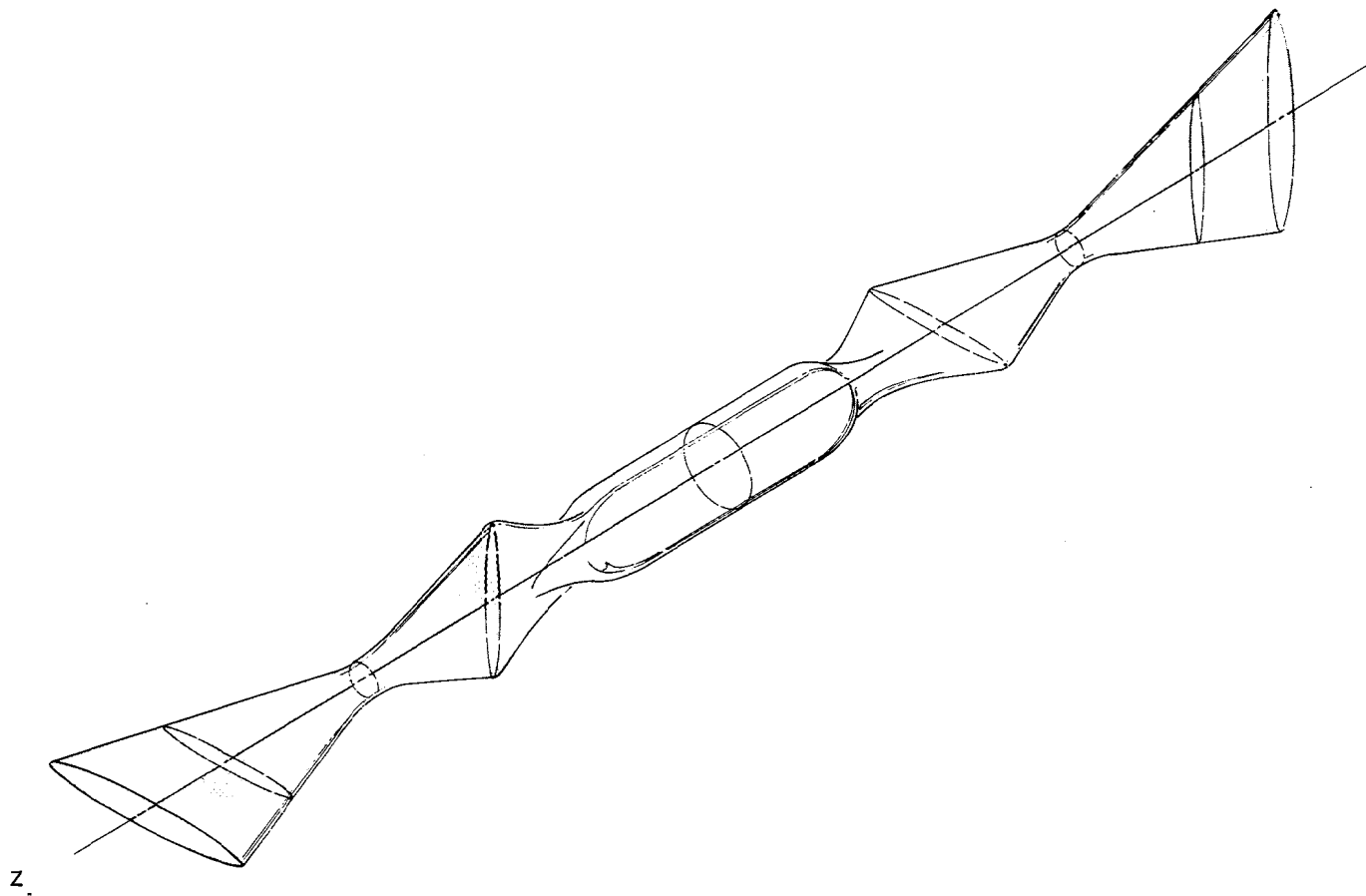


Fig. C-5. Magnetic flux shape.

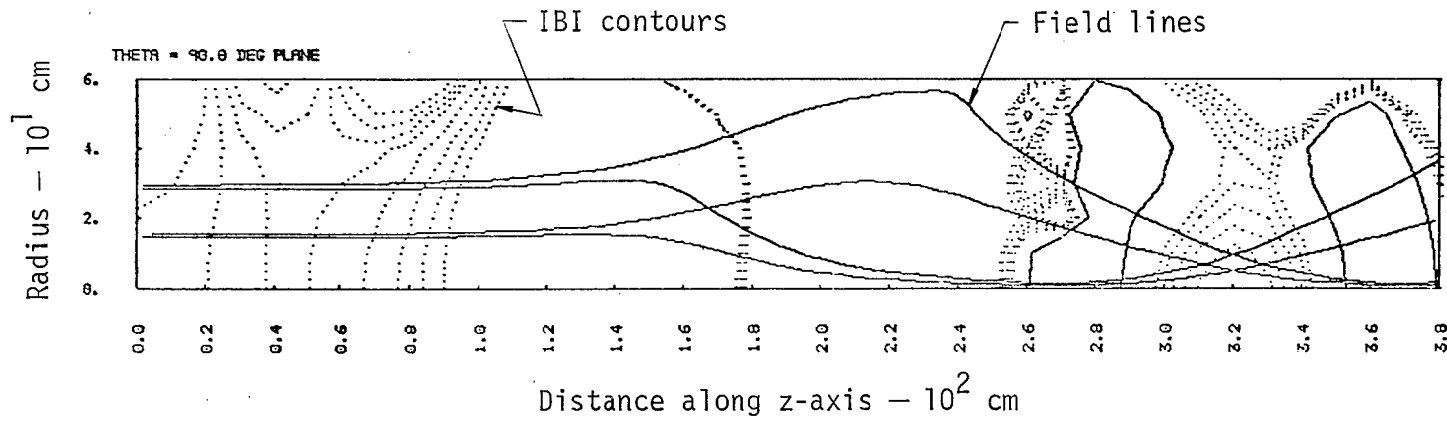


Fig. C-6. Magnetic field plot on  $90^\circ$  plane.

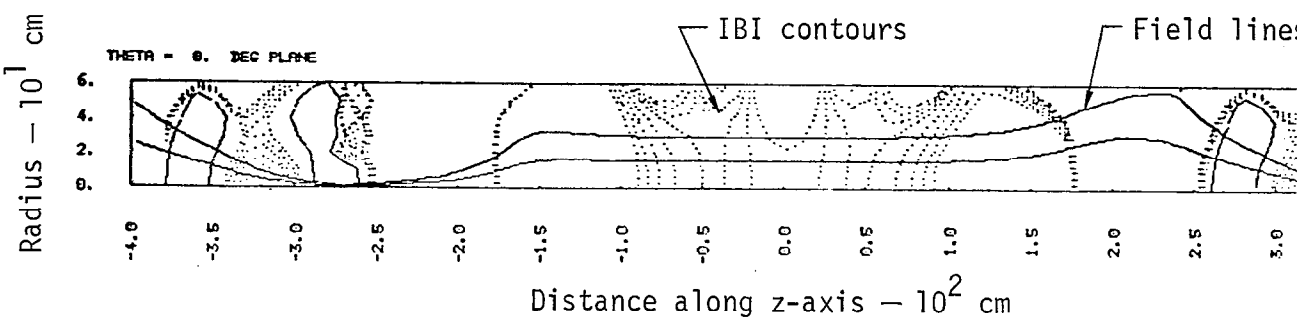


Fig. C-7. Magnetic field line plot on  $0^\circ$  plane.

Table C-1. TMX Magnet Parameters.

Magnet Type - Plug	Baseball plus "C" coil pair
- Transition	Ioffe bars
- Central Cell	Solenoids
Distance between inner mirrors	5.5 m
Distance between plug mirrors	0.9 m
Plug central field	1.0 T
Center-cell field <sup>a</sup>	0.05 to 0.3 T
Plug mirror ratio, axial <sup>a</sup>	1.3 to 3.5
Plug mirror ratio, radial <sup>a</sup> (at 10 cm)	0.98 to 1.04
Maximum plasma radius	
- In plug	0.2 m
- In center cell	0.7 m
Total stored energy	40 MJ

<sup>a</sup>For some of this range, a field of 1.0 T in the center of the plug can be achieved. The extremes of this range can be attained at somewhat lower plug fields. (See text.)

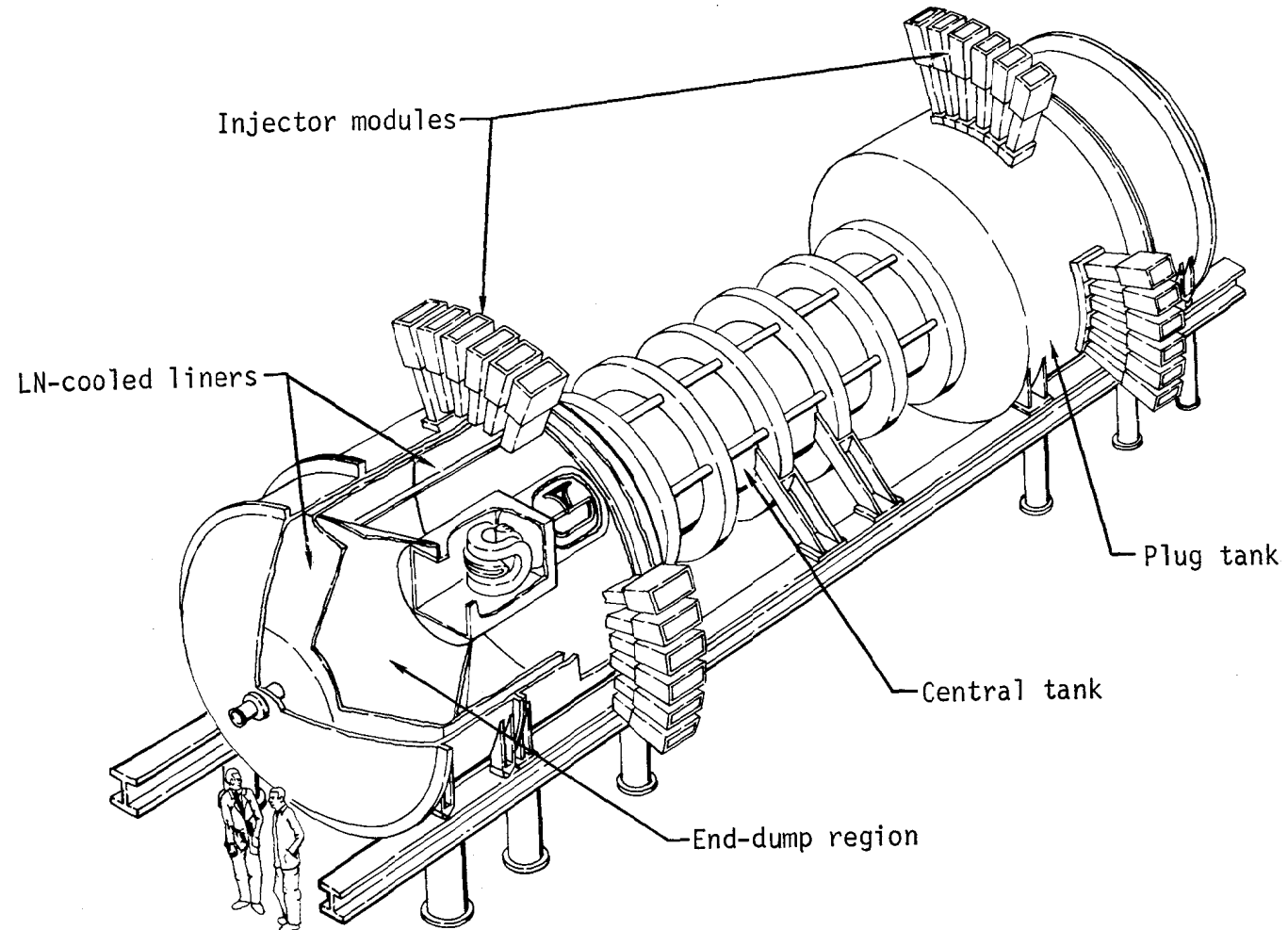


Fig. C-8. TMX configuration.

The forces and magnetic pressures in the Baseball and "C" coils were calculated with the EFFI code. C2 The results are shown in Figs. C-9 and C-10. The total forces in one octant of the plug coil set are:

$$F_x = 2.03 \times 10^6 \text{ N} \quad (4.56 \times 10^5 \text{ lb})$$

$$F_y = 1.88 \times 10^6 \text{ N} \quad (4.22 \times 10^5 \text{ lb})$$

$$F_z = 1.95 \times 10^6 \text{ N} \quad (4.38 \times 10^5 \text{ lb})$$

Although the total forces in the x-, y-, and z-directions are approximately equal, the critical force is that in the x-direction because it tends to open the coil over the mirror region. Since the plasma leakage fan must be kept free of obstructions, direct tension support is not allowed, and the forces must be transferred to the outside of the coil by a structure such as a beam. Figure C-11 shows such an arrangement. This particular design was used for sizing the system and is somewhat conservative. The Baseball coil acts as a support to the "C" coils and provides structure to support both the "opening" and axial forces.

The transition Ioffe coil (Fig. C-1) is lightly loaded and does not present any difficult structural problems.

The Ioffe coil surrounding the central cell (Fig. C-1) is built on the surface of the central vacuum tank, which provides required structural strength. The solenoidal coils surrounding the central cell are supported against attractive forces by a structure similar to that used with the same coils on the 2XIIB experiment.

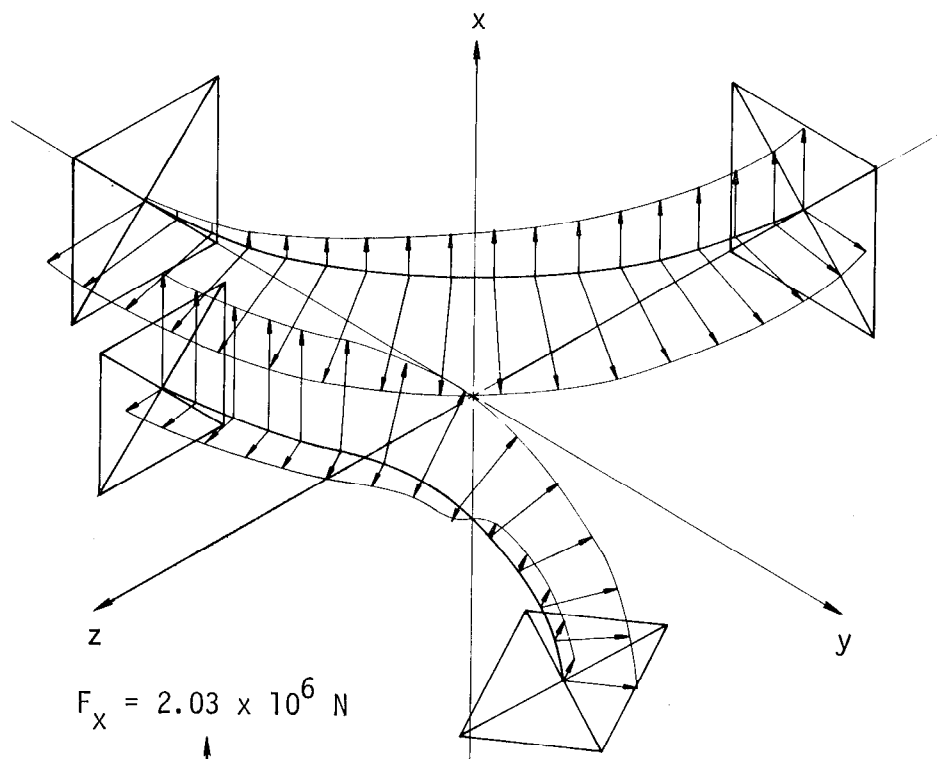
#### Magnet Construction

The coils are all fabricated of square, hollow, copper conductor suitably insulated and bound into an epoxy/glass/copper-composite structure. The internal coils are jacketed in stainless steel to reduce the outgassing of the conductor bundle to an acceptable level.

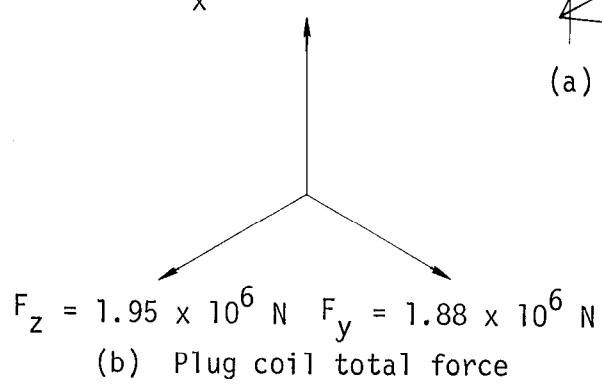
The construction of these coils is within the capabilities of the magnet fabrication facilities at LLL that were used to wind the 2XIIB and Baseball II coils.

#### Thermal Design

As noted above, the plug magnets and central-section magnets are made from square, hollow, copper conductor. All these coils operate near room temperature in a pulse mode. The coils are cooled by continuously circulating loss-conductivity water (LCW) from existing cooling towers. We calculate the



(a) Plug coil force distribution



(b) Plug coil total force

Fig. C-9. Plug coil force, showing (a) force distribution and (b) total force.

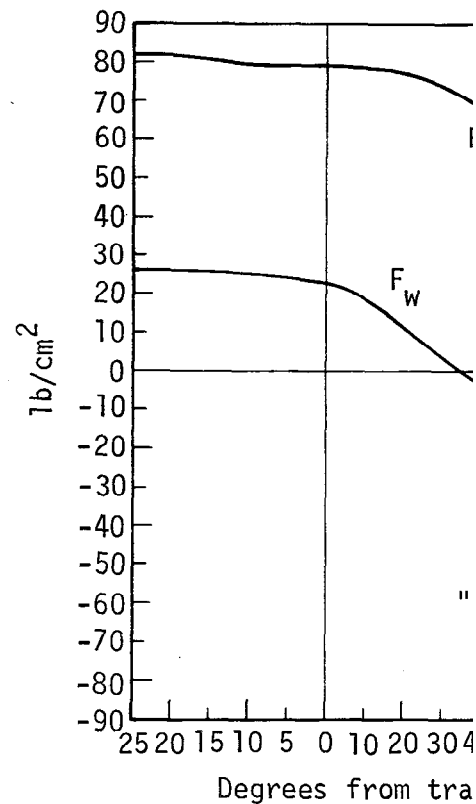
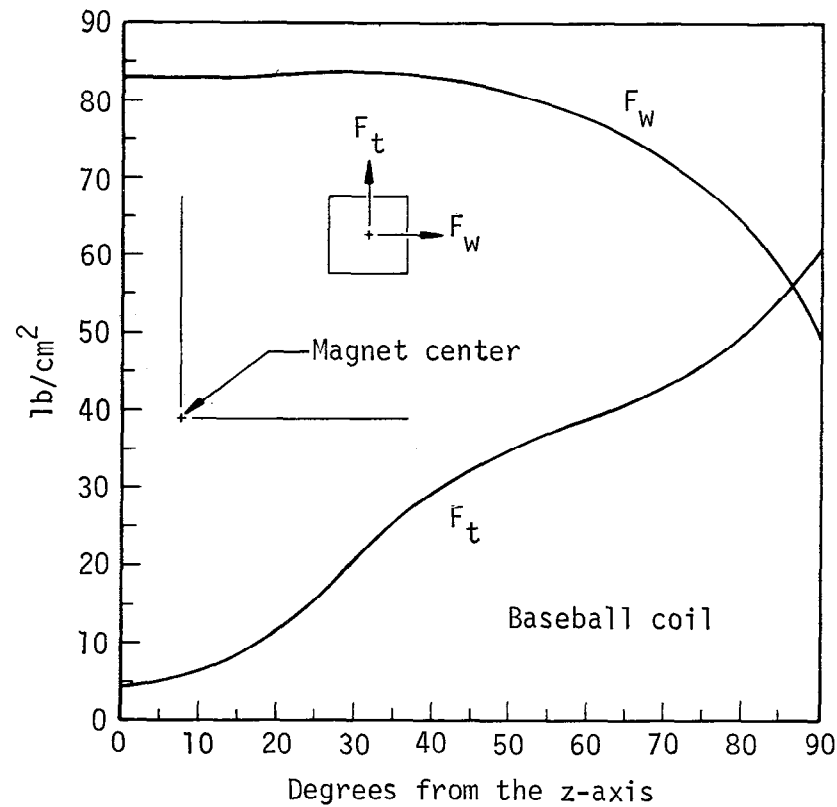


Fig. C-10. Conductor pressure for Baseball and "C" coils.

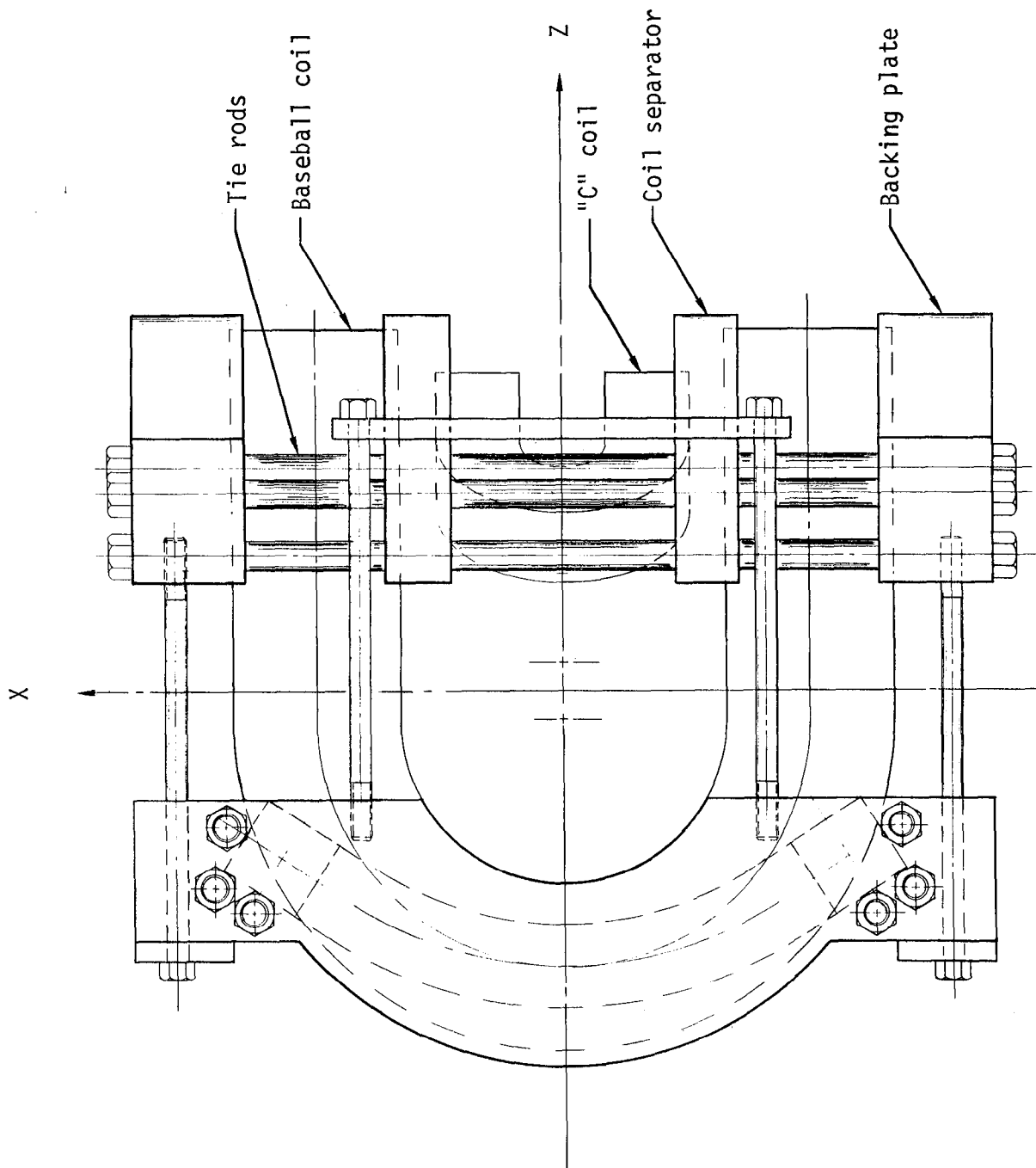


Fig. C-11. Plug coil set.

peak power for the coils to be 20 MW. The total stored energy of all the coils will be 40 MJ. The copper has more than enough mass to store 40 MJ of energy during each pulse. Assuming a maximum temperature rise of 60 K, the cooling time required between each pulse is about 2.0 minutes. The available LCW is sufficient because the cooling tower capacity is 6.5 MW. The average current density in these magnets is less than  $2000 \text{ A/cm}^2$ . This is conservative from a thermal standpoint, but the extra copper is required to match the power supply impedance.

#### Magnet Power Supply System

To power the water-cooled, copper coils of the TMX machine, an existing substation power distribution system and existing dc power supplies are used.

The available substation (Fig. C-12) consists of three 13.8-kV to 480-V step-down transformers with the following ratings:

Bank No.	Power (MVA)	Rated Secondary current (A)
151	3.75	4510
561	3.00	3600
705	3.00	3600
Total	9.75	11,710

It is possible to draw about twice rated power from this 480-V power system for "on times" up to 10 s at duty cycles of 10% or less. The time limit is imposed by the protective fuses and circuit breaker equipment. In operation, "on time" would be limited to 5 to 7 s by the available thermal capacity of the copper coils.

Adequate 480-V secondary cabling from the three step-down transformers exists to the circuit breaker distribution panels in Bldg. 436 (Figs. C-13 and C-14), which will house the required dc power supplies.

Twenty-five 300-kW dc power supplies are available for use in this magnet power supply system. Of that total, 15 power supplies are now installed in Bldg. 436. These units are built to a specification which requires that they be capable of operating either at 4 times rated current for up to 20 s with a duty factor of 5% or at 3 times rated current for up to 60 s with a 16% duty factor.

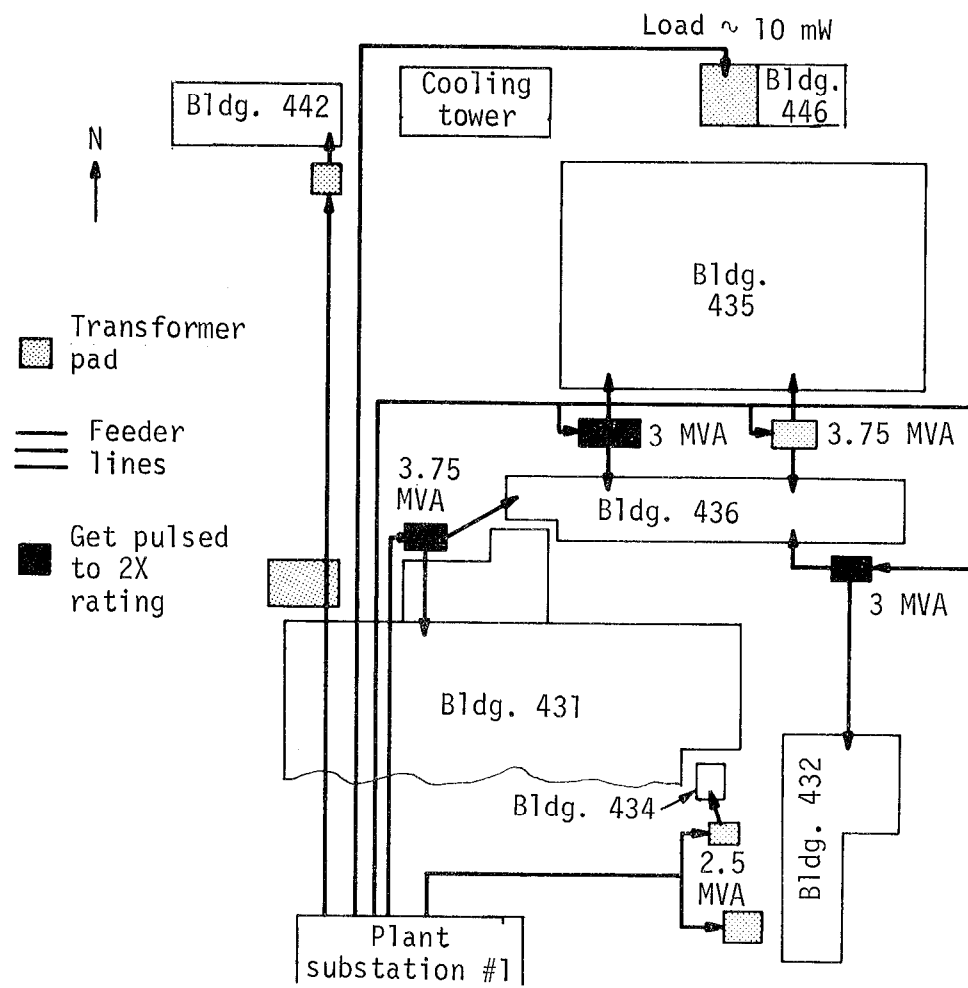


Fig. C-12. 13.8-kV service from existing substations.

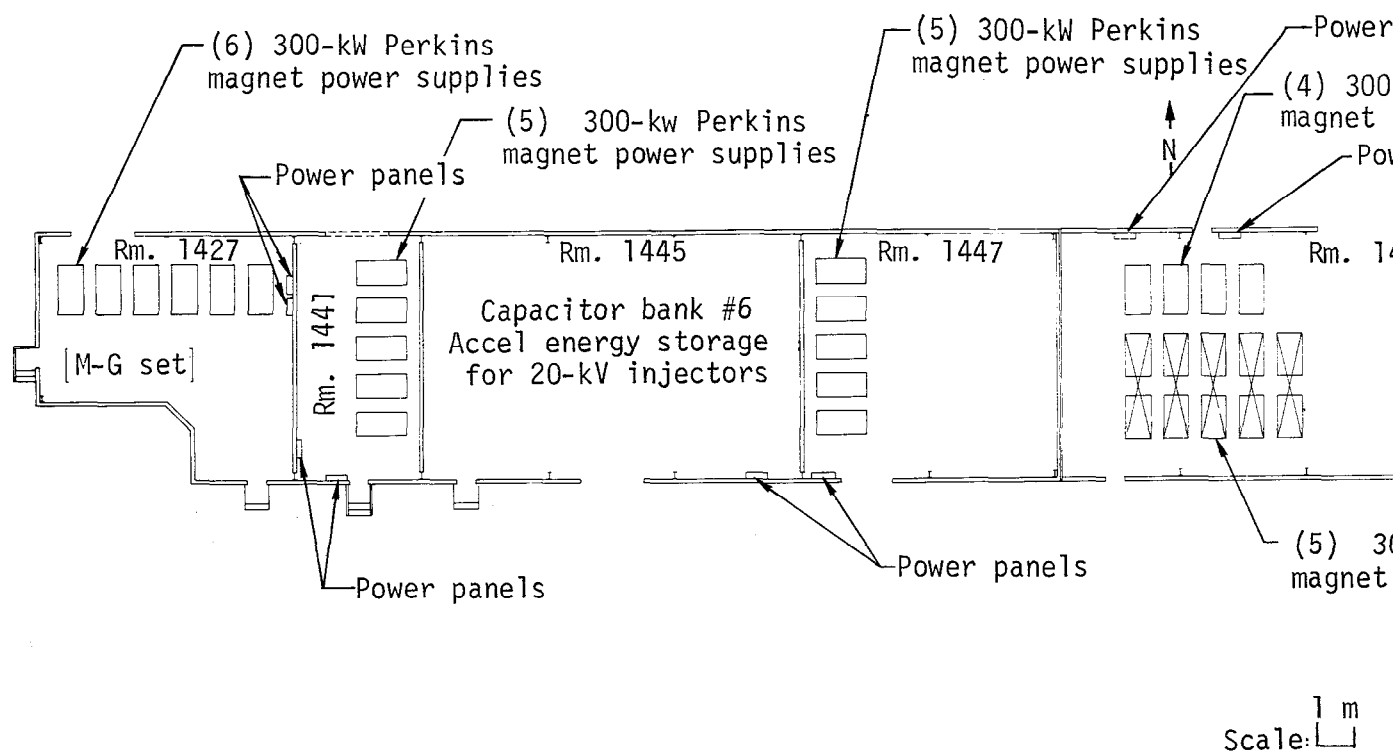


Fig. C-13. Power supply in Building 436.

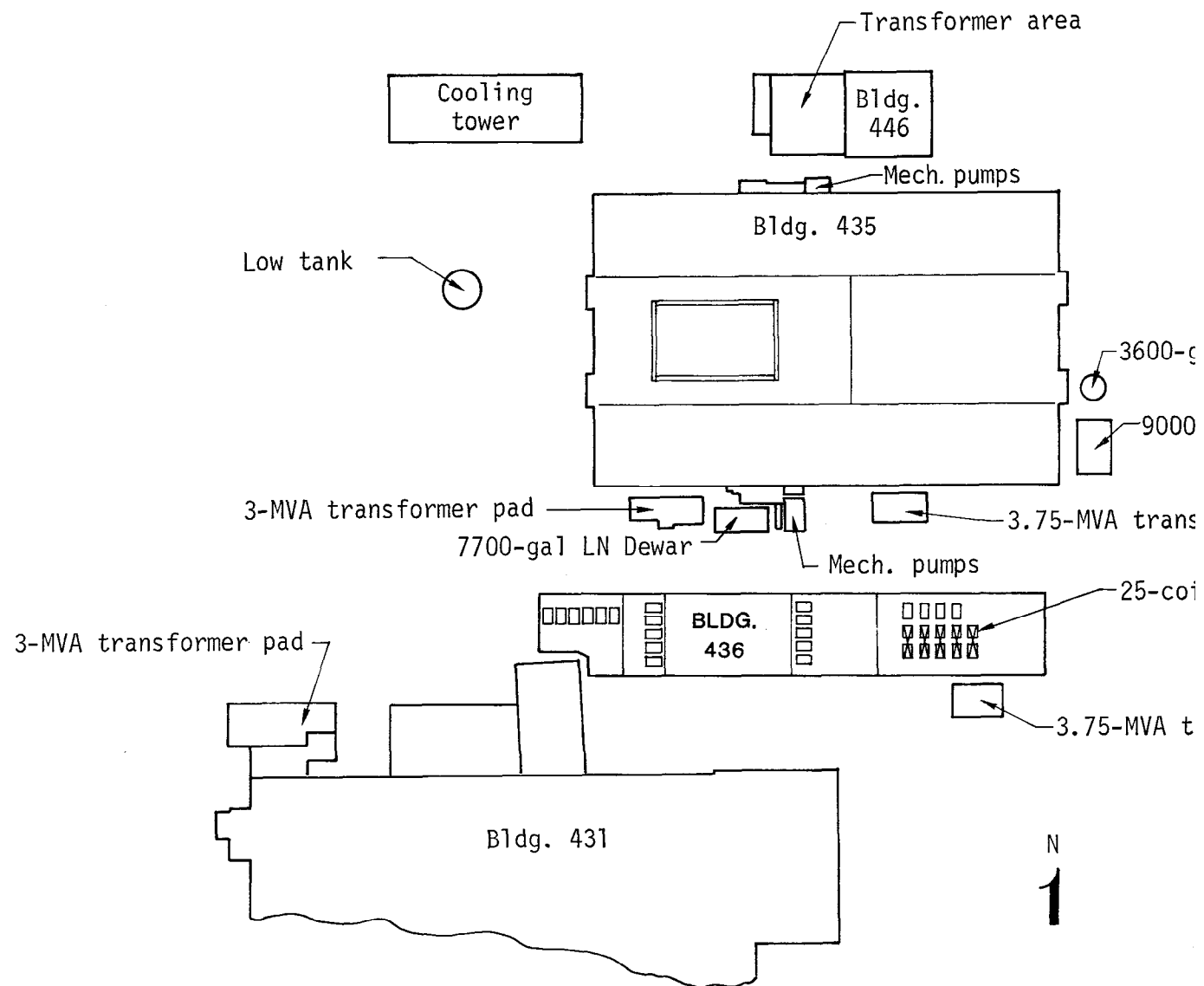


Fig. C-14. Site plan.

Previous load tests on these relatively simple "brute force" power supplies show that they have a conversion efficiency (power out/power in) of about 80%. Also, it has been determined that near rated output voltage can be maintained for output currents up to about 2.5 times rating. Therefore, one can expect to draw up to 750 kW from these nominal 300-kW cw rated power supplies.

Reserving three of the 25 power supplies for energizing the central solenoid coils and operating the remaining 22 units at about 750 kW each would provide a maximum of 16.5 MW of power to the plug/transition-coil combinations. At an overall conversion efficiency of 80%, this would require about 20 MVA from the 480-V power distribution system, which is the expected limit.

By redistributing the 13.8-kV loads at the LLL plant substation, it would be possible to isolate this short-duration, low-duty factor (5%), heavy-pulsed load. This would minimize the effects of this pulse loading on other plant loads.

The magnets can be turned on and off by simply closing and opening the contactors at the 480-V, three-phase, primary input to each power supply. Since the output circuit of these supplies is a three-phase, full-wave bridge rectifier, when the primary power is interrupted, the magnets will discharge through the dc bus and the bridge rectifiers. The discharge will be governed primarily by the time constant of the coils themselves. This ratio will be in the range of 0.2 to 0.5 s.

## C2. VACUUM SYSTEM

### Introduction

This section discusses the design of the primary vacuum system required to handle the molecular gas associated with the operation of the two gas box injectors and 24 neutral-beam injector modules.

### Components of the Vacuum System

The primary components of the TMX vacuum system are the two plug tanks and the central tank. The plug tanks are subdivided by liquid nitrogen-(LN-) cooled liners that serve both as pumping surfaces and as differential pumping volumes (see Figs. C-15 and C-16). The coil region encloses the plug coil and plasma. The plasma-dump region pumps the particles that are lost axially from the plasma.

The injector regions one and two provide pumping for the un-ionized gas from the beam sources. The dump region pumps the neutral-beam particles that penetrate through the plasma.

The gas box provides a region for the injection of cold gas. All regions are interconnected by orifices that provide either for beam access into or out of the plasma or for the continuity of the plasma. The plug and central regions are water cooled, and all other regions are LN-cooled. All regions except the gas box are Ti-gettered for pumping.

### Surface Pumping

A fresh coating of titanium will be deposited on the pumping surfaces shortly before each experimental shot. The gettering film is deposited on both sides of the inner LN liners and on the inner surface of the vacuum wall liner. In addition, the inner surfaces of the plug coil are gettered. These surfaces, which operate at  $\sim 300$  K, must absorb the high flux of energetic neutrals produced by charge-exchange reactions.

Present-day Ti-Ta alloy wire of 3-mm diameter has a measured sublimation rate of  $50 \text{ mg/m}^2 \cdot \text{min}$ . It has a lifetime of  $\sim 200$  min, so it will provide 200 1-min evaporation. Because it is desirable to provide for more shots before wire replacement, three to five sets are used in rotation. The total surface area to be gettered is  $\sim 176 \text{ m}^2$  per plug tank and  $\sim 25 \text{ m}^2$  in the central region

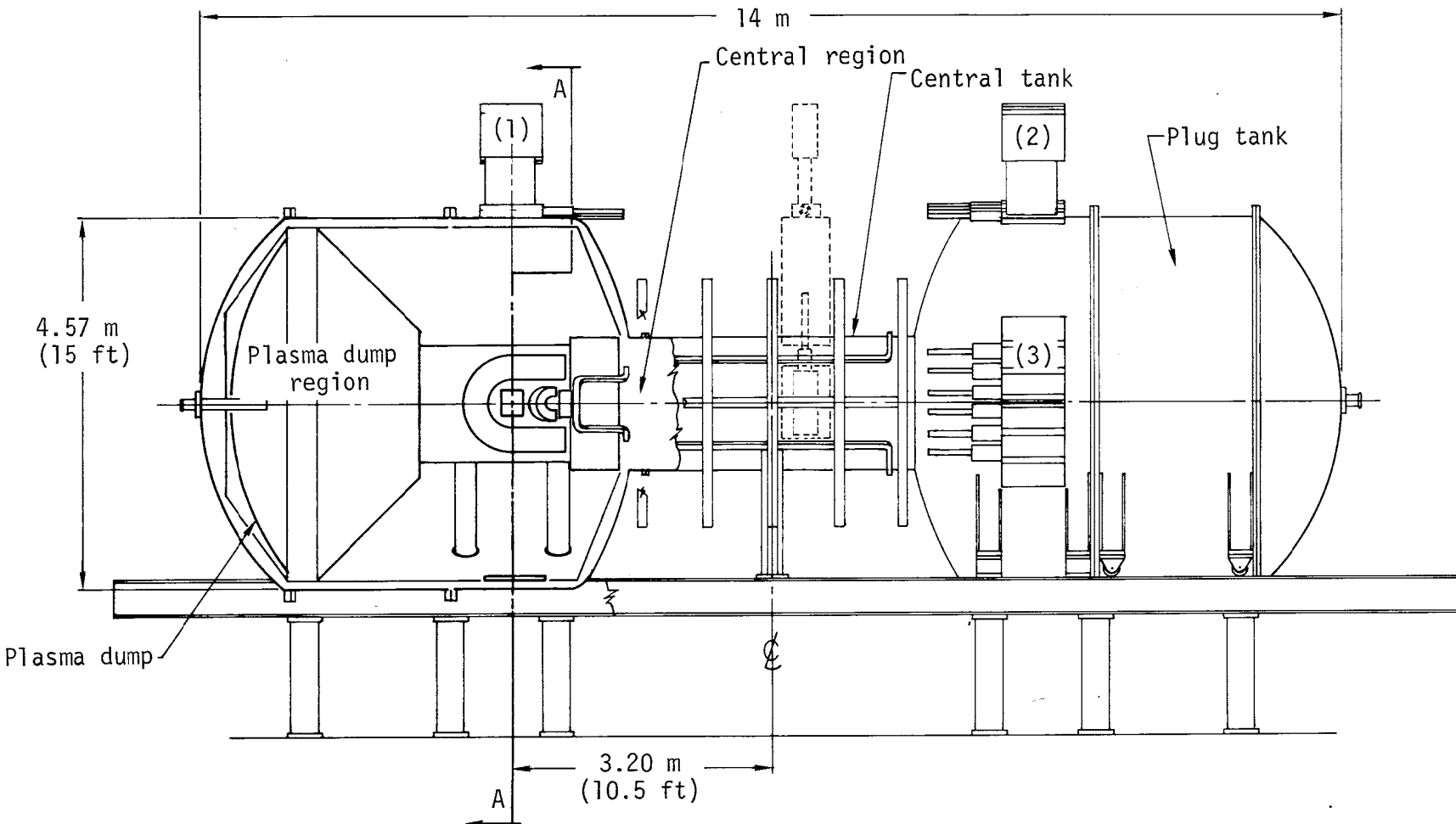


Fig. C-15. Vacuum system (elevation); (1), (2), and (3) are injector module arrays.

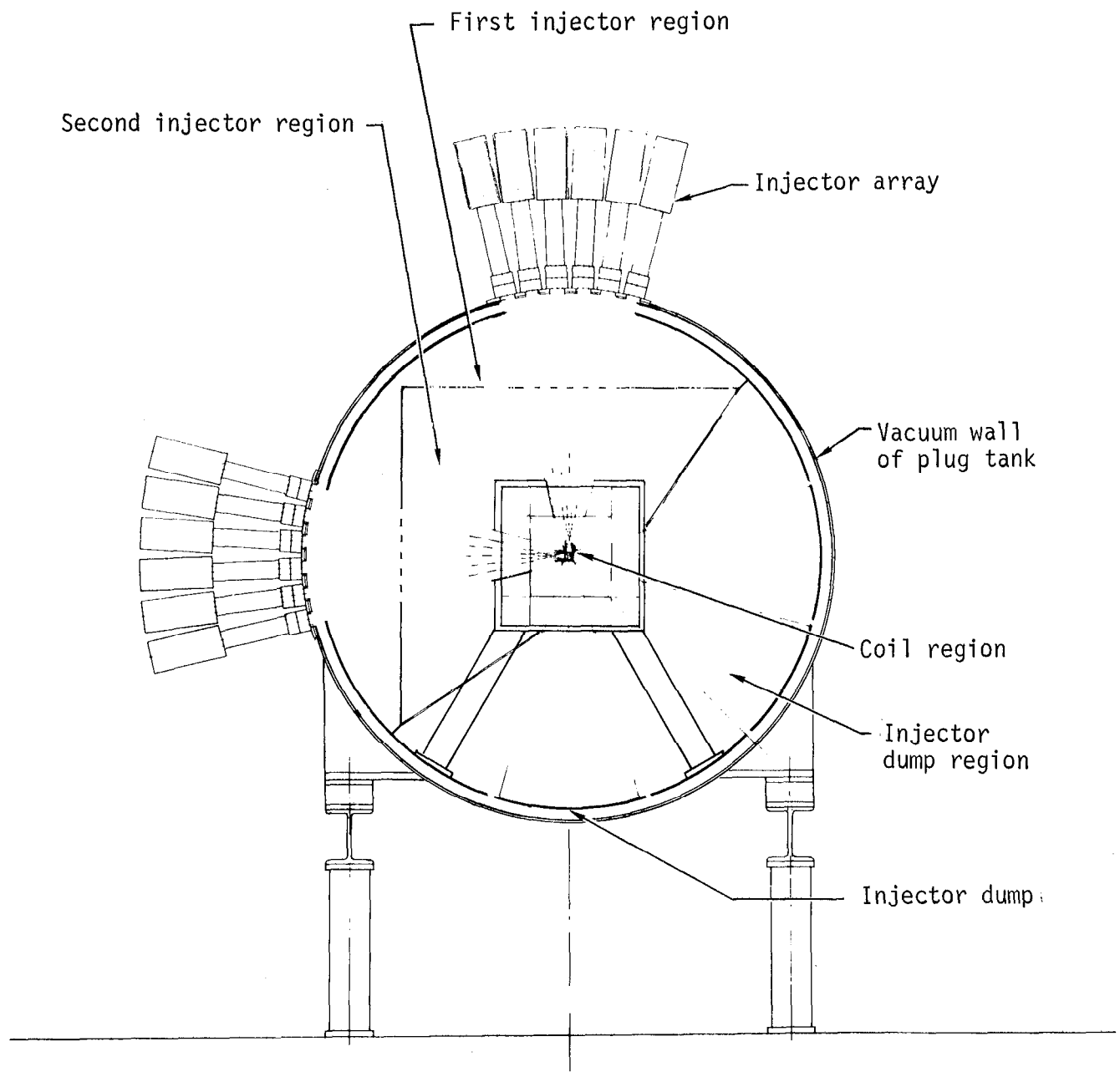


Fig. C-16. Vacuum system (cross section through plane A-A of Fig. C-15).

(see Table C-2). Thus, for a deposition of 20 monolayers ( $5 \times 10^{16}$  molecules/cm<sup>2</sup>) of Ti atoms in 1-min,  $\sim 280$  m of wire per set is distributed throughout the machine. This distribution must be such that a uniform coating is achieved.<sup>C3</sup>

The sublimator fixtures include mostly fixed wires, with some retractable units that can be removed from the plasma region and the beam lines during a shot by remote control. It is advantageous to design for removal of any getter unit from outside the vacuum wall, so that wire can be replaced without personnel having to enter the machine. This will be done wherever practical.

#### LN Liners

The LN liners are designed of stainless steel with a pillowed cross section and are similar to those used in 2XIIIB. This cross section provides for storage of sufficient LN to remove the heat absorbed during gettering while holding the temperature near 77 K. In addition, panels are heated by radiation from room-temperature surfaces. The resistance of the getter wire has been measured to be  $\sim 0.215$  Ω/m when run at 106 A.<sup>C4</sup> Thus, the total heat load for  $\sim 280$  m of getter wire is  $\sim 675$  kW, or an average of  $\sim 2$  kW/m<sup>2</sup>.

#### Plasma and Injector Dumps

The surfaces that the energetic particles strike in the two dump regions must handle the heat load imposed by the bombardment. They will be heated to improve pumping, since the sticking coefficient of high-energy H<sub>2</sub> and D<sub>2</sub> particles on warm Ti surfaces has been found to approach 0.95 for a 200°C surface<sup>C5</sup> (0.8 is used for our calculations.).

The pressure in the plasma dump region must remain low so as to minimize the introduction of cold electrons into the plug region. This pressure is estimated to be  $\sim 4 \times 10^{-6}$  Torr at equilibrium.

A second function of the injector dump will be to act as a calorimeter for focusing and aiming the neutral-beam sources.

#### Gas Load Sources

There are two main sources of gas loading: the gas box injectors and the neutral-beam injectors. For the latter, we assume that the input gas is 30 Torr·l/s for both the 40-keV source module and for the 20-keV source module.

Table C-2. Areas and volumes of regions in TMX.

Region	Volume (m <sup>3</sup> )	Pump area (m <sup>2</sup> )
Central	10	25
Plug-coil region (each of 2)	3	10
End dump (each of 2)	18	40
Injector regions		
First (each of 4)	5	23
Second (each of 4)	6	20
Dump (each of 4)	9	20
Gas box (each of 2)	<1	0
Plug tank total:	61	176
Total for machine:	132	377

(One standard molecular Torr $\cdot$ l/s is equal to  $3.29 \times 10^{19}$  molecules/s or, multiplying by  $e = 1.60 \times 10^{-19}$ , 5.28 molecular "amperes".) The 40-keV modules produce  $\sim 40$  "A" of energetic neutral atoms, whereas the 20-keV modules produce 50 "A". Thus, after subtracting the energetic atoms the molecular gas per source array with the two 40-keV sources operating (two arrays per plug) is 52.4 Torr $\cdot$ l/s.

The regions in which the energetic fraction is seen depend on the details of the neutral beam/plasma interaction and the molecular-gas/plasma interaction. Discussions of these interactions follow.

The gas load from the gas box injector is 150 "A". Nearly all of it appears at the plasma dump as the result of ionization reactions. A small fraction appears as molecular gas in either the plug or central region.

In addition to these two actual gas sources, there are the effective sources of gas resulting from the fraction of plasma that is refluxed as cold gas from the plasma dump and the portion of the penetrating neutral beam that strikes the injector dump and is refluxed as cold gas.

#### Neutral-Beam/Plasma Interaction

An injected neutral incident on the plasma can either undergo an ionization or charge-exchange collision or it can penetrate entirely through the plasma. In TMX, a penetrating neutral passes out of the plasma region into the injector dump region. There, it impinges on the injector dump and is either trapped or appears in the injector dump region as molecular gas to be pumped by the vacuum system. The nonpenetrating neutral becomes a trapped plasma ion. However, if it has undergone a charge-exchange collision, a new energetic neutral is produced from the former plasma ion. If the new neutral is not re-ionized in the plasma, it escapes and travels in a straight path until it encounters a solid surface. There, it loses its energy and is either pumped or refluxed as cold gas. We assume the particles are refluxed. The trapped plasma ions eventually scatter into one of the mirror loss cones and leak from the plug plasma region either into the central plasma region or out into the end-loss region. There, they strike the plasma dump and are either trapped or refluxed as cold gas.

The gas loading in the various regions will depend on the fractions of penetrating ( $f_p$ ), charge-exchange ( $f_{cx}$ ), and trapped neutrals ( $f_t$ ). These

fractions are functions of the injection energy, the plasma energy distribution, the injection beam and plasma geometries, and the plasma density.

#### Molecular-Gas/Plasma Interaction

It is assumed that all gas molecules encountering the plasma surface are converted into cold ions and ejected by the plasma potential into either the end region or the central region. Some of the encounters produce energetic charge-exchange neutrals that escape the plasma, impinge on a surface, and are either pumped or refluxed as cold gas. It is conservatively assumed that all these charge-exchange neutrals are refluxed as cold gas inside either the coil region or the central region. The fraction of neutrals that is ionized and that does not result in charge-exchange neutrals depends on the plasma energy, density, and geometry.

#### Gas-Balance Analysis

A final gas-balance analysis must depend on the factors discussed in the gas-flow section. However, a preliminary analysis has been performed using the relationship for a single region:

$$P(t) = \frac{Q_{in}}{(S + C_{out})} \left[ 1 - \exp \left( \frac{[S + C_{out}]}{V} \cdot t \right) \right],$$

and

$$Q_{out} = C_{out} \cdot \Delta P ,$$

where

- P(t) = pressure as a function of time (Torr),  
ΔP = pressure differential across outlet orifice (Torr),  
Q<sub>in</sub> = gas inflow (Torr·l/s)  
Q<sub>out</sub> = gas outflow (Torr·l/s),  
S = pumping speed (l/s),  
C<sub>out</sub> = conductance of outlet orifice (l/s),  
t = time (s), and  
V = region volume (l)

The pumping speed is the sum of the pumping speed of the gettered surfaces in the region plus the pumping speed of the plasma in regions where plasma is present (assuming unity reflux of charge-exchange neutrals).

Thus,

$$S = S_s + S_p,$$

$$S_s = 3.638 \left( \frac{T}{M} \right) \cdot (A_s) (a_s),$$

$$S_p = 3.638 \left( \frac{T}{M} \right) \cdot (A_p) (a_p),$$

where

$S_s$  = surface pumping speed ( $\ell/s$ ),

$S_p$  = plasma pumping speed ( $\ell/s$ ),

$T$  = gas temperature (K),

$M$  = gas molecular weight (amu),

$A_s$  = pumping surface area ( $\text{cm}^2$ ),

$A_p$  = plasma surface area ( $\text{cm}^2$ ),

$a_s$  = sticking coefficient for surface, and

$a_p$  = ionized (trapped) fraction of neutrals incident on plasma.

We assume that the sticking coefficient for Ti is 0.2 at 77 K and 0.03 at room temperature.<sup>C6</sup>

In addition to the molecular gas that enters the plasma region by molecular flow, there is a fraction,  $f_{ST}$ , that streams directly from a source through the apertures. This fraction is assumed to be entirely incident on the plasma. If the source is modeled as a point gas source,

$$f_{st} = \frac{A}{2\pi r^2},$$

where

$A$  = aperture area ( $\text{cm}^2$ ), and

$r$  = distance from point source to aperture (cm).

A model for the TMX vacuum system is shown in Fig. C-17. This model shows only half of the machine, since all calculations can be done on the basis of one plug tank.

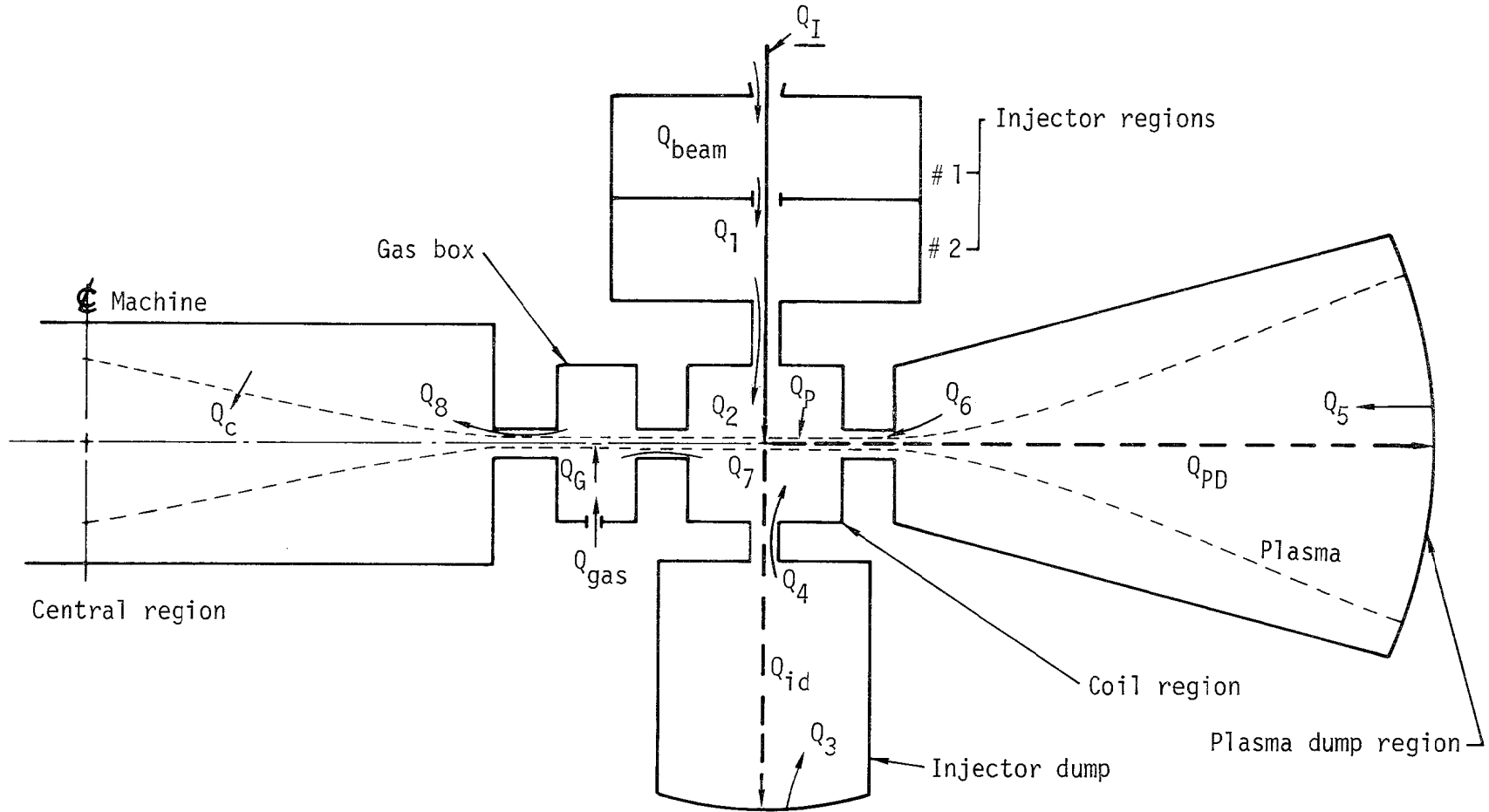


Fig. C-17. Schematic of primary vacuum system (showing one plug).

Preliminary analysis has shown that ~71% of the molecular gas that flows into the plug regions will be pumped by the plasma. Based on this analysis plus the assumptions that all trapped or pumped particles appear at the plasma dump and that the pressures in the coil and central regions remain low relative to other regions, a rough estimate of the plasma gas load for the plug can be made. The estimated flows are shown in Table C-3.

This analysis was based on an injected current of 160 A (full rated value) and a trapped current ( $Q_T$ ) of 19.2 A per plug, with  $f_T = 0.12$ . The estimate was for  $f_{cx} = 0.18$ ; therefore,  $f_p = 0.70$ . The ratio of incident gas ( $Q_p$ ) to trapped current then is

$$\frac{Q_p}{Q_T} \approx 1.6.$$

This is a highly conservative estimate; a more detailed analysis is in progress.

Table C-3. Gas flow into the coil region.

Description	Symbol	(Torr·l/s)	Value (A)
<b>From injector region</b>			
Molecular flow	$Q_2$	0.18	4.0
Streaming flow	$Q_{ST2}$	0.43	4.5
<b>From injector dump region</b>			
Molecular flow	$Q_4$	0.10	1.1
Streaming flow	$Q_{ST4}$	0.01	0.1
<b>From plasma dump region</b>			
Molecular flow	$Q_6$	0.08	0.8
Streaming flow	$Q_{ST6}$	0.01	0.1
From gas box (molecular flow)	$Q_7$	0.29	3.1
From charge-exchange neutrals	$Q_{cx}$	2.73	28.8
Total gas load on plug plasma	$Q_p$	2.85	30.1

### C3. INJECTION SYSTEM

#### General Description

The injection system of the TMX experiment includes the target-plasma generators, the neutral-beam injectors, and the gas-stabilization system. A streaming-plasma gun in each plug tank will create a target plasma for the 24 neutral-beam source modules that inject neutral deuterium atoms to replace losses and to heat a plasma stabilized by streaming cold gas applied by the gas-box system. The neutral-beam sources operate for 25 ms, and in that time deliver to the target plasma 800 A of neutrals from the 20-keV injectors together with 320 A of neutrals from the 40-keV injectors. These are the total rated currents and include the half- and third-energy components as well as full-energy ions.

Two groups of neutral beams, each containing 6 beams, are mounted on each end plug tank as shown in Fig. C-18. The single-column array of six modules shown in Fig. C-19 contains four 20-keV, 50-A modules and two 40-keV, 40-A modules and is one of four typical groups. Two of the 20-keV modules can be used to inject into the central-cell plasma for additional ion heating as shown in Fig. C-18. Both the 20-keV and 40-keV neutral beams from 2XIIB will be used; additional beam modules will be built as needed. Specifications for these sources are listed in Table C-4, and a source schematic is shown in Fig. C-20. All of the beam sources are located at a radial distance of 3.2 m and are aimed at the machine centerline. To minimize refluxed gas to the plasma, the two six-source groups shown in the cross-sectional view of Fig. C-16 have been positioned to inject the beam that passes through the plasma into a dump region opposite the injector modules. This arrangement requires the smallest aperture sizes and thereby offers a higher impedance to gas streaming from the source. The apertures accommodate beam divergences of  $\pm 0.5^\circ$  in the direction of the grid wires and  $\pm 2^\circ$  transverse to the grid wires.

Figure C-21 shows the typical arrangement of source, shielding, neutralizer, and isolation valve. The source module is mounted on an adjustable plate platform that incorporates a rectangular metal bellows and provides for adjustment with two degrees of freedom. A segmented calorimeter together with a laser mounted on the source arc chamber as a reference are used to align the sources. Once the mounting plate has been positioned, it need not be readjusted except when the aim of the sources is being changed.

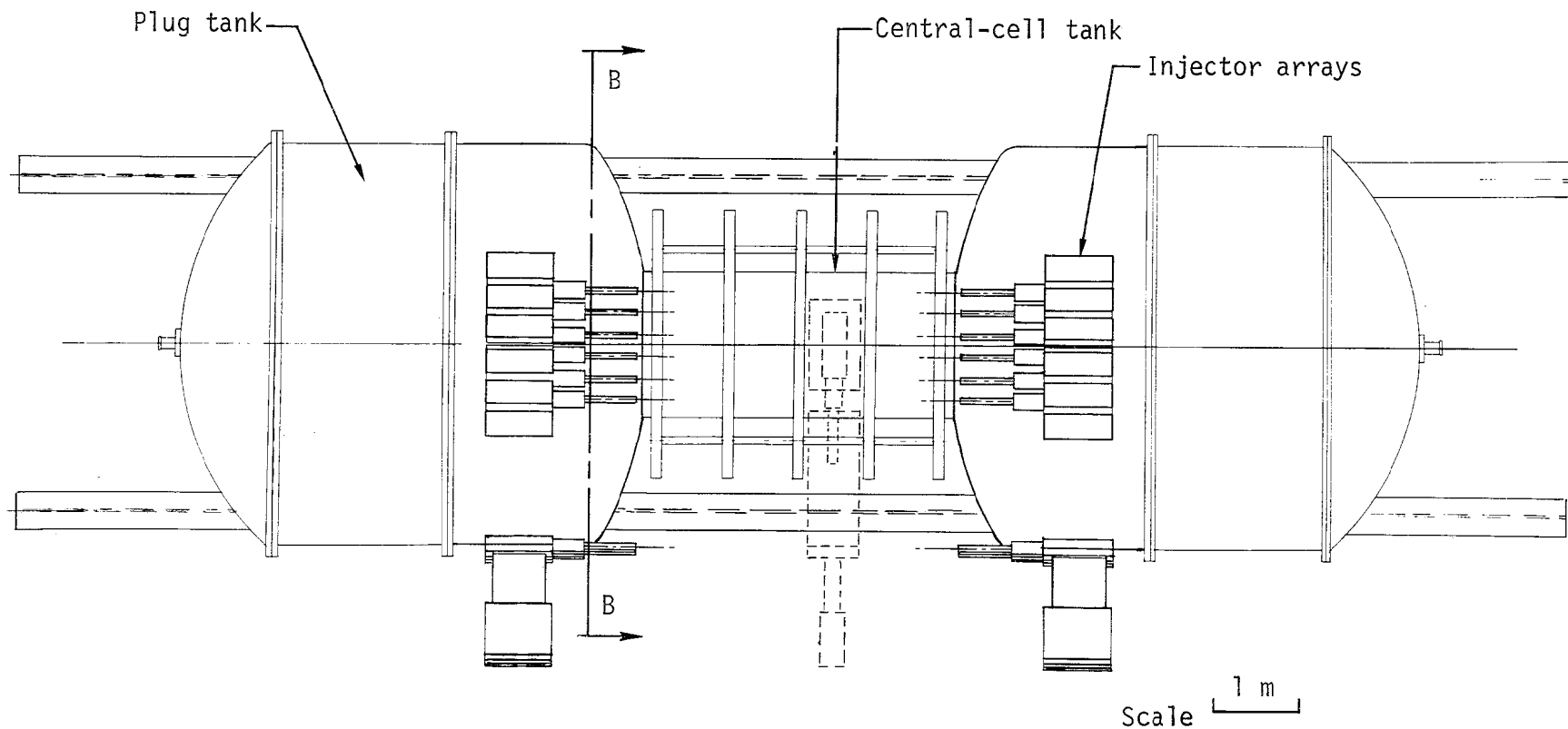


Fig. C-18. Injection system (plan view).

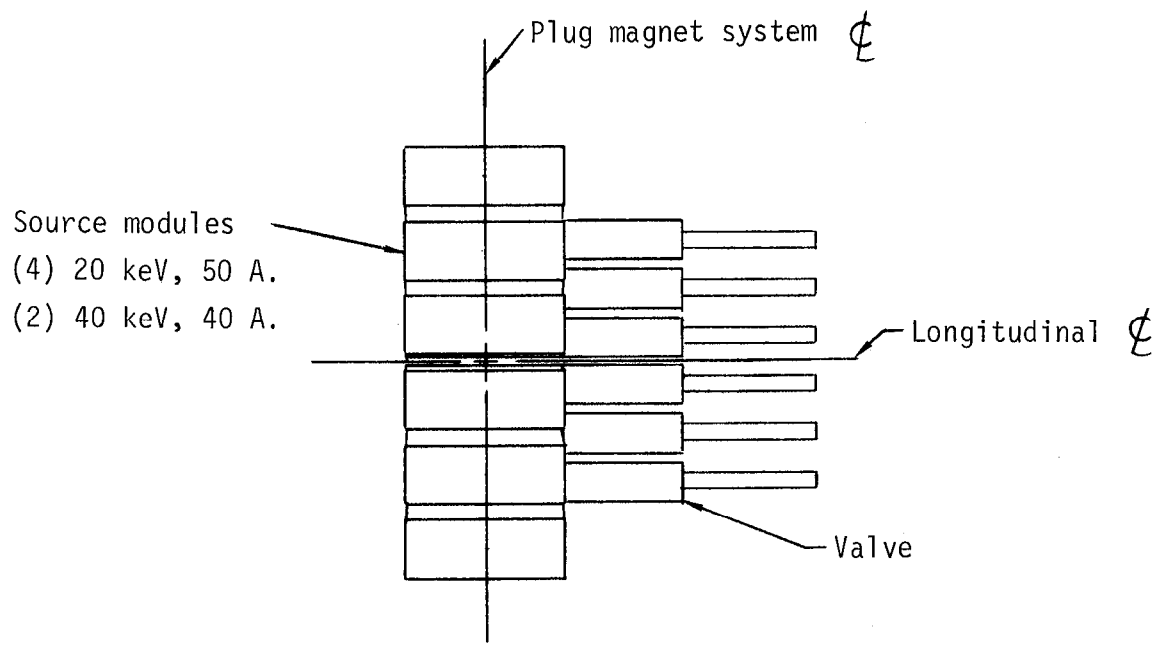


Fig. C-19. Injection system (end view through single-column array of 6 neutral-beam modules).

Table C-4. Neutral injector module specifications.

Parameter	20-keV Module	40-keV Module
Max. neutral beam energy	20 keV	40 keV
Avg. neutral beam energy	~15 keV	~29 keV
Power supply drain	80 A	65 A
Extractor current density	0.5 A/cm <sup>2</sup>	0.4 A/cm <sup>2</sup>
Extractor dimensions	7 cm × 35 cm	7 cm × 35 cm
Overall dimensions	20 cm × 58 cm	20 cm × 58 cm
Pulse length	25 ms	25 ms
D <sub>2</sub> gas inlet	30 Torr·l/s	30 Torr·l/s
Beam divergence	±2° W × ±0.5° H	±2° W × ±0.5° H
Beam at plasma (rated value)	50-A neutrals in 10 cm high × 33 cm wide.	40-A neutrals in 10 cm high × 33 cm wide.

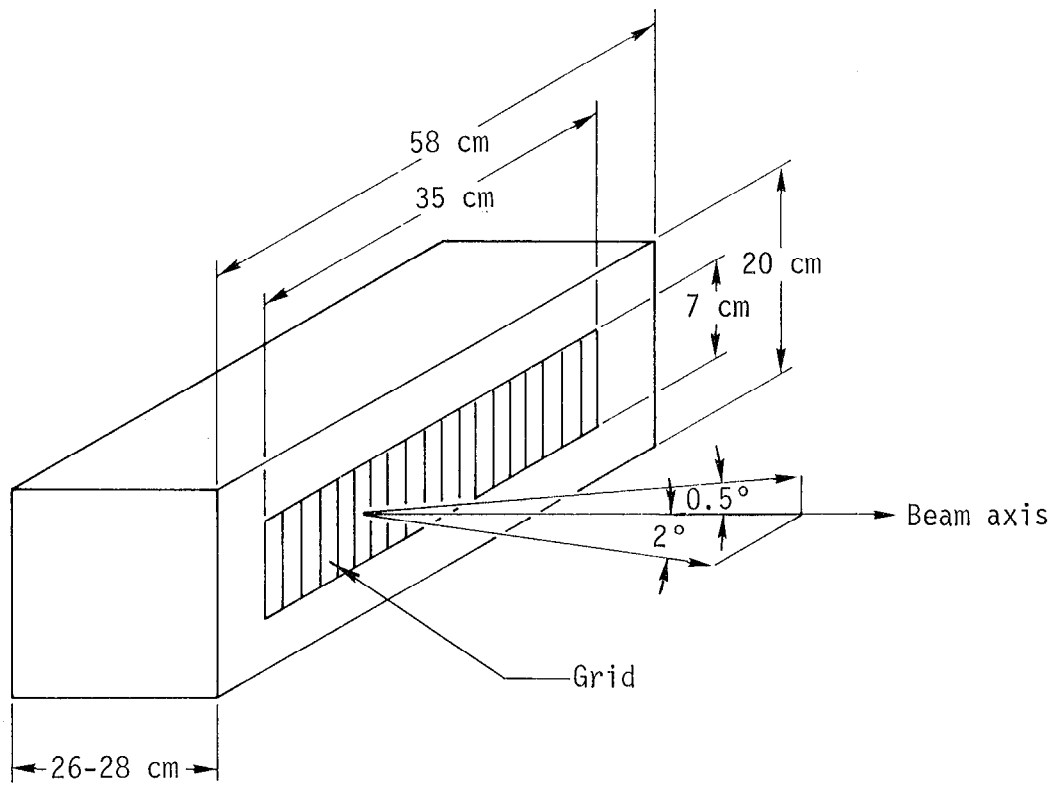


Fig. C-20. Simplified diagram of a neutral-beam injector module.

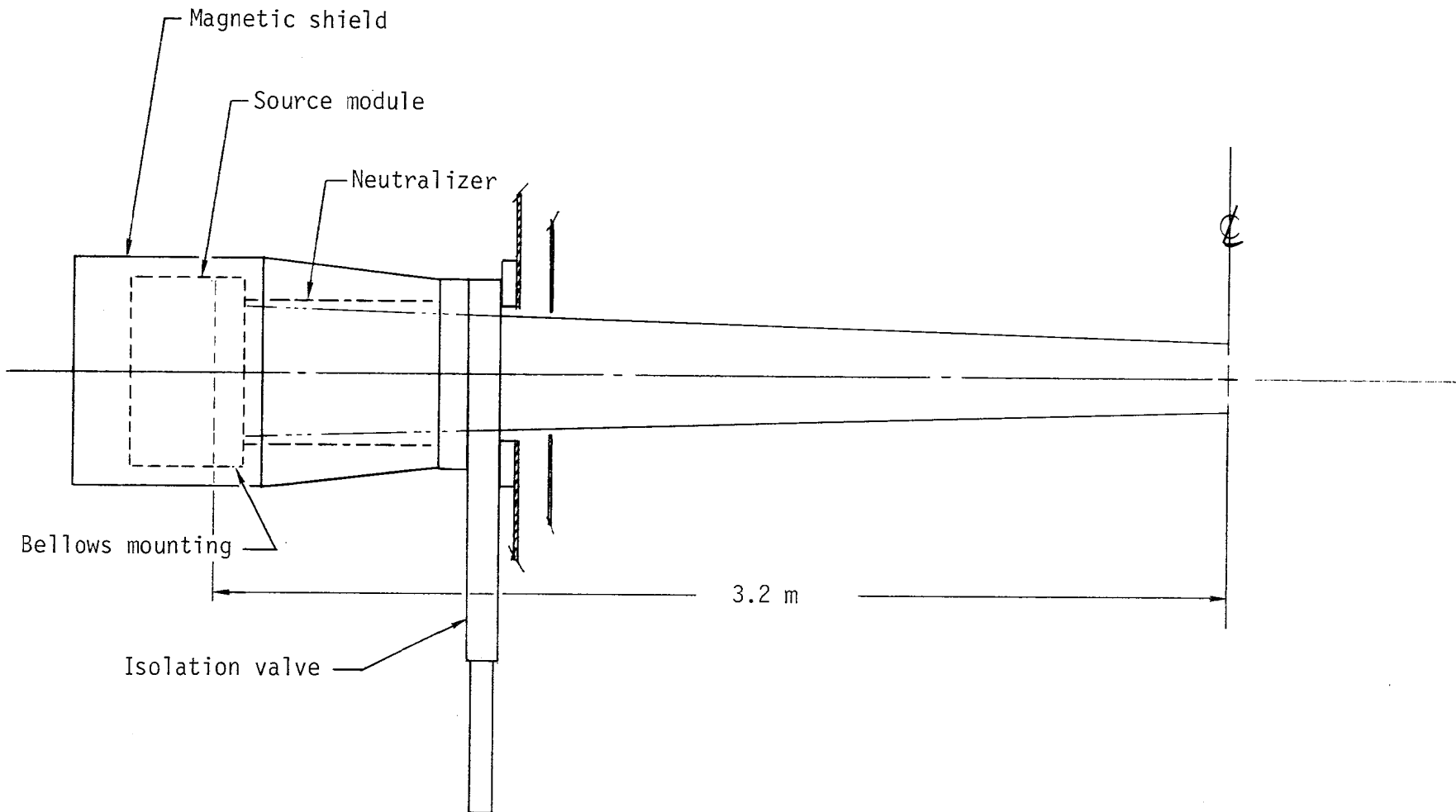


Fig. C-21. Typical arrangement of source shielding, neutralizer, and isolation valve in the injection system.

### Injector Magnetic Shielding

Because the neutral-beam sources are sensitive to magnetic fields, they are shielded against a magnetic intensity approximately equal to that at the 2XIIIB modules. The magnetic field intensity perpendicular to the centerline of the neutralizer must be  $\leq 0.5$  mT. Neutrals exiting the neutralizer thus experience a displacement no greater than 2.0 cm at the plasma. The basic shield design has an outer layer of 0.95-cm-thick 1010 steel within which are fitted one or more 0.13-cm-thick layers of a high-permeability material. The shielding isolates a space beginning approximately 0.4 m behind the first source grid and extending to the front for a length of about 0.7 m. A prime requirement of the high-permeability shells is that there be no breaks throughout their lengths in order to preclude conducting flux into the shielded space. To determine material combinations and thicknesses required to reduce the field to acceptable values, we use the LLL JASON<sup>C7</sup> computer code together with experience gained on the 2XIIIB and Baseball II experiments. The JASON computer code was developed to solve complex electrostatic problems using finite-element methods. A module spacing of approximately 30 cm is provided to reduce the need for a gas dielectric ( $SF_6$ ) to prevent electric breakdown from the 40-kV extraction structure. However, to be conservative, the magnetic shields will be designed to provide a gas dielectric environment if needed. The 20- and 40-keV sources use the same mounting hardware, magnetic shields, etc., and are thus interchangeable, except perhaps for neutralizer length.

### Isolation Valves

A key factor to maintaining an experimental machine in a running mode is the ability to perform maintenance on the injector modules while preserving vacuum conditions. Minimum exposure of the cryogenic surfaces to atmosphere is also desirable. Thus, each module is assembled with an isolation valve located forward of the neutralizer section (see Fig. C-21). These vacuum valves have a rectangular gate plate sized to the 10- by 40-cm cross section of the beam. The direction of movement in these valves is constrained to parallel the long direction of the opening because of the proximity of adjacent modules. This subsystem is interlocked to prevent inadvertent operation if a module has been removed or if a mounted module has not yet been pumped down.

### Target-Plasma Generator

One of the two streaming-plasma guns used to create the startup plasma in the TMX experiment is mounted on the axis at each end of the vacuum chamber. These guns inject a plasma column approximately 10 cm in diameter through apertures in the end-plate surfaces of the expander. Individual vacuum valves provide system isolation for maintenance of the guns, each of which is a cylinder 7.6 cm in diameter by 87 cm long.

### Gas Stabilization System

The two gas box systems shown in Fig. C-22 provide plasma particles for the central cell, whose end losses stabilize the plasma in the plug magnets. About 150 A of deuterium gas is bled into each gas box by four fast pulse valves, which are shown in Fig. C-22. Only about half of this gas becomes ionized in the plug plasma; the remainder leaks past the elliptically shaped cutouts in the face plates of the gas box. This gas will be pumped at a rate sufficient to maintain a lower pressure in the plug tanks than in the central cell. The elliptical cutouts in the face plates are shaped to match the cross section of the plasma fan.

### Neutral-Beam Power Supplies

Each neutral beam requires accelerating, filament, arc, and decelerating power supplies and controls. The characteristics of these power supplies are given in Table C-5. The power supply complement includes one additional unit to be used on a test stand for breaking in source modules. Figure C-23 shows how the power supplies are connected to the source.

The accelerating power supply consists of a capacitor bank discharged through a hard tube modulator. Existing electrolytic capacitor banks will be rewired to supply the 40-kV supplies. The 20-kV supplies are powered from the oil capacitor bank now used to power the 2XIIB magnet. The present series switch ignitrons will be converted to crowbar the bank in the event of a fault. In addition to existing modulators, seven new modulators are required.

The existing filament supplies are driven from the 480-V ac line through a delta primary and dual secondary (delta and wye), with full-wave rectification. The dc outputs are paralleled. Eight new supplies are required. These new filament supplies use 10 batteries in each unit. The supply is fully protected with fuses, and a separate charging supply is used for each of the eight supplies.

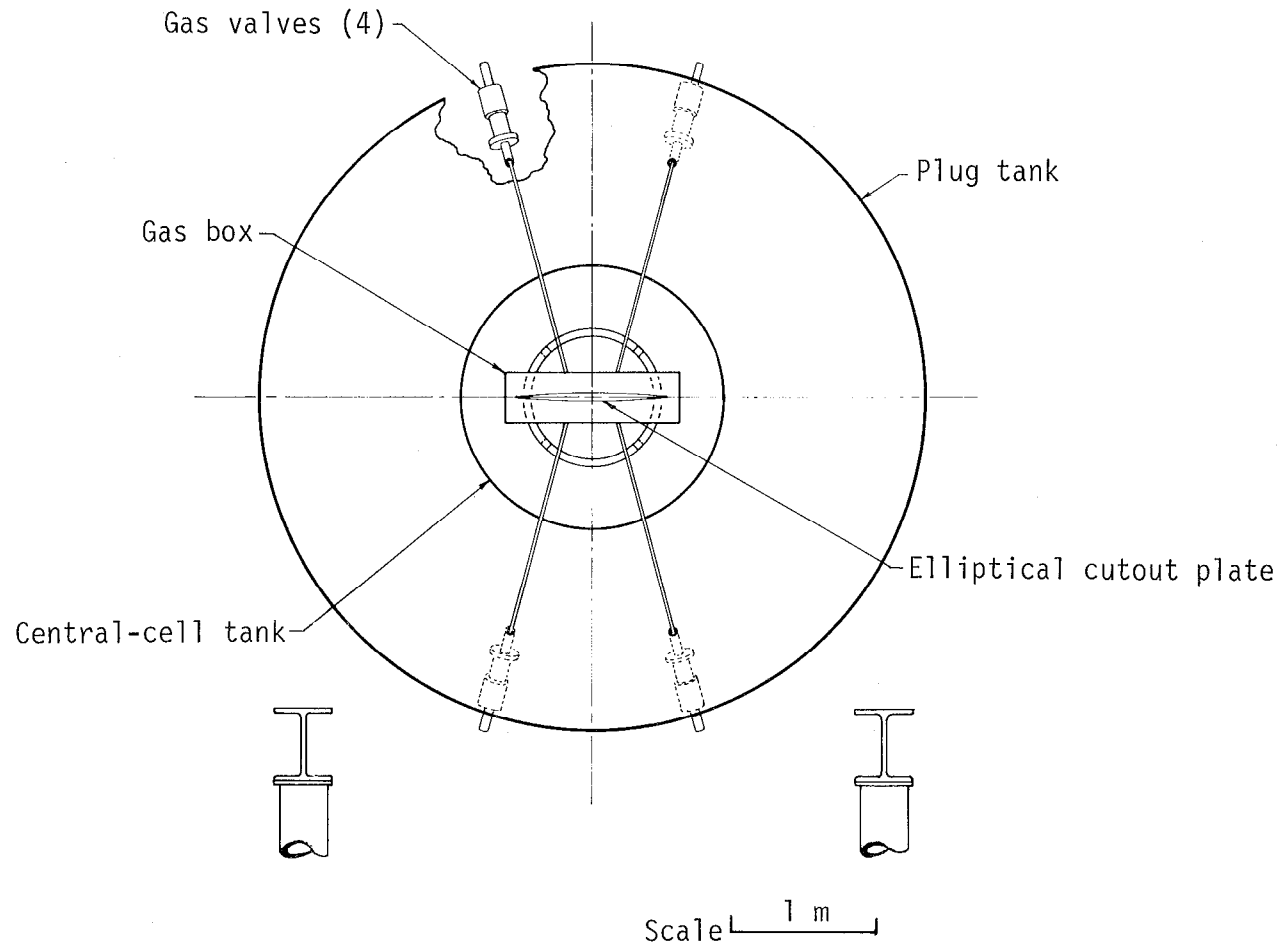


Fig. C-22. Gas-stabilization system (section B-B from Fig. C-18).

Table C-5. Summary of neutral-beam power supplies.

	Number	Voltage		Current	Time	
Accel	9	40	kV	80 A	25	ms
	16	20	kV	80 A	25	ms
Decel	25	5	kV	20 A	25	ms
Arc	25	50	V	5000 A	25	ms
Filament	25	11.4	V	2400 A	1.5 s	

Note: One 40-kV power supply to be used on test stand.

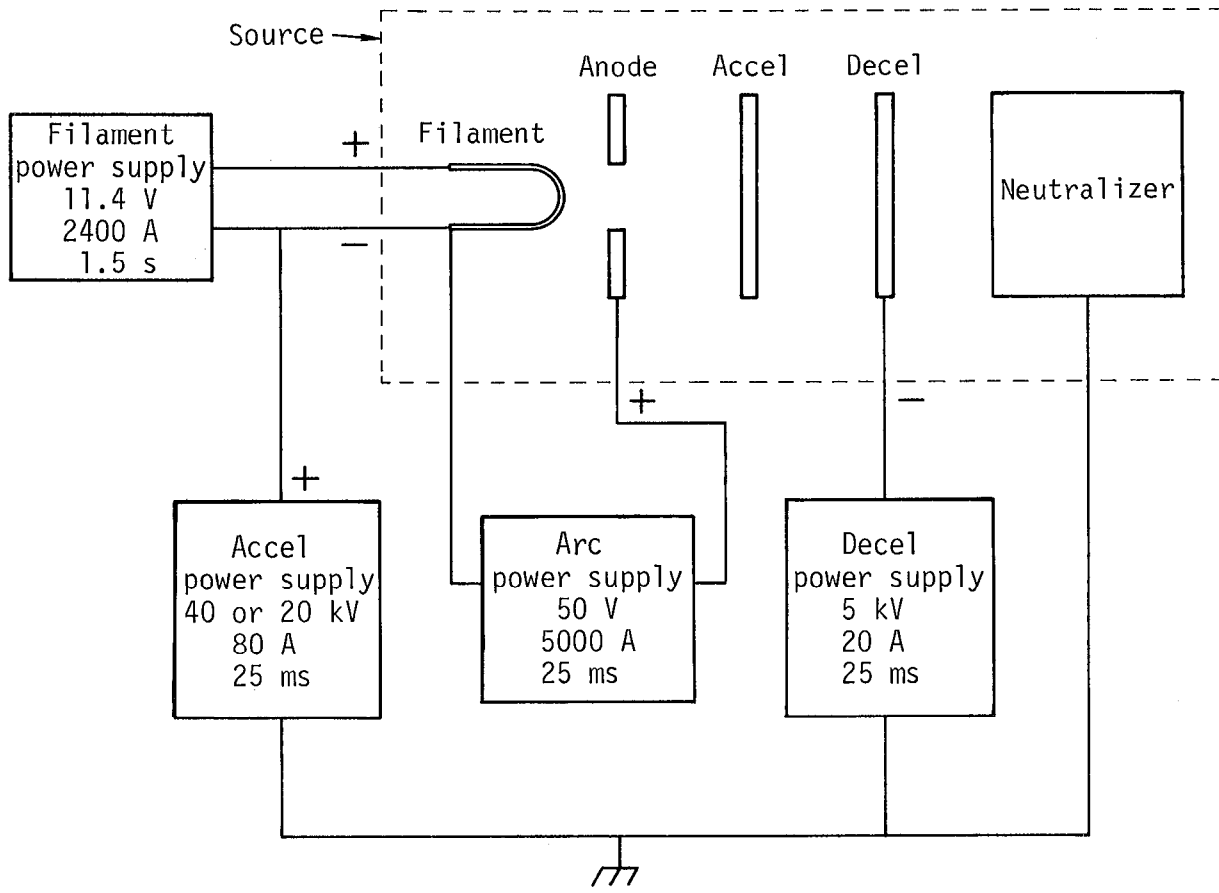


Fig. C-23. Power supply for neutral-beam source. The accel, anode, and filament are tied together electrically by the plasma created by the arc.

The arc supplies are of two types. Eight supplies are made by wiring two existing lumped-parameter pulse-forming networks in series to form the arc-pulse line (APL). This configuration is necessary to lengthen the pulse to 25 ms. Three and one-half new 25-ms APL's are required in combination with existing APL's for the north side of the machine where space is limited. All 12 arc supplies on the south side are new supplies of the battery type. Sixty-four batteries are used per supply; each battery supplies 1290 A·h. Each supply is charged by a separate charging supply.

The decel power supplies must be modified for 25-ms operation by increasing the capacitance. Eighteen existing supplies together with seven new supplies are needed.

Twelve control systems for neutral beams exist, and 13 new ones are required. The new controls are modeled after the old ones except where differences exist due to the battery supplies. Table C-6 contains a summary of the existing supplies and required new supplies.

#### Target-Plasma Generator Power Supply

We have the two streaming-plasma guns. Each gun is required to operate independently and has its own timing/triggering controls and charging power supplies.

To initiate the firing cycle, the power supply furnishes two 5- $\mu$ s ionizing pulses (one 10-kV, the other 70-kV) to the gun. To create the streaming plasma, the power supply then delivers stored energy from the pulse-forming network (PFN) to the gun. Figure C-24 shows the block diagram for this system. The power supply operates from either manual or computer control. The PFN voltage is controllable over a range of 50% to 100%.

Table C-6. Summary of the existing and new supplies.

Equipment	Existing	New
20-kV power supply		
Accel	16	-
Filament	16	-
Arc	8	8
Decel	16	-
Controls	12	4
40-kV power supply		
Accel	2	7
Filament	1	8
Arc	1/2	8-1/2
Decel	2	7
Controls	-	9

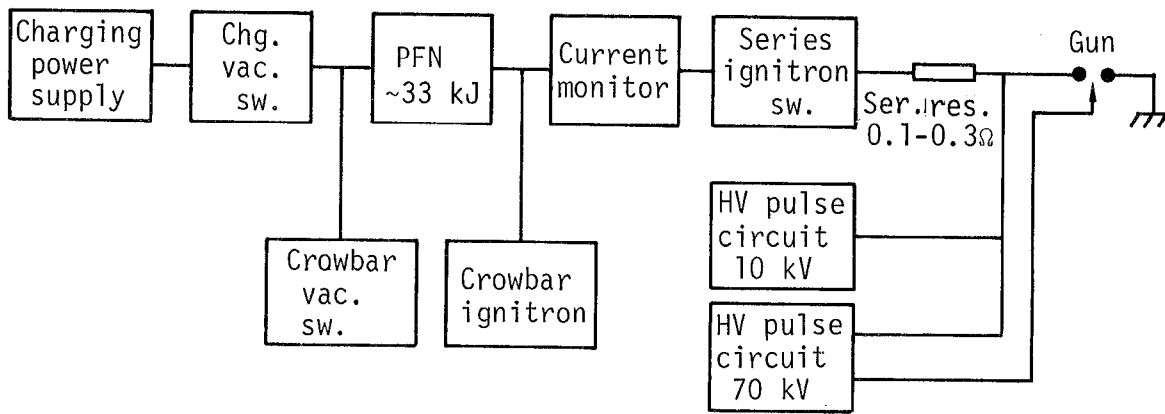


Fig. C-24. Power supply for streaming plasma gun. This system uses pulse-forming network energy storage with auxiliary 70-kV and 10-kV ionizing pulses to trigger the gun.

#### C4. FACILITY

##### Description

The TMX machine and its support facilities will be located in LLL's Bldgs. 435, 436, and 446, utilizing areas previously occupied by the Baseball II-T experiment and by parts of the 2XIIB experiment. The west high-bay area of Bldg. 435, which will house the vacuum vessel, control rooms, and most of the power supplies for the neutral-beam source, is approximately 60 ft by 120 ft (Fig. C-25). The vacuum vessel is oriented east-west in the high bay; it is set in a pit to provide 360° access and is surrounded by a concrete neutron shield. The machine is flanked to the north and south by tiers for supporting the power supplies for the neutral beams and streaming-plasma guns. Other power supplies, located in Bldg. 436, energize the coil set through existing tunneling into the high-bay area. All systems are controlled from racks along the east side of the high-bay area.

Plasma diagnostics are performed in the existing 2XIIB facility. This allows the diagnostic facility and data-retrieval system to be used for either TMX experiments or for 2XIIB experiments. The ground floor of the high bay, the mezzanine levels, and the outlying rooms provide approximately 21,000 ft<sup>2</sup> of floor space that can be utilized by the experiment. The high-bay area is served by a 17-ton-capacity bridge crane.

##### Building and Site Preparation

Most of the west high-bay area is now occupied by the Baseball II-T experiment. Much of the utility piping, conduit, and cabling associated with that experiment will be removed to make room for new construction. The vacuum vessel, coil, source tank, and burial tank will all be removed to a storage area, along with the entire target plasma generator, and the clean room and its associated air conditioning and filtering systems. Rooms 1020, 2020, 1143, and 1153 will be cleared of all old furniture, benches, racks, and cabling. Rooms 1143 and 1153 will serve as temporary storage for all the electronic equipment that must be cleared out of the racks in the high-bay area before excavation of the pit can begin. Existing racks at the southwest, southeast, and north sides of the high-bay area will be removed. All reusable equipment such as valves and mechanical pumps will be stored until needed.

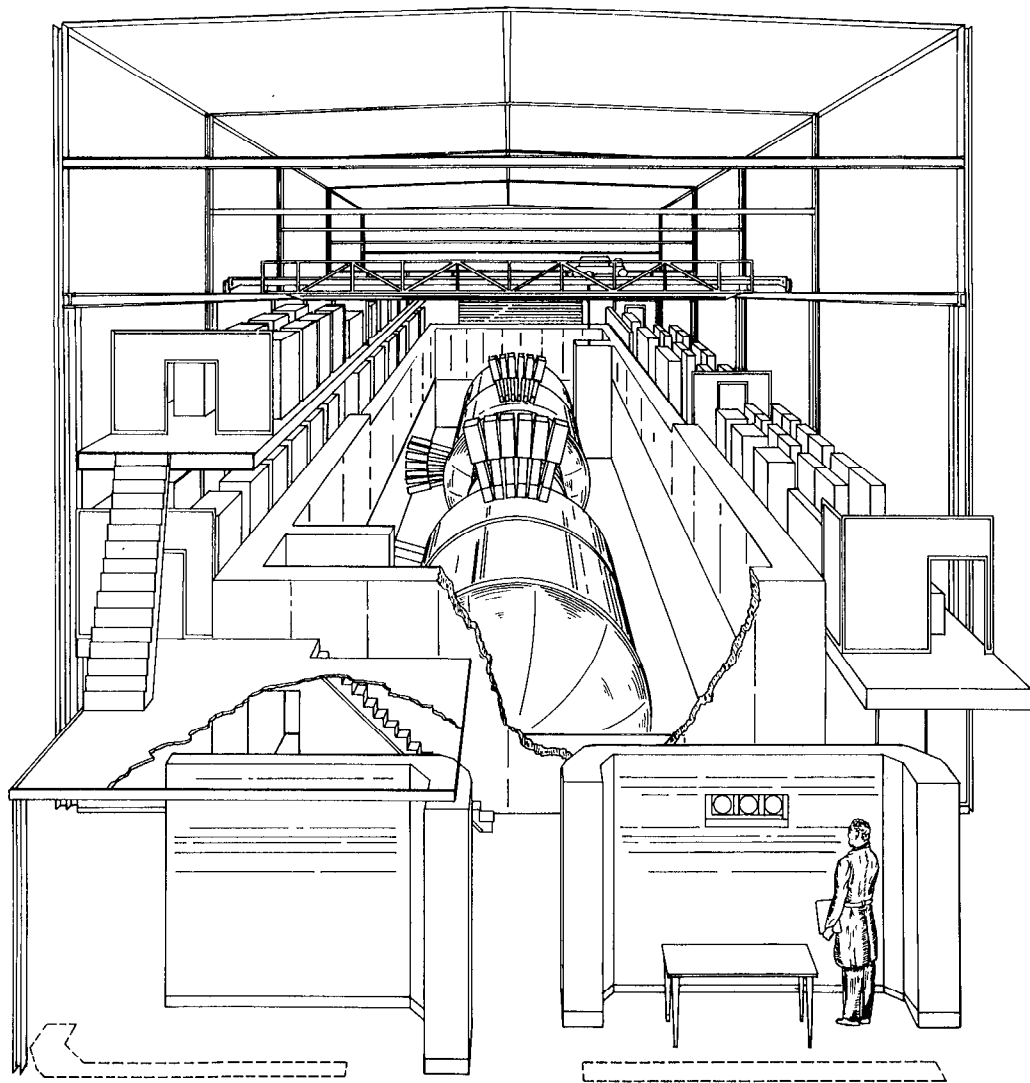


Fig. C-25. Conceptual drawing of the TMX facility.

The helium liquifier, purifier, and 10,000-litre Dewar will be moved to other locations. Liquid-nitrogen feed and exhaust lines to the high-bay area will be upgraded to meet the vacuum vessel pumping requirements.

Adequate electrical power exists in the area to supply both the neutral beams and the coils (see Fig. C-14). The continuous-load line power available in the area is 9.75 MVA; however, the line power can be pulsed to 20 MVA for 5 s at 2-min intervals to accommodate the coil power supplies in Bldg. 436. To isolate the building utilities from this pulsed line loading by the TMX machine, a new 13.8-kV feeder line will be brought through existing conduit to the transformer pad southeast of Bldg. 435. We are also considering the feasibility of upgrading the 13.8-kV lines to 40-MVA capacity from the present 22.5 MVA by redistributing loads at the plant substation.

Building 436 now houses 15 coil power supplies for the 2XIIIB experiment (see Fig. C-13). To allow expansion of the power supply banks to 25 modules, some existing mechanical equipment must be relocated. Also, the existing oil capacitor banks will be used to store neutral-beam energy. Electrolytic capacitor banks in Bldg. 436 and batteries on the high-bay tiers will provide energy storage for the remaining neutral beams.

#### Building Modifications and Additions

Major modifications to Bldg. 435 are necessary to accommodate the TMX machine. In the high-bay area, a large pit will be centrally located between two existing tunnels to accommodate the vacuum vessel and its required pumping and to provide 360° access for diagnostic probes and neutral-beam assemblies (see Fig. C-26). The pit, which will be 32 ft wide by 56 ft long by 12 ft deep, will cut through the existing tunnels that will provide cabling access. The pit depth is determined by allowing sufficient clearance for mechanical pumping yet minimizing the scaffolding required to service ports on the vacuum vessel (Fig. C-27). The vacuum vessel centerline will be approximately at the high-bay ground level. Recessing the vacuum vessel into a pit serves a secondary purpose of reducing the height of the neutron shielding required. The pit width is determined by the requirements of neutral-beam assembly positioning in the radial direction with respect to the tank z-axis and by crane access to the pit for removal and installation of mechanical equipment without disturbing the vacuum vessel. The pit also requires the installation of utility lighting

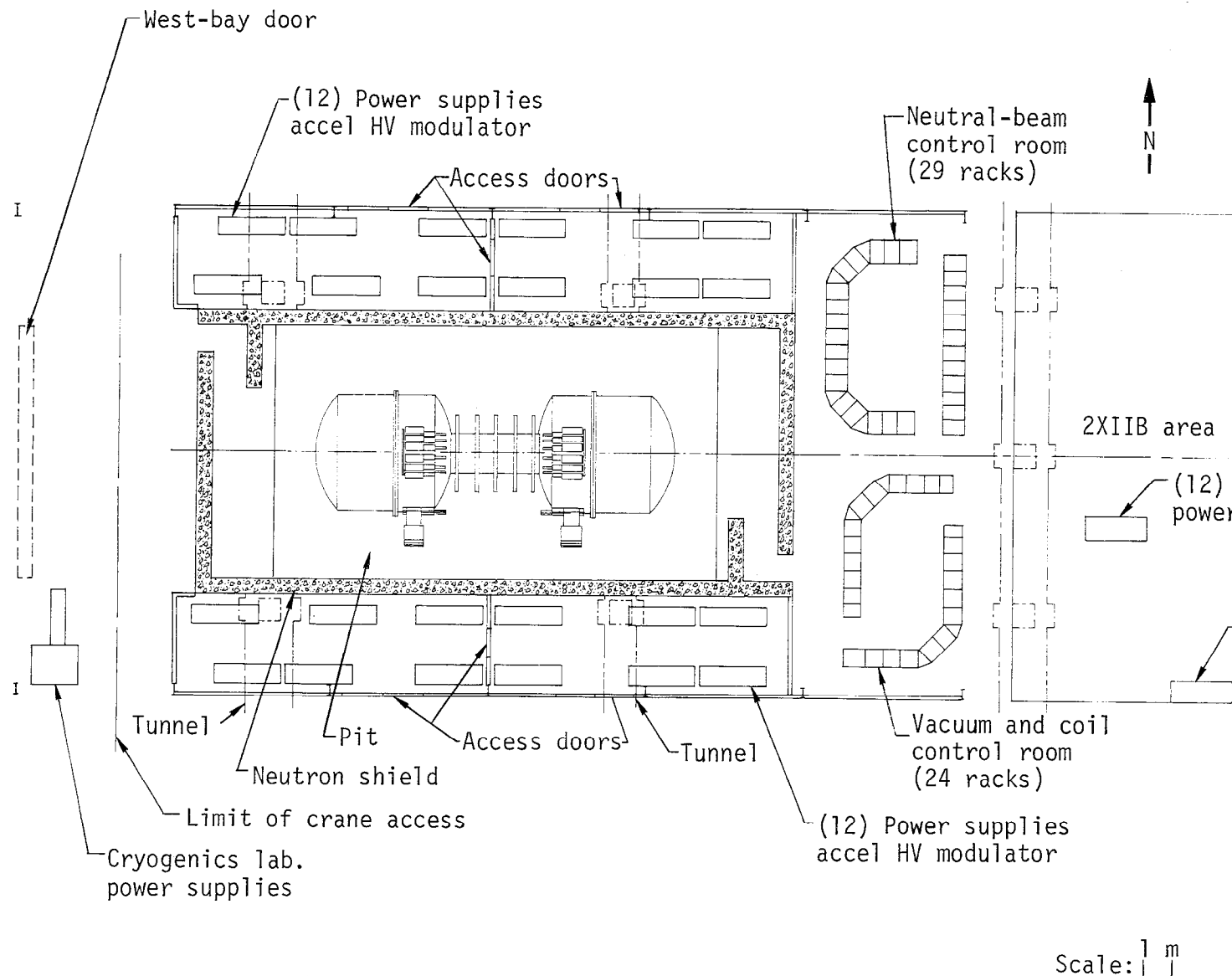


Fig. C-26. Ground-level plan of Building 435 high-bay area.

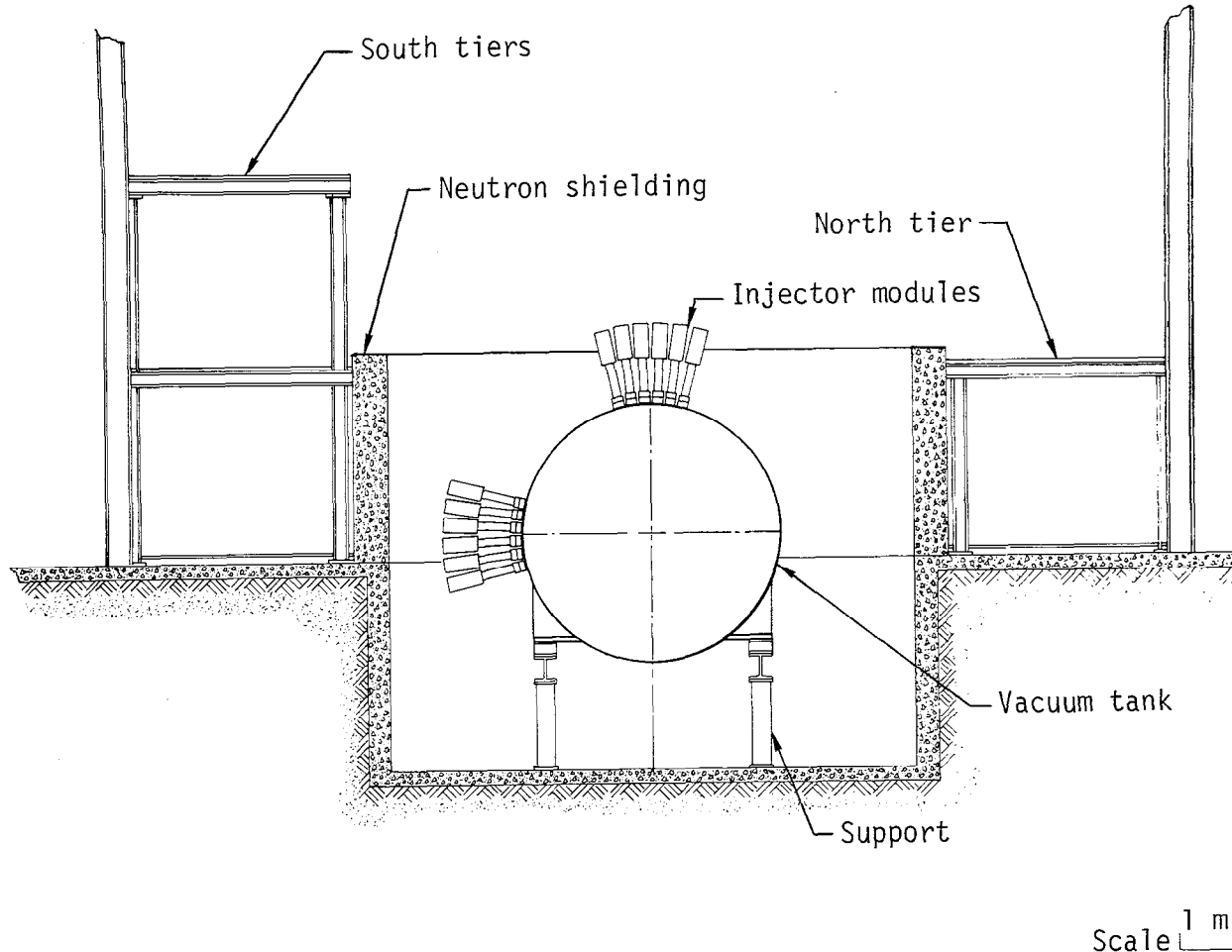


Fig. C-27. West elevation of Building 435 high-bay area.

and power, a sump pump, LCW and standard water lines, and an air-circulation ventilation system. High-load columns in the pit will support the TMX machine.

Surrounding the pit is a 72-ft-long by 32-ft-wide concrete neutron shield. The neutron shield consists of a modular, block construction bounded on the north and south sides by tiers of neutral-beam power supplies, on the east by control rooms, and on the west by the high-bay crane access. The height of the east wall will be 14 ft; portions of the north and south walls will be 12 ft; the remainder will be 10 ft. To provide adequate protection against the anticipated levels of neutron flux the walls must be 2 ft thick. The extent of the neutron shield is dependent on the degree of protection needed for personnel on the high-bay floor and in outlying second-floor areas of Bldg. 435. Not only the plasma is considered a source of neutrons; both machine and air-refluxing effects must also be considered in shield design. The neutron shielding requirements are discussed in more detail in Appendix C-5. With installation of the concrete-block wall, provision will be made for utility lighting and power.

Tiers for the neutral-beam power supplies to the north and south of the neutron shield wall in the high-bay area will be 12 ft above the ground floor (see Fig. C-28) and will have an area approximately 12 ft by 80 ft each. The south tier will also have a second level (see Fig. C-29) that will be 22 ft above the ground floor. These three tiers and the floor space beneath provide about 4,800 ft<sup>2</sup> for the power supplies for the neutral beams and the streaming-plasma gun. Some floor preparation will be required to support the tier columns. The hallway areas flanking the high bay have adequate utility feeder size to furnish required lighting, neutral-beam power, LCW, and fire sprinklers.

Using salvaged racks and others in storage, a new, 29-rack neutral-beam control room will be constructed in the northeast high-bay area. The existing southeast high-bay area racks, which would control the machine vacuum and coils, consist of 24 racks. The existing platform over the southeast racks will remain for utility equipment mounting, e.g., air conditioning, that may be needed to support the control rooms.

Plasma diagnostics will be performed in the existing 2XIIB facility. Room 2020 will have the existing partitioning removed, the west wall sealed, and adequate lighting, power, and air conditioning added to allow a later expansion of the diagnostics facility. The east wall will be broken through to the 2XIIB diagnostics area to allow physical access and cabling.

-0/1

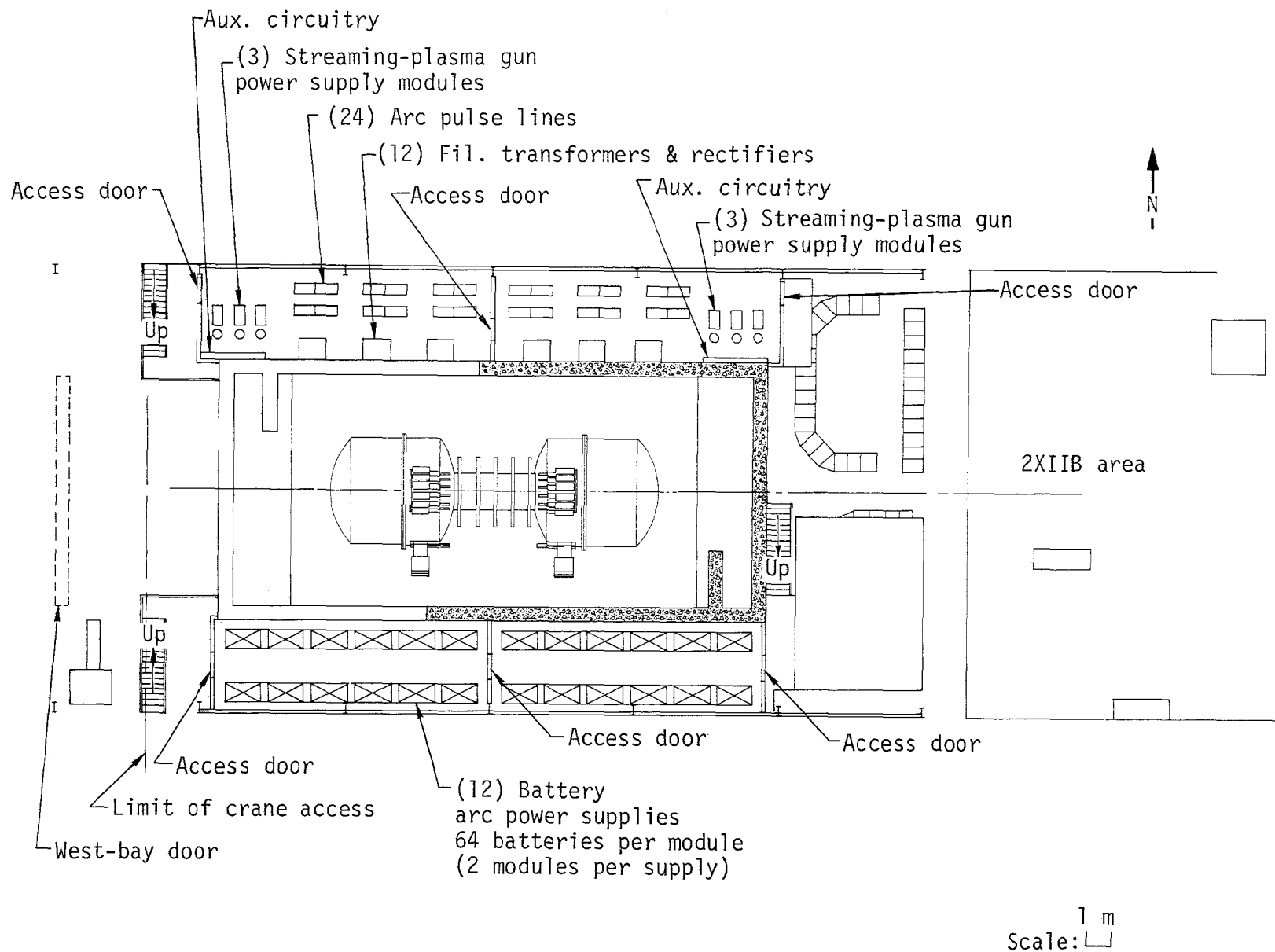


Fig. C-28. First tier level plan of Building 435 high-bay area.

-171-

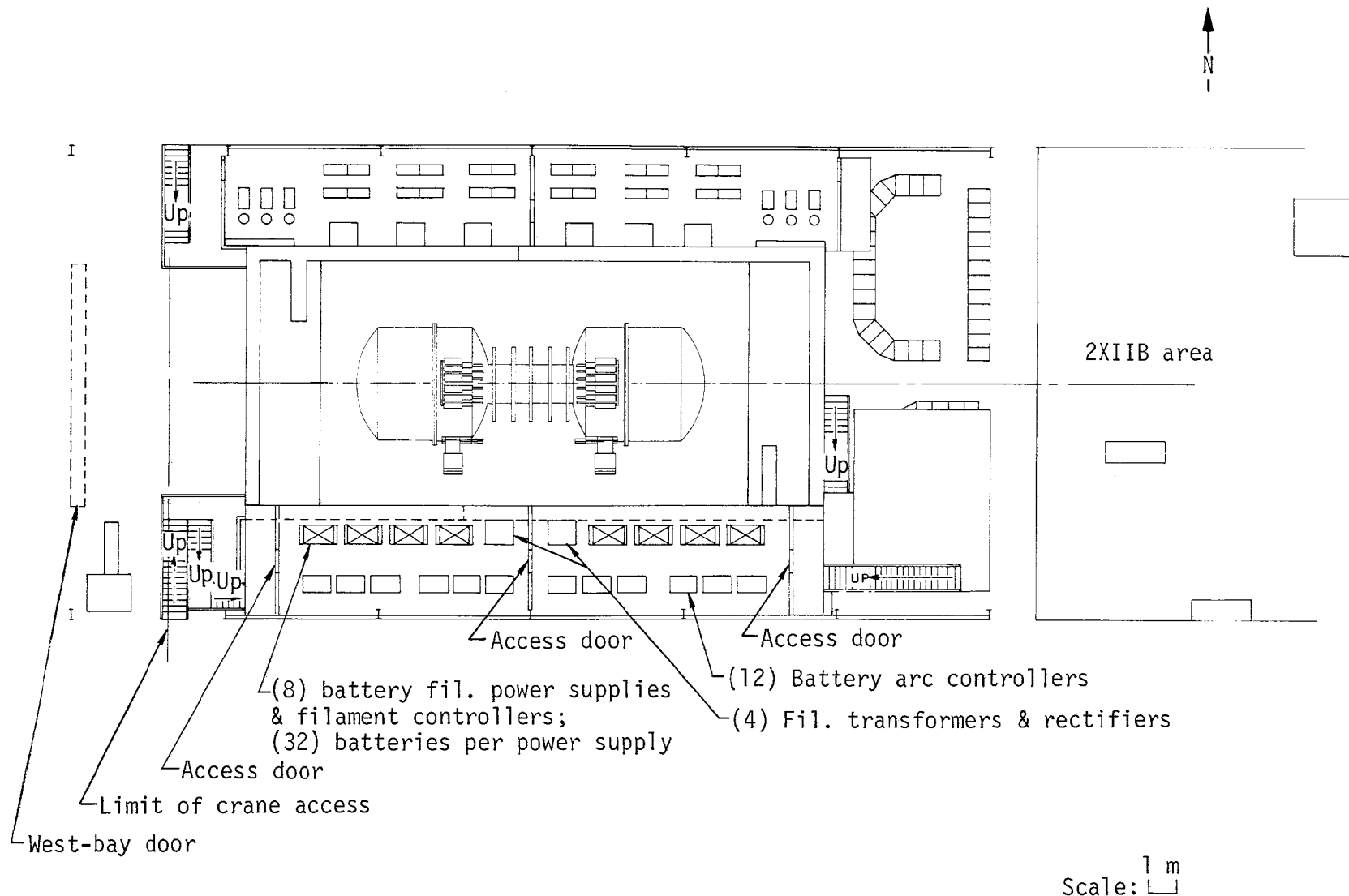


Fig. C-29. Second tier level plan of Building 435 high-bay area.

#### External Vacuum Pumping System

On the TMX machine, the external vacuum pumping system consists of all vacuum components placed outside the vacuum vessel. Using a scheme similar to the Baseball II-T system, it will consist of a system of mechanical vacuum pumps, mercury diffusion ejectors, and mercury diffusion pumps (see Fig. C-30). The system will serve to initially pump-down the vacuum vessel and to help maintain vacuum against the surface outgassing load in the vessel.

Initial pump-down will take approximately 8 hours. Four hours of rough pumping using new trochoid piston pumps will reduce the system pressure from 760 Torr to 0.1 Torr. Two hours further pumping with existing conventional piston pumps will bring the system pressure down to 0.01 Torr. At this point, diffusion pumps backed by a diffusion ejector pump will be started to bring the system pressure down to  $10^{-6}$  Torr within 2 hours. Afterwards, the LN liners can be chilled.

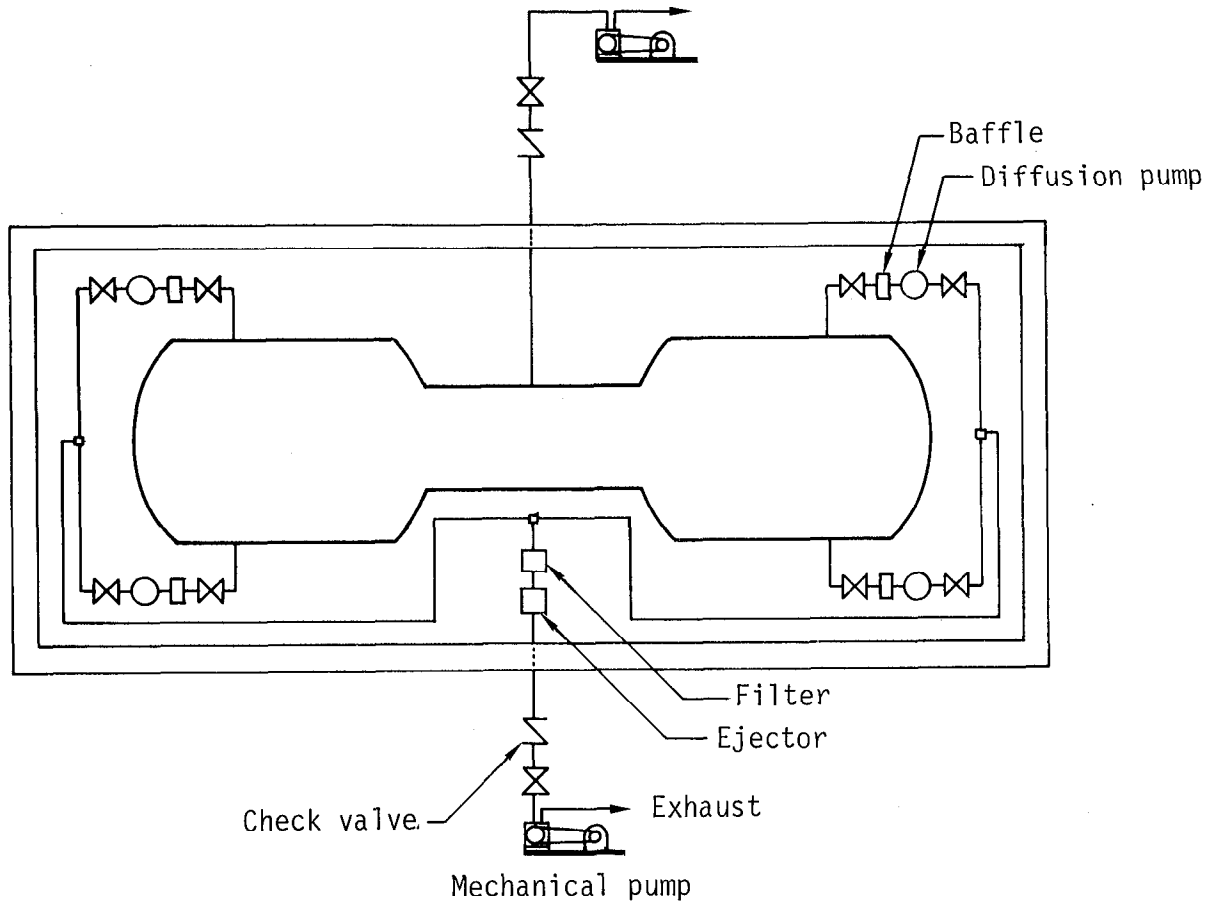


Fig. C-30. Diagram of external vacuum pumping system.

## C5. NEUTRON SHIELD DESIGN AND ANALYSIS

### Introduction

The steps taken to design a shield for this experiment are to

- Specify design source strength and type of primary radiation source.
- Estimate dose rates without any shielding.
- Specify allowable and design dose rates.
- Develop analytical model for shielding analysis.
- Lay out a preliminary shield design using analytical model.
- Analyze and upgrade preliminary shield design using three-dimensional Monte Carlo techniques.

For shield design purposes, the time average source strength is  $3 \times 10^8$  DD fusion neutrons (2.5 MeV/s), half from each of the two end-plug plasmas. This is based on an estimated instantaneous source strength of  $8 \times 10^{12}$  neutrons/s, and 100 0.1-s pulses/80-h week.<sup>C8</sup>

With no shielding or other material attenuation, the dose rate by uncollided neutrons from a  $3 \times 10^8 \text{ s}^{-1}$  point source of 2.5-MeV neutrons is 8.6 mrem/h at 20 ft and drops to 6.5 mrem/h at 80 ft. [The 2.5-MeV neutron-flux-to-dose-rate conversion factor used here ( $0.13 \text{ mrem/h/n/cm}^2 \cdot \text{s}$ ) is from Ref. C9, Part III, p. 5.]

For the first stage of our shield design effort, our design criterion for maximum time-average dose rate in controlled inhabited areas is 0.5 mrem/h. This is 20% of the allowable 40 h/week average occupational exposure rate as specified by ERDA (Ref. C9, Part I, p. 1; Part V, p. 9). As more detailed shield design work is undertaken, we use the more demanding criteria of 500 mrem/yr (0.24 mrem/h) for facility personnel and 50 mrem/yr at the site boundary, or less depending on how much shielding can be provided at a cost of \$1000/man-rem saved.<sup>C9</sup>

With no shielding, the dose rate at 20 ft is 17 times the design level of 0.5 mrem/h. To reduce this dose rate to the design level will require a modest amount of shielding.

Two feet of concrete will reduce the direct dose rate by ~2 orders of magnitude.<sup>C10</sup> The magnet coils will provide some shielding, but the holes through the coil structures should dominate. To be conservative, no shielding credit is taken for the coils.

The shielding must protect people from both this direct radiation and indirect scattered radiation. While the most effective shield arrangement

would be to completely surround the experiment, there are both economic and accessibility advantages to leaving the top of the experimental cell uncovered. With no overhead shielding, scattered radiation over the shield becomes an important contributor to the total biological dose rates.

#### Analytical Model

The first step taken to design the shield was to develop a simple analytical model for a shadow shield that could be used to lay out a preliminary shield design. The resulting expression, displayed below, approximates the dose rates from both air-scattered neutrons and neutrons coming directly through the shield.

$$\begin{aligned} \text{Dose rate (air + direct)} \approx S & [ (3.85 \times 10^{-8} \cdot \exp(-0.037\alpha) \cdot d^{-1}) + \\ & (1.11 \times 10^{-5} \cdot \exp(-2.3t) \cdot d^{-2}) ] \text{ mrem/h}, \end{aligned} \quad (\text{C1})$$

where

S = average DD neutron source strength (neutrons/s)

$\alpha$  = minimum angle formed between edge of shield, source,  
and detector ( $^{\circ}$ )

d = distance between source and detector (ft) ( $< 100$  ft)

t = shield thickness (ft)

Note: for  $\alpha \leq 0$ , t = 0.

The derivation of this model is described in Ref. C11.

The design of the TMX facility is determined by factors other than shield performance. Therefore, shield composition, thickness, and height are the only parameters available to provide the required shielding.

Using the analytical expression (C1) as a guide, a preliminary shield design was developed. This shield consists of 2-ft-thick ordinary concrete walls ranging in height from 10 ft at the west end of the experimental cell to 14 ft at the east end. Shield height is varied because personnel are stationed at varying heights around the experiment. The dose rates at various locations outside the shield, as predicted by expression (C1), are listed in Table C-7. The location of the six detector locations considered are shown in Fig. C-31. Detector heights are all 6 ft above the various floor levels.

Table C-7. Shield performance based on analytical model.

Detector Location <sup>a</sup>	Height <sup>b</sup> (ft)	Shield height (ft)	East source <sup>c</sup>		West source <sup>c</sup>		Dose rates		
			d (ft)	$\alpha$ (°)	d (ft)	$\alpha$ (°)	Direct	Air total (mrem/h)	
1	6	10	30	9.6	50	5.6	0.026	0.233	0.26
2	6	12	20	19.0	20	19.0	0.084	0.29	0.37
3	6	14	50	10.0	30	17.0	0.025	0.182	0.21
4	18.5	12	52	9.6	43	11.0	0.015	0.166	0.18
5	20	14	80	2.7	60	9.4	0.007	0.139	0.15
6	20	12	82	1.6	66	3.9	0.006	0.142	0.15

<sup>a</sup>Detector locations are displayed on plan view of experimental area, Fig. C-31.

<sup>b</sup>All heights are from ground floor level; source height is 0.5 ft.

<sup>c</sup>d = distance between source and detector;  $\alpha$  = angle formed between detector, source, and top of shield.

Key: shield heights

I 10 ft

II 12 ft

III 14 ft

Detector locations - ① through ⑥

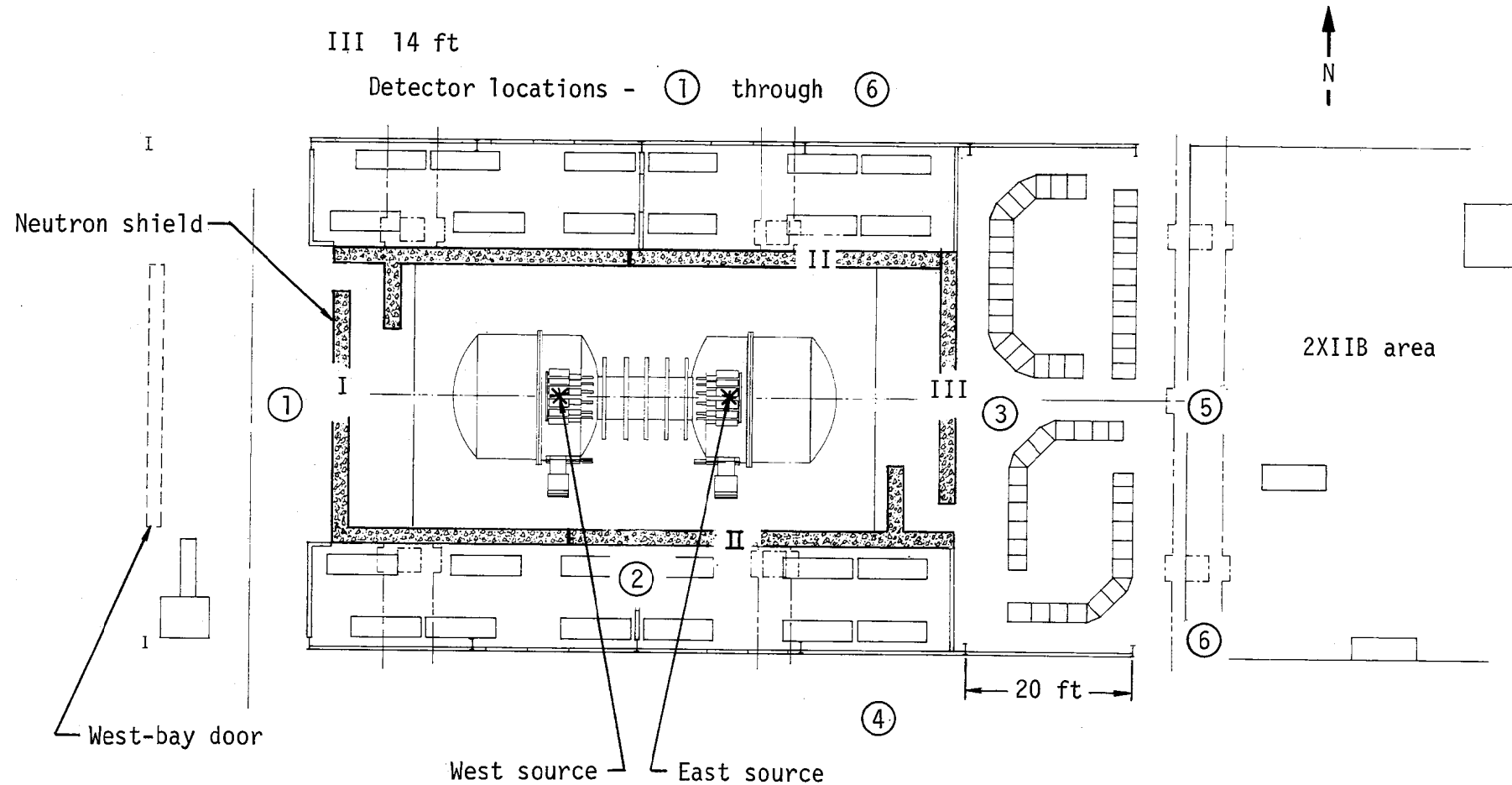


Fig. C-31. Plan view of facility used for shielding analysis.

All locations considered have dose rates below the design target of 0.5 mrem/h.

#### Monte Carlo Calculations

The next step was to analyze the preliminary shield with much more exact three-dimensional Monte Carlo methods. Dose estimates inside and outside the experimental cell from the neutrons and secondary gammas were calculated using the MORSE-L<sup>C12</sup> program and the coupled 30-group neutron and 15-group gamma structure cross-section library.<sup>C13</sup> Dose-flux conversion constants used in the calculations for gammas and neutrons were interpolated from.<sup>C14</sup>

The dose equivalent rates from direct and scattered neutrons inside the experimental cell are given in Table C-8. The neutron sources used in the calculations were spherical, 1 m in diameter (center is 0.5 m from the floor). The detectors are located north of the center of the source located on the west side.

The biological hazard potential is not severe. For safety considerations, however, an operational safety procedure common to Livermore accelerators shall be adopted by the Laboratory Management in accordance with the Laboratory Safety Manual,<sup>C15</sup> and shall be in effect at the time of TMX operation.

The calculated neutron and secondary gamma dose-equivalent rate in mrem/h per neutron/s as a function of concrete slab thickness is shown in Fig. C-32. To reduce the dose rate below 0.25 mrem/h (500 mrem/yr) outside the nearest wall requires approximately 54 cm of concrete. A 60-cm-thick concrete wall reduces this to 0.2 mrem/h. Since there will be some contributions from skyshine, it is preferable to build walls 60-cm thick.

The direct and skyshine dose-equivalent rates as a function of distance from the center of the containment vessel are shown in Fig. C-33. The dose rates are for  $3 \times 10^8$  neutrons/s with no roof shield and assuming that thickness of an ordinary concrete wall is 60 cm.

#### Shielding Cost/Benefit

Table C-9 summarizes the estimates for dose-commitment for the Laboratory employees and doses at the nearest site boundary, under the assumptions that the facility is operated for 3 years and that the source strength is  $3 \times 10^8$  neutrons/s. The dose-committment from direct penetration through shielding

Table C-8. Dose equivalent rates inside the experimental cell.

Location (cm)	Dose rate (rem/h)
25	1.813
350	$2.20 \times 10^{-2}$
750	$1.81 \times 10^{-1}$

Table C-9. Dose equivalent outside the shielded areas.

Wall thickness (cm)	Roof thickness (cm)	Site boundary (rem/yr)	Laboratory direct (man-rem/3 yr)	Skyshine (man-rem/3 yr)
60	0	0.0002	4	40

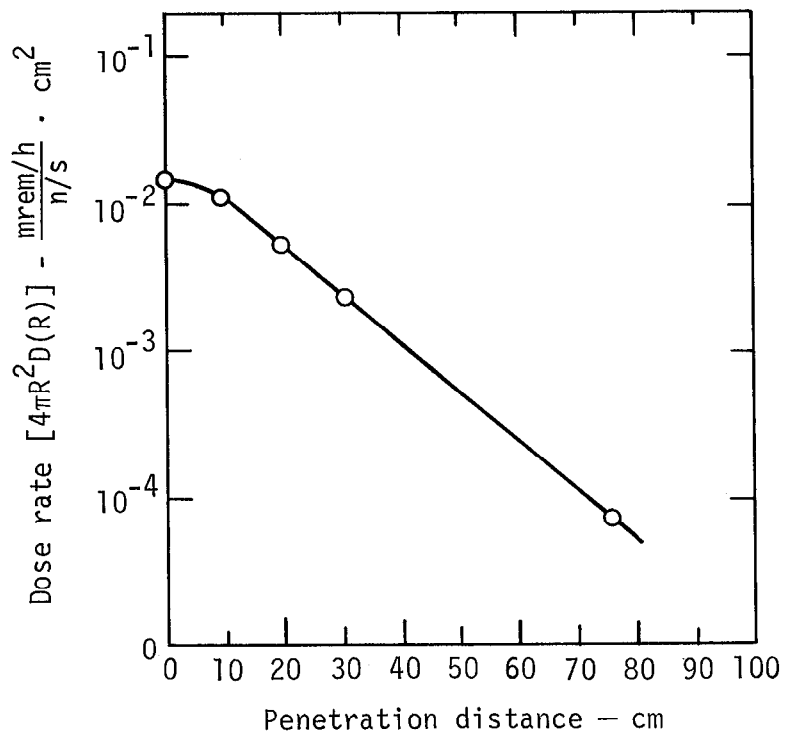


Fig. C-32. Calculated 2.7-MeV neutron dose rates (multiplied by  $4\pi R^2$ ) in ordinary ( $2.3 \text{ g/cm}^3$ ) concrete as a function of distance  $R$ .

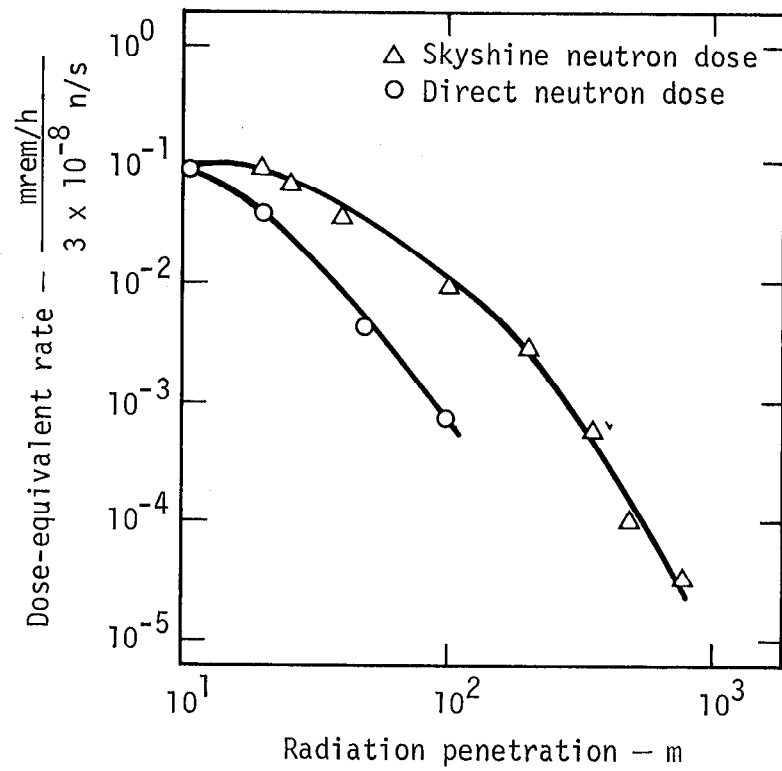


Fig. C-33. Penetration of radiation through 60-cm-thick concrete walls and unshielded roof as a function of distance M.

walls can be lowered from 4 man-rems to 0.4 at a cost of \$50,000; and dose-committment from sky shine can be lowered from 40 to 4 man-rems at a cost of \$75,000 to \$85,000. In both cases, man-rem savings at a cost of greater than \$1,000/man-rem are not cost effective.

#### Summation

Analysis to date indicates that TMX should be surrounded by shielding for the protection of personnel. Both analytical modeling and three-dimensional Monte Carlo calculations predict that at the time-averaged design source strength of  $3 \times 10^8$  DD neutrons/s, ordinary concrete walls ~2 ft thick and 10 to 14 ft high will limit personnel exposure to less than 0.5 mrem/h. A cost/benefit appraisal indicates that additional shielding would not be cost effective.

In light of more recent neutron-yield calculations (see Appendix A-10), we believe our analysis is conservative. Besides reduced neutron source pulse time, the shielding effects of experimental components (principally the magnet coils) have been ignored. On the other hand, our analysis has yet to consider the effects of neutron scatter from the roof and walls of the building, or from experimental components viewed by both source and detector. Due to the size of the building, we do not believe that scatter from the roof or walls will be a problem, but it would be prudent to keep experimental components out of neutron source line-of-sight. Our calculational effort is presently addressing these scattering questions.

## C6. CONTROL SYSTEMS

The controls area for the TMX experiment is conveniently partitioned into the following subsystems: vacuum system, getter system, magnet system, neutral-beam injector system, and personnel safety interlock system.

### Vacuum Control System

A manually controlled, hardwired, vacuum control system will be provided. Its function is to control vacuum pumps and valves so that the "pump-down" and "up-to-air" sequences are easily controlled. A number of vacuum gauges monitor the pressure in the various tanks and display this information on panel meters. A vacuum map visually indicates the status of the various valves and pumps in the system. In addition, interlocks are provided to prevent inadvertent operation of certain critical valves and pumps.

### Getter Control System

The getter power supplies and controls system from 2XIIIB are used on TMX as is. This system utilizes a minicomputer to automatically operate the getter wires at their evaporation temperature and to keep a log of the status and history of each wire.

### Magnet Control System

The magnet power supplies are controlled with a manual, hardwired control system. Each power supply can be preset to its desired operating voltage. Voltages and currents at both the magnet and the power supply are monitored and displayed on panel meters.

### Personnel Safety Interlocks

The safety interlock system is a hardwired system designed to provide an automatic, fail-safe environment free of all controllable hazards that may be encountered when access to the machine or related equipment is attempted. Knowledge about the system is not required to assure personnel safety. The interlock system cannot be compromised by operation of any control either intentionally or inadvertently.

### Neutral-Beam and Streaming-Plasma Gun Control

The control system for the 24 neutral beams on TMX is designed to provide the best control facility possible for the minimum cost. Accordingly, the

entire control system for the 12 beams on 2XIIB, including the computer control and monitoring equipment, will be moved to the TMX neutral-beam control room and used directly with minimum modifications. The 12 beams not controlled by this equipment are controlled manually with control equipment built to existing designs with minor modifications. The 12 manual beam controls include computer-compatible interfaces so that computer control may be added in the future if desired.

## C7. DIAGNOSTIC SYSTEM

Many of the diagnostic measurements to be made on TMX are processed by a minicomputer-based data acquisition system. In addition to providing raw data storage and archiving (to enable complex data processing at a later time), this system can provide on-line data reduction. Diagnostic data can be processed and presented to the experimenter in an easily understood form, giving him the necessary information to evaluate and direct the course of the experiment.

Most of the proposed data acquisition system (including diagnostic instrumentation and computer gear) is available from the 2XIIB and Baseball II experiments. New diagnostic instrumentation, in addition to that already available on 2XIIB and Baseball, is discussed in Appendix A8.

## C8. REFERENCES

- C1. W. A. Perkins and T. C. Brown, *MAFCO-A Magnetic Field Code for Handling General Current Elements in Three Dimensions*, Lawrence Livermore Laboratory, Rept. UCRL-7744-Rev. II (1966).
- C2. S. J. Sackett, "Calculation of Electromagnetic Fields and Forces in Coil Systems for Arbitrary Geometry," in *Proc. 6th Symp. on Engineering Problems of Fusion Research*, San Diego, 1975 (IEEE, 75CH1097-5-NPS, 1975) p. 935.
- C3. C. J. Anderson and V. A. Finlayson, "Operating Characteristics of a 85% Ti 15% Ta Alloy Getter Wire," *J. Vac. Sci. Technol.*, 7, (1970).
- C4. S. M. Hibbs, Lawrence Livermore Laboratory, *Internal Memorandum*, (1975). Readers outside the Laboratory who desire further information on LLL internal documents should address their inquiries to the Technical Information Department, Lawrence Livermore Laboratory, Livermore, California 94550.
- C5. G. Haas, M. Keilhacker, W. Poschenrieder, and F. Wagner, "Divertor Pumping Systems of ASDEX," in *Proc. 9th Symp. Fusion Technology, Garching, Fed. Rep. of Germany, 1976* (Max-Planck-Institute für Plasmaphysik, in preparation) Paper A1-8.
- C6. J. Bohdansky, J. Roth, M. K. Sinha, and W. Ottenberger, "Trapping Coefficient of Energetic Hydrogen (0.3 - 8 keV) in Ti at High Doses," presented at *Int. Conf. Surface Effects in Controlled Fusion Devices, San Francisco, 1976* (to be published in *J. Nucl. Mater.*).
- C7. S. J. Sackett, *JASON - A Program for the Solution of Nonlinear Elliptical P.D.E.'s in Two Independent Variables, Part 2: Users Manual*, Lawrence Livermore Laboratory, Rept. (in preparation).
- C8. W. Nexsen, Lawrence Livermore Laboratory, *Internal Memorandum*, October 13, 1976.
- C9. "Standards for Radiation Protection," in *ERDA Manual*, Ch. 0524 (April 1975).
- C10. N. M. Schaeffer, ed, *Reactor Shielding for Nuclear Engineers*, USAEC, Rept. TID-25951 (1973).
- C11. J. D. Lee, Lawrence Livermore Laboratory, *Internal Memorandum*, (December 8, 1976).
- C12. T. P. Wilcox, Lawrence Livermore Laboratory, *Internal Document*, MOR-6 (September 1, 1976).

- C13. T. P. Wilcox, Lawrence Livermore Laboratory, *Internal Document MOR-13* (July 9, 1973).
- C14. *ICRP Publication 21, Data for Protection Against Ionizing Radiation from External Sources: Supplement to ICRP Publication 15.* (Pergamon Press, Oxford, 1973).
- C15. *Livermore Health and Safety Manual*, Lawrence Livermore Laboratory, Rept. M-017, Sect. 33.00 (1977).

APPENDIX D . DETAILED COST BREAKDOWN

(A. K. Chargin and G. E. Vogtlin)

Table D-1. Summary of Detail Cost Breakdown by Subsystem (K\$)

	Engineering				In-House Fab.				Purchase				Technicians				Equipment				Physics		Total		Total	
	ME	EE	ME	EE	ME	EE	ME	EE	ME	EE	ME	EE	ME	EE	ME	EE	+ Comp.	Manpower	77	78	77	78	77	78	77	78
Fiscal Year	77	78	77	78	77	78	77	78	77	78	77	78	77	78	77	78	77	78	77	78	77	78	77	78	77	78
Magnet System	93	124	10	79	20	40	0	13	67	221	0	91	105	236	0	146	0	0	0	50	0	0	208	585	87	365
Vacuum System	123	98	0	0	47	154	0	0	83	839	0	0	60	180	0	0	0	0	0	0	0	0	183	278	130	993
Inject. System	28	117	21	120	2	161	34	96	4	703	41	51	0	200	27	183	0	0	432	149	0	0	76	620	81	1011
Facility	97	70	26	50	8	90	5	11	3	209	2	70	102	243	40	30	13	105	0	0	0	0	265	393	18	380
Controls	0	5	70	62	0	0	10	40	0	0	23	55	0	0	10	65	0	0	75	80	0	0	80	132	33	95
Diagnostics	5	45	43	20	8	7	0	0	0	5	0	88	25	175	19	160	0	0	0	400	0	0	92	400	8	100
System Design & Integration	129	102	59	80	0	0	0	0	0	0	0	0	0	25	0	20	0	0	0	0	177	390	365	617	0	0
Administration	0	0	0	0	0	0	0	0	29	265	0	0	0	0	0	0	0	0	0	98	274	98	274	29	265	
Totals	475	561	229	411	85	452	49	160	186	2242	66	355	292	1059	96	604	13	105	507	679	275	664	1367	3299	386	3209
<hr/>																										
Capital Equipment Subtotal																										
Manpower & Expense Subtotal																										
Contingency																										
<hr/>																										
Totals																										
9500																										

Table D-2. Detail Cost Breakdown for the Magnet System (K\$)

Fiscal Year	Engineering				In-House Fab.				Purchase				Technicians				Equipment				Physics		Total Manpower		Total Expense		Total Equip.		Total Cost	
	ME 77	EE 77	ME 78	EE 78	ME 77	EE 77	ME 78	EE 78	ME 77	EE 77	ME 78	EE 78	ME 77	EE 77	ME 78	EE 78	ME 77	EE 77	ME 78	EE 78	+ Comp. 77	78	77	78	77	78	77	78		
Field Calc.	10	5	0	0	0	0	0	0	0	0	0	0	0	0	0	0	0	0	0	0	10	5	0	0	0	0	0	15		
Conductor, 9 coils	4	0	5	0	0	0	0	0	30	4	0	0	0	0	0	0	0	0	0	0	9	0	30	4	0	0	0	43		
Winders,9 coils	16	0	0	0	10	0	0	0	15	0	0	0	15	0	0	0	0	0	0	0	31	0	25	0	0	0	0	56		
Insulation, 9 coils	4	3	0	0	2	0	0	0	15	0	0	0	5	10	0	0	0	0	0	0	9	13	17	0	0	0	0	39		
Cooling, 9 coils	0	13	0	0	0	2	0	0	0	5	0	0	0	6	0	0	0	0	0	0	0	19	0	7	0	0	0	0	26	
Plug Structure	36	10	0	0	0	6	0	0	0	95	0	0	0	15	0	0	0	0	0	0	36	25	0	101	0	0	0	162		
Ioffe Bars Structure	10	6	0	0	0	6	0	0	0	31	0	0	0	7	0	0	0	0	0	0	10	13	0	37	0	0	0	60		
Solenoid Struc.	0	10	0	0	0	4	0	0	0	15	0	0	0	5	0	0	0	0	0	0	0	15	0	19	0	0	0	34		
Assembly & Checkout	0	10	0	0	0	10	0	0	0	5	0	0	0	25	0	0	0	0	0	0	0	35	0	15	0	0	0	50		
Power Supplies	1	2	5	75	0	0	0	13	0	0	0	91	0	0	0	146	0	50	0	0	6	223	0	104	0	50	0	383		
Plug Magnet Support	2	15	0	0	0	2	0	0	0	12	0	0	0	8	0	0	0	0	0	0	2	23	0	14	0	0	0	39		
Elec. Feedthrus	0	10	0	4	0	2	0	0	0	4	0	0	0	30	0	0	0	0	0	0	0	44	0	6	0	0	0	50		
Wind. CEE coils	3	5	0	0	8	0	0	0	0	0	0	0	85	15	0	0	0	0	0	0	88	20	8	0	0	0	0	116		
Wind. BB coils	4	20	0	0	0	6	0	0	0	0	0	0	0	85	0	0	0	0	0	0	4	105	0	6	0	0	0	115		
Wind. Ioffe Bars	3	15	0	0	0	2	0	0	0	0	0	0	0	30	0	0	0	0	0	0	3	45	0	2	0	0	0	50		
Misc. Materials	0	0	0	0	0	0	0	0	7	50	0	0	0	0	0	0	0	0	0	0	0	0	7	50	0	0	0	57		
Totals	93	124	10	79	20	40	0	13	67	221	0	91	105	236	0	146	0	0	0	50	0	0	208	585	87	365	0	50	1295	

Table D-3. Detail Cost Breakdown for the Vacuum System (K\$)

Fiscal Year	Engineering				In-House Fab.				Purchase				Technicians				Equipment				Physics		Total		Tc Exp
	ME 77	EE 78	ME 77	EE 78	ME 77	EE 78	ME 77	EE 78	ME 77	EE 78	ME 77	EE 78	ME 77	EE 78	ME 77	EE 78	+ Comp. 77	Manpower 77	77	78	77	78	77		
Plug Tanks	15	5			0	10			35	245			0	13							15	18	35		
Central Cell Tank	6	5			0	10			0	30			0	10							6	15	0		
Tank Supports	10	5			8	5			30	30			25	10							35	15	38		
Central Cell Liner	5	4			0	3			0	10			0	10							5	14	0		
Source Gas Liners	15	5			0	4			0	130			0	15							15	20	0		
Plasma Dump Liners	10	5			0	3			0	110			0	15							10	20	0		
Coil Liners	5	5			0	3			0	25			0	10							5	15	0		
Liner Feed-Throughs	4	10			0	12			0	40			0	5							4	15	0		
Coil Liner Getters	14	5			0	20			0	10			0	5							14	10	0		
Source Liner Getters	10	5			10	14			8	9			8	10							18	15	18		
Plasma Dump Getters	6	5			10	14			0	10			0	12							6	17	10		
Central Cell Getters	8	2			12	8			0	10			6	2							14	4	12		
Plasma Dump Burial Target	6	10			0	6			0	50			0	6							6	16	0		
Plasma Dump Grid	6	5			0	6			0	50			0	10							6	15	0		
Ports, Flanges, and Bellows	2	12			4	16			10	30			9	24							11	36	14		
General Installation	1	10			3	20			0	50			12	23							13	33	3		
Totals	123	98	0	0	47	154	0	0	83	839	0	0	60	180	0	0	0	0	0	183	278	130			

Table D-4. Detail Cost Breakdown for the Injector System (K\$)

	Engineering				In-House Fab.				Purchase				Technicians				Equipment				Physics		Total	Tc Exp	
	ME 77	EE 78	ME 77	EE 78	ME 77	EE 78	ME 77	EE 78	ME 77	EE 78	ME 77	EE 78	ME 77	EE 78	ME 77	EE 78	+ Comp. 77	Manpower 77	77	78	77	78	77		
Fiscal Year	77	78	77	78	77	78	77	78	77	78	77	78	77	78	77	78	77	78	77	78	77	78	77		
Stream. Guns	2	12	0	5	0	4	0	7	0	5	0	1	0	20	0	10	0	0	2	47	0				
20-keV Sources	2	10	0	0	0	22	0	0	0	55	0	0	0	32	0	0	0	0	2	42	0				
40-keV Sources	2	10	0	0	0	72	0	0	0	215	0	0	0	72	0	0	0	0	2	82	0				
Magnetic Sh'd & Source Supports	11	25	0	0	0	14	0	0	0	165	0	0	0	19	0	0	0	0	11	44	0				
Source Valves	11	14	0	0	2	5	0	0	4	120	0	0	0	5	0	0	0	0	11	19	6				
Bellows Assemblies	0	10	0	0	0	6	0	0	0	55	0	0	0	3	0	0	0	0	0	13	0				
Source Dump Targets	0	10	0	0	0	14	0	0	0	20	0	0	0	4	0	0	0	0	0	14	0				
Source Diagnostics	0	4	0	0	0	10	0	0	0	8	0	0	0	15	0	0	0	0	0	19	0				
Gas Box	0	15	0	0	0	13	0	0	0	55	0	0	0	20	0	0	0	0	0	35	0				
Source Ass'y Stands	0	5	0	0	0	1	0	0	0	5	0	0	0	10	0	0	0	0	0	15	0				
Accel Pwr Supply	0	0	0	73	0	0	0	18	0	0	0	16	0	0	5	56	196	72	5	129	0				
Decel Pwr Supply	0	0	5	6	0	0	4	1	0	0	12	0	0	0	2	2	0	0	7	8	16				
Arc Pwr Supply	0	0	8	15	0	0	14	47	0	0	12	15	0	0	9	43	228,	53	17	58	26				
Filament Pwr Supply	0	0	4	9	0	0	9	4	0	0	8	2	0	0	3	12	8	24	7	21	17				
Cabling	0	0	1	6	0	0	5	18	0	0	9	16	0	0	6	55	0	0	7	61	14				
Test Stand	0	2	3	6	0	0	2	1	0	0	0	1	0	0	2	5	0	0	5	13	2				
Totals	28	117	21	120	2	161	34	96	4	703	41	51	0	200	27	183	0	0	432	149	0	0	76	620	81

Table D-5. Detail Cost Breakdown for the Facility (K\$)\*

	Engineering				In-House Fab.				Purchase				Technicians				Equipment				Physics		Total		Tot
	ME	EE	ME	EE	ME	EE	ME	EE	ME	EE	ME	EE	ME	EE	ME	EE	ME	EE	ME	EE	+ Comp.	Manpower	77	78	77
Fiscal Year	77	78	77	78	77	78	77	78	77	78	77	78	77	78	77	78	77	78	77	78	77	78	77	78	77
Neutron Shield	20	10	6	0	0	5	0	0	0	0	0	2	0	30	0	3	0	105				26	43	0	
Tiers	25	13	5	0	0	6	0	0	0	100	2	10	0	40	0	7	0	0				30	60	2	
Clear Main Bay	5	0	4	0	0	0	3	0	0	0	0	0	35	0	15	0	0	0	0			59	0	3	
Clear Side Rooms	3	0	2	0	0	0	1	0	0	0	0	0	25	0	7	0	0	0	0			37	0	1	
Equip. Storage	2	2	1	0	1	0	0	0	0	0	0	0	10	0	8	0	0	0	0			21	2	1	
Access																									
Platforms	13	5	0	0	0	18	0	0	0	25	0	0	0	25	0	0	0	0	0			13	30	0	
External Vacuum System	10	5	0	8	7	24	0	0	0	30	0	3	17	35	3	2	0	0				30	50	7	
Control Rooms	1	3	0	5	0	0	0	4	0	4	0	3	0	15	3	3	0	0				4	26	0	
Diagnostic Rooms	3	3	2	5	0	0	1	4	0	13	0	4	10	15	4	2	0	0				19	25	1	
Raised Floors	0	5	0	3	0	0	0	0	0	5	0	25	0	10	0	0	0	0				0	18	0	
LN <sub>2</sub> System	10	6	0	8	0	20	0	3	3	15	0	5	5	30	0	2	0	0				15	46	3	
LCW/H <sub>2</sub> O/Air	0	11	0	1	0	4	0	0	0	13	0	0	0	23	0	0	0	0				0	35	0	
Ventilation	3	3	1	2	0	5	0	0	0	2	0	5	0	10	0	3	3	0				4	18	0	
Air Conditioning	0	2	0	2	0	8	0	0	0	2	0	2	0	10	0	0	10	0				0	14	0	
Pwr & Lighting	2	1	5	13	0	0	0	0	0	0	8	0	0	0	6	0	0	0				7	20	0	
Intercom	0	1	0	3	0	0	0	0	0	0	3	0	0	0	2	0	0	0				0	6	0	
Totals	97	70	26	50	8	90	5	11	3	209	2	70	102	243	40	30	13	105	0	0	0	265	393	18	

\*The cost of excavating and constructing the pit within Building 435 is covered by LLL General Plant Fund. The estimated amount

Table D-6. Detail Cost Breakdown for the Control System (K\$)

	Engineering				In-House Fab.				Purchase				Technicians				Equipment				Physics		Total		To
	ME	EE	ME	EE	ME	EE	ME	EE	ME	EE	ME	EE	ME	EE	ME	EE	ME	EE	+ Comp.	Manpower	77	78	77	78	77
Fiscal Year	77	78	77	78	77	78	77	78	77	78	77	78	77	78	77	78	77	78	77	78	77	78	77	78	77
Vacuum Controls	0	1	26	9		1	2		5	9		4	7		16	4			30	17	6				
Getter Pwr & Controls	0	1	4	4		1	0		8	0		2	12		0	0			6	17	9				
Magnet Control	0	1	10	5		3	0		5	8		2	5		4	13			12	11	8				
Safety Interlocks	0	1	0	13		1	6		0	20		2	12		0	32			2	26	1				
Beam Controls	0	1	30	31		4	32		5	18		0	29		55	31			30	61	9				
Totals	0	5	70	62	0	0	10	40	0	0	23	55	0	0	10	65	0	0	75	80	0	0	80	132	33

Table D-7. Detail Cost Breakdown for the Diagnostic System (K\$)

Fiscal Year	Engineering				In-House Fab.				Purchase				Technicians				Equipment				Physics		Total Manpower		Total Expenses	
	ME 77	EE 77	ME 78	EE 78	ME 77	EE 77	ME 78	EE 78	ME 77	EE 77	ME 78	EE 78	ME 77	EE 77	ME 78	EE 78	ME 77	EE 77	ME 78	EE 78	Total 77	Total 78	Total Manpower	Total Expenses		
Ion Beam Probe	2	75	10	2	4	2			0	0	0	20	10	30	10	32		0	150			32	79	4	2	
Low Energy Neut. Analyzer	2	10	10	2	4	2			0	0	0	20	10	21	9	21		0	75			31	54	4	2	
Thomson Scat- tering System	1	5	10	2	0	3			0	5	0	12	5	16	0	20		0	50			16	43	0	2	
2-mm Microwave Interferometer	0	2	5	2	0	0			0	0	0	12	0	15	0	12		0	50			5	31	0	1	
High Energy Neut. Analyzers	0	4	5	1	0	0			0	0	0	12	0	35	0	25		0	25			5	65	0	1	
Langmuir Probes	0	1	0	1	0	0			0	0	0	2	0	12	0	8		0	10			0	22	0	0	
R. F. Probes	0	1	0	1	0	0			0	0	0	2	0	14	0	12		0	5			0	28	0	0	
End Loss Analyzers	0	4	0	1	0	0			0	0	0	2	0	5	0	3		0	15			0	13	0	0	
Beam Attenuation Detectors	0	1	3	4	0	0			0	0	0	2	0	10	0	10		0	10			3	25	0	0	
X-Band Microwave Interferometers	0	1	0	2	0	0			0	0	0	2	0	7	0	10		0	5			0	20	0	0	
Diamagnetic Loops	0	1	0	2	0	0			0	0	0	2	0	10	0	7		0	5			0	20	0	0	
Totals	5	45	43	20	8	7	0	0	0	5	0	88	25	175	19	160	0	0	0	400	0	0	92	400	8	10

APPENDIX E. ENVIRONMENTAL IMPACT ASSESSMENT

(B. N. Odell)

Description of the Proposed Action and  
Its Anticipated Benefits

The proposed action involves modifying the interior of Bldg. 435 so that the new TMX mirror machine and its associated equipment can be installed and operated in the existing building. Some of the supporting equipment will also be located in nearby Bldgs. 436 and 446. In addition, 2-ft-thick shielding blocks will be installed around the TMX machine to protect personnel from neutrons.

Existing cranes will be used to install the TMX equipment and shielding blocks.

Building 435 was designed and constructed as an experimental physics facility so that it could be easily modified to accommodate various experiments. The facility presently houses the Baseball II and 2XIIB experiments. The Baseball II experiment has been terminated, and the TMX machine will be installed in the Baseball II area. The 2XIIB experiment will be shut down, and much of its equipment will be used for the TMX machine.

The TMX machine will provide the essential steps in extending our knowledge of the mirror program plasma physics leading, eventually, to magnetic fusion energy.

Potential Environmental Impact

Neither the building modification nor the operation of this facility will significantly alter the impact of this facility on the environment for the following reasons:

- During construction, the only adverse environmental impact will be that typical of excavation and construction. The construction will take place within existing Bldg. 435, and the pit within the building will be enlarged.
- There are no native trees near this building and no soil erosion will take place from the modification. The Livermore site does not contain any known items of archaeological interest. Appropriate safety measures will be taken to minimize hazards and avoid injuries during the construction phase of this project.
- During operations, actual and potential environmental impact will be kept as low as practicable by engineered safety features, operating procedures, and a quality assurance program.

- The shielding will be designed to limit the dose rate to personnel in the facility to less than 500 mrem/yr. (If cost effective, this dose rate will be further reduced by adding additional shielding.) The dose rate from this machine to the nearest Site boundary will be less than 0.2 mrem/yr compared to a background dose rate of 60 mrem/yr.
- Existing cooling water facilities will be used.
- ac power will be supplied by an existing substation located nearby.
- Connections to the existing sewer will remain the same.

Identification of Known or Potential Conflicts with  
Federal, State, Regional, or Local Plans and Programs

The proposed action will be located within the LLL site boundaries and will not conflict with any known plans or programs sponsored by federal, state, regional, or local agencies.

Alternatives

Possible alternatives to the proposed modification of Bldg. 435 and the operation of the TMX machine in that facility are:

- Constructing a new facility on the LLL site.
- Not performing the experiment.

Constructing and operating a new facility on the LLL site would cause about the same environmental impact as that created by modifying Bldg. 435 and conducting the experiment in it. However, costs would be considerably higher and more time would be required for construction. This alternative would delay the advancement of the technology required to understand plasma physics and develop energy-producing fusion reactors by as much as 2 years.

Not performing the experiment would cause the least impact from the environmental standpoint. However, the TMX experiment would involve relatively minor adverse environmental impacts.

TMX is designed to provide an experimental link between previous magnetic fusion energy experiments and practical mirror fusion reactors.

The benefits obtained from performing this experiment far outweigh the environmental costs.

EXHIBIT A. 2XIIB PLASMA CONFINEMENT EXPERIMENTS\*

F. H. Coensgen, J. F. Clauser, D. L. Correll, W. F. Cummins,  
C. Gormezano, B. G. Logan, A. W. Molvik, W. E. Nixsen  
T. C. Simonen, B. W. Stallard, and W. C. Turner

---

\* This paper was originally prepared for publication in the Proceedings of the Sixth International Conference on Plasma Physics and Controlled Nuclear Fusion Research, Berchtesgaden, Federal Rep. of Germany, October 6-13, 1976.

## 2XIIIB PLASMA CONFINEMENT EXPERIMENTS\*

F. H. Coensgen, J. F. Clauser, D. L. Correll, W. F. Cummins,  
 C. Gormezano<sup>†</sup>, B. G. Logan, A. W. Molvik, W. E. Nexsen,  
 T. C. Simonen, B. W. Stallard, and W. C. Turner

Lawrence Livermore Laboratory, University of California  
 Livermore, California, U.S.A. 94550

## ABSTRACT

This paper reports results of 2XIIIB neutral-beam injection experiments with plasma-stream stabilization. The plasma stream is provided either by a pulsed plasma generator located on the field lines outside the plasma region or by ionization of neutral gas introduced at the mirror throat. In the latter case, the gas is ionized by the normal particle flux through the magnetic mirror. A method of plasma startup and sustenance in a steady-state magnetic field is reported in which the plasma stream from the pulsed plasma generator serves as the initial target for the neutral beams. After an energetic plasma of sufficient density is established, the plasma generator stream is replaced by the gas-fed stream. Lifetimes of the stabilized plasma increase with plasma temperature in agreement with the plasma stabilization of the drift-cyclotron loss-cone mode. The following plasma parameters are attained using the pulsed plasma generator for stabilization:  $\bar{n} \approx 5 \times 10^{13} \text{ cm}^{-3}$ ,  $\bar{W}_i \approx 13 \text{ keV}$ ,  $T_e = 140 \text{ eV}$ , and  $n\tau_p \approx 7 \times 10^{10} \text{ cm}^{-3}\cdot\text{s}$ . With the gas feed, the mean deuterium ion energy is 9 keV and the peak density  $\bar{n} \approx 10^{14} \text{ cm}^{-3}$ . In the latter case, the energy confinement parameter reaches  $n\tau_E = 7 \times 10^{10} \text{ cm}^{-3}\cdot\text{s}$ , and the particle confinement parameter reaches  $n\tau_p = 1 \times 10^{11} \text{ cm}^{-3}\cdot\text{s}$ .

---

\* This work was performed under the auspices of the U.S. Energy Research & Development Administration, under contract No. W-7405-Eng-48.

<sup>†</sup>On leave from Association Euratom-CEA, Grenoble, France.

## 1. INTRODUCTION

Several results from the 2XIIIB magnetic-mirror confinement experiment are reported in this paper. In these experiments using injected neutral beams, it is necessary to stream warm plasma along the magnetic field lines [1] to obtain improved ion confinement and to produce high plasma betas. The stream reduces the amplitude of ion-cyclotron fluctuations and, consequently, the turbulent diffusion loss of ions. The experimental results are described in considerable detail by the quasilinear theory [2,3] for the drift-cyclotron loss-cone (DCLC) mode [4]. Earlier experimental results [5,6] are also explained by this theory. According to this theory, the ion velocity distribution evolves to a marginally stable state as turbulent diffusion from either the hot-ion population or from an external stream fills in the ambipolar hole. In the latter case, the hot-ion confinement is improved.

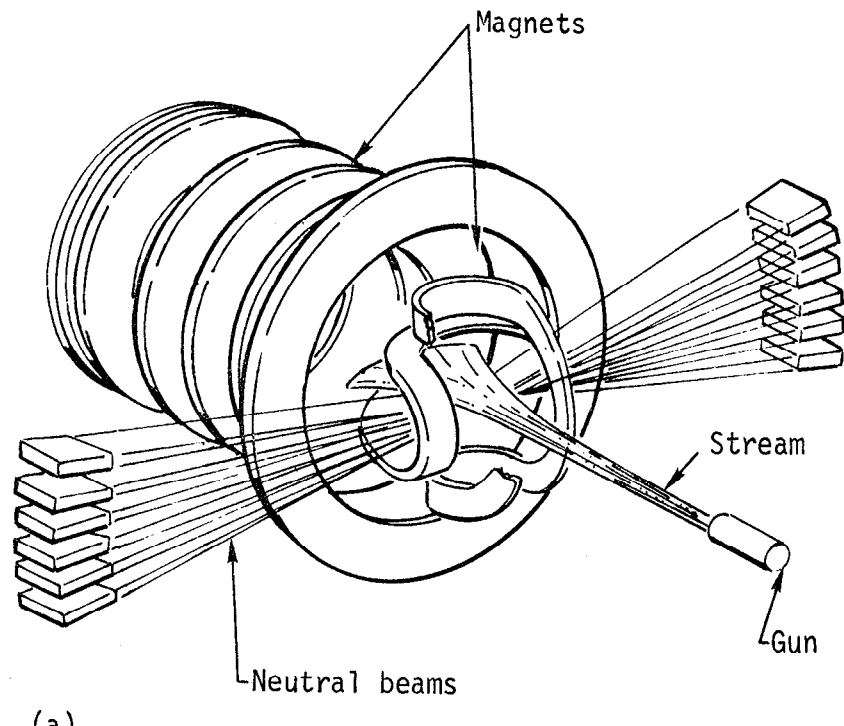
The 2XIIIB magnet is a minimum-B, Yin-Yang set with a 0.67-T central field, a 2:1 mirror ratio, and 150-cm mirror-to-mirror length. The size of the magnet is similar to that of the 2XII magnet but differs in that it has considerably larger openings for neutral-beam injection. The 2XIIIB neutral-beam system consists of 12 injectors [7] operating with extraction energies between 15 and 20 keV. Up to 4.8 MW of neutral deuterium atoms with an equivalent current of 370 A have been injected. This current is divided between full-, half-, and one-third-energy components. The stream is supplied either by a deuterium-loaded-titanium washer gun [8] or by ionization of gas injected at the mirror throat as shown in Fig. 1.

We discuss two modes of operation of the 2XIIIB device. In the first, described in Section 2, the target plasma is formed by trapping and adiabatically compressing a plasma injected along a magnetic field in the manner of the previous 2XII experiments [6]. In this mode, the target plasma has a density  $n_e \approx 4 \times 10^{13} \text{ cm}^{-3}$ , mean ion energy  $\bar{W}_i \approx 3 \text{ keV}$ , and electron temperature  $T_e \approx 100 \text{ eV}$ . Approximately 50% of the neutral beam injected into this target is trapped by charge exchange and ionization; the mean ion energy of the contained plasma is raised to 13 keV within a few hundred microseconds. In the second mode of operation, described in Section 3, plasma and beam injection begin after the magnetic field has reached its maximum. In this mode, beam trapping and exponentiation are initiated on the colder and lower-density plasma stream in a quasisteady-state magnetic field.

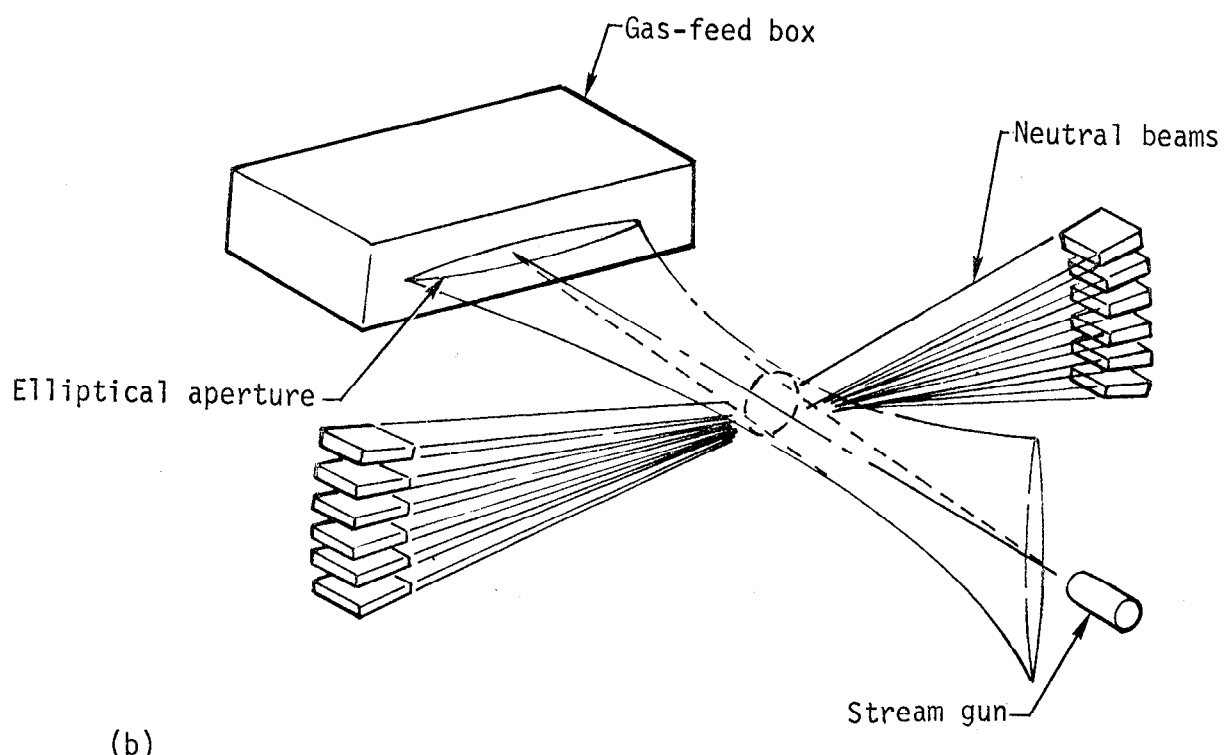
## 2. STREAM STABILIZATION AND ENERGY SCALING

The data in Fig. 2, taken with a plasma target trapped and heated by magnetic compression, show the effect of the stabilizing plasma stream. Neutral-beam injection begins at the peak of compression (1.1 ms). With the plasma stream, the neutral-beam current and duration are 200 A and 1.6 ms; without the plasma stream, they are 200 A and 1.2 ms.

Figure 2(a) shows the central plasma electron density  $n_e$  versus time. These data were obtained by dividing microwave interferometer measurements of line density by the measured (14-cm) mean plasma diameter [9]. The plasma target densities are comparable with and without streaming plasma. With no stream, the neutral beam maintains the density for a brief 0.3 ms. Afterwards, the beam input rate cannot overcome the plasma losses due to the increasing amplitude of the ion-cyclotron fluctuations. By contrast, the density with a plasma stream continues to build up until the neutral beams are shut off.



(a)



(b)

Fig. 1. Schematic diagrams illustrating (a) injection of plasma stream and (b) injection of gas at mirror throat.

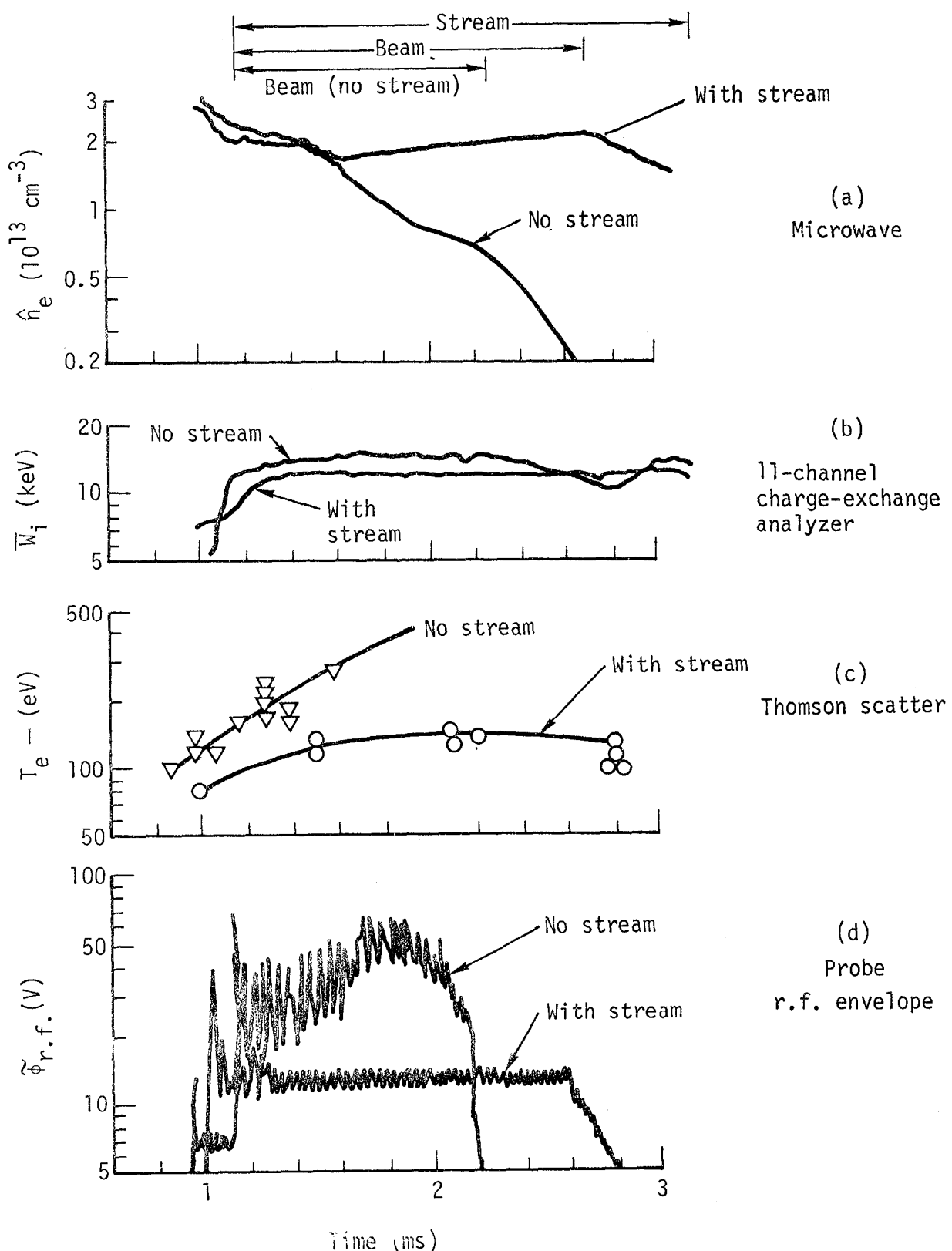


Fig. 2. Plasma parameters versus time, showing that the plasma stream (a) permits density buildup, (b) results in small decrease in average ion energy, (c) cools electrons, and (d) reduces ion-cyclotron fluctuations.

The mean deuteron ion energy is shown in Fig. 2(b). Without the stream, the mean ion energy increases rapidly. With the streaming plasma, the mean ion energy rises more slowly to 12 keV within 0.3 ms of beam turn-on. The 12-keV mean ion energy has been verified by absolute measurements of fast-atom charge-exchange flux, plasma diamagnetism, and absolute measurements of neutron production [10].

Electron temperature versus time measurements were made by Thomson scattering. In Fig. 2(c), the electron temperature with no stream rises rapidly to 250 eV. With the stream, the electron temperature increases from 75 eV to about 140 eV in 0.5 ms, and then remains relatively constant.

Ion-cyclotron fluctuations are detected with electrostatic probes [11] located beyond the mirrors and with microwave beams [12] at the center of the plasma. Figure 2(d) illustrates that the stream lowers the ion-cyclotron fluctuation amplitude by a factor between 2 and 4. Increasing the streaming-plasma input further reduces the fluctuation amplitude. The large decrease in fluctuation amplitude at 2.2 ms with no stream occurs when the hot-plasma density drops to a low enough level that the plasma is stabilized by background cold gas, much the same as in partially gettered operation [5,6]. The dominant fluctuation frequency is centered near the ion-cyclotron frequency [13], corrected for finite beta. Experimental observations of turbulent ion energy diffusion are obtained from measurements of charge-exchange flux at 12 discrete energies from 0.5 to 38.9 keV. The observed diffusion is reproduced theoretically by the quasilinear theory [14].

Longitudinal density measurements [9] with a movable microwave interferometer indicate that the axial plasma length is ~40 cm. Inverting this density profile [15] determines an ion-angular distribution peaked nearly perpendicular to magnetic field lines. This distribution indicates that the ions, injected near 90°, diffuse primarily in the perpendicular velocity direction by electron drag and wave turbulence, rather than in pitch angle, in agreement with the quasilinear theory.

The scaling of the plasma confinement parameter  $n\tau_p$  with mean ion energy has been determined from 3 to 13 keV by varying the neutral-beam extraction voltage. Particle lifetime  $\tau_p$  is obtained from the density decay rate after the neutral beams are turned off [1,16]. Such measurements indicate that particle confinement increases with ion energy, from  $n\tau_p = 1.5$  to  $2.0 \times 10^{10} \text{ cm}^{-3}\cdot\text{s}$  at 3 keV up to  $n\tau_p = 7 \times 10^{10} \text{ cm}^{-3}\cdot\text{s}$  at 13 keV. The beam current required to sustain the plasma at  $10^{13} \text{ cm}^{-3}$  density decreases with mean ion energy, indicating improved energy confinement at higher ion energies.

Energy confinement time  $\tau_E$  is calculated from energy balance once steady state is achieved. Quantitative determination of  $\tau_E$  is not available because the power input from the streaming gun is not well known. However, with gas-feed stabilization and with all power being supplied by the neutral beams,  $n\tau_E = 7 \times 10^{10} \text{ cm}^{-3}\cdot\text{s}$ .

Electron temperature measurements using Thomson scattering are available for a limited number of shots and indicate a slow increase in electron temperature with ion energy. The hot-ion cooling rate depends on the electron temperature and follows the Spitzer [17] drag dependence  $n\tau_d = 4.4 \times 10^7 T_e^{3/2}$  over a range of electron temperatures  $30 < T_e < 140 \text{ eV}$ .

### 3. HIGH-BETA BUILDUP IN A STEADY MAGNETIC FIELD

We have found that the streaming plasma used for stabilization can be injected into a quasi steady-state magnetic field to form a suitable target

plasma [18]. With an injected beam current of 260 A, the data in Fig. 3(a) show that the density of the hot plasma increases exponentially, reaching densities and energies similar to those achieved previously with target plasmas that were trapped by pulsed magnetic fields. The points are computed from a density buildup code [19]. This procedure offers a simple solution to the important technical problem of plasma startup in d.c. magnetic-mirror machines.

Using a single deuterium-loaded-titanium washer gun to provide startup and stabilizing plasma stream, a maximum beam-injected plasma beta of 0.4 is reached. Here beta is defined by  $\beta \equiv 8\pi \hat{n}_i \bar{W}_i / B_{vac}^2$ , where  $\hat{n}_i$  is the central hot-ion density,  $\bar{W}_i$  is the average ion energy, and  $B_{vac}$  is the applied central field. The beta is limited by end losses associated with periodic bursts of ion-cyclotron fluctuations and not by the available neutral-beam current. Increasing the amount of stabilizing plasma stream with three guns raises the beta to 0.6, but  $\beta$  is again limited by the same phenomenon.

To further increase the plasma stream, a gas-feed system [20] was installed as shown in Fig. 1(b). A ceramic box, with elliptical apertures conforming to the flux tube passing through a 12-cm-diam circle at the central midplane, is located just beyond one mirror throat of the minimum-B field. Hydrogen or deuterium gas is injected at a controlled rate into the box above and below the plasma fan by four pulsed gas valves. Gas neutrals are ionized in the box by electrons ( $T_e \approx 100$  eV) conducted along the field from the central plasma. Because the mean free path of gas neutrals is short compared to the thickness of the plasma fan, few neutrals leak out of the box. Measurements of charge-exchange flux from the center of the machine indicate a charge-exchange lifetime on background gas greater than 5 ms. This loss rate was negligible compared to other losses of the hot ions.

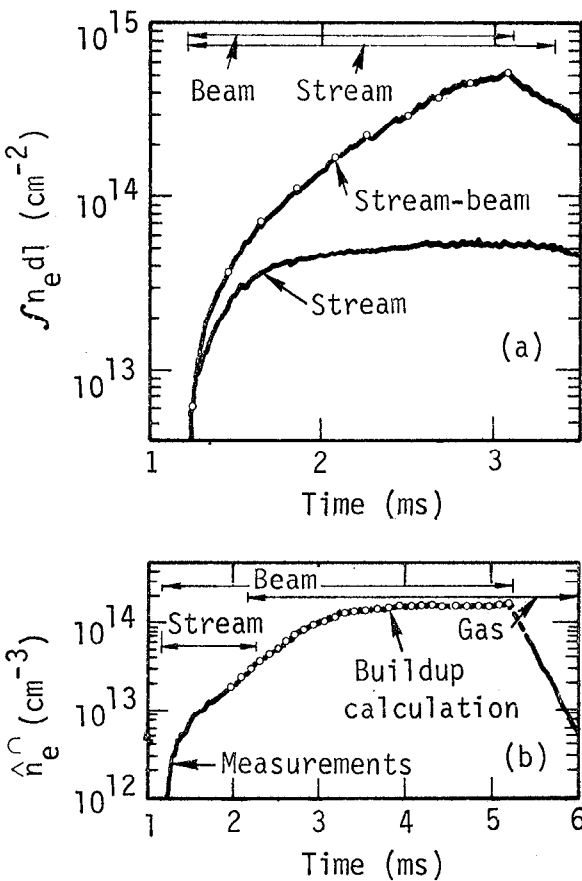


Fig. 3. Density buildup history on streaming plasma target, showing (a)  $\int n_{dl}$  without gas feed and (b)  $\hat{n}_e$  with 8000-A hydrogen gas feed.

To start ionization of injected gas, a hot plasma is initially created as described above. Figure 3(b) shows buildup with 225-A of beam injection. The guns are turned off, and gas injection begins with 8000-A atom equivalent of hydrogen gas. The central density reaches  $1.5 \times 10^{14} \text{ cm}^{-3}$  and is sustained for the duration of beam injection. No strong bursts of ion-cyclotron fluctuations are observed, indicating that the stabilizing plasma is not limited with the gas feed. Similar results were obtained with deuterium.

The dots shown in Fig. 3(b) are obtained by fitting the observed time dependence of the plasma density to the rate equation

$$\frac{dn}{dt} = a(1 - e^{-bn}) - \frac{n^2}{\langle n\tau_p \rangle}. \quad (1)$$

The coefficient  $a$  is the beam current trapped per unit volume calculated for Gaussian plasma and beam density profiles and taking into account reionization of charge-exchange neutrals. The parameter  $b = \langle \sigma v \rangle (2\bar{r}_p)/v_b$  is an attenuation factor averaged over the energy components of the neutral beam. Here,  $\langle n\tau_p \rangle$  is a density-independent loss parameter, appropriate for particle loss by ion-ion scattering and electron drag. For a constant 10% fraction of cold plasma, the best fit of Eq. (1) to the measured density buildup gives a plasma volume  $V = 4.5$  litres (defined by  $\hat{n}_e V = \text{total number of particles}$ ), and  $\langle n\tau_p \rangle = 1.2 \times 10^{11} \text{ cm}^{-3} \cdot \text{s}$ .

Hydrogen was used in the gas feed with deuterium neutral-beam injection so that hot beam-injected ions could be distinguished from warm ions trapped from the streaming plasma by the mass-selective neutral analyzer. At the high-density saturation, after correcting for reionization of charge-exchange neutrals the mean ion energy was calculated to be 9 keV. The maximum fraction of cold ions, hydrogen, and impurities is estimated to be less than 20%.

The dashed line in Fig. 4 shows the average plasma diamagnetism  $\bar{\Delta}B/B_{\text{vac}}$  measured by a compensated diamagnetic loop around the vacuum chamber. The excluded flux of the plasma is normalized to the total flux excluded by a field-free metal object ( $\Delta B = B_{\text{vac}}$ ) of the same volume as the plasma, placed at the position of the plasma for calibration. For constant plasma dimensions, the measured diamagnetic flux will be proportional to the average field reduction  $\bar{\Delta}B/B_{\text{vac}}$  within the plasma. Because of the substantial reduction in field, the mean ion gyroradius is comparable to the plasma radius. Accordingly, the frequency of ion-cyclotron fluctuations decreases with  $\bar{\Delta}B/B_{\text{vac}}$ , as indicated by the point labeled  $(\Delta\omega_{ci}/\omega_{ci})_{\text{vac}}$  in Fig. 4.

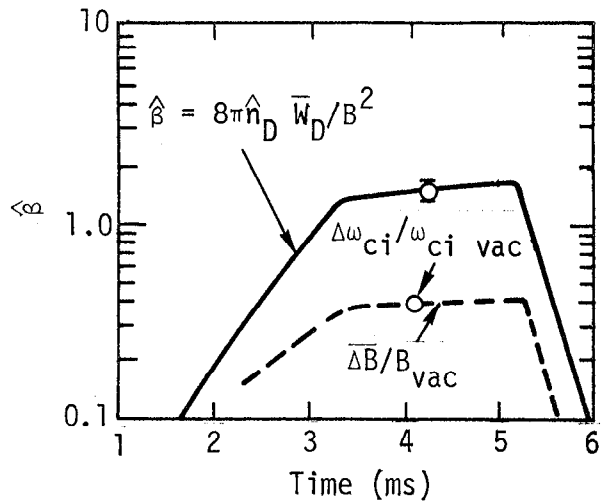
The solid line in Fig. 4 gives the peak value  $\hat{\beta}$  obtained from the measured central density  $\hat{n}_D$  and average ion energy  $\bar{W}_D$ . The central beta reaches a value well above unity. The error bar shows the uncertainty in peak density and cold plasma fraction. Because of the short axial length of the plasma ( $L_p/\bar{r}_p \approx 3$ ) and the high plasma pressure, the field lines are likely to have substantial curvature; therefore, a central beta value of roughly 2 is required to depress the on-axis field to zero.

Figure 5 shows how the energy confinement parameter  $\hat{n}\tau_E$  scales with neutral-beam current  $I_b$  for constant average beam energy  $\bar{E}_b$ . The average plasma energy lifetime in steady state is calculated from

$$\tau_E = (\hat{n}_D V) \bar{W}_D / (f I_b \bar{E}_b). \quad (2)$$

In Eq. (2), the numerator is the energy content of a total number of ions ( $\hat{n}_D V$ ) at average energy  $\bar{W}_D = 9$  keV, and the denominator is the fraction  $f$

Fig. 4. Central values of beta, diamagnetic flux, and ion-cyclotron frequency shift versus time.



of incident beam power that is absorbed in the plasma. This fraction varies with density, but it reaches typical values of 0.6. At  $I_b = 225$  A,  $\hat{n}\tau_E = 7 \times 10^{10}$  cm $^{-3}$ .s. Averaging over an ion orbit from the center of the plasma rather than taking the central density gives  $\bar{n}\tau_E \approx 5 \times 10^{10}$  cm $^{-3}$ .s. At  $I_b = 225$  A, a Thomson scattering measurement of the central electron temperature  $T_e = 100 \pm 20$  eV gives a confinement parameter of  $n\tau_d = 4.4 \times 10^{10}$  cm $^{-3}$ .s  $\pm 30\%$  due to electron drag. Thus, ion losses are largely accounted for by classical electron drag, consistent with the quasilinear theory for marginal stability [2]. Figure 5 shows that the central beta increases with beam current (at constant beam energy), with no apparent saturation. No evidence is found of a beta limit due to the mirror mode, the Alfvén ion-cyclotron mode, or nonadiabatic effects. Comparison of diamagnetic measurements with density measurements indicates that the energy of the plasma ions remains approximately constant with increasing beta. The energy containment time  $\tau_E$  is found to be nearly constant over the range of beam current shown in Fig. 5. The product  $n\tau_E$  in Fig. 5

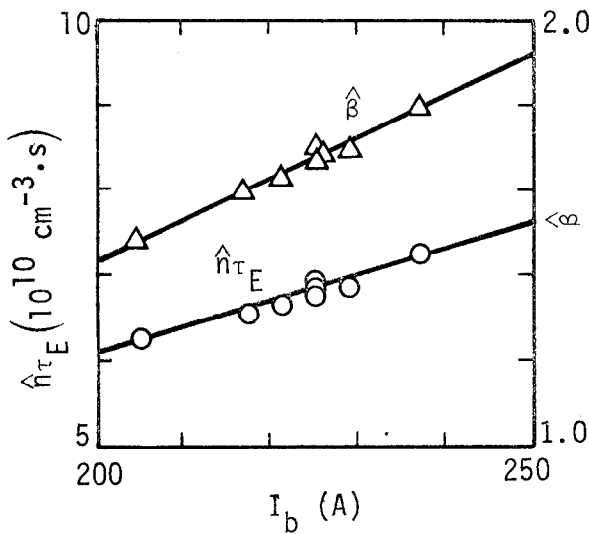


Fig. 5. Energy confinement  $\hat{n}\tau_E$  and  $\hat{\beta}$  increase with neutral-beam current  $I_b$ .

increases proportionally to beta (density) as the beam power is increased. Preparations are underway to pursue this favorable scaling of  $\Delta nT_E$  to higher neutral-beam power.

#### 4. CONCLUSIONS

In summary, the principal results of the 2XIIIB experiments are:

- Demonstration that stabilization is provided by a small fraction of warm plasma.
- Demonstration of plasma heating and sustenance by neutral-beam injection.
- Demonstration that the plasma confinement parameters  $nT_p$  and  $nT_E$  increase with ion energy.
- Achievement of startup in a steady-state magnetic field.
- Attainment of central plasma beta greater than unity.

Two fundamental properties of mirror systems are shown: the increase in  $nT$  with ion energy and the ability to contain high-beta plasmas. The energy scaling and the satisfactory theoretical interpretation of these data establish a basis for the design of future open-geometry experiments. The high-beta result has particular significance for mirror fusion reactor design, since high-beta operation enhances the fusion energy balance.

## REFERENCES

- [1] COENSGEN, F.H., CUMMINS, W.F., LOGAN, B.G., MOLVIK, A.W., NEXSEN, W.E., SIMONEN, T.C., Phys. Rev. Lett. 35 (1975) 1501.
- [2] BALDWIN, D.E., BERK, H.L., PEARLSTEIN, L.D., Phys. Rev. Lett. 36 (1976) 1051; also see Paper CN 35/C2, these Proceedings.
- [3] BERK, H.L., GORMEZANO, C., STEWART, J.J., submitted to Nucl. Fusion.
- [4] POST, R.F., ROSENBLUTH, M.N., Phys. Fluids 9 (1966) 730.
- [5] GOTTF, YU.V., IOFFE, M.S., KANAEV, B.S., MOTLICK, A.G., PASTUKHOV, V.P., SUBOLEV, R.J., YUSHMANOV, E.E., 4th Conf. Plasma Physics and Controlled Fusion Research (Proc. Conf. Tokyo, 1974) 1, IAEA, Vienna (1975) 341.
- [6] COENSGEN, F.H., CUMMINS, W.F., MOLVIK, A.W., NEXSEN, W.E., SIMONEN, T.C., STALLARD, B.W., 4th Int. Conf. Plasma Physics and Controlled Fusion Research (Proc. Conf. Tokyo, 1974) 1, IAEA, Vienna (1975) 323.
- [7] BAKER, W.R., BERKNER, K.H., COOPER, W.S., EHLERS, K.W., KUNKEL, W.B., PYLE, R.V., STEARNS, J.W., 4th Int. Conf. Plasma Physics and Controlled Fusion Research (Proc. Conf. Tokyo, 1974) 1, IAEA, Vienna (1975) 329.
- [8] COENSGEN, F.H., CUMMINS, W.F., SHERMAN, A.E., Phys. Fluids 2 (1959) 350; also STEINHAUS, J.F., OLESON, N.L., BARR, W.L., Phys. Fluids 8 (1965) 1720.
- [9] STALLARD, B.W., CUMMINS, W.F., MOLVIK, A.W., NEXSEN, W.E., SIMONEN, T.C., TURNER, W.C., Bull. Am. Phys. Soc. 20 (1975) 1231.
- [10] NEXSEN, W.E., LOGAN, B.G., COENSGEN, F.H., MOLVIK, A.W., CUMMINS, W.F., Bull. Am. Phys. Soc. 20 (1975) 1232.
- [11] SIMONEN, T.C., to be published in Phys. Fluids.
- [12] POWERS, E.J., SIMONEN, T.C., to be published in J. Appl. Phys.
- [13] TURNER, W.C., CUMMINS, W.F., NEXSEN, W.E., POWERS, E.J., SIMONEN, T.C., STALLARD, B.W., Bull. Am. Phys. Soc. 20 (1975) 1232; also see POWERS, E.J., Phys. Fluids 16 (1973) 1374.
- [14] TURNER, W.C., BERK, H.L., STEWART, J.J., submitted to Phys. Rev. Lett.
- [15] HALL, L.S., SIMONEN, T.C., Phys. Fluids 17 (1974) 1014.
- [16] COENSGEN, F.H., CLAUSER, J.F., CORRELL, D.L., CUMMINS, W.F., GORMEZANO, C., LOGAN, B.G., MOLVIK, A.W., NEXSEN, W.E., SIMONEN, T.C., STALLARD, B.W., TURNER, W.C., LLL Rept. UCID-17037 (1976).
- [17] SPITZER, L. Physics of Fully Ionized Gases, 2nd ed., Wiley, New York (1962).
- [18] COENSGEN, F.H., CLAUSER, J.F., CORRELL, D.L., CUMMINS, W.F., GORMEZANO, C., LOGAN, B.G., MOLVIK, A.W., NEXSEN, W.E., SIMONEN, T.C., STALLARD, B.W., TURNER, W.C., Phys. Rev. Lett. 37 (1976) 143.
- [19] STALLARD, B.W., LLL Rept. UCRL-51784 (1975).
- [20] LOGAN, B.G., LLL Rept. UCID-16851 (1975).

EXHIBIT B. THEORETICAL EXPLANATION OF PRESENT MIRROR EXPERIMENTS  
AND LINEAR STABILITY OF LARGER SCALED MACHINES\*

H. L. Berk, D. E. Baldwin, T. A. Cutler, L. L. Lodestro, N. Maron,  
L. D. Pearlstein, T. D. Rognlien, J. J. Stewart, and D. C. Watson

---

\* This paper was originally prepared for publication in the Proceedings of the Sixth International Conference on Plasma Physics and Controlled Nuclear Fusion Research, Berchtesgaden, Federal Rep. of Germany, October 6-13, 1976.

## THEORETICAL EXPLANATION OF PRESENT MIRROR EXPERIMENTS AND LINEAR STABILITY OF LARGER SCALED MACHINES\*

H. L. BERK, D. E. BALDWIN, T. A. CUTLER, L. L. LODESTRO, N. MARON,  
L. D. PEARLSTEIN, T. D. ROGNLIEN, J. J. STEWART, D. C. WATSON  
University of California, Lawrence Livermore Laboratory,  
Livermore, Calif., United States of America

### ABSTRACT

A quasilinear model for the evolution of the 2XIIIB mirror experiment is presented and shown to reproduce the time evolution of the experiment. From quasilinear theory it follows that the energy lifetime is the Spitzer electron drag time for  $T_e \lesssim 0.1T_i$ . By computing the stability boundary of the DCLC mode, with warm plasma stabilization, we predict the electron temperature as a function of radial scale length. In addition, the effect of finite length corrections to the Alfvén cyclotron mode is assessed.

### INTRODUCTION

Both the 2XIIIB [1] and PR-7 [2] mirror experiments have demonstrated stabilization of an ion-cyclotron frequency instability by the axial injection of cold plasma, herein termed a "stream." This conformed to a theoretical prediction that the drift-cyclotron-loss-cone (DCLC) mode would be stabilized by the presence of a low-density warm component [3]. In the following, we describe a quasilinear calculation for the ion evolution together with a model for the time evolution of the electron temperature. The composite theory is shown to be in quantitative agreement with many aspects of the 2XIIIB experiment. The diffusion due to fluctuations, competing with transit loss of the unconfined stream, heats the low-temperature stream to partially fill the loss cone of the hotter confined

---

\* This work was performed under the auspices of the U.S. Energy Research and Development Administration under contract No. W-7405-Eng-48.

plasma, thereby achieving marginal stability at a low fluctuation level. In the absence of the stream, a higher fluctuation level and a turbulent decay result. Next, we discuss the implication of this stabilizing mechanism in larger-radius machines. Finally, we describe certain finite geometry effects on the anisotropy-driven Alfvén-ion-cyclotron (AIC) mode which is predicted to exist in mirror machines at high  $\beta$ .

#### GENERAL CONSIDERATIONS

Ions are contained in a mirror machine only if  $v_{\perp}^2 > (v_{\parallel}^2 + 2q\Phi/M)/(R - 1)$ , where  $v_{\perp}$  and  $v_{\parallel}$  are the midplane components of the velocity relative to the magnetic field, R is the mirror ratio, q and M are the charge and mass, and  $\Phi$  is the ambipolar potential which is typically positive and several times  $T_e/|e|$  when  $T_e/T_i \ll 1$ . Particles lying outside this region of velocity space are lost axially in a transit time. When the velocity-space transport rate is slow compared to this transit rate, which is generally the case for mirror-confined plasmas, the distribution function for unconfined particles is small compared to its value for confined particles. The resulting non-monotonic energy distribution can then be subject to microinstabilities, termed loss-cone modes [4,5]. A sufficient level of turbulence results in a velocity diffusion which competes with the axial transit rate. The result is that the low-energy portion of the distribution partially fills in so that it becomes marginally stable. However, the existence of a significant density of unconfined particles implies a large loss flux which must be supplied either from the confined particles or from an external source such as demonstrated by stream stabilization [1].

In the absence of an external source, the requirement for maintenance of a stable distribution implies that the ratio of the lifetimes of confined to unconfined ions will vary as the respective densities. Thus, it was thought that a distribution which is well spread in pitch angle would have a lifetime of only a few axial transit times [6]. However, a distribution that is highly peaked in pitch angle, as results from neutral injection normal to  $\vec{B}$  together with diffusion principally in  $v_{\perp}$  and energy drag on cold electrons, has a hole in velocity space that is characteristic of the ambipolar energy. The ratio of densities will then vary as  $E_i/q\Phi$ , where  $E_i$  is the average ion energy. In addition, because the axial flow rate of unconfined ions is here the ion acoustic speed, the lifetime

of peaked distribution exceeds that of a well spread distribution of equal energy by a factor  $(E_i/q\Phi)^{3/2}$ .

If cold ions are supplied, as by an injected plasma stream, the lifetime of confined ions can be further enhanced. The turbulence no longer is required to replenish the loss flux of unconfined ions from the confined ions, but only to heat the injected cold ions to uniformly fill the region  $0 < v_{\perp}^2 < 2q\Phi/M$ . The loss flux of unconfined ions is then also an energy flux which, assuming the power comes from the confined ions, results in a lifetime enhancement factor  $(E_i/q\Phi)^{5/2}$ . In this text, it is shown that for 2XIIB parameters this lifetime is longer than the Spitzer drag time, so that the lifetime of the energetic ions is determined by this latter classical process.

#### QUASILINEAR MODEL

To quantify these notions, we have added to an existing two-dimensional (2-D)  $(v_{\perp}, v_{\parallel})$  Fokker-Planck code, which included Coulomb collisions, charge exchange, and neutral-beam input sources [7], a quasi-linear diffusion in  $v_{\perp}$  and a low-energy source to represent the stream. Particles in the unconfined regions were assumed lost at a rate inverse to their transit time. In addition, a simplified and faster one-dimensional (1-D) code for  $F(v_{\perp}, t) = \int dv_{\parallel} f(v_{\parallel}, v_{\perp})$ , valid when  $\langle v_{\parallel}^2 \rangle \ll \langle v_{\perp}^2 \rangle$ , has been constructed [8,9]. Results of the two codes will be compared here.

The turbulence model is driven by the DCLC for which  $k_{\parallel} = 0$  and  $k_{\perp} a_i > 1$ , where  $k_{\parallel}, k_{\perp}$  are the wave number components relative to  $\vec{B}$ , and  $a_i$  is the mean ion Larmor radius. Near marginal stability, noise is resonant near a cyclotron harmonic  $m$ , and the velocity diffusion coefficient is taken as

$$\hat{\vec{D}}(\vec{v}_{\perp}) = \frac{\hat{\vec{v}}_{\perp} \hat{\vec{v}}_{\perp}}{v_{\perp}^2} \sum_k \left| \frac{q\tilde{\Phi}_k}{M} \right|^2 \frac{m^2 \omega_{ci}^2}{\Delta\omega_k} J_m^2 \left( \frac{k_{\perp} v_{\perp}}{\omega_{ci}} \right), \quad (1)$$

where  $\tilde{\Phi}_k$  is the fluctuating potential,  $\Delta\omega_k$  is the correlation frequency determined by the transit rate of ions moving in a non-uniform magnetic field [10],  $\Delta\omega_k \approx \omega_{ci} (\langle v_{\parallel}^2 \rangle^{1/2} \omega_{ci}^{-1} |d \ln B/ds|)^{1/3}$ , and  $s$  is distance along  $B$ . The amplitude  $|\tilde{\Phi}_k|^2$  is proportional to the wave energy density,

$$\epsilon_k = \left| \frac{q\tilde{\Phi}_k}{Mv_{\perp}^2} \right|^2 \frac{n_e M v_{\perp}^2}{\sigma_k^2},$$

where  $n_e$  and  $v$  are a normalized density and velocity, and  $\sigma_k$  is a time-dependent parameter that is determined by the solution of the dispersion relation and that in this work is modelled as a constant.  $\epsilon_k$  is determined by the equation

$$\frac{\partial \epsilon_k}{\partial t} = 2\gamma_k \epsilon_k + \alpha_k ,$$

where  $\alpha_k$  is the thermal source of noise, and the growth rate is given by

$$\frac{\gamma_k}{\omega_{ci}} = \sigma_k \frac{v^2}{n_0} \int dv^3 \frac{\partial f}{\partial v_\perp^2} J_m^2 \left( \frac{k_\perp v_\perp}{\omega_{ci}} \right) \frac{m\omega_{ci}}{\Delta\omega_k} . \quad (2)$$

In a machine such as 2XIIIB with a radius of only a few Larmor radii, DCLC is unstable when the "matrix element" on the right-hand side of Eq. (2) is positive over a large range of  $k_\perp$ . For larger machines, the dispersion relation restricts the range of unstable  $k_\perp$ , even when the matrix element is positive, and a more realistic form must be used for  $\omega(k)$  and  $\sigma_k$ . This case is currently under investigation.

The electron temperature plays an important role in determining both the electron drag rate and the ambipolar potential. It can be calculated using either the electron Fokker-Planck equation or equivalently from the energy balance equation

$$\frac{d}{dt} \left( \frac{3}{2} n T_e \right) = n v_d E_i - \eta T_e J_{loss} , \quad (3)$$

where  $v_d$  is the Spitzer ion-electron energy exchange rate,  $E_i$  is the mean ion energy,  $J_{loss}$  is the electron particle flux per unit volume lost axially, and  $\eta T_e$  is the mean energy per unit volume of the axially-lost electrons. The identification  $\eta T_e = q\Phi + T_e$  reduces the model predictions to those of the electron Fokker-Planck code used in the 2-D code. Larger values of  $\eta$  allow a phenomenological means for accounting for processes such as ionization, secondary emission, etc.; and a value  $\eta = 8$ , used in the 1-D code, was typical of the values found to describe the  $T_e$  history of 2XII [11]. The ratio  $q\Phi/T_e$  is determined by the requirement of equal ion and electron loss rates [12]; typically, with stream we find  $q\Phi/T_e \approx 3$ .

The codes show that the stream reduces the fluctuation level in the plasma, allowing buildup with sufficient energetic beam current and an extended lifetime in the absence of beams. Without stream, the enhanced fluctuations prevent buildup to steady state, and turbulent decay results.

By using the experimentally measured time evolution of the plasma stream and background charge exchange, a quantitative comparison with experiment is possible. In Fig. 1, we compare density, ion temperature, and electron temperature measured in the 2XIIB experiment with the predictions of the 1-D and 2-D codes. The experimental results can be duplicated quite accurately with both codes. However, the modelling of the physics in the two codes is somewhat different, resulting in small quantitative differences in the plasma evolution. Consequently, to replicate the experiment, the stream current in the 2-D code was a factor 1.5 greater than that in the 1-D code, while the charge-exchange loss rate from background gas was a factor 0.75 of the 1-D code. Both of these adjusted factors are within the experimental error for the respective measured quantities. For a more detailed discussion of the 1-D results, see Refs. [8] and [9].

The scaling laws for the steady state follow from the requirement for marginal stability and from Eq. (3) with the loss flux estimated as  $J_{\text{loss}} = v_t n_u$ , where  $v_t \approx (q\Phi/M)^{1/2}/2L_p$  is the transit rate of unconfined particles,  $L_p$  is the axial scale length, and  $n_u$  is the unconfined plasma density. Using  $q\Phi \approx 3T_e$ , we find

$$T_e (\text{keV}) = 3.3 \times 10^{-7} \left( \frac{n^2 L_p E_i^2}{n_u \eta} \right)^{1/3}, \quad (4)$$

where  $E_i$  is the mean ion energy. For 2XIIB ( $R_p/a_i \approx 2$  to 3),  $n_u$  at marginal stability is given by  $n_u \approx n\lambda q\Phi/E_i \approx 3n\lambda T_e/E_i$ , with  $\lambda$  a constant  $\approx 0.5$ . For this case, we obtain

$$T_e = 1.1 \times 10^{-5} \left( \frac{n L_p E_i^2}{\lambda \eta} \right)^{1/4}. \quad (5)$$

When the stream current  $J_{\text{strm}}$  is much larger than the beam current, it follows that in steady state  $J_{\text{strm}} \approx J_{\text{loss}}$ . When the mean ion energy is roughly the mean input beam energy, which occurs with sufficiently intense beams and stream, both the steady-state density and electron temperature are controlled by the stream and mean ion beam energy,

$$\begin{aligned} n &= 0.7 J_{\text{strm}}^{8/11} L_p^{5/11} E_i^{2/11} \eta^{3/11} / \lambda^{5/11}, \\ T_e &= 1.0 \times 10^{-5} J_{\text{strm}}^{2/11} L_p^{4/11} E_i^{6/11} / \eta^{2/11} \lambda^{4/11}. \end{aligned} \quad (6)$$

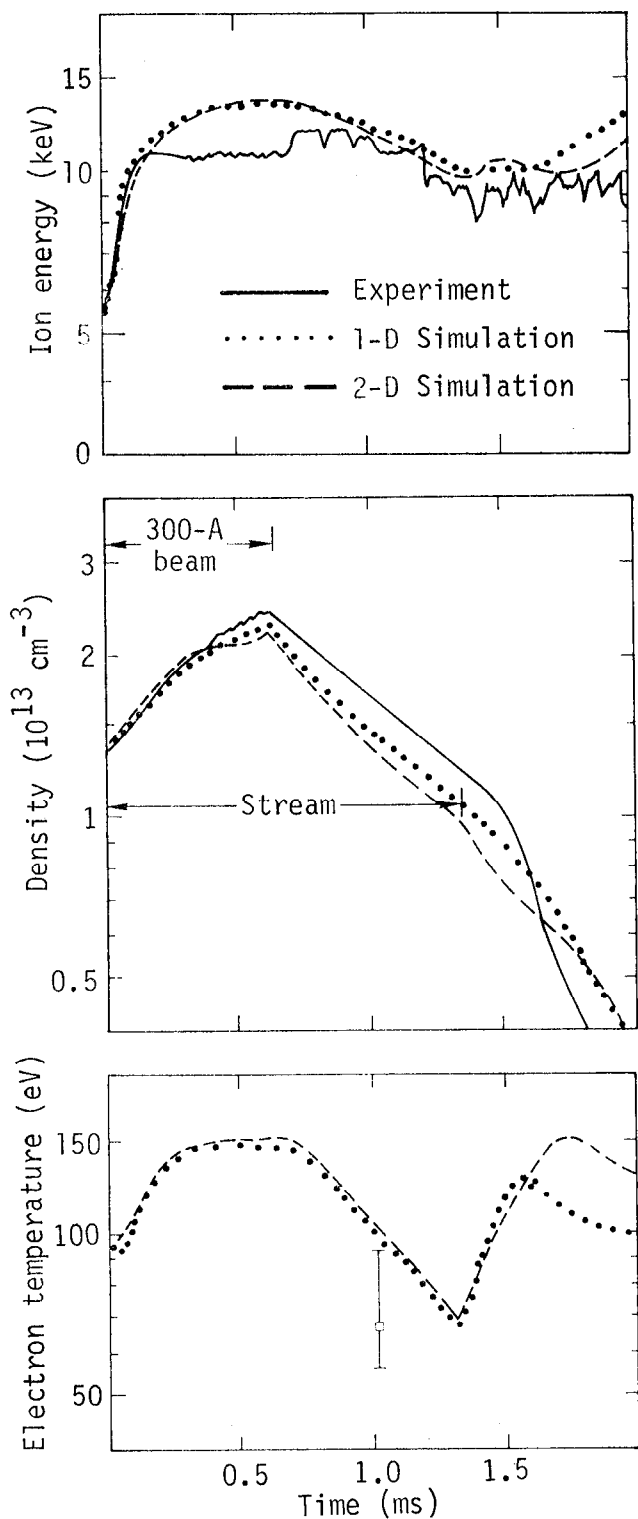


FIG. 1. Comparison of the time evolution of the plasma parameters in the 2XIIIB experiment with the 1-D and 2-D quasilinear codes. The electron temperature was measured at one point in time as shown.

Note that when these conditions are fulfilled, the steady-state  $n$  and  $T_e$  are independent of the input beam current. This result manifests itself in the density buildup in Fig. 1. For the first 300  $\mu s$ ,  $J_{\text{strm}}$  and thus  $n_u$  are greater than this minimum value required for stability at the prevailing density, and the density builds up at the beam input rate. After 300  $\mu s$ , further density increase is determined by the prevailing stream, and the subsequent increase in density while the beam is on requires an increasing stream current with time as inferred from the end loss measurements.

Ions lose energy both by classical drag on the electrons at a rate  $v_d n E_i$  and via fluctuations that supply the power drain of the unconfined ions given by  $\frac{1}{2} q \Phi J_{\text{loss}}$ , where  $\frac{1}{2} q \Phi$  is the average energy of the unconfined ions. From Eq. (3) in steady state, it may be seen that the power drain from electron drag is larger than the turbulent energy transfer by a factor  $2\eta/3$ , so that the ion energy confinement time is dominated by classical electron drag, with the electron temperature depressed by the presence of the stream.

#### DRIFT-CYCLOTRON-LOSS-CONE STABILITY

For mirror machines with larger radii, the electron temperature is still given by Eq. (7) with the ratio  $n_u/n_H$  determined by the marginal stability condition. This is evaluated from the flute-averaged dispersion relation of the DCLC mode [10], given by

$$\int_0^L ds k_\perp^2 I(\omega, k_\perp, s) = 0 , \quad (7)$$

where

$$I = \frac{\omega_{pe}^2}{\omega_{ce}^2} + 1 + \frac{\omega_{pi}^2}{\omega_{ci}^2} \left\{ \frac{\omega_{pi}^2}{k_\perp^2 c^2} - \frac{\omega_{ci}}{k_\perp R_p} \frac{1 + \frac{\beta_\perp}{2}}{\omega + ik_\perp^2 D_e(\omega/k)/\omega_{ci}^2} \right. \\ + \sum_{n \neq 0} \frac{\omega_{ci}^2}{k_\perp^2} \int d^3 v \frac{1}{v_\perp} \frac{\partial F_i}{\partial v_\perp} \frac{\omega}{\omega - n\omega_c + ik_\perp^2 D_i(\omega/k)/\omega_{ci}^2} J_n^2 \left( \frac{k_\perp v_\perp}{\omega_{ci}} \right) \\ \left. + \frac{\omega_{ci}^2}{k_\perp^2} \int d^3 v \frac{1}{v_\perp} \frac{\partial F}{\partial v_\perp} \left[ J_0^2 \left( \frac{k_\perp v_\perp}{\omega_{ci}} \right) - 1 \right] \right\} \quad (8)$$

is the local dispersion relation, and  $D_i(\omega/k)$  is the magnitude of the turbulent diffusion coefficient at the phase velocity of the wave. As a representative function, we use

$$F(v_{\perp}^2) = \frac{(n - n_u)}{v_H^2 - v_h^2} \left[ \exp\left(-\frac{v_{\perp}^2}{v_H^2}\right) - \exp\left(-\frac{v_{\perp}^2}{v_h^2}\right) \right] + \frac{n_u}{v_u^2} \exp\left(-\frac{v_{\perp}^2}{v_u^2}\right). \quad (9)$$

In Eq. (8),  $D_i$  is obtained from the quasilinear, marginally stable state and can be estimated from the requirement for power balance with the stream. Assuming the turbulence transfers energy from the hot plasma to the unconfined plasma, whose lifetime is a transit time  $v_t^{-1}$ , this balance gives

$$\frac{nv_H^2}{\tau_E} = n_u v_t v_u^2, \quad (10)$$

where  $\tau_E$  is the turbulent-energy lifetime of the hot plasma. By using a diffusive scaling law, we have  $D_i(v_H) \approx v_H^2/\tau_E$ ; and from Eq. (1) we have  $D_i(v_{\perp}) \approx (\omega/kv_{\perp})^3 D_i(\omega/k)$  for  $\omega/kv_{\perp} \lesssim 1$  where  $\omega \approx m\omega_{ci}$ . Hence, using Eq. (10), we find

$$D_i\left(\frac{\omega}{k}\right) = \frac{a_i^3}{L_p} \frac{n_u}{n_H} \left(\frac{kv_H}{\omega}\right)^3. \quad (11)$$

MX, an experiment proposed by Lawrence Livermore Laboratory, has the parameters  $B_{vacuum} = 20$  kG and  $L_p = 170$  cm. The fraction of warm plasma ( $n_u/n$ ) required for marginal stability and the implied electron temperature at  $\beta = 0.5$  (the electron temperature determines the energy lifetime) are plotted in Fig. 2 as a function of plasma radius for two values of  $(v_H/v_u)^2$  and  $D_e = D_i$ . In scaling from 2XIIB to MX, there is a six-fold reduction in the required warm plasma ratio. The marked reduction in the size of the stable radius from the case of no warm plasma to the case with warm plasma is due to two cooperative effects. One is the stabilizing effects of warm plasma and beta reported elsewhere [3,13,14] and the other is orbit diffusion which strongly stabilizes the large  $k_{\perp}$  modes.

#### ALFVÉN-ION-CYCLOTRON MODE

In addition to inverted populations in velocity space that generate the previously described loss-cone modes, a mirror-confined plasma supports an anisotropic velocity distribution, which is an additional source

of instability. A mode of recent concern [15] that taps this source is a left-hand, circularly polarized Alfvén wave. This mode, which will be referred to as the Alfvén-ion-cyclotron (AIC) mode, occurs at a sufficiently large  $\beta_{\perp}$ . Previous calculations of this mode [15,16] ignored finite-geometry effects and produced growth rates and frequencies for real  $k_{\parallel}$ . In this paper, we present preliminary theoretical results for the stability of this mode in mirror machines of finite extent. Specifically, we determine the boundary between absolute and convective instability ( $d\omega/dk_{\parallel} = \text{Im}\omega = 0$ ) and the influence of finite geometry on this boundary by solving the phase integral [3]

$$\int_{-s_t}^{s_t} k_{\parallel}(s) ds = (2n + 1)\pi; \quad n = 0, 1, 2; \quad \frac{dk_{\parallel}}{ds} (s = \pm s_t) = 0, \quad (12)$$

where  $s$  is the distance along a field line. We evaluate Eq. (12) by approximating  $k_{\parallel}$  as

$$k_{\parallel}(B) = k_{\parallel}[B(0)] + \left. \frac{dk_{\parallel}}{dB} \right|_{B=0} \frac{s^2}{L^2} B(0).$$

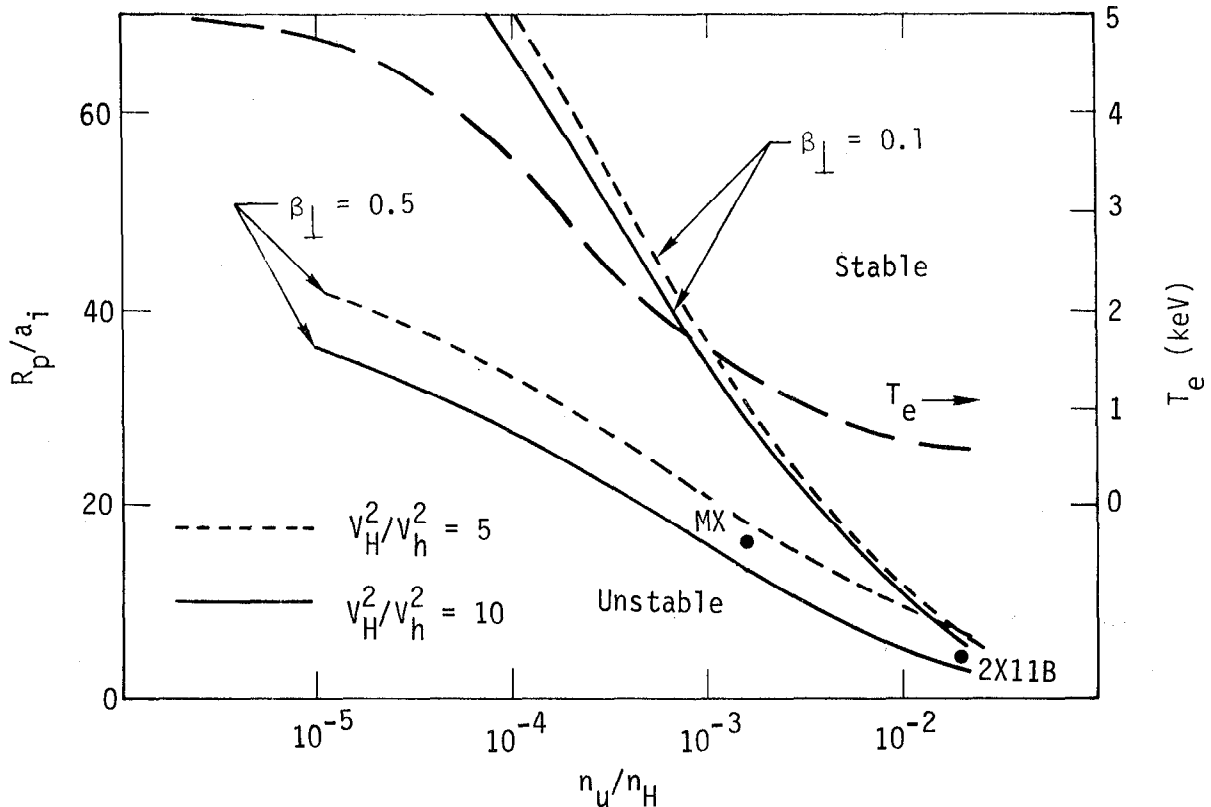


FIG. 2. Plasma-radius stability boundary and predicted electron temperature for the MX experiment vs the fraction of warm plasma. Stable regions are for larger radii.

The dispersion relation for the AIC mode is given in Ref. [15]. To evaluate stability boundaries, we consider two specific distributions: a bi-Maxwellian distribution (which is a model of the drag-dominated distribution computed by Fokker-Planck codes),

$$f \approx e^{-\alpha_{\perp} v_{\perp}^2} e^{-\alpha_{\parallel} v_{\parallel}^2},$$

and a collisional-type distribution,

$$f \approx e^{-\alpha v^2} g(v_{\perp}^2/v^2).$$

Our results are depicted in Figs. 3(a) and 3(b), where we plot the boundary of absolute instability for AIC for a uniform plasma and compare it to the shifted boundary obtained from a Wenzel, Kramers, and Brillouin (WKB) calculation for 2XIIB and MX configurations.

Due to inhomogeneities, there is a substantial shift of the stability boundary for the 2XIIB configuration. However, the beta observed in that experiment is still in excess of the predicted threshold for AIC. Possible explanations are:

- The depression in the field is less than that predicted by the long, thin approximation for the equilibrium, implying less local  $\beta_{\perp}$  for the mode.
- The simple parabolic expansion of the phase integral is inaccurate, because the WKB approximation typically fails when the calculated frequency shift is comparable to the homogeneous plasma frequency shift.

We have examined the effect on the mode of finite  $k_{\perp} \approx 1/R_p$  and find it to be less important than the finite plasma length.

Finally, it should be noted that the SUPERLAYER code described in paper CN-35/C3 in these Proceedings shows buildup through reversal without disruption by AIC, provided the plasma is not too long, i.e., if it is on the order of 2XIIB lengths. If it is finite length which stabilizes AIC in 2XIIB, then MX with its longer scale length should be affected by this mode at high beta.

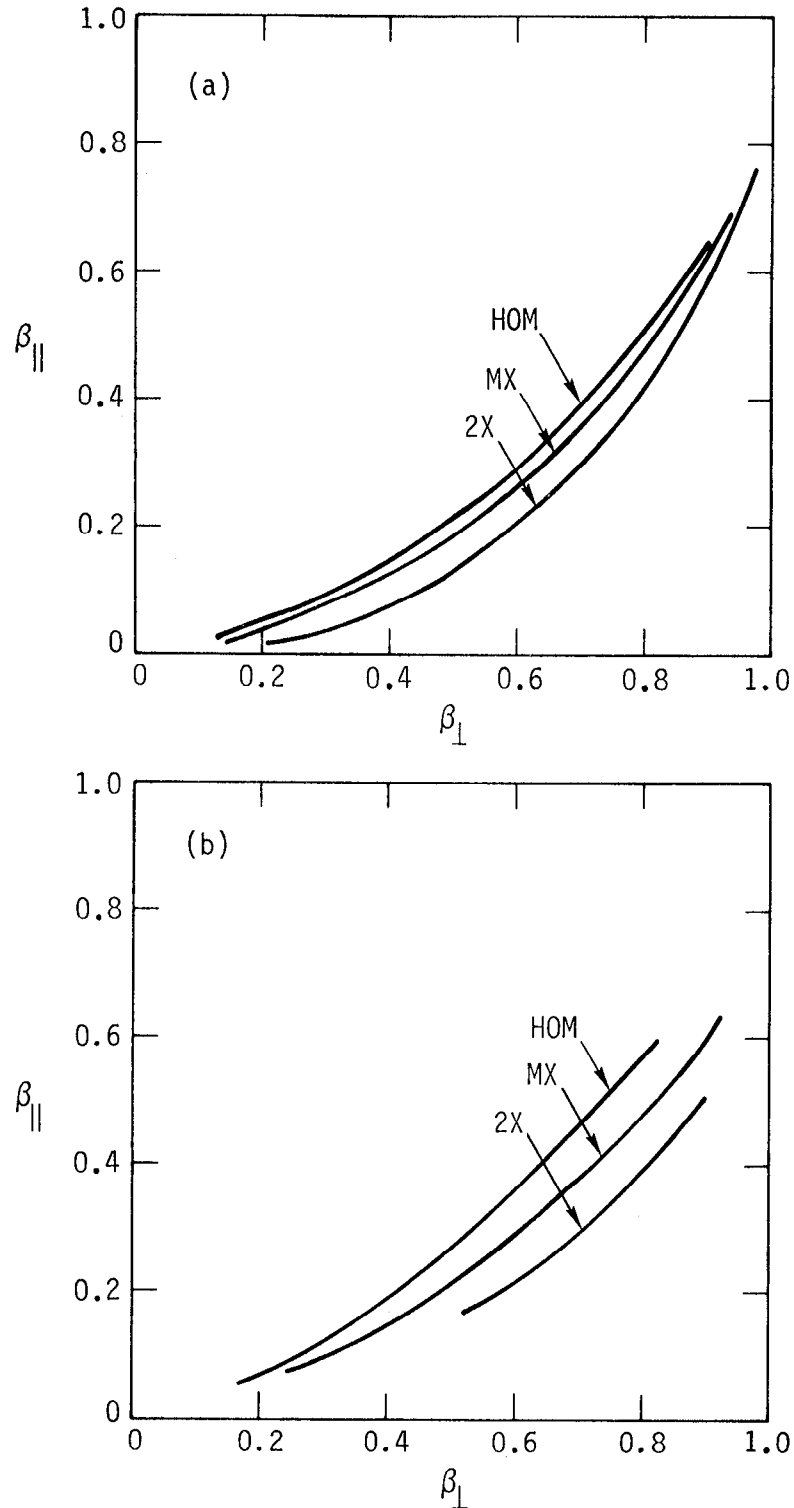


FIG. 3. Alfvén-ion-cyclotron stability boundaries in the  $\beta_{\perp}$ - $\beta_{\parallel}$  plane. Boundary curves labelled "HOM," "MX," and "2X" correspond to homogeneous plasma and to scale lengths of 25 and 7 ion Larmor radii respectively. Figures 3(a) and 3(b) correspond to bi-Maxwellian and collisional ion velocity distributions, respectively.

## REFERENCES

- [1] COENSGEN, F. H. et al., Phys. Rev. Lett. 35 (1975) 1501.
- [2] BAIBORODOV, Y. T. et al., 6th Eur. Conf. Controlled Fusion and Plasma Physics (Proc. Conf. Moscow, 1973) 2, U.S.S.R. Academy of Sciences, Moscow (1973) 122.
- [3] BERK, H. L. et al., 3rd Int. Conf. Plasma Physics and Controlled Nuclear Fusion Research (Proc. Conf. Novosibirsk, 1968) 2, IAEA, Vienna (1969) 151.
- [4] ROSENBLUTH, M. N., POST, R. F., Phys. Fluids 8 (1965) 547.
- [5] POST, R. F., ROSENBLUTH, M. N., Phys. Fluids 9 (1966) 730.
- [6] GALEEV, A. A., 2nd Int. Conf. Plasma Physics and Controlled Nuclear Fusion Research (Proc. Conf. Culham, 1965) 1, IAEA, Vienna (1966) 341.
- [7] FUTCH, A. H., HOLDREN, J. P., KILLEEN, J., MIRIN, A. A., Plasma Phys. 14 (1972) 211.
- [8] BERK, H. L., STEWART, J. J., Lawrence Livermore Laboratory Rep. UCRL-78407 (1976) (submitted to Phys. Fluids).
- [9] BERK, H. L., GORMEZANO, C., STEWART, J. J., Lawrence Livermore Laboratory Rep. UCRL-78401 (1976) (submitted to Nucl. Fusion).
- [10] BALDWIN, D. E. et al., 4th Int. Conf. Plasma Physics and Controlled Nuclear Fusion Research (Proc. Conf. Madison, 1971) 2, IAEA, Vienna (1971) 735.
- [11] COENSGEN, F. H. et al., 5th Int. Conf. Plasma Physics and Controlled Nuclear Fusion Research (Proc. Conf. Tokyo, 1974) 1, IAEA, Vienna (1975) 323.
- [12] PASTUKHOV, V. P., Nucl. Fusion 14 (1974) 3.
- [13] TANG, W. M., PEARLSTEIN, L. D., BERK, H. L., Phys. Fluids 15 (1972) 1153.
- [14] GERVER, M. J., Electronic Research Laboratory Rep., University of California, Berkeley (1976) (to be published in Phys. Fluids).
- [15] DAVIDSON, R. C., OGDEN, J. M., Phys. Fluids 18 (1975) 1045.
- [16] For a list of earlier references, see CORDEY, J. G., HASTIE, R. J., Phys. Fluids 15 (1972) 2291.

CKM/jj/vt/jf/lmc

G. P. O. /789-009/7940